THE UNIVERSITY OF HULL

INVESTIGATION OF NOVEL MICRO-CHANNEL, MINI-CHANNEL PV/T AND THERMAL MODULES BASED SOLAR HEAT PUMP SYSTEMS

being a Thesis submitted for the Degree of Doctor of Philosophy

at the University of Hull

by

Jinzhi Zhou

MSc University of Science and Technology of China, China
BEng Hefei University of Technology, China

November 2018

CONTENT

PUBLICATIONS

Book chapter

1. Xudong Zhao, Xiaoli Ma, Peng Xu, Diallo Thierno, Zishang Zhu, and **Jinzhi Zhou**, Cases of Energy System in a Green Building in UK (Chapter 15), Handbook of Energy Systems in Green Buildings, DOI 10.1007/978-3-662-49088-4_15-1, Springer-Verlag GmbH Germany 2017; pp.1-55.

Journal Publications

1. **Jinzhi Zhou**, Xudong Zhao, Xiaoli Ma, ZhongzhuQiu, Jie Ji, Zhenyu Du, Min Yu. Experimental investigation of a solar driven direct-expansion heat pump system employing the novel PV/micro-channels-evaporator modules. Applied Energy 178 (2016) 484-495.
2. **Jinzhi Zhou**, Xudong Zhao, Xiaoli Ma, Yi Fan. Clear-days operational performance of a hybrid experimental space heating system employing the novel mini-channel solar thermal & PV/T panels and a heat pump. Solar Energy 155 (2017) 464-477.
3. Thierno Diallo, Min Yu, **Jinzhi Zhou**, Xudong Zhao, Jie Ji, David Hardy. Analytical investigation of the Heat-Transfer Limits of a Novel Solar Loop-Heat Pipe Employing a Mini-Channel Evaporator, Energies 2018, 11(1), 148.
4. Min Yu, Thierno Diallo, Xudong Zhao, **Jinzhi Zhou**, Zhenyu Du, Jie Ji, Yuanda Cheng. Analytical study of impact of the wick's fractal parameters to the heat transfer capacity of a novel micro-channel loop heat pipe. Energy 158 (2018) 746-759.
5. Thierno Diallo, Min Yu, **Jinzhi Zhou**, Xudong Zhao, Samson Shittu, Guiqiang Li, Jie Ji. Energy performance analysis of a novel solar PVT Loop Heat Pipe heating system employing a microchannel heat pipe evaporator and a PCM triple heat exchanger. Energy 167 (2019) 866-888.

Patents

1. Xudong Zhao, **Jinzhi Zhou**, Zhenyu Du. A micro-channel Photovoltaic/thermal (PV/T) panel, Chinese patent, CN 201610090634.X, 2016.

Conference Proceedings and Presentations

1. **Jinzhi Zhou**, Xudong Zhao, Xiaoli Ma, Yi Fan. Experimental performance of mini-channel solar thermal & PV/T panels in summer season. The 2nd UK-China workshop for renewable energy and phase change energy storage technologies in building. Hull, UK. 29th-31st, July, 2018.
2. **Jinzhi Zhou**, Xudong Zhao, Xiaoli Ma, Yi Fan. Study on a hybrid solar indirect-expansion heat pump system associated the novel mini-channel solar thermal & PV/T panels for space heating. 16th International Conference on Sustainable Energy Technologies (Set 2017), Italy, 17th - 20nd July 2017.
3. **Jinzhi Zhou**, Xiaoli Ma, Xudong Zhao. Experimental study of a novel PV/micro-channel-heat-exchanging collector based heat pump system, 15th International Conference on Sustainable Energy Technologies (Set 2016), Singapore, 19th -22nd July, 2016.

Posters

1. **Jinzhi Zhou**, Xudong Zhao, Xiaoli Ma. Investigation of a novel PV/micro-channel-heat-exchanging panel based heat pump system – an approach towards the renewable heating for buildings. Poster for Postgraduate Research Posters at the University of Hull, UK, 22th March 2016.

ACKNOWLEDGEMENT

I would like to express a sincere gratitude to my excellent Professor Xudong Zhao. His patient guidance and support encouraged me to overcome all of the obstacle during the process of PhD study, and complete my PhD work successfully. His rigorous and meticulous style has always been an example in my work and study, and his inspiring teaching and diverse ideas have given me endless inspiration.

I would also like to thank the University of Hull for the financial support of the International Fee-Bursary, as well as Shanxi Jingxu Renewable Energy Co. , Ltd for the support to living costs. Thanks to Dr. Zhongzhu Qiu, Mr. Fan Yi and the technician from Shanxi Jingxu Renewable Energy Co. , Ltd for helping me to construct the prototype systems and test them. Also, thank you to Dr. Xiaoli Ma for the many constructive suggestions to my journal papers.

A particular thank you to my research group colleagues, Mr. David Hardy, Dr. Diallo Thierno, Miss. Min Yu, Mr. Samson Shittu and Mr. Kai Zhang. Thank you for your hard work, we had a good time together.

Lastly, I would like to thank my parents and girlfriend, their support and encouragement was the driving power for me to move forward in my work.

ABSTRACT

Regarding the building energy consumption optimisation, there is a developmental trend to replace traditional fossil fuel sourced energy with, rapidly growing, clean renewable energy. The main source of energy consumption is from hot water, cooling and space heating, which is normally provided by electric heater, gas boiler and/or coal boiler. However, these existing systems have their own drawbacks, such as high operating costs (electric heater), being inconvenient to obtain (gas boiler) and causing environmental pollution (coal boiler). Therefore, it is necessary to develop a clear and convenient energy system to replace these traditional ones, i.e., solar energy, biomass energy.

This research aims to investigate two kinds of novel photovoltaic thermal modules (PV/T) based heat pump systems, one with direct-expansion and the other with an indirect-expansion style, to be used for the purpose of space heating, hot water supply and power generation. Compared to existing PV/T modules, the new modules possess novel features that lead to enhanced heat transfer, improved solar efficiency and extended module lifetime. The strength and innovation of PV/T technology in this thesis are as follows: (1) a micro-channel and mini-channel tube is selected as the heat exchanger tube. This special structure improves the heat transfer rate of working fluid inside, enhancing both solar, thermal and electrical efficiencies; (2) compared to existing copper tube heat exchanger, the micro-channel has a much larger contact area, increasing the heat transfer rate; (3) the material of the micro-channel tube and header is aluminum, which has a low cost. These designs were intended to overcome some of the drawbacks and provide experimental data for the development of PV/T technology.

For the solar direct-expansion heat pump system, more than one-month time testing was carried out, and according to the result on a sunny winter day, the average electrical, thermal and overall efficiencies of the micro-channel panels were 13.1%, 56.6% and 69.7% respectively, which were respectively higher by 11.0%, 11.8% and 11.4% than the similar system. The Coefficient of Performance (COP) of the system had a similar variation trend to the solar radiation, with the average COP in the testing day being 4.7.

For the solar indirect-expansion heat pump system, again tested in winter, it was found that the average electrical, thermal and overall efficiencies of the mini-channel PV/T panels were 14.5%, 31.7% and 46.2% respectively, which has 9.0%, 5.8% and 6.2% higher efficiency than the existing similar systems. In addition, the mean thermal efficiency of the mini-channel thermal panels is 49.9%, which is a 5% increase compared to existing collector. The average COP of the heat pump is 4.6 during the working time. In summer, the average electrical efficiency of the PV/T panel was 11.5%, and the average thermal efficiency of the thermal panel was 46.8%. The temperature of water in the tank increased from 23^{o}C to 60^{o}C, therefore this water could be used for various applications.

The annual economic and environmental analysis results, based on the local weather data, indicate that although the two systems have a higher initial cost, they have a much lower operating cost. Based on the weather data of Taiyuan city, the payback time of these direct and indirect expansions systems are 8.7 years and 5.8 years, respectively. Additionally, these direct and indirect expansion systems can, respectively, reduce CO_2 emission by around 91.4 t and 109.1 t annually. Based on the weather data of London, the payback time of the two systems are 6.6 years and 3.5 years, while the CO_2 emission reduction are 44.8 t and 76.2 t, respectively.

Based on these research results, some amendments are required to improve and promote the systems in the future. These include improving the structure and material of the PV/T panel, reducing manufacturing cost, further optimisation of the system and long-term measurement under real-world conditions. Additionally, seeking policy support is needed from the government to reduce the initial and operating cost.

This research shows that these two solar heat pump systems provide a reasonable alternative to the traditional heating system for space heating in rural house. Most of the existing solar energy systems are small scale and designed for producing hot water, while the large-scale solar energy system for space heating in rural houses is rarely researched. Therefore, the experimental and simulation results on these two systems provides fundamental data for developing and improving large-scale solar energy systems.

LIST OF FIGURES

LIST OF TABLES

NOMENCLATURE

A	Area, m^2
C	Currency, A
E	Output power, W
F	Price, GBP
G	Solar radiation, W/m^2
H	Efficiency,
I	Interest rate per year,
K	Thermal conductivity, W/(m·K)
L	Characteristic length, m
M	Quality, kg
O	Salvage value, GBP
P	Pressure, Bar
Q	Energy, W
R	Thermal resistance, K/W
S	Speed, m/s
T	Temperature, K
U	Voltage, V
V	Displacement per revolution, m^3
W	Distance between the tubes, m
W_p	Watt peak capacity, W
W_e	Watt of electricity, W
X	Result value,
Y	Thermal capacity, W/(kg·K)
B_o	Boiling number,
CCE	Carbon credit earned, ton/year
C_D	Mass flow coefficient,
CRF	Capital recovery factor,
C_p	Thermal capacity, W/(kg·K)
CPP	Cost payback period, year
D_h	Hydraulic diameter, m
EE	Primary energy saving efficiency,
$EPBT$	Energy payback time, year

EPF	Energy production factor,
F'	Efficiency factor,
F''	Fin efficiency,
F_R	Heat removal factor,
Gr	Grashof number,
LCE	Life cycle conversion efficiency,
LCNC	Life-cycle net cost,
L_F	Wetted perimeter, m
L_H	Heated perimeter, m
MRE	Mean relative error,
Nu	Nusselt number,
PO	Power output, W
PP	Present value,
Pr	Prandtl number,
Re	Reynolds number,
P_R	Reduced pressure, Bar
Ra	Rayleigh number,
RC	Radius of curvature, m
RE	Relative error,
$SDHP$	Solar direct-expansion heat pump system
$SIHP$	Solar indirect-expansion heat pump system
W_b	Length of the panel, m
We_{lo}	Weber number,
WI	Input power, W
α	Heat transfer coefficient, W/(m^2·K)
β	Efficiency temperature coefficient, 1/K
β'	Thermal diffusivity, m^2/s
γ	Transmittance,
ϖ	Ratio of specific heats at constant pressure and volume
δ	Declination of the sun,
ε	Emissivity,
ζ	Coverage factor,
η	Efficiency,
θ	Incident angle of sunlight to the plane, ^{o}

κ	View factor,
ϱ	Adiabatic compressibility factor,
λ	Absorption rate,
μ	Dynamic viscosity, Pa·s
ξ	Exergic efficiency,
ρ	Density of refrigerant, kg/m^3
Σ	Stefan-Boltzmann constant, W/(m^2·K^4)
τ	Time, s
χ	Dryness of the refrigerant,
χ_{tt}	Lockhart–Martinelli parameter,
ω	Solar hourly angle,
ς	Relative pressure loss, Bar
d	Thickness, m
dy	Width of the selected microelement, m
f	Friction factor,
f''	Frequency of power input, Hz
f'	CO_2 emission factor, kg/kWh
h	Enthalpy of refrigerant, KJ/kg
m	Mass flow rate, kg/s
$\overline{m}$	Mass velocity, kg/(m^2·s)
$\dot{m}$	Mass flow rate, kg/(m^2·s)
N	Number,
n'	Rotational speed of compressor, r/s
o	Volumetric thermal expansion coefficient of air, 1/K
q_H"	Effective heat flux,
r	Reflectance of glass,
u	Thermodynamic property,
ν	Kinematic viscosity, m^2/s
Π	Number of poles in the motor,
Υ_m	Conversion rate from electricity to thermal energy,
ϕ	Latitude of local place,
ψ	Coefficient,
Ω	Equivalent intensity, kg/kWh
ϑ	Diffused radiation fraction,

Subscripts

E	Generated electricity
L	Energy loss
CHE	Condenser heat exchanger
EVA	Ethylene-vinyl acetate
LT	Lifetime
TPT	Tedlar-Polyester-Tellar
τ	Time
$\gamma\lambda$	Transmittance-absorption coefficient of glazing cover
A	Energy being absorbed
b	Aluminium plate
c	Critical
E	Electrical
g	Gas
i	Inside of Tube
l	Liquid
o	Outside of Tube
p	Pipe
s	Surrounding environment
T	Thermal
U	Useful energy
v	Volumetric
w	Water
z	Bond between the fin and tube
am	Ambient
air	Air
al	Absorption losses
bi	Selected microelement
cb	Convective boiling dominant
cl	Collector
co_2	Carbon dioxide
com	Compressor
$d.a$	Days

em	Electrical motor
$e.r$	Expected returns per year
eva	Evaporator
eev	Electronic expansion valve
$f.i$	Inlet of the panel
f, m	Mean temperature
$f.o$	Outlet of the panel
gas	Gas
gc	Glass cover
gf	Ground floor
gt	Gas transmission efficiency
hcg	Heat-conducting glue
$h.w.d$	Hot water demanded
$i.c$	Initial investment
ie	Indicated efficiency
if	Infill Tube
in	Inlet
$input$	Energy input
lk	Leakage
$m.c$	Maintenance cost per year
mc	Mini-channel
ml	Mortar levelling layer
nb	Nucleate boiling dominant
oa	Overall
oc	Open-circuit
out	Outlet
ppr	PPR pipe
pr	Phenolic resin
ps	Pea stone layer
pst	Stainless steel pipe
pv	PV cell
pvt	PV/T panel
ref	Refrigerant
rc	Reference condition

rl	Reflection losses
ro	Room
sat	Saturated condition
$save$	Energy save
sg	Silicone grease
sc	Supercooled
So	Energy sored by panel
su	Short-circuit
sun	Sun light
st	Superheated
th	Thermal
tk	Tank
$total$	Total
wd	Wind
wf	Working fluid
$wall$	Wall of the building
am_gc	Ambient air and glass cover
am_if	Ambient air and infill tube
am_p	Ambient air and pipe
b_am	Aluminium plate and ambient
b_gc	Aluminium plate and glass cover
b_pv	Aluminium plate and PV cell
com_ac	Actual input power
com_in	Inlet of compressor
com_out	Outlet of compressor
com_to	Theory input power
con_in	Inlet of condenser
con_out	Outlet of condenser
eva_out	Outlet of evaporator
eva_in	Inlet of evaporator
eev_in	Inlet of EEV
eev_out	Outlet of EEV
gf_ro	Ground floor and room

gas_b	Gas boiler
gas_out	Outlet of gas boiler
gas_in	Inlet of gas boiler
g_c	Condensing
g_e	Evaporating
gr_gc	Ground and glass cover
p_b	Pipe and aluminium plate
p_c	Copper pipe
p_in	Internal diameter of pipe
pc_in	Inside surface of copper tube
pc_out	Outside surface of copper tube
pv_gc	PV cell and glass cover
pv_p	PV cell and pipe
pv_if	PV cell and infill tube
p_w	Pipe and water
ppr_ro	PPR pipe and room
ppr_in	Inside surface of PPR tube
ppr_out	Outside surface of PPR tube
pst_in	Inside surface of stainless steel pipe
pst_out	Outside surface of stainless steel pipe
pvt_out	Outlet of PV/T panel
pvt_in	Inlet of PV/T panel
r_com	Refrigerant in the compressor
ref_eva	Refrigerant in evaporator
r_f	Tube and refrigerant
r_g	Superheated region
r_p	Refrigerant in pipe
s_gc	Surrounding environment and glass cover
sky_gc	Sky and glass cover
t_c	Temperature coefficient
w_c	Circulating water
wf_am	Working fluid and ambient

wf_p	Working fluid and pipe
wf_in	Working fluid at inlet of tank
wf_out	Working fluid at outlet of tank
wf_pst	Working fluid and stainless steel pipe
w_in	Water at the inlet of tank
w_out	Water at outlet of tank
w_ro	Water and room

CHAPTER 1: INTRODUCTION

1.1 Background

Today the whole world faces several challenges in the field of energy policy, as it seeks to ensure the security of the energy supply, address climate change and deal with fluctuating energy costs. The increasing consumption of fossil fuels is contributing to global warming, through greenhouse gas emission, and air pollution. To overcome these problems, many governments have drawn up several effective solutions to reduce the environmental impact of increasing energy consumption. Reducing energy consumption is the best way to save energy which can provide effective and low-cost solutions to overcome these challenges, i.e., (1) Cutting the CO_2 emissions caused by energy generation, (2) Avoiding negative economic impacts caused by steadily rising energy prices. Another important way of working to reduce the impact of increasing energy consumption is by improving the research and application of renewable energy, using sunlight, wind, rain, tides, waves, and geothermal heat.

As shown in **Fig. 1-1**, 44% of all energy consumed in the EU is used in buildings, being domestic, tertiary or industrial [1.1], with buildings accounting for 36% of Europe's CO_2 emissions [1.2]. Most buildings we occupy today were constructed at a time when energy efficiency was not a major concern, and as a result, a large amount of energy is used for heating, cooling and lighting. Space heating and cooling takes the largest share, using between 50 % and 70 % of the total residential energy usage (**Fig. 1-2**, [1.3]).

In China, according to the China Energy Consumption Research Report (2016) [1.4], the buildings account for around 19% of energy consumption (**Fig. 1-3**) and about 50% of China's CO_2 emissions [1.5]. Space heating and hot water supply also contribute a large proportion of energy consumption (about 68%) (**Fig. 1-4**, [1.6]).

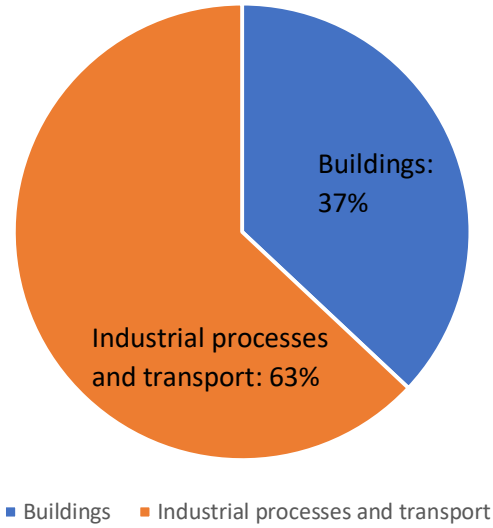

Fig. 1- 1: Share of total EU energy consumption [1.1]

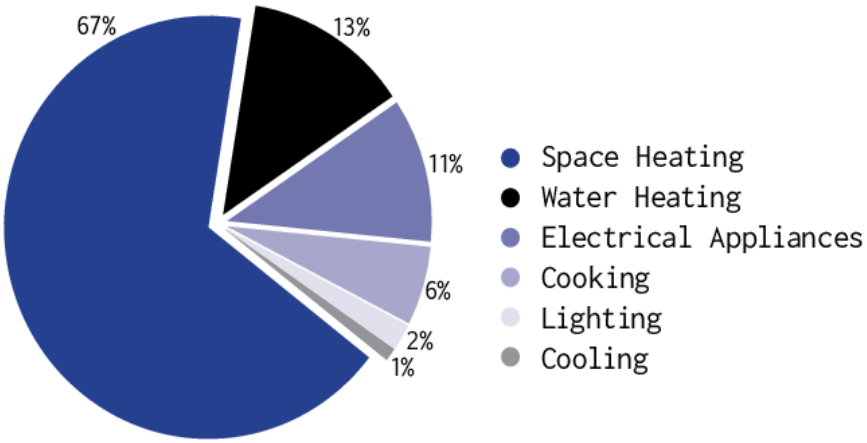

Fig. 1- 2: Residential end-use energy split EU [1.3]

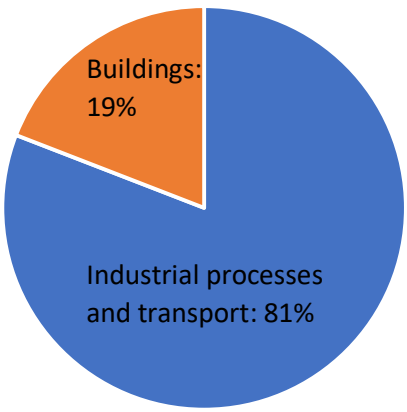

Fig. 1- 3: Share of total China energy consumption [1.4]

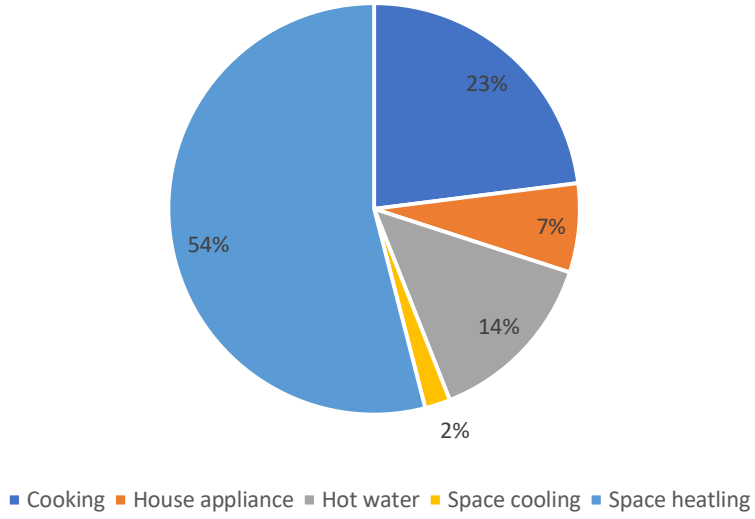

Fig. 1- 4: Residential end-use energy split China [1.6]

To reduce the energy consumption of buildings, two effective solutions can be carried out: (1) Developing low-energy buildings. The "2010 Energy Performance of Buildings Directive" and "2012 Energy Efficiency Directive" [1.7] are the EU's main legislation covering the reduction of energy consumption of buildings. On 30th November 2016, the Energy Performance of Buildings Directive was updated to help promote the use of smart technology in buildings, and to streamline the existing rules. (2) Development of renewable energy. In EU and China, the share of renewable energy in building sectors are 10% [1.8] and 2.6% [1.6], respectively, representing very small percentage. Hence the potential for the application of renewable energy technologies into buildings is unlimited. As solar is commonly the most convenient technology to integrate into a building, many different types of solar energy have been researched and developed.

Regarding solar energy, solar thermal and solar electrical power are two different technologies that are based on solar thermal collectors and photovoltaic (PV) panels, respectively. A PV panel involves the conversion of light into electricity, using semiconducting materials, with photovoltaic capacity expanding in recent years worldwide. A solar thermal collector is a device which collects solar energy and converts it into thermal energy. Currently, this conversion procedure has become the most common method to achieve hot water.

From 2007 to 2016, the installed capacity of PV panel in the EU grew from 4.94 GWp to 104.3 GWp [1.9], and in China, the figure increased from 0.1 GWp to 78.07 GWp [1.10]. Although the proportion of electricity generated by PV is currently very low, with the pressure of decreasing CO_2 production, and supporting of government policy, it has huge potential to replace more conventional energy. With the cost of a PV cell and PV system decreasing (about 50%), it is predicted that within the next twenty-five years (2016-2040, **Fig. 1-5**), the total installed capacity of solar PV across the globe could reach around 3,900 GWe. This takes the largest share of total installed capacity (29%) and would generate 15% of the world's electricity [1.11]. This application of PV systems would reduce CO_2 emissions by about 3 giga-tonnes (Gt) of CO_2 per year.

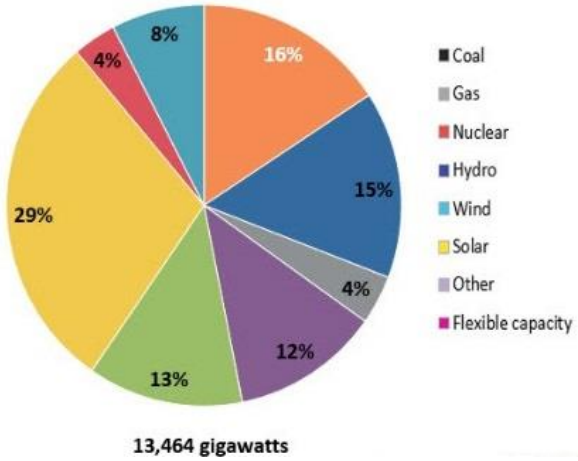

Fig. 1- 5: Expected world mix capacity in 2040 [1.10]

According to application purpose and output temperature, there are three types of thermal collectors, those for low-temperature use (hot water, space heating, drying and distilling), medium-temperature use and high-temperature use (concentrated solar power, solar cooker). In a variety of applications, the low-temperature type is currently the most studied and obvious application, because of that it can be applied to building easily. In 2015, solar thermal capacity in operation in Europe, was about 33.2 GW_{th} [1.12]. This figure could reach at least 200 GW_{th} by 2030, with solar thermal energy be used in most of European buildings. The typical share of solar thermal energy in meeting the heating and cooling demands of a single building will increase dramatically, to more than 50%, and up to 100% [1.13]. In 2016, the solar thermal capacity in China was 324.5 GW_{th} [1.14], and this

capacity could be increased to 840 GW_{th} by 2030, which takes an 80% share of the global capacity. The inclusion of a thermal collector could reduce air pollution output by 51.4 giga-tonnes (Gt) CO_2, 1.4 giga-tonnes (Gt) SO_2 and 14 giga-tonnes (Gt) dust particulates [1.15].

Both the PV panel and solar thermal collector have similar limitations, a large portion of energy is wasted, especially for the PV panel (nearly 80%). To avoid this energy waste, the concept of solar photovoltaic thermal (PV/T) panel was presented. A PV/T panel, as the combination of a solar thermal collector and a PV module, can give a higher overall solar efficiency and reduce space occupancy, compared to separately lay solar thermal collectors and PV modules [1.16]. However, the promotion of this system is limited by its high price and application environment. With PV panel price decreasing, and families distributed photovoltaic power station expanding, it proves a developing chance for PV/T to replace the PV panel, which not only generate electricity to sell, but also provide thermal energy for family. The market of PV/T systems would likely prove to be to fast-growing, with its outstanding performance, and also in its support for environmentally growing government policies.

1.2 Research objectives

The aim of this thesis is to overcome the barriers of existing PV/T panels and develop two novel, high efficiency, low cost, and low carbon solar heat pump systems for rural homes in cold areas. The solar direct expansion heat pump has the advantage of high efficiency and COP, and the system presented in this thesis owns 22 m^2 PV/T panel which is designed for space heating, but it is wasteful to supply hot water, because of its high operating cost. Therefore, the solar indirect expansion heat pump system is introduced and can provide energy for space heating and hot water in different seasons with little operating cost. This work is expected to increase the overall energy efficiency by around 10% to the existing PV/T panels. To achieve this aim, this thesis has set out four objectives, as follows:

(1) To develop a conceptual design for a micro-channel PV/T module based heat pump system, with the goal of increasing the overall energy efficiency by around 10%;

(2) To develop the components' performance and use a computer simulation model to optimise the configuration of the solar heat pump systems, and predict the system's performance to obtain technical goals;

(3) To design, construct and test a prototype solar heat pump system in the real weather conditions. The real weather data will be used in the simulation model, with the simulation result then compared to experimental results, checking the accuracy and rationality of the model.

(4) To predict the economic and environmental performance of the solar heat pumps with the simulation model and local annual weather data.

1.3 Research concept

Two different types of solar associated heat pump systems will be studied. The first system is the solar driven direct-expansion heat pump system, employing the novel PV/micro-channels-evaporator modules. As shown in **Fig. 1-6**, the PV/micro-channel direct-expansion heat pump is designed for space heating in winter and generating electricity annually. The system is comprised four major components: (1) the PV/micro-channels-evaporator modules; (2) a brushless motor driven compressor; (3) a heat exchanger was inserted into a water storage tank which works together to act as the condenser; (4) an electro-magnetic expansion valve; (5) four batteries and one inverter for electricity storage and consumption. On the hot water side, the piping layout is configured to deliver the hot water directly to embedded under-floor heating elements, which can emit the heat to the room space at the designed rate.

When the refrigerant passed through the PV/micro-channel-evaporator modules, it changes phase from the liquid to vapour state by absorbing the heat from the rear of the PV panel. The vaporized refrigerant is then directed into a compressor where it is pressurized and heated, becoming high-pressure super-critical vapour. This vapour is then delivered to the condenser where heat exchange between the vaporized refrigerant and heating loop water takes place. This action leads to a temperature rise in the heating loop water which is used for providing heating for the targeted room space in a building. This leads to the condensation of the refrigerant vapour, generating liquid

refrigerant at the outlet of the condenser. This liquid refrigerant is then forced through the electro-magnetic expansion valve, leading to a significant fall in both the pressure and temperature. After that, the low temperature liquid refrigerant is once again delivered into the PV/micro-channels-evaporator to absorb the heat from the PV panel.

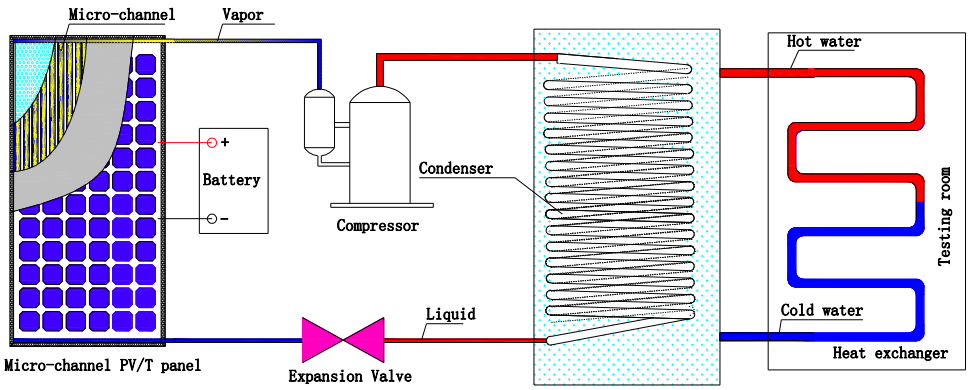

Fig. 1- 6: Solar direct-expansion heat pump system employing the novel PV/mini-channels-evaporator modules

The second system in this study, is solar associated indirect-expansion heat pump system, employing the novel mini-channel solar thermal and PV/T panels. As shown in **Fig. 1-7**, the system comprises four major components: (1) the mini-channel-based solar thermal panels; (2) the mini-channel-based PV/T panels; (3) a heat pump; (4) a heat storage tank; and (5) four batteries and one inverter for electricity storage and consumption. These components were appropriately linked together using the dedicated pipe lines, thus forming a hybrid experimental space heating system that can make use of the benefits of each component.

Overall, the proposed system can be divided into three functional parts: (I) energy collection, (II) energy upgrading and transportation, and (III) energy releasing. Within part I, the PV/T and thermal panels were arranged in parallel, to provide hot water to part II and also electricity to the batteries; within the part II which is for energy upgrading and transportation, there are multiple flow paths laid off that allow the working fluid to pass selectively. Within the part III, a heating loop comprising several heat emitters and a heat exchanger, is integrated into the room space of a house. This allows the heat carried by the loop fluid to be released to the room space. Furthermore, the heating loop

has a few channels that allow the fluid from the solar loop to be fed and the fluid within the loop to be released.

The major advantage of the system lies in the multiple functions of providing energy for space heating in winter and domestic hot water in other seasons, as well as generating electricity annually to balance the electricity demand of the system.

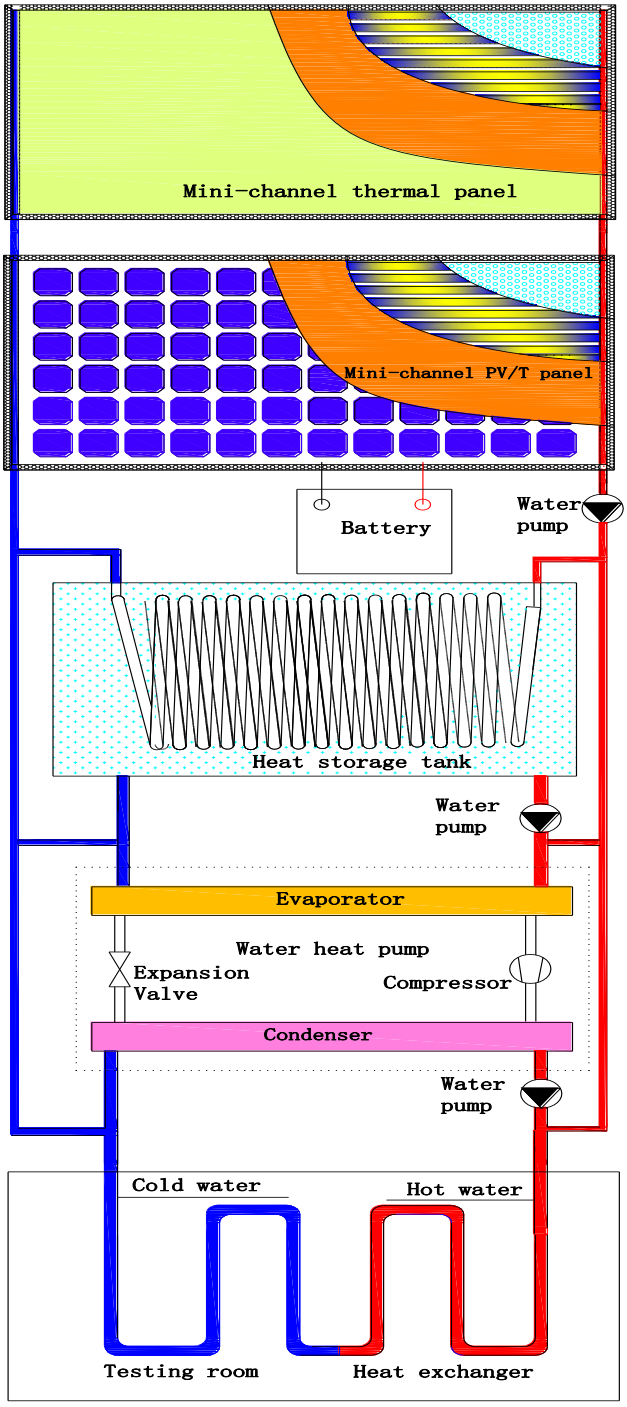

Fig. 1- 7: Solar indirect-expansion heat pump system employing the novel mini-channel solar thermal & PV/T panels

1.4 Research novelty and added value of the thesis

Considering the current PV/T technology and potential opportunity future development, the strength and innovation of PV/T technology in this thesis is as follows:

(1) **Micro-channel and mini-channel tube are selected to be the heat exchanger tube, which can enhance solar thermal and electrical efficiencies.** For the phase-changing medium, the increased vapor flow velocity in micro-channels (hydraulic diameter < 2 mm [1.17]) would generate a higher shear stress exerted upon the film interface. This would greatly decrease the thickness of the liquid film on the channel wall, resulting in very high evaporation rate of the liquid on the channel wall or condensation rate of the vapor within the core space of the channel [1.18, 1.19 and 1.20]. For the single-phase medium, the mini-channel tubes (2 mm < hydraulic diameter < 8 mm [1.21]) have a flat exterior surface that can be exactly bound to the PV cells, while their interior cross-sectional areas are smaller than the existing flat-plate panels, thus creating a higher flow velocity and therefore higher heat transfer rate.

(2) **Larger contact area and higher heat transfer rate.** For existing PV/T panels, the heat exchanger copper tube is welded on the base panel, and the connection area is a straight line. Contrastingly, the micro-channel connection to the base panel has a much larger contact area, increasing the heat transfer rate between the medium and base panel;

(3) **Low manufacture cost.** The material of the micro-channel tubing and header is aluminum, which is much cheaper than copper tubing, improving the economic performance.

These designs were intended to overcome some of the drawbacks and provide experimental data for the development of PV/T technology.

The research into these two solar heat pump systems provides a reasonable way to replace the traditional heating system in rural homes. Therefore, the experimental and simulation results of the two systems provide useful data for developing and improving the solar energy systems.

1.5 Research Methodology

The aim of this research is to develop two new solar heat pump systems for space heating, hot water supply and electricity generation. To achieve the objectives, mentioned previously (**1.2**), these methods are, briefly, described as follows:

Approach to objective 1- Conceptual development of the two new solar heat pump systems.

This approach is designed to develop two new solar heat pump systems, whose energy efficiency is expected to be 10% higher when compared to similar existing systems. The steps toward to this include (1) design the scale of the systems based on the heat load of building by completing drawings of all the components and overall systems; (2) design the new micro-channel and mini-channel heat exchanger; (3) determining the connection method between the components and selecting equipment for testing and collecting the necessary data.

Approach to objective 2 - Developing the components' parameters and computer simulation model to predict the performance of the systems.

This approach will achieve the technical objective with the method of numerical simulation. This steps includes (1) completing the simulation models of all the selected components and combining them together to form an integral system; (2) running the simulation model to analyse the electrical, thermal and overall efficiency of the PV/T panels, energy output and COP of the heat pump, which will show the performance of the systems in different seasons and potential efficiency improvement of the systems relative to the existing systems. This analyses of performance of the systems is theoretical and provides the fundamental data for comparison with the experimental result in the following **Approach 3**.

Approach to objective 3 - Constructing and testing the systems and verifying the computer model with the testing result.

This approach is designed to check the rationality and accuracy of the computer model with the test result. These steps include (1) constructing two solar heat pump systems with the design schemes; (2) testing the performance

of the two systems in real weather conditions, i.e., the electrical, thermal and overall efficiencies of the PV/T panels, energy output and COP of the heat pump, and (3) verifying the computer simulation model developed in **Approach 2**. With the test result, the performance improvement of the systems can be determined, when compared to similar existing systems. This approach will help to improve the rationality and accuracy of the computer simulation model and provide a much better result on the prediction of the annual energy and economic performance.

Approach to objective 4 - Energy, economic and environmental performance of the solar heat pump systems.

This approach is designed to calculate the cost target, annual energy output and environmental performance of the two systems. These predictions will include initial cost, operating cost and saving cost compared to traditional system installed in a local area, as well as the annual energy performance, lifetime data, payback time and CO_2 emission performance. This approach will show the economic and environmental advantages of the two new solar heat pump systems, which provides fundamental data to replace traditional systems.

1.6 Thesis structure

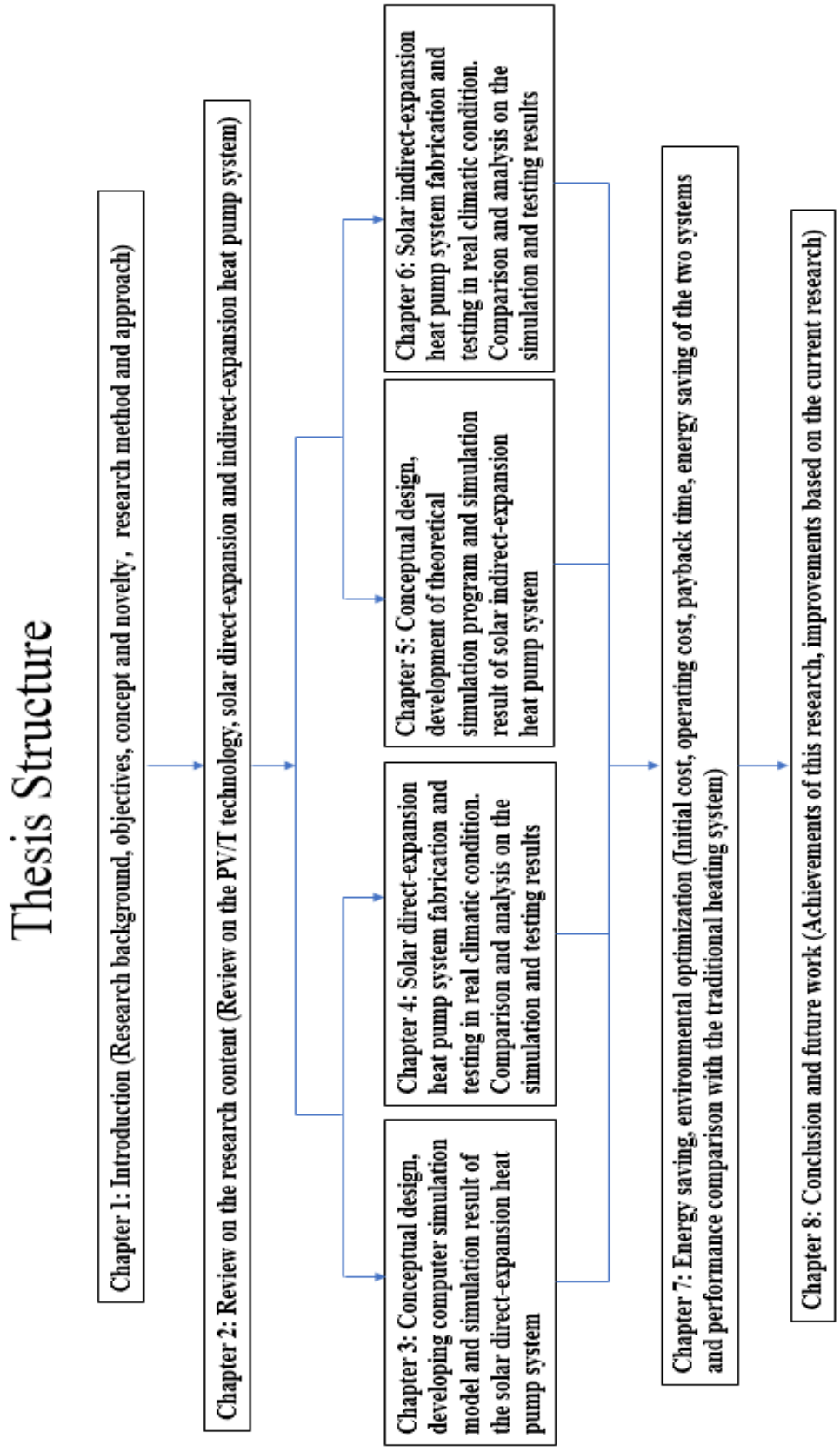

Fig. 1- 8: Thesis structure

Fig. 1-8 shows the structure of the thesis, and the detail of every chapter is described as follows:

Chapter 1 - Introduction: describes the research background, objectives, concept, novelty, research method and approach.

Chapter 2 - Review on the research content: presents the development process of the PV/T panels, the investigation of the solar direct-expansion and indirect-expansion heat pump system, including the different types, strengths and weaknesses and application. The limitation of these systems is summarised, and the potential development tendencies are analysed.

Chapter 3 - Conceptual design, developing computer simulation model and simulation result of the solar direct-expansion heat pump system: introduces research based on these systems, the working principle of the proposed system and creates a schematic design for key components. A group of computer simulation models are developed based on the selected components, including the micro-channel PV/T panel (evaporator), compressor, water storage tank (condenser) and electrical expansion valve. Based on these models and local weather data, the performance of the system is predicted and analysed. These preparations provide a fundamental condition for the comparison between the experimental and simulation results.

Chapter 4 - Solar direct-expansion heat pump system fabrication and testing in real climatic condition. Comparison and analysis on the simulation and testing results. The prototype system is constructed in outdoor conditions, a short time testing is carried out in real climatic conditions. These test results are used to verify simulation results and provide foundational data for seasonal simulation.

Chapter 5 - Conceptual design, development of theoretical simulation program and simulation result of solar indirect-expansion heat pump system: describes the structure, operating process and control strategy of the system. In addition, the numerical simulation models of the mini-channel PV/T and thermal panel, water storage tank, water source heat pump and gas boiler are developed. Typical local weather data is selected as input data and used to run simulation models for predicating the performance of the system.

These results provide foundational data for prototype construction, experiment testing and result analysis.

Chapter 6 - Solar indirect-expansion heat pump system fabrication and testing in real climatic condition. Comparison and analysis on the simulation and testing results. The prototype system is constructed on the roof of one building and tested at a minimum of one month. The experimental and simulation results are highly similar, indicating that the simulation model is reliable and can be used to predict the performance of the system long term.

Chapter 7 - Energy saving, environmental optimization: based on the test results, a simple simulation model is created to forecast the performance, the running cost, energy saving, contribution on the carbon emission of the two systems in Taiyuan and London. Compared to traditional heating system, the strength and weakness of the studied systems is analysed, and the corresponding improvement is presented.

Chapter 8 - Conclusion and future work: describes the main results and conclusions from the simulation and test results of the research. Based on the results, some improvements are presented and the reasonability of them to be researched in the future.

All above chapters are combined to achieve the stated research objectives. The novel PV/T panels, which are applied as the evaporator in the solar direct-expansion heat pump system or energy source of the indirect-expansion heat pump system, show a high electrical and thermal efficiencies. These systems could provide enough thermal energy for space heating during the winter daytime and generate electricity annually for sale, to balance the operating cost. The application of these systems could significantly reduce fossil fuel consumption and carbon emission.

CHAPTER 2: LITERATURE REVIEW

2.1 Chapter introduction

This chapter will provide a development progress, research review and practical application of the PV/T technology, the main content is given as follows:

(1) Describe the concept of PV/T technology and performance evaluation method.
(2) Give the economic and environmental evaluation of the PV/T panel.
(3) Present comprehensive review on the development, research and practical application of PV/T technologies.
(4) According to the application type, analyse the performance of PV/T and PV/T heat pump systems.
(5) Identify the major features, current R&D status, research highlights and application of various PV/T technologies.
(6) Discuss the opportunities for further development of PV/T technologies based on the barriers mentioned in previous chapter.

This part of work provided foundational information of the investigation and presented the study and developed status, practical application of existing PV/T technologies. Based on this review, some new methods and technologies are presented to overcome the drawbacks of existing ones.

2.2 Basic concept and theory development, performance evaluation standard of PV/T technology

2.2.1 Basic concept and theory analysis of the PV/T panel

(a) Basic concept and structure of PV/T panel

The current use of solar energy is mainly concentrated in the solar thermal, photoelectricity, photochemistry and photo-biological conversion. For a photovoltaic panel, only a part of the light can be absorbed and converted into electrical energy by PV cell. At present, the PV cell photoelectric conversion efficiency is very low, generally only 5% to 20%, which is measured under the standard test condition [2.1] (1,000 W/m^2 solar irradiance, 25 ^{o}C module

temperature and air mass 1.5). The low electrical efficiency is caused by two reasons: (1) Suffering from the material of the PV cell. The material of the PV cell is always simplex, such as polysilicon, monocrystalline silicon and amorphous silicon. These materials only can absorb a specific light wave band and the rest of light would be wasted. (2) Impact of the high temperature. Most of the light is converted into thermal energy. One part of the thermal energy is released to the air, and the other energy is absorbed by the PV panel, which raise the temperature of PV cell and decrease the electrical efficiency of it, as shown in **Fig. 2-1**. The efficiency of the PV with different materials decreasing when the temperature increasing. From 25 ^{o}C to 200 ^{o}C, silicon's efficiency drops to 5%, whereas the other materials (Gallium selenide, Gallium phosphide, Cadmium sulphide and Gallium arsenide) are near 12% [2.2]. Silicon is a good material for ambient temperature terrestrial uses; it fails in high-temperature applications.

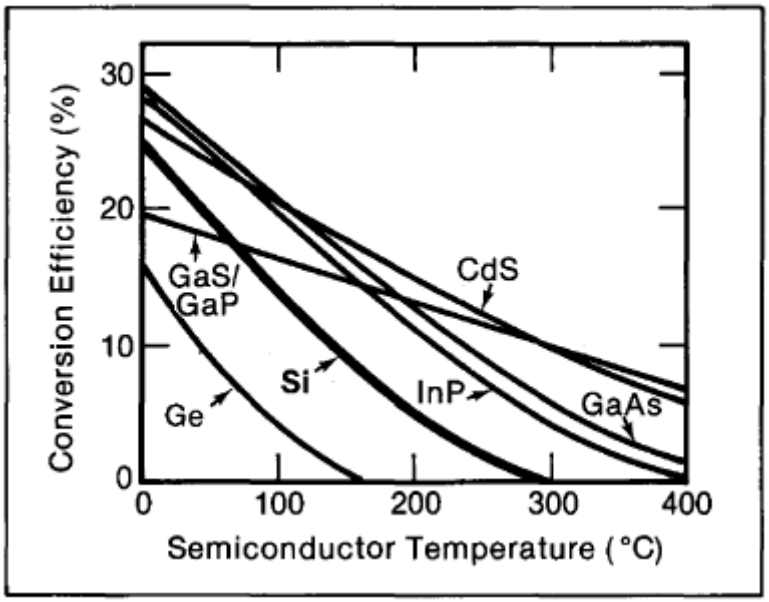

Fig. 2- 1: Solar cells efficiency versus temperature for various materials [2.2]

To keep the PV panel working at a low temperature and outputting at high efficiency, it is necessary to carry out an appropriate solution to remove the surplus energy and collect it for other uses. PV/T technology has been developed to achieve this aim. The PV/T panel combines PV panel and solar thermal collector into one integrated component that removes generated heat from the solar PV thereby improving electrical efficiency and providing solar heat for users. Compared to PV panel and thermal collector which has a single

foundation, the PV/T panel can make maximal use of the solar energy, providing the electricity and thermal energy at the same time.

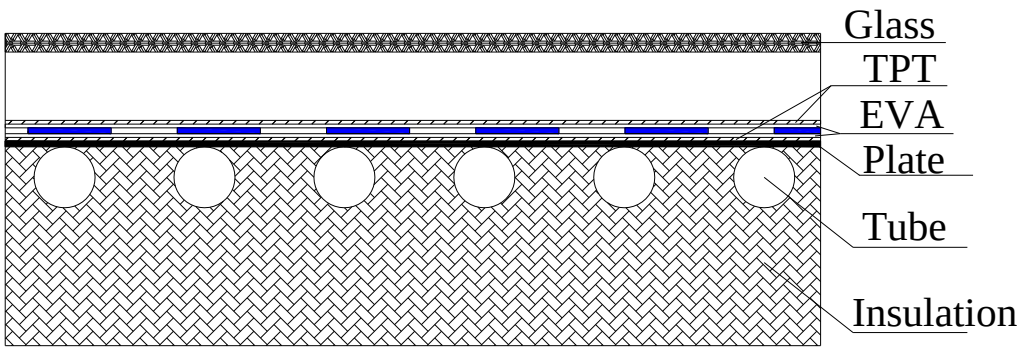

Fig. 2- 2: PV/T panel with air gap [2.3]

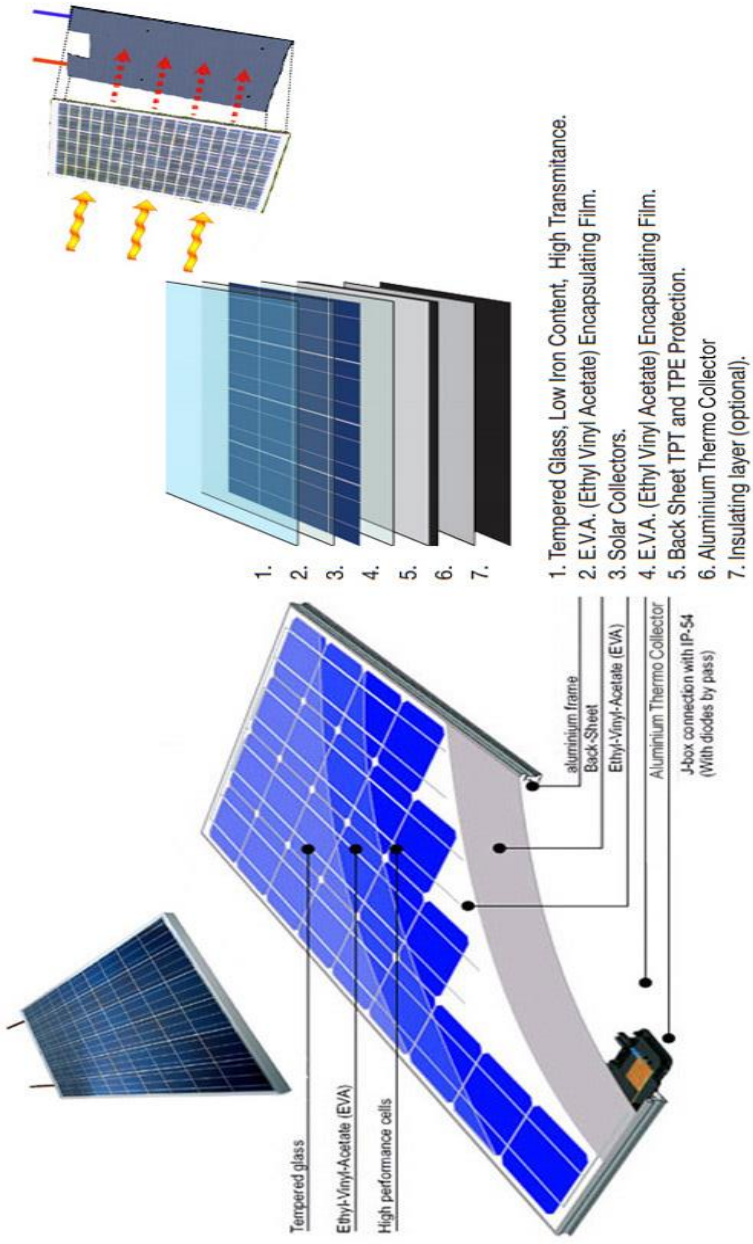

Fig. 2- 3: PV/T panel without air gap [2.3]

A typical PV/T panel comprises several parts: (1) a glazed cover (preventing the dust and protecting the PV cells), (2) an air gap, which is for preventing heat loss (**Fig. 2-2,** [2.3]) or not (**Fig. 2-3,** [2.3]), (3) several PV cells (converting solar energy into electricity), two Ethylene-vinyl acetate (EVA) layers (as the adhesive to connect the cover) and a Tedlar-polyester-Tedlar (TPT, layer (as the electrical isolation), (4) an aluminium absorb plate (absorbing the sunlight which cannot be converted into electricity), (5) several tubes (cooling down the aluminium plate when working fluid passes across the tube), (6) the insulation layer (preventing the heat loss), and (7) a holding-up framework (to keep these components together).

(b) Basic theory of PV/T panel

To improve the comprehensive utilization efficiency of solar energy and reduce the solar energy utilization cost, Kern and Russell first proposed the combination of a PV panel and thermal collector in 1978, that is, laying the flow path on the back of the PV module, dissipating heat by fluid and collecting heat for other use. According to the simulation [2.4] and experimental [2.5] result, it is indicated that the overall efficiency of PV/T panel is much higher than these single foundation panels (PV panel and thermal collector) at the same operating condition. The PV/T technology opened a new way for the development of solar energy and played a significant role in promoting.

The PV/T panel gives consideration to PV panel and thermal collector, which can provide electricity and thermal energy at the same time. As shown in **Fig. 2-4**, the solar energy absorbed by the PV/T panel (Qa) can be divided into four parts: (1) the collected useful energy (Qu), the heat loss to the surrounding air (Q_L), the generated electricity energy (Q_E), and the energy stored by the panel (Qso). The equation which describes the relationship of them can be given as [2.6]:

$$Q_a = Q_u + Q_E + Q_L + Q_{so} \quad [2\text{-}1]$$

$$Q_a = A_{cl} G(\gamma\lambda) \quad [2\text{-}2]$$

$$Q_E = A_{cl} G \eta_e \quad [2\text{-}3]$$

$$Q_u = A_{cl} G \eta_t \quad [2\text{-}4]$$

$$Q_L = A_{cl} G (T_{pv} - T_{am}) \quad [2\text{-}5]$$

$$Q_{so} = C_p M_{cl} \frac{dT}{d\tau} \quad [2\text{-}6]$$

Where, G is the solar irradiation (W/m^2); A_{cl} is the collecting area of the panel (m^2); $(\gamma\lambda)$ is the transmittance-absorption coefficient of glazing cover; η_e and η_t are the electrical and thermal efficiency respectively; T_{pv} and T_{am} are the PV cell temperature and ambient (K); C_p is the thermal capacity of the PV/T panel (W); M_{cl} is the quality of absorber (kg); τ is the time.

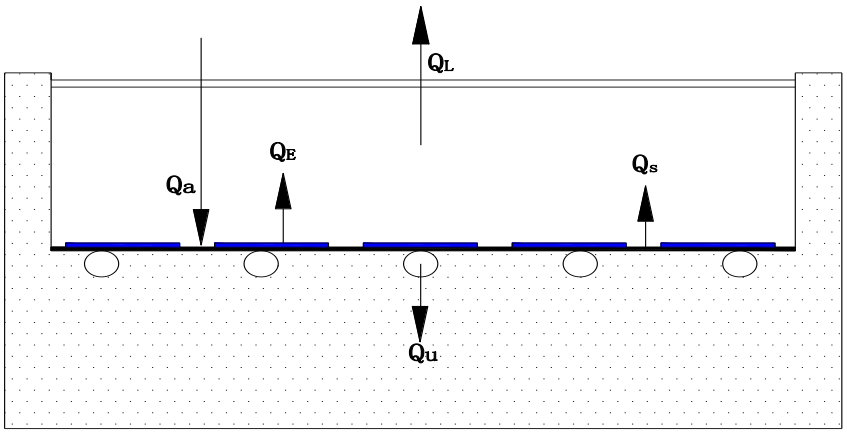

Fig. 2- 4: Energy distribution diagram of PV/T panel

(1) Electrical efficiency

The electrical efficiency is related to the operating temperature of the PV cell, and the relationship between them can be described as [2.7]:

$$\eta_e = \eta_{rc}[1 - \beta_{PV}(T_{pv} - 298.15)] \quad [2\text{-}7]$$

Where, η_{rc} is the initial electrical efficiency at reference temperature (298.15K); β_{PV} is the cell efficiency temperature coefficient (1/K); T_{pv} is the PV cell temperature (K).

The electrical efficiency can be calculated as the ratio of output power to the incident solar irradiation, when it is working in practical condition [2.8].

$$\eta_e = \frac{PO_{pv}}{GA_{cl}} \quad [2\text{-}8]$$

Where, PO_{PV} is the output power of the PV/T panel (W).

(2) Thermal efficiency

The thermal efficiency of the flat-plate PV/T panel is the ratio of useful thermal energy to the incident solar irradiation, and it can be given [2.6]:

$$\eta_{th} = \frac{Q_u}{GA_{cl}} \quad [2\text{-}9]$$

The useful thermal energy can be calculated as [2.6]:

$$\mathrm{Q_u} = \frac{MC_p(T_{f.o} - T_{f.i})}{GA_{cl}} \quad [2\text{-}10]$$

Where, M is the mass flowrate of cooling fluid (kg/s); C_p is the thermal capacity of the cooling liquid (kJ/(kg·K)); $\mathrm{T_{f,i}}$ and $T_{f.o}$ are the temperature of cooling liquid at the inlet and outlet of the panel (K).

At the steady working station, the thermal efficiency also can be given as [2.6]:

$$\mathrm{Q_u} = A_{cl}[G(\gamma\alpha) - \mathrm{U_L}(T_{pv} - T_{am})] - Q_E \quad [2\text{-}11]$$

Where, $\mathrm{Q_u}$ is the useful thermal energy (W); $\mathrm{U_L}$ is the heat loss coefficient ($\mathrm{W/m^2/K}$).

Normally, the temperature of PV/T panel depends on its structure type and the inlet temperature of the cooling liquid. It is a function which includes several parameters. Hottel and Whillier presented and confirmed the theoretical model of thermal collector [2.8, 2.9], and the equation of useful thermal energy can be given as:

$$\mathrm{Q_u} = F'A_{cl}\left[G(\gamma\alpha) - \mathrm{U_L}(\mathrm{T_{f,m}} - \mathrm{T_{am}})\right] - Q_E \quad [2\text{-}12]$$

Or

$$\mathrm{Q_u} = F_R A_c\left[G(\gamma\alpha) - \mathrm{U_L}(\mathrm{T_{f,i}} - \mathrm{T_{am}})\right] - Q_E \quad [2\text{-}13]$$

Where, F' is the efficiency factor; F_R is the heat removal factor; $\mathrm{T_{f,m}}$ is the mean temperature of the cooling liquid.

The F' depends on the structure type of the panel, which has the different expression as follows due to the different structure type (**Fig. 2-5**, **Fig. 2-6**, and **Fig. 2-7** [2.6]).

(I)

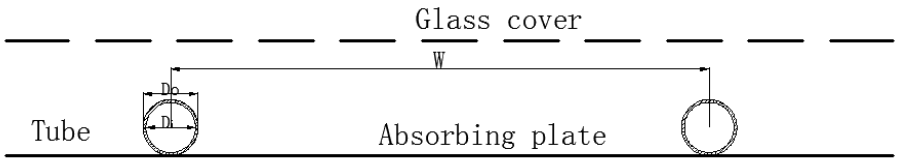

Fig. 2- 5: Tube sheet absorbing plate (I) [2.6]

$$\left\{\begin{array}{c} Eq_1 = \frac{WU_L}{K_z} + \frac{w}{(W-D_o)F''} \\ Eq_2 = \frac{D_o}{W} + \frac{1}{Eq_1} \\ F' = \frac{1}{\frac{WU_L}{\pi D_i \alpha_{f,i}} + \frac{1}{Eq_2}} \end{array}\right\} \quad [2\text{-}14]$$

(II)

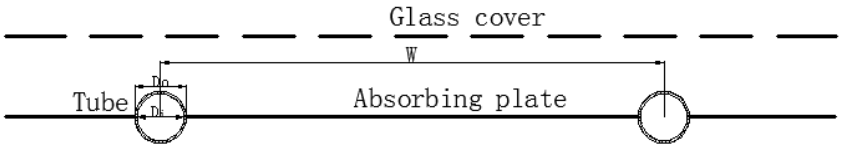

Fig. 2- 6: Tube sheet absorbing plate (II) [2.6]

$$F' = \frac{1}{\frac{WU_L}{\pi D_i \alpha_{f,i}} + \frac{W}{D_o + (W-D_o)F''}} \quad [2\text{-}15]$$

(III)

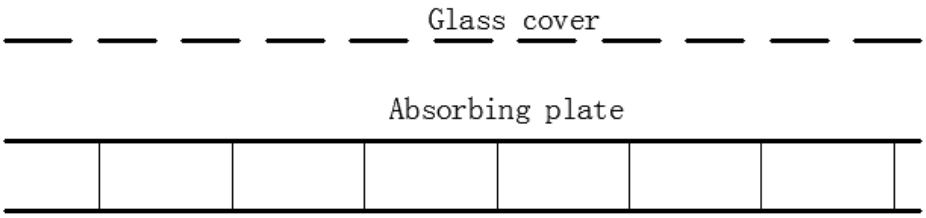

Fig. 2- 7: Flat aluminium box absorbing plate [2.6]

$$F' = \frac{1}{1 + \frac{U_L}{\alpha_{f,i}}} \quad [2\text{-}16]$$

$$F_R = \frac{GC_p}{U_L}\left[1 - \exp\left(-\frac{F'U_L}{GC_p}\right)\right] \quad [2\text{-}17]$$

Where, W is the distance between tubes (m); D_o and D_i are the outside and inside diameter of flow tubes (m); K_z is the thermal conductance of the bond

between the fin and tube (W/m/K); $\alpha_{f,i}$ is the heat transfer coefficient of working medium (W/m^2/K); F'' is the fin efficiency, which is given by [2.6]:

$$F'' = \frac{tgh[\sqrt{\left(\frac{U_L}{K\delta}\right)}\left(\frac{W-D_o}{2}\right)]}{\sqrt{\left(\frac{U_L}{K\delta}\right)}\left(\frac{W-D_o}{2}\right)} \quad [2\text{-}18]$$

Where, K is the thermal conductivity of the fin (W/m/K) and δ is the fin thickness (m).

(3) Overall energy efficiency

The overall efficiency is the most important evaluation standard. It can be defined to be ratio of electricity gain and heat gain to the incident solar irradiation striking the collector's absorbing surface. It can be given as [2.8]:

$$\eta_{oa} = \eta_e + \eta_{th} \quad [2\text{-}19]$$

Where, η_{oa} is the overall efficiency of the PV/T panel; η_e and η_t are the electrical and thermal efficiencies, respectively.

(4) Coefficient of Performance (COP) of the heat pump

The efficiency of refrigeration systems and heat pumps is denoted by its coefficient of performance (COP). The COP is determined by the ratio between energy usage of the compressor and useful heat extracted from the condenser. The equation of the COP of the heat pump can be given as [2.9]:

$$COP = \frac{Q_{use\_heat}}{Q_{com}} \quad [2\text{-}20]$$

2.2.2 Developed process of the PV/T technology

Over the last 40 years, many different types of PV/T panel have been investigated. They can be classified in different structures, foundation and cooling medium. For the different structure, it can be described as [2.10]:

- 1a - Unglazed without thermal insulation.
- 1b - Unglazed without thermal insulation, heat exchanger as a separate unit under PV module.
- Unglazed with thermal insulation.
- Glazed PV cells are placed on the absorber.

- Glazed PV cells are placed right under the transparent insulation/glass panel.
- PV/T solar collectors with concentrators.

(1) a - Unglazed without thermal insulation

For this type of PV/T panel, a collector (usually a roll bond plate for liquid collectors) is adhered to the backing of a standard PV module with micro-bore connectors either passing through the side of the aluminium frame or providing flexible connection pipes on the back of the plate (**Fig. 2-8, [2.10]**).

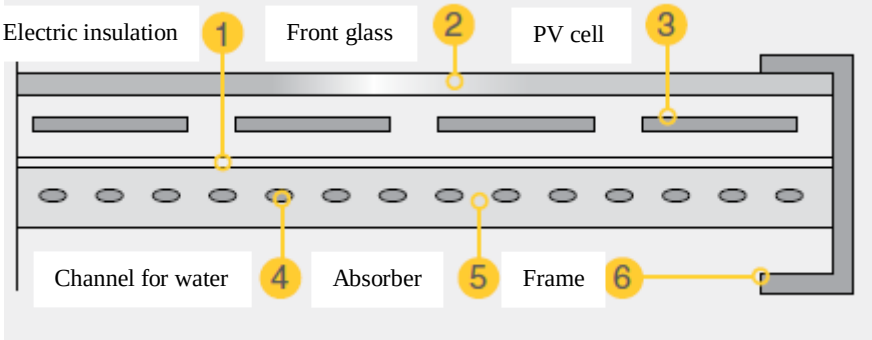

Fig. 2- 8: Unglazed without thermal insulation [2.10]

When the collector temperature is lower than the ambient temperature, the collector absorbs heat both from the PV module and surrounding air. When the collector temperature is higher than the ambient temperature, the collector absorbs heat from PV module and at the same time, releases heat to the air. Hence it is suitable to be installed in area with high ambient temperature.

The advantage of this approach is the relatively simple construction, providing an efficient method of cooling the solar PV cells. The technology is modular and therefore scalable (to a point), allowing systems to be sized effectively for different hot water/ space heating/ hybrid energy system requirements. By using standard solar PV modules, it is possible to use standard mounting systems and integrate the systems within a larger solar PV array, providing a uniform aesthetic. The low profile of the PV/T modules also makes it possible to integrate into a roof or façade.

(1) b - Unglazed, without thermal insulation, heat exchanger as a separate unit under PV module

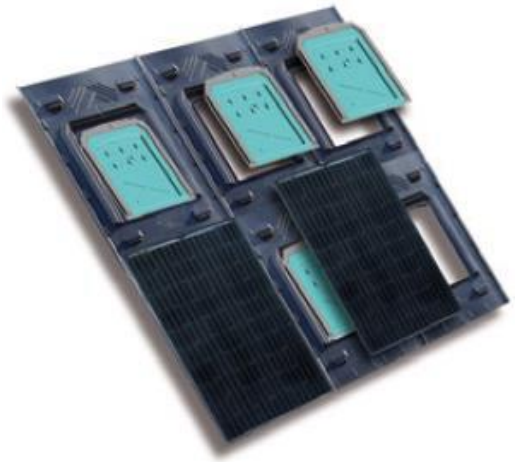

Fig. 2- 9: Unglazed, without thermal insulation, heat exchanger as a separate unit under PV module [2.10]

For this type of PV/T panel, the thermal collector (heat exchanger) is designed as a base, and any PV module can be combined with it and hybridised into a PV/T panel (**Fig. 2-9, [2.10]**).

The advantages of this are similar to those of type (1) a, providing a scalable system that is easily integrated into a roof. Type (1) b products generally allow more flexibility with regarding to the choice of solar PV module that is used, meaning that they can be retrofitted to existing PV systems. The main disadvantage of a type (1) b system is that it does not necessarily maximise the heat transfer between the two elements, resulting in a lower heat transfer coefficient. In addition, some systems are limited in their application only providing one method of heating system integration, i.e., warm air.

(2) Unglazed with thermal insulation

For this type of PV/T panel (**Fig. 2-10, [2.10]**), it has a similar structure as the (1) a, adding an insulation at the back of thermal collector which can prevent the heat loss from the back in low temperature ambient.

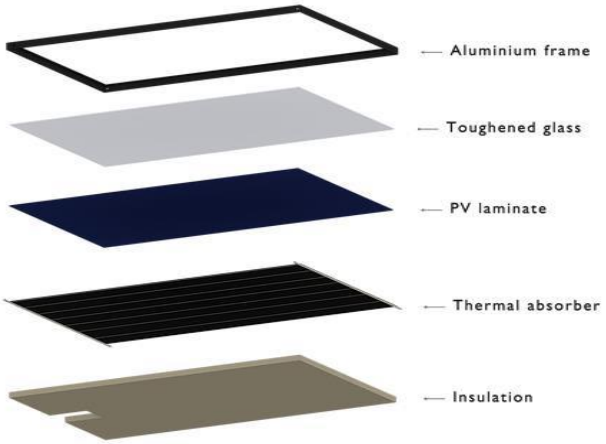

Fig. 2- 10: Unglazed with thermal insulation [2.10]

(3) Glazed PV cells are placed on the absorber

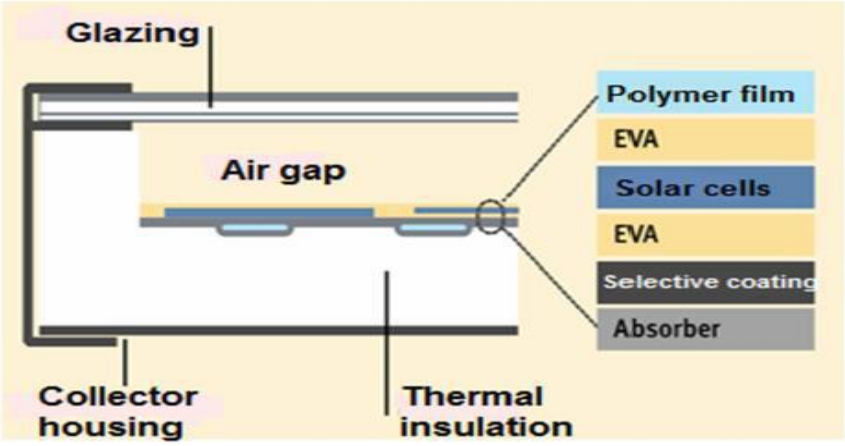

Fig. 2- 11: Glazed PV cells placed on the absorber [2.10]

For this type of PV/T panel (**Fig. 2-11, [2.10]**), the PV cells are laminated on the absorber, and an air gap is designed to prevent the heat loss from the front surface. The advantages of this PV/T panel are higher working temperature and lower heat loss, leading a higher overall efficiency. The disadvantage of it is that the lamination of combining PV cell and aluminium plate together may cause the disconnection of PV panel, which is caused by the different degree of expansion between the PV cell and aluminium plate, resulting in the wire adrift.

(4) Glazed PV cells are placed right under the transparent insulation/glass pane

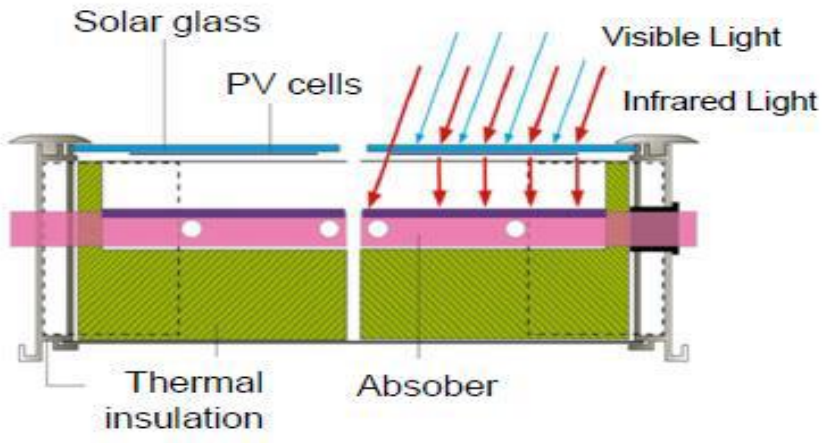

Fig. 2- 12: Glazed PV cells placed right under the transparent insulation/glass pane [2.10]

For this type of PV/T panel, a standard PV panel replaces the glass cover of conventional flat-plate panel (**Fig. 2-12, [2.10]**). Most of the sunlight are absorbed by PV cell, and small part of sunlight can go through the glass and be absorbed by the absorber. On the one hand, the PV cell can be cooled down via the glass surface by the air surrounding, and on the other hand, the cooling medium can't absorb the heat directly from the PV cell, because of the air gap between the PV cell and absorber plate. Hence the PV cell will not experience high temperature nor low temperature, meaning that it doesn't have an advantage in electrical efficiency, but the air gap will impact the thermal efficiency.

(5) PV/T solar collectors with concentrators

Fig. 2- 13: PV/T solar collectors with concentrators [2.10]

For this type of PV/T panel, a blank of Fresnel reflectors or trough concentrators are used to focus solar irradiance on a strip of PV cells mounted on a collector (**Fig. 2-13, [2.10]**). The Solarus Power Collector features two strips of solar PV cells that absorb the solar energy reflected by two parabolic mirrored troughs running underneath the PV cell strips. The heat generated within the semi-circular tubes is extracted as hot air. The main advantage of a CPV/T collector is that high temperatures that can be reached (typically 65-90 °C), making it suitable for hot water applications. There are also fewer material costs associated with the Fresnel reflector approach. The disadvantage to the system is traditionally its lack of scalability and a decrease in solar PV efficiency as the result of the high temperatures. Systems with tracking are also inherently expensive and require more maintenance.

Typically, the PV/T panel is installed for hot water or space heating. Different types of PV/T panels can be integrated into different systems. The method in which heat is extracted i.e., by air or liquid, will often dictate the best type of heating systems to integrate with. To achieve a high overall efficiency, the PV/T is expected to work at a low temperature (40-50 °C), hence the temperature of hot water it provides is between 35-45 °C. It is a good choice for pre-heating for hot water or as a heat source of a heat pump. Domestic PV/T systems are normally installed for the following purposes [2.10]:

- To provide a pre-heat for a hot water cylinder or thermal store to supply hot water.
- To provide a pre-heat feed into a boiler for hot water and/or space heating.
- To provide a pre-heat or direct feed for an air source heat pump.
- To provide heat to charge a ground loop, borehole, earth bank or other inter-seasonal storage for a GSHP.
- To provide a pre-heat or direct feed for HVAC warm air heating systems.

2.2.3 Performance Evaluation Standards and Indicators

(a) Performance evaluation standards

Currently, there are several evaluation standards for PV panel and thermal panel testing. The part of the details is listed in **Table 2-1.** However, there is no single product standard available which includes both the PV and thermal

panel. There are also no overarching standards or generic guidance that describe how the PV/T systems should be designed and installed. All such guidance is product specific and published by the PV/T manufacturers. For effectively describing the performance of the PV/T system, several evaluating methods are presented by researchers, including overall energetic efficiency, overall exergetic efficiency, primary energy saving efficiency. The economic performance of the PV/T systems is measured by the life-cycle cost and cost payback time (CPT). The environmental benefit of a PV/T system is justified using life-cycle carbon saving or energy payback time (EPT) and greenhouse gas payback time (GPBT).

Table 2- 1: Standards for PV panel and thermal collector [2.10]

PV panel	
Item	**Title**
IEC 60068-2-78	Environmental testing - Part 2-78: Tests - Test Cab: Damp heat, steady state
IEC/EN 61215	Crystalline silicon terrestrial photovoltaic modules - Design Qualifications and type approval
IEC/EN 61646	Thin-film terrestrial photovoltaic (PV) modules Design qualification and type approval
IEC/EN 61730	Photovoltaic (PV) module safety qualification - Part 1: Requirements for construction Part 2: Requirements for testing
IEC 62108	Concentrator photovoltaic (CPV) modules and assemblies - Design qualification and type approval
UL 1703	Flat-Plate Photovoltaic Modules and Panels
ASTM E1171	Test Methods for Photovoltaic Modules in Cyclic Temperature and Humidity Environments
Thermal collector	
Item	**Title**
EN ISO9806	Solar Energy - Solar thermal collectors - Test Methods
BS EN12975 - 1:2006+A1	Thermal solar systems and components. Solar collectors. General requirements
BS EN 12976-1:2006	Thermal solar systems and components. Factory made systems. General requirements
BS EN 12976-2	Solar thermal systems and components - Solar collectors and Factory-made systems

(b) Performance evaluation indicators

(1) Overall efficiency of PV/T system

A PV/T panel can provide electrical and thermal energy at the same time. The overall efficiency is an intuitive way to evaluate the performance of PV/T system, which can be defined to be the ratio of the generated electricity and collected thermal energy to the incident solar radiation striking a PV/T absorber. It describes the percentage of solar energy being used, ignoring the difference of the electricity and thermal energy in terms of energy grade.

(2) Primary energy saving efficiency

The primary energy saving efficiency is another method to describe the performance of the PV/T panel [2.11, 2.12]. It is the ratio of all the energy gained by the PV/T system (electricity and thermal) which has been converted to be thermal energy to the total solar input energy. It can be estimated as [2.11]:

$$EE_{oa} = \eta_{th} + \frac{\eta_e}{\Upsilon_m} \quad [2\text{-}21]$$

Where, EE_{oa} is the primary energy saving efficiency; Υ_m is the electrical power generation efficiency for a conventional power plant at 0.38.

(3) Economic performance and the environmental benefit of PV/T system

The economic performance and environmental benefit of PV/T system can be evaluated by the expressions for energy matrices, carbon credits and cost parameters [2.13]. Energy matrices give an idea about the annual, lifetime, and economical performances of the system. The energy matrices have been determined based on the annual energy/exergy gain from the system. It includes the energy payback time (EPBT), energy production factor (EPF), Life cycle conversion efficiency (LCE) [2.11].

To analyse the energy sustainability of the PV/T system, EPBT is one of the main parameters, which can be expressed as [2.11]:

$$EPBT = \frac{Q_{input}}{Q_{save}} \ (years) \quad [2\text{-}22]$$

Where, Q_{input} is the energy input during the module life cycle (which includes the energy requirement for manufacturing, installation, energy use during operation, and energy needed for decommissioning) and Q_{save} is the annual energy savings due to electricity and thermal energy generated by the PV/T module.

Energy production factor of the PV/T system is used to predict the overall performance. It is based on the lifetime of the system and can be expressed as [2.11]:

$$EPF = \tau_{LT} \times \frac{Q_{save}}{Q_{input}} \quad [2\text{-}23]$$

Where, EPF is the energy production factor; τ_{LT} is the lifetime of PV/T system.

Life cycle conversion efficiency is the net energy production of the PV/T system with respect to the solar input (radiation) over the life time of the PV/T system (τ_{LT}, years) and can be expressed as [2.11]:

$$LCE = \frac{(Q_{save} \times T_{LB}) - Q_{input}}{Q_{sun} \times \tau_{LT}} \quad [2\text{-}24]$$

Where, LCE is the Life cycle conversion efficiency; Q_{sun} is the annual solar radiation.

The corresponding carbon credit earned from the mitigation of CO_2 (in tons/year) can be determined using the relation as [2.14]:

$$CCE = \frac{E_{save} \times \Omega_{co_2}}{1000} \times F_{co_2} \quad [2\text{-}25]$$

Where, CCE is the carbon credit earned; F_{co_2} is the price of 1 tone of CO_2 \$14:5 [2.12, 2.14]; Ω_{co_2} is the average CO_2 equivalent intensity for electricity generation from coal (2.04 kg CO_2/kWh).

The cost payback period can be calculated as [2.15]:

$$CPP = \frac{F_{i.c} + F_{m.c}}{F_{e.r}} \quad [2\text{-}26]$$

Where, CPP is the cost payback period; $F_{i.c}$ is the initial investment; $F_{m.c}$ is the maintenance costs; $F_{e.r}$ is the expected returns per year.

In summary, the energy is the most convenient and effective method to evaluate the performance of PV/T system. The primary energy saving efficiency describes the saving capacity of the PV/T system on the fossil energy. The energy payback time (EPBT), energy production factor (EPF), Life cycle conversion efficiency (LCE) and payback period (PBP) describes the economic and environmental performance of the PV/T system. These testing and evaluation methods provides feasibility scheme for the evaluation of PV/T system and references for the standard building in the future.

2.3 R&D Progress of PV/T, PV/T assisted heat pump technology and Practical Applications of PV/T technologies

2.3.1 Review on the R&D progress of the PV/T technology

Several types of PV/T panels have been researched and developed for different functions since the concept was presented. The PV/T panel can provide electricity and thermal energy for hot water, space heating and drying. According to the cooling medium, the PV/T panel can be classified into air-cooled, liquid cooled and heat pipe-cooled types. They can either stand-alone or combine with other devices, such as a heat pump, and or thermoelectric module, which are described as follows:

(1) PV/T panel

(a) Air-cooled PV/T panel

The development of a hybrid system or mixed mode technologies to improve the drying process reduces energy consumption and therefore reduces its environmental impact. The hybrid solar provides an alternative to the use of fossil fuel but the intermittent nature and the low intensities of solar radiation is a problem. However, the problems can be remedied by the use of heat storage, auxiliary energy sources, control systems and a larger surface collector [2.16-2.19]. Moreover, the hybrid solar drying system was designed incorporating with a PV/T system. One of the ingenious methods of solar energy conversion systems is the photovoltaic thermal air collector or hybrid solar collector, which converts solar radiation to both thermal and electrical energies for use in drying systems. The integrated arrangement for utilizing thermal energy, as well as electrical energy, with a PV module is referred to as hybrid PV/T system. Owning to the low specific heat capacity, the air has

a high temperature at the outlet of PV/T panel, which is reasonable for drying [2.20-2.22] and space heating [2.23-2.28].

(b) Liquid-cooled PV/T panel

In liquid-based PV/T system, the solar thermal system consists of metal absorber plates and metal tubes embedded behind a photovoltaic panel to extract its heat and keep the PV panel cool transfers. The photovoltaic panel transfer heat to liquid flowing across the tubes embedded behind the PV panel. The electrical efficiency of photovoltaic panel increases due to the decrease in its temperature [2.29-2.36]. Ji et al. [2.30] investigated that with increase in mass flow rate of water, the temperature of the PV drops and its electrical efficiency increases. Deng et al. [2.35] carried out an experimental investigation on electrical and thermal performance of photovoltaic/thermal system and found 13.76%, 11.92%, 13.71% and 14.65% of electrical efficiency with 31.62%, 33.07%, 24.99% and 17.24% of thermal efficiency.

(c) Heat pipe PV/T panel

A heat pipe is a heat transfer device which can transfer heat energy efficiently under Isothermal state. The heat pipe has the advantage of that: 1), no moving parts and don't need energy to operate; 2), long life time; 3), minimum maintenance; and 4) flexible size [2.37]. Therefore, it can be combined with the PV/T panel easily. The straight heat pipe PV/T panels showed a low thermal performance, because of the high thermal resistance and less heat exchange area at the condenser part [2.38-2.41]. In winter, their thermal efficiency ranged from 20% to 31.8% [2.38-2.40]. The loop heat pipe PV/T panel is another type PV/T, which has the ability to operate against gravity and achieve a higher maximum heat transport capacity [2.42]. Wei He and Xingxing Zhang [2.43, 2.44] investigated the loop heat pipe PV/T assisted heat pump system. It was found that the thermal efficiency of PV/T was 71% and 39.3%, respectively at selected condition. Hong Li [2.45] tested another loop heat pipe assisted heat pump system annually whose average daily electrical efficiency is from 11.6% to 12.4% and mean daily thermal efficiency ranges from 42.1% to 48.1%. Thierno M.O. Diallo [2.46] simulated the energy performance of a micro-channel heat pipe PV/T system, which has the mean electrical and thermal efficiency of 12.2% and 56.6%, respectively.

(2) Solar indirect-expansion heat pump system

It is a common way to combine solar energy and heat pump technology together to provide energy for hot water and space heating, which includes solar direct-expansion and indirect-expansion heat pump systems. The solar indirect-expansion heat pump system can be applied much more conveniently, because it is modular and easy to install. Most of the energy source of this system is from mixture of solar energy and air, water and ground source [2.47].

The air source is a natural and convenient energy which is available anywhere. It is acceptable to provide energy for building by air source and solar energy together. Guodong Qiu [2.48] compared the performance of a solar air heat pump system within the low, middle and high temperature condition. Yin Liuc [2.49] introduced fin tube and tube heat exchanger into heat pump system, which can increase heat capacity from 51% to 62% and COP from 49% to 59% under selected condition. Xu Dong [2.50] presented an experimental investigation of a solar integrated air source heat pump system under different condensing temperature.

Normally, the water source is from the hot/warm water which is heated by solar panel. This process not only can improve the efficiency of solar panel, but also benefit to the COP of the heat pump. T. T. Chow [2.51] presented a practical case study of a combined hybrid PV/T solar assisted heat pump (SAHP) system for a sports centre's hot water production. Wei He [2.52] presented a dedicated theoretical investigation of a novel solar loop-heat-pipe facade-based heat pump water heating system which is suitable for different refrigerant. Taehoon Kim [2.53] compared the efficiency and COP performance of three different types of solar indirect solar assisted heat pump system.

The geothermal heat pump or Ground source heat pump (GSHP) becomes an important renewable energy technology for its capability of producing heating and cooling simultaneously and because ground temperature is relatively constant, it makes this energy source reliable and environmentally friendly [2.54]. By combining PV/T technology and GSHP together, the system could produce heating, cooling and electricity more efficiently and low operating cost, compared to the conventional system that uses

a boiler and chiller for heating, cooling and electricity from the grid [2.55]. Euy Joon Lee [2.56] studied a photovoltaic/thermal (PV/T)-ground source heat pump hybrid system by using fuzzy logic control. M. Bakker [2.57] found that the PV/T panel was able to cover nearly all (96%) of the system electricity use, and that the COP of the heat pump was around 2.60.

(3) Solar direct-expansion heat pump system

The solar direct-expansion heat pump system makes use of the solar collector as the heat pump evaporator, thus enabling the direct collection of the heat from the striking solar radiation. With a low temperature of two-phase refrigerant keeping passing the heat exchanger behind of the PV and absorber, the PV/T panel was operating in a low temperature condition, which can enhance both the electrical and thermal efficiency absolutely.

Some solar direct-expansion heat pump systems used PV/T panels as the energy source [2.58-2.61] to provide hot water. While the PV/T panel also can be designed to provide energy for heat pipe and heat pump together [2.62]. It can work in different modes with different seasons, and it shows a much better economic performance than the single heat pipe PV/T panel or solar heat pump system. Jie Ji investigated a PV/T-air double source heat pump system [2.63-2.65], which can work in low temperature condition. It shows that the COP of the heat pump system increase with the solar radiation increasing. Gang Pei presented another double source solar heat pump system, it showed a high overall efficiency and high COP [2.66]. These multiple sources expand its application area.

Owning to different type and structure, these PV/T panels showed different performance, and their parameters are described in **Table 2-2**.

Table 2- 2: The characteristics comparison of different PV/T types [2.16-2.66]

Panel type	Efficiency	Advantage	Disadvantage
Air-cooled PV/T Type [2.18-2.26]	24%–47%	- Low cost - Simple structure	- Low thermal mass - Large air volume - Poor thermal removal effectiveness - High heat loss
Liquid-cooled PV/T type [2.27-2.34]	33%–59%	- Low cost - Direct contribution - High thermal mass - Low flow volume	-Still high PV temperature - Unstable heat removal effectiveness - Complex structure - Possible pipe freezing
Heat pipe PV/T type [2.36-2.44]	20%–56.6%	- Low PV temperature - Stable performance - High solar efficiency -Effective heat removal - Reduced power input	- High cost - Risk of damage - Complex structure
PV/T assisted indirect expansion heat pump [2.46-2.54]	39.3% -71%	- Low PV temperature - Stable performance - High efficiency -Effective heat removal	- High cost - Difficult to operate
PV/T assisted direct expansion heat pump [2.55- 2.63]	56%–74%	- Low PV temperature - Stable performance - High efficiency -Effective heat removal	- Risk of leakage -Unbalanced liquid distribution - High cost - Difficult to operate

2.3.2 Practical application of PV/T technology

Due to the limitation of the technology, application environment and high price, most of the PV/T technologies are at the stage of researching. But there are still several commercial products which were developed for practical application. The information of them is as below:

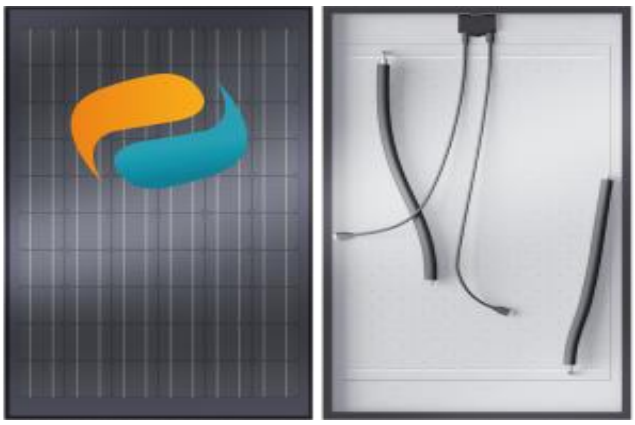

Fig. 2- 14: DualSun's innovative hybrid solar panel [2.67]

DualSun's Wave Company designed a type of PV/T panel, which intelligently integrates a photovoltaic panel with a heat exchanger on the back sheet [2.67]. it can recover the wasted heat from the photovoltaic cells to produce hot water (**Fig. 2-14**).

The Anaf Solar Company [2.68] also made a similar PV/T as the DualSun's. The PV panel is cooled by the water, increasing the electrical efficiency and providing thermal energy (**Fig. 2-15**).

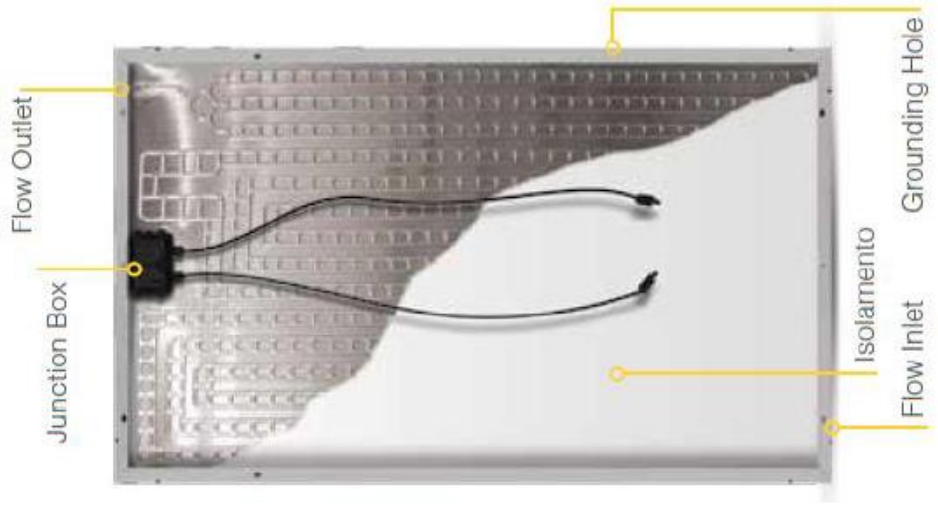

Fig. 2- 15: Anaf Solar's innovative hybrid solar panel [2.68]

This company also developed the Heat & Sanitary Water Configuration system, which includes the PV/T panel, heat pump, water storage tank and water pump (**Fig. 2-16**).

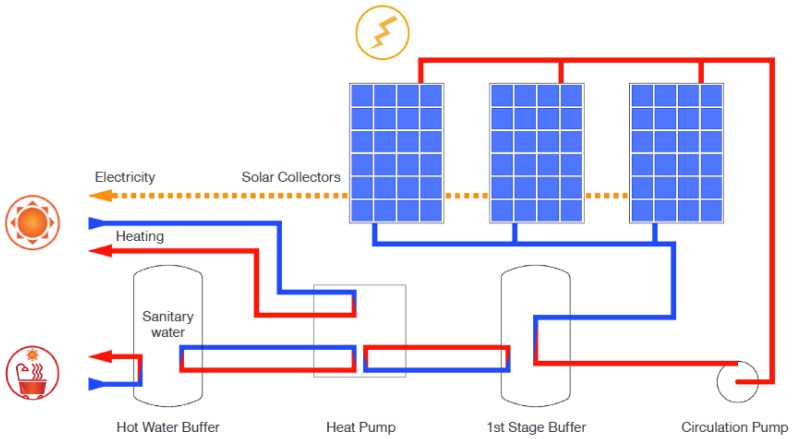

Fig. 2- 16: Heat & Sanitary Water Configuration System [2.68]

GSE AIR'SYSTEM [2.69] (**Fig. 2-17**) combined with the GSE Integration system collects the heat generated by the photovoltaic panels for heating,

domestic hot water (thermodynamic water heater, heat pump, double flow CMV) or drying crops.

Fig. 2- 17: GSE AIR'SYSTEM [2.69]

C. Bosch's Solator [2.70] and Systovi's R-Volt [2.71] have the similar structure of PV/T productions, which use serpentine copper tube as the heat exchanger (**Fig. 2-18**).

Fig. 2- 18: Systovi's SYSTEM [2.71]

Fototherm AL Series [2.72], Natural Technology Developments (NTD) Limited Solar Angel [2.73] (**Fig. 2-19**), Solimpeks Volther Powervolt and Powertherm [2.74] manufactured the unglazed PV/T with thermal insulation which can reduce heat losses and enhance the output of thermal energy.

Fig. 2- 19: Unglazed PV/T module with insulation from Solar Angel [2.73]

The Naked Energy Company [2.75] designed the vacuum tube PV/T module (**Fig. 2-20**). The vacuum tubes have low thermal losses and will produce abundant hot water / heat regardless of being installed in hot or cold climates.

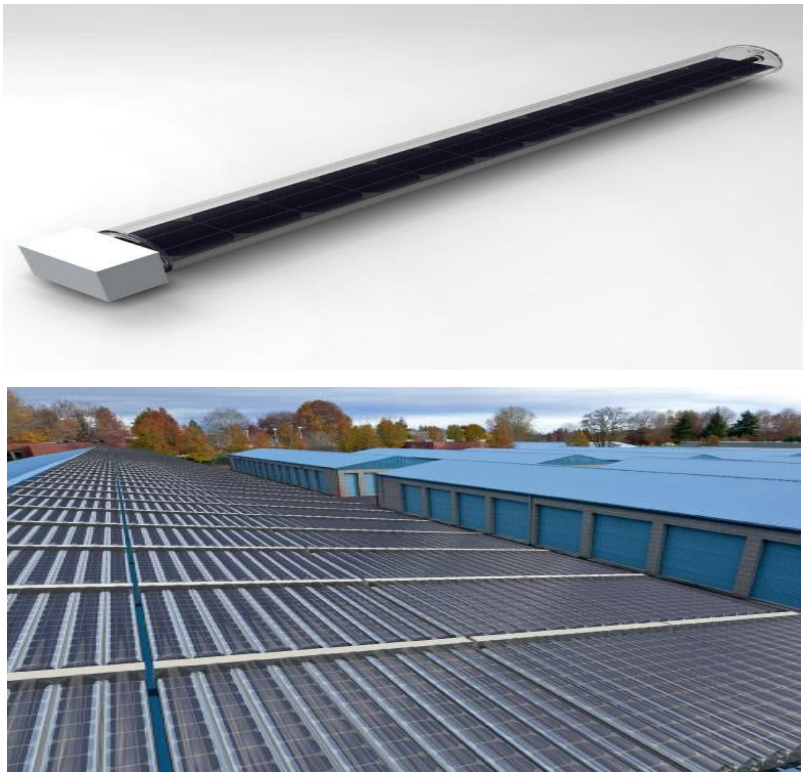

Fig. 2- 20: Vacuum tube PV/T module from Naked Energy [2.75]

The Energyntegration Company [2.76] in Italy can supply the EY-Hybrid PV/T panel (**Fig. 2-21**). There is a gap between the PV cell and absorber, and it is designed to be applied on the roof of house.

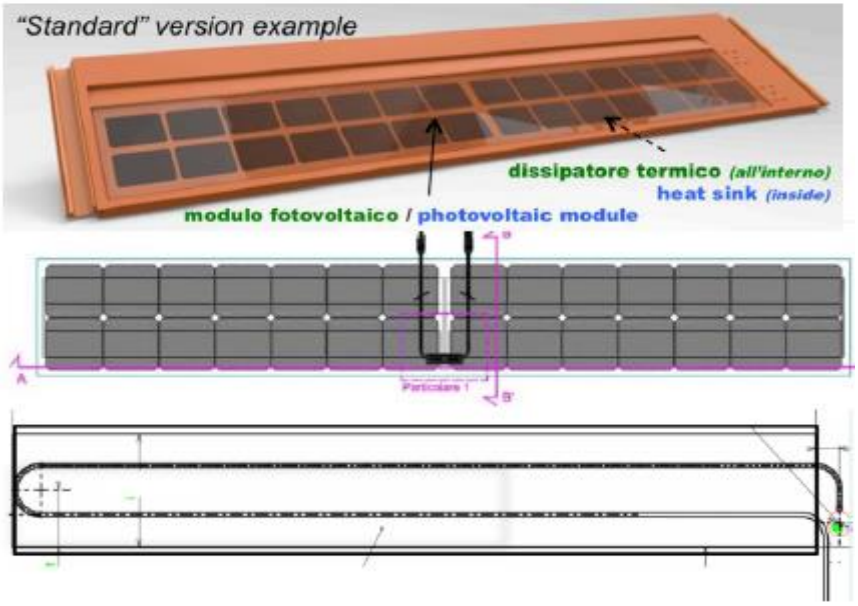

Fig. 2- 21: EY-Hybrid PV/T panel from Energyntegration [2.76]

The Solarus and Cogenra Solar Company [2.77] focus on the concentrated PV/T (CPV/T) products (**Fig. 2-22**). For this product, a curved mirror was used to reflect as much concentrated sunlight onto the receiver as possible and to maximize the amount of power collected and ensure that annual coverage is as even as possible - without the need for complicated tracking systems.

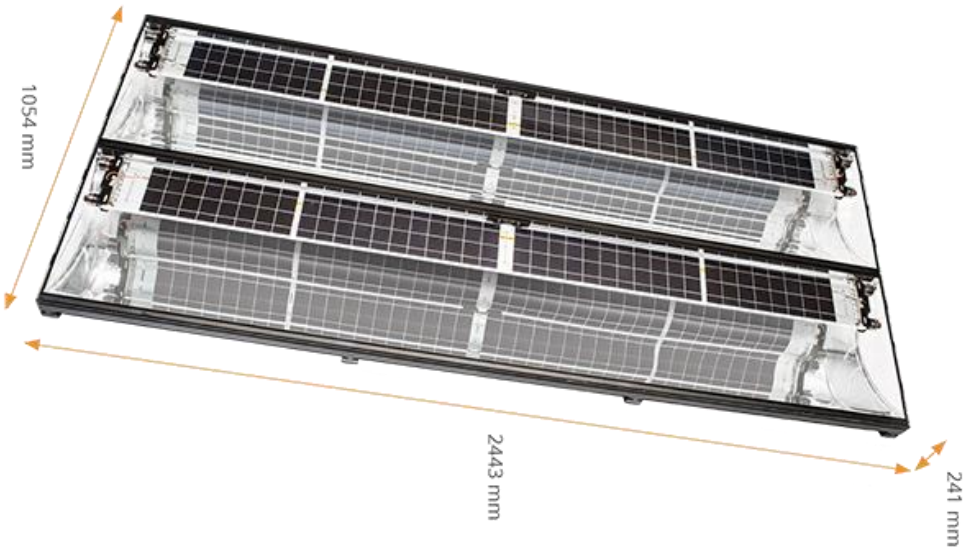

Fig. 2- 22: Concentrated PV/T (CPV/T) from the Solarus and Cogenra Solar [2.77]

The main parameters of all the products which are manufactured by these companies are listed in **Table 2-3**.

Table 2- 3: Specifications of the practical applied PV/T panel [2.67-2.77]

Technical specification					
Manufacturer	**Cooling method**	**Electrical efficiency**	**Thermal efficiency**	**Advantage**	**Disadvantage**
DualSun's Wave	Water	-	-	Generating much more heat than PV panel	Low electrical efficiency
Anaf Solar	Water	-	-	High electrical efficiency	No insulation, high heat loss
GSE AIR'SYSTEM	Heat pump	-	-	High electrical and thermal efficiency	High initial cost
C. Bösch	Water	17.11-18.3%	55-56 %	High electrical, thermal efficiency, low weight	High operating cost
Systovi	Water	16.5%	-	High temperature water	High operating cost
Fototherm	Water	14.6-15.8 %	58%	High electrical, thermal efficiency,	Unglazed and high heat loss
NTD Limited	Water	-	-	High electrical,	Unglazed and high heat loss
Solimpeks	Water	14.9%	-	High electrical,	Unglazed and high heat loss
Naked Energy	Water	-	-	High thermal efficiency,	Low electrical efficiency
Energyntegration	Water	-	-	Low weight	Difficult to install
Solarus, Cogenra	Water	-	-	Low cost	Difficult to be applied

2.3.3 Boundary condition of PV/T panel

The performance of the PV/T system can be impacted by many factors, i.e., the material, flow rate and temperature of the cooling fluid, solar radiation, panel type and other factors [2.78-2.105]. These boundary conditions provided special operating condition and requirement to investigate the working process of the PV/T systems.

(1) Temperature

The performance of the PV/T panel can be determined by the operating temperature, i.e., ambient temperature, fluid temperature at the inlet of panel,

thermal absorber temperature. It was found that decreasing both the fluid and ambient temperature can enhance both the electrical and thermal efficiency of PV/T panels [2.78]. With the measured temperature as the boundary condition, the convective coefficients were higher than expected due to leading edge effects and the turbulent nature of the flow [2.79].

(2) Material of cooling fluid

The material of the cooling fluid can be classified into air, liquid and refrigerant. The air is mainly used for space heating and drying [2.20-2.28]. The water is mainly for hot water and space heating [2.29-2.36]. The refrigerant is always used in heat pump or heat pipe system for hot water and space heating [2.58-2.66]. The water has a much higher specific heat capacity than the air, resulting in a lower operating temperature and higher thermal efficiency [2.80]. While some new types of liquid were introduced into the PV/T panels, i.e., Phase Change Material [2.81], nanofluids [2.82- 2.84], which can improve the solar efficiency of the PV/T panel absolutely, because of their special feature. The PV/T panel which acts as the evaporator of solar direct-expansion heat pump with two phase fluid going through it showed the best performance, owning to the help of compressor which keep the panel working at a very low temperature [2.85].

(3) Flow rate of the cooling fluid

The flow rate of cooling fluid will determine the Reynolds number and flow status of it, which always impacts the heat transfer rate. With the flow rate of cooling liquid increasing, the working temperature of the solar PV/T is also increasing too, meaning that the electrical and thermal efficiency are increasing [2.84-2.88], while the efficiency cannot increase unlimited. At the beginning, it increases very fast, and then slowly rise to the maximum value, where it finally plateaus [2.89].

(4) Solar radiation

The solar radiation not only can impact the working temperature, but also can influence the flow rate of the working fluid, meaning that the higher the temperature, the lower viscosity [2.90]. At the same operating condition, high solar radiation can reduce the proportion of energy loss to the surroundings, meaning that it performs with a higher thermal efficiency [2.90]. While the

high temperature will lower its electrical efficiency [2.91, 2.92]. For the solar direct-expansion heat pump system, the thermal efficiency will decrease with the increasing solar radiation, it was caused by the limited cooling capacity of the compressor, which cannot match the increasing solar energy [2.92, 2.93].

(5) Structure of the PV/T panel

The structure of PV/T panel is another factor which can impact its performance, i.e., glass cover, the heat exchanger behind the PV cell. The difference between the glazed and unglazed PV/T panel is that whether an air gap is designed between the glass cover and PV cell, which can reduce the heat loss in front of the panel. Normally, the glazed PV/T panel has a much higher working temperature than the unglazed one, leading to a higher thermal efficiency and lower electrical efficiency [2.94, 2.95]. The heat exchangers of PV/T panel are round pipe, micro-channel tube, heat pipe and flat box, et [2.96-2.100], and the micro-channel structure showed a much better heat transfer capacity than the other [2.101], therefore, this type own the best performance in solar energy, and the round pipe has the lowest efficiency, but the electrical efficiency is similar [2.102].

(6) Other boundary conditions

Several other kinds of boundary conditions can also impact the working result of the PV/T panel, i.e., the material of PV, finned heat exchanger and heat loading. It found that the type of PV/T panel with mono-crystalline Si solar cells has a higher value than the one with multi-crystalline Si solar cells both in electrical and thermal efficiency [2.103]. The finned flat-PV/T panel had a 1% higher annual heat gain and 3% higher electrical gain than the un-finned one. Similarly, the compound parabolic concentrating (CPC) PV/T panel also showed a better performance than the un-finned one [2.104]. Recovery ratio and heat loading are considered as the boundary condition for the PV/T system [2.105].

2.3.4 Energy, economic and environmental performance analysis of the PV/T panel

(a) Energy performance analysis of PV/T panel

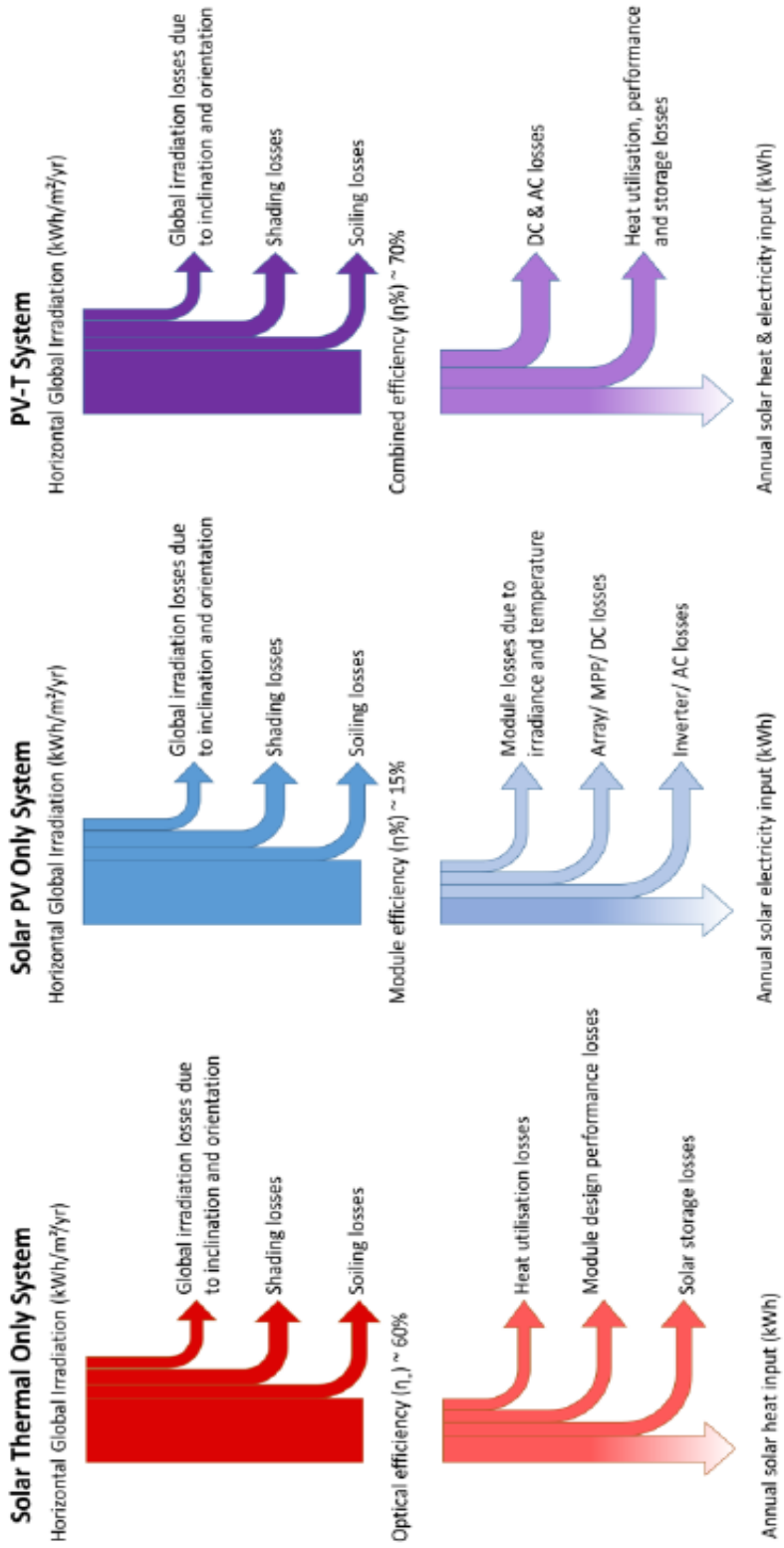

Fig. 2- 23: Comparing system efficiencies of single solar technology systems and a PV/T system [2.10]

The design concept of a PV/T system is to produce heat and electricity as efficiently as possible, maximising the amount of solar energy that is converted into useful energy. The performance of the PV/T panel is affected by its own characteristics, the system (i.e., pipework, water pump, and storage), the system integration (indirect-expansion heat pump, direct-expansion heat pump), operation condition and control. **Fig. 2-23** illustrates the difference of energy loss between the PV panel, thermal collector and PV/T panel. The result showed that the PV/T panel could output nearly the same efficiency of both the separated PV panel and thermal collector. The PV/T modules are designed to be less thermally efficient due to the requirement to operate at lower temperatures than the standard solar thermal collector is.

The performance of a PV/T system can be described in the following ways: (1) Electrical efficiency; (2) Thermal efficiency; (3) System efficiency (%); (4) Energy savings (kWh/yr.); (5) Cost benefit (£/year, payback in years, ROI %); (6) Environmental benefit (kg CO_2 offset).

The Electrical generation, thermal generation and system efficiency are very important factors to evaluate the performance of the PV/T module. There are four primary heat transfer mediums used in PV/T panel, air, water, water/glycol and refrigerant. For these types of PV/T panel, the performance of them would be affected by the temperature of medium at input, the flow rate and the ambient temperature. The air-based PV/T technology are most used for space heating and drying. With a poor thermodynamic parameter, the air can't transfer too much energy and own a much higher output temperature than other mediums (water and refrigerant). The result is that the air-based PV/T panel would operate in a high temperature condition, resulting in a lower electrical and thermal efficiencies (**Fig. 2-24, [2.106]**). Due to the different testing condition, the electrical, thermal and overall efficiencies range from 6.9% to 12.3%, 19.4% to 27.7% and 45% to 53.6%, respectively [2.107- 2.109]. The water-based PV/T panel is the most common type, which can provide hot water and space heating. The electrical and thermal efficiencies range from 12% to 17% and 25% to 54.6%, respectively [2.110, 2.111, 2.112, 2.38, and 2.113] (**Fig. 2-25**). There are two types of refrigerant medium PV/T panels, which are heat pipe PV/T panel and solar direct-

expansion heat pump system. The refrigerant medium can evaporate in the heat exchanger with a very low temperature, keeping the panel working at a low temperature. Therefore, the overall efficiency of this type is much higher than the air and water medium. The testing result showed that the electrical efficiency is more than 17.5%, and thermal efficiency is around 55.0%. The overall efficiency could achieve as high as 81.2%, and the COP ranged from 3.8 to 6.1[2.59, 2.60, 2. 60, 2.114, and 2.115].

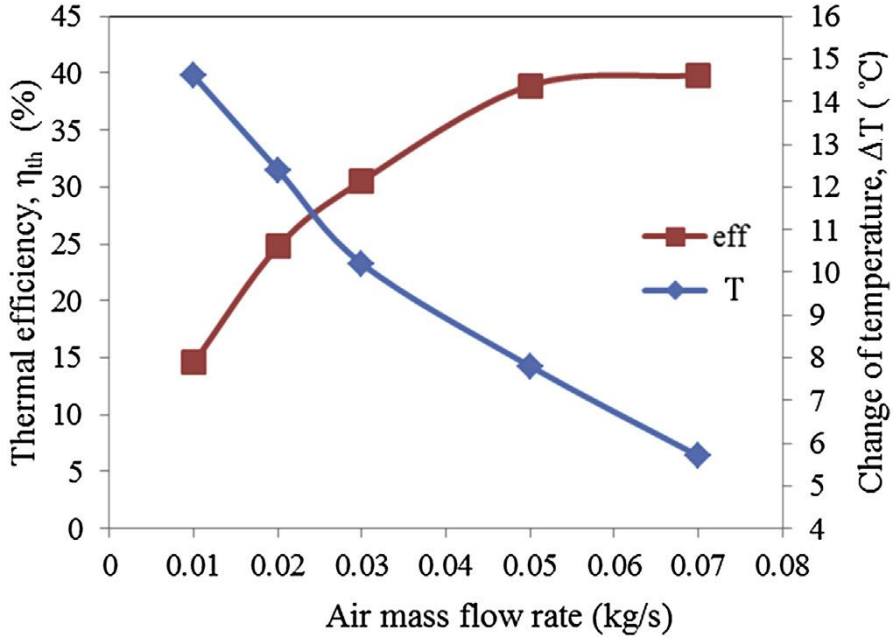

Fig. 2- 24: Performance of PV/T panel with different air mass flow rate [2.106]

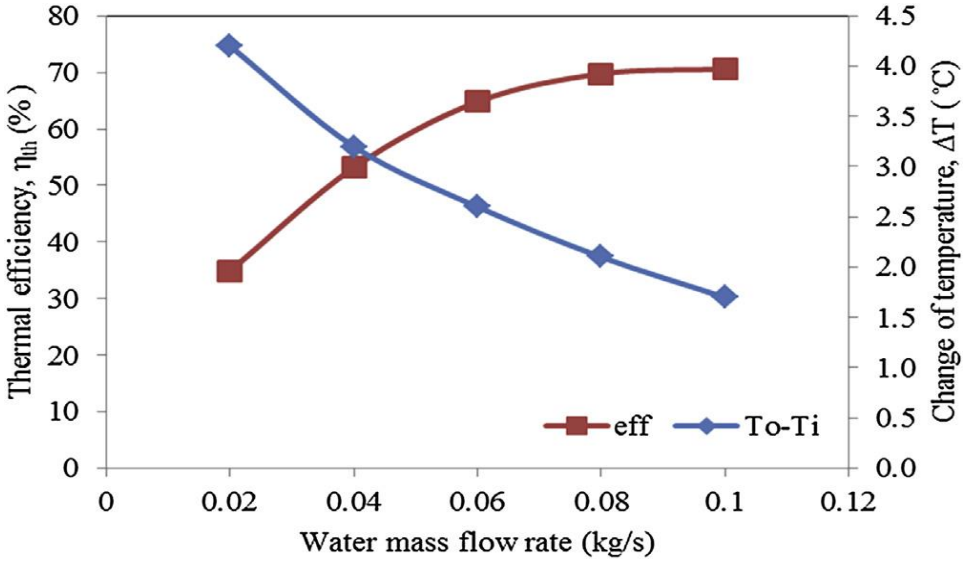

Fig. 2- 25: Performance of PV/T panel with different water mass flow rate [2.106]

Another assessment result is completed by the manufacturers or professional evaluators, which is normally carried out in the constant or standard condition. There is no testing standard formulated for PV/T technology, and the standards for PV panel and thermal collector can be used to predict the performance of PV/T panel. For the PV part, the main parameters are (1) Electrical efficiency at maximum output power; (2) Maximum output power, (3) Output voltage at maximum output power, (4) Output current at maximum output power, (5) Open-circuit voltage; and (6) Short-circuit current. These parameters are impacted by the area of the panel, quantity, layout and the material of the PV cell. The electrical efficiency of the PV panel is mostly impacted by the materials under the same designed parameters. The comparison of different materials [2.116] is as shown in **Table 2-4**. For the thermal part, the performance of the panel is impacted by the structure of itself, i.e., glazed or unglazed, heat exchanger, absorber plate. The assessment form is unusually by the efficiency with the combined factor of (Tp/Ta)/G, as shown in **Fig. 2-26** [2.117]. Although the testing standard for the PV/T panel has not been established, several testing [2.118, 2.119] on it was carried out in indoor or constant condition. These testing provided fundamental data for the standard established in the future.

Table 2- 4: Performance of different materials of the PV cell [2.116]

Materials	**Electrical efficiency in standard condition**	
	Maximum	**Commercial production**
Monocrystal silicon	16-20%	24%
Polycrystalline silicon	14-16%	18%
Amorphous silicon	8-10%	14.6%
Thin-film solar cells	19.5%	-

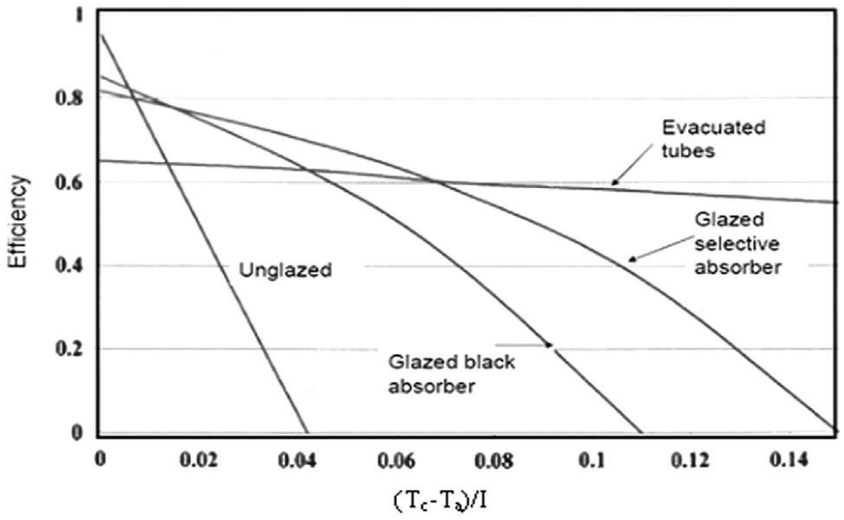

Fig. 2- 26: Variations of the efficiency with the combined factor of (Tc-Ta)/G for typical solar collectors [2.117]

The energy saving normally is calculated annually which always based on the experimental and simulation result. As shown in **Fig. 2-27**, the annual electricity gain, thermal energy gain and exergy gain would be included [2.120]. The annually result is always predicted by the numerical simulation [2.121-2.123]. It is difficult to simulate the performance of the system correctly without considering the complicated impactors, i.e., the local weather, dust and geography. Therefore, the experimental testing is needed to supply the based data and compared to simulation result [2.110, 2.111, 2.124 -2.131]. With the comparative result, the model could be adjusted and controlled reasonably, which would be used to predict the annual performance veritably.

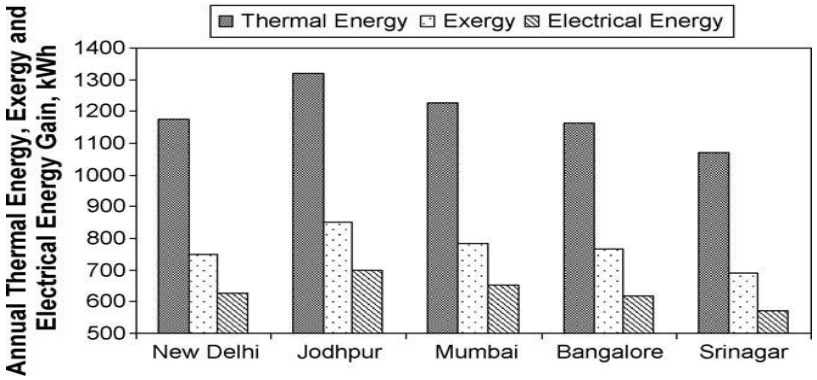

Fig. 2- 27: Annual thermal energy, Exergy and electrical energy [2.119]

(b) Economic and environmental performance of the PV/T panel

The economic and environmental performance of the PV/T panel is the most important indicator for its application and promoting. In items of economic issue, the maintenance and operation cost, energy saving, lifetime and payback time would be considered. In items of environmental issue, life-cycle carbon emission reduction is the main parameter to be analysed.

Some investigations on the economic and environmental performance were presented [2.132-2.135]. The comparison result between the separated PV, thermal collector and PV/T panel are shown in **Fig. 2-28**, **Fig. 2-29** and **Table 2-5** [2.132].

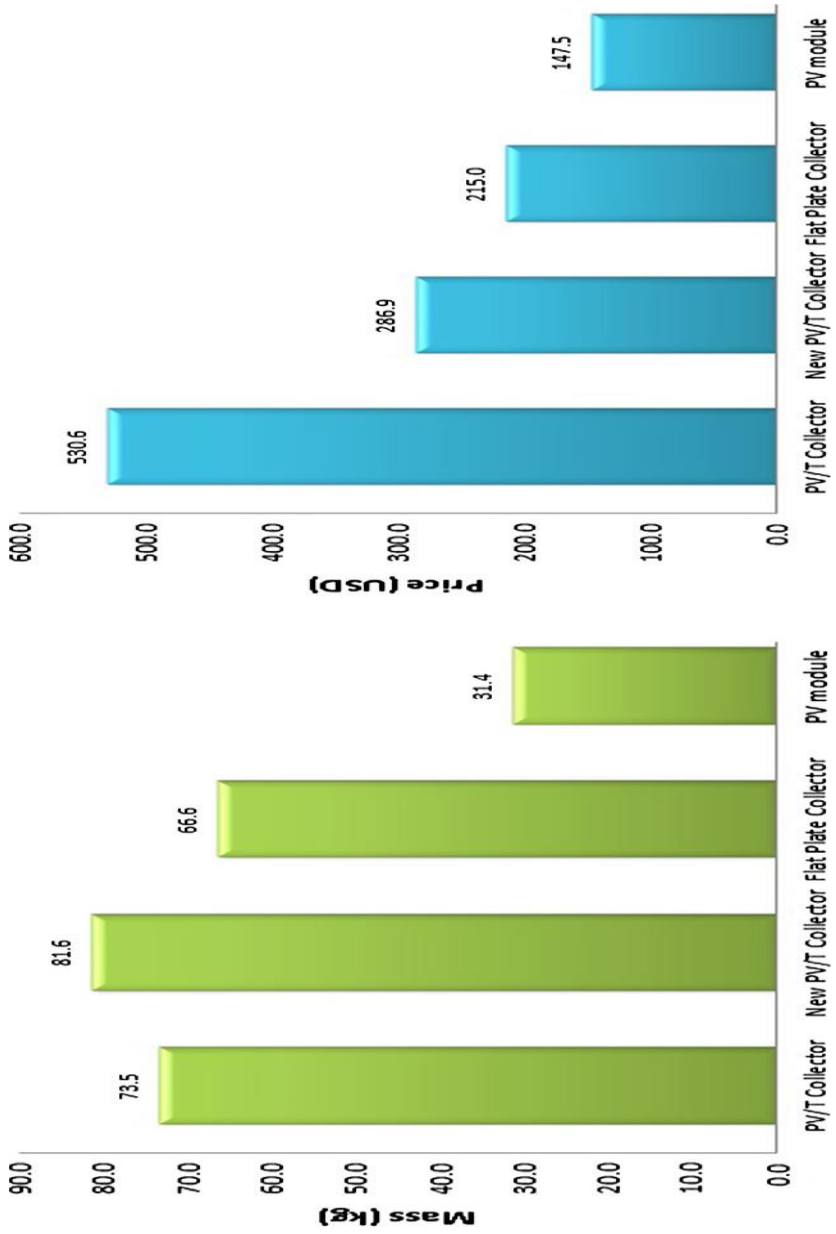

Fig. 2- 28: Mass and cost of the different solar collectors [2.10]

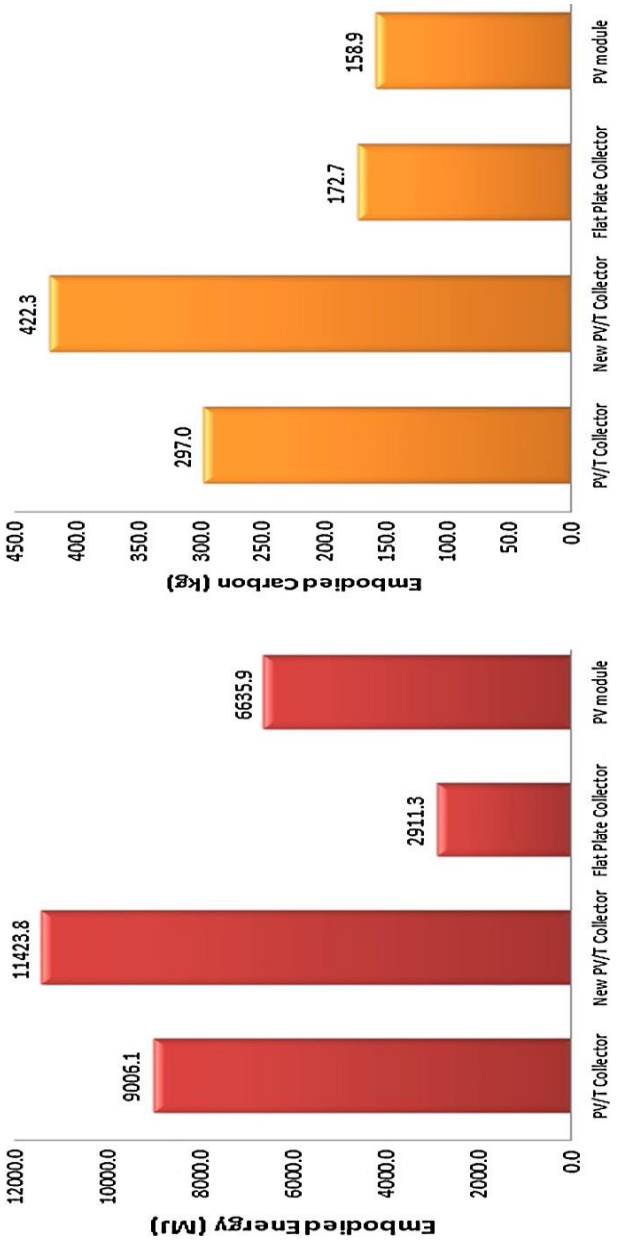

Fig. 2- 29: Embodied energy and embodied CO_2 emission of the different solar collectors [2.10]

Table 2- 5: Results of the economic analysis and environmental impact of flat plate roof mounted solar energy systems [2.132]

Parameter		SWH system	PV system	PV/T system
Calculated mass of the collector (kg)		66.5	31.3	81.5
Total calculated mass of the system (kg)		139.2	87.9	193.8
Calculated cost of the collector (GBP)		166.5	114.2	222.3
Actual cost of the collector (GBP)		173.8	164.9	NA
Total calculated cost of the system (GBP)		398.2	337.9	633.5
Actual cost of the system (GBP)		399.7	337.7	NA
Total calculated embodied energy (MJ)		6324.4	8139.3	15740.1
Annual useful energy (MJ)	Electrical	NA	1357.3	1415.4
	Thermal	7115.4	NA	4256.2
Annual overall useful thermal energy (MJ)		7115.4	4138.3	8571.8
Energy Pay Back Time (years)		0.8	1.9	1.8
Energy Yield Factor		28.1	12.7	13.6
Total calculated embodied CO_2 emission (kg)		424.1	183.5	694.8
Annual CO_2 emission mitigation (kg)		3122.8	1816.2	3762
Carbon Pay Back Time (years)		0.13	0.10	0.18
Annual Certified Emission Reduction (GBP)		40.2	23.3	48.5
Simple Payback Period (years)		2.3	13.3	3.1
Return on Investment (%)		42.4	7.5	31.9
Net Present Value (GBP)		1138.5	-102.7	1203.1
Benefit to Cost ratio		3.8	0.6	2.8
Internal Rate of Return (%)		42.4	6	31.8
Unit Cost of Energy (GBP/kW h)		0.024	0.11	0.03

In summary, the performance of the PV/T panel can be evaluated by several methods, i.e., the operational efficiency, the capacity of energy saving, the economic and environmental performance. However, most of the current work are based on the simulation result, therefore the comprehensive experimental investigation based on the long-term on the PV/T panel should be carried out which could give a much more realistic analysis on it.

2.3.5 Strength and barriers of the current PV/T technology

The PV/T panel is designed to combine the PV panel and thermal collector to be a component that can provide electricity and heat energy at the same time. Its strengths are (1) more efficient use of area; (2) high overall efficiency, and

(3) performance versatility. In items of the barriers, there are two problems need to be solved, which are related to the technical and application.

(1) Technical barriers

The main technical barriers (1) have a low heat transfer coefficient between the heat transfer medium and base panel, which is normally caused by the structure of the heat exchanger and the connection type between the tube and base panel; (2) have an inappropriate combination method between the PV cell and base panel.

Most of the current commercial PV/T panels or thermal collectors use copper tubes as the heat exchanger, and laser welding technology to connect the copper tubes and base panel, as shown in **Fig. 2-30** [2.136]. For the copper tubes, the large hydraulic radius and low flow rate of the medium inside have a negative impact on the heat transfer performance. Additionally, the cost of the copper tube is relatively high which increases the initial cost of the PV/T panels, and the combination of both PV panel and thermal panel together make PV/T panel own a much higher weight, which is not easy to combine with architecture. In terms of connection type, laser welding technology is suitable for welding two components with different materials (copper and aluminium), but the connection area is a straight line, which limits for heating transfer. Furthermore, when the wheel is crossing the base panel, a huge pressure is applied to the PV cell, potentially damaging it.

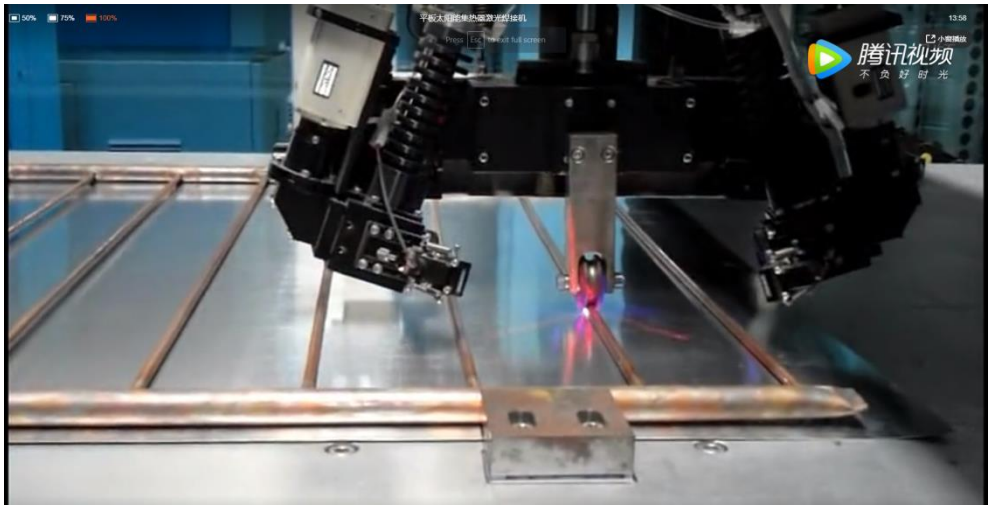

Fig. 2- 30: Laser welding technology connecting copper tube and absorber [2.136]

The laminating machine is the main equipment used for connecting the PV cell and glass or PV cell and base panel. The unglazed PV/T panel with air gap between the glass and PV cell has a much higher thermal efficiency, but if the PV cell is laminated on the base panel directly, the outage of PV would occur in six to twelve months [2.89], caused by the different thermal stress between the PV cell and base panel. Therefore, it is necessary to find a reasonable connection method to keep the PV operating well with a large temperature difference.

(2) Application barriers

The aim of the PV/T technology is to obtain more energy than the traditional PV system, and it is accepted that a rise in solar PV module temperature of 1°C causes about a 0.5% drop in electricity generation [2.137]. To achieve a higher efficiency, the PV/T panel and its combined system should be designed to be more complex than the separated PV or thermal collector. With a more complex system, the system installation space and technical requirement will also need to be improved. The working temperature of PV/T panels should be controlled at a low point, avoiding effects on the lifetime and output of the PV cell. However, this would result in an output temperature that is not high enough for domestic needs. This more complex system can also lead to economic and commercial barriers, i.e., high initial investment, high cost of labor. The 'payback' time for a domestic or small commercial PV/T installation, without any governmental policy support, will depend on how much of the electricity generated is used to displace imported grid electricity, and how much of the heat generated is useable. A simple analysis of the costs against savings suggest that PV/T payback is approximately 15-21 years at current prices [2.10].

2.4 Potential opportunity for the development of PV/T technology in the future

2.4.1 Reducing thermal resistance between heat exchanger and base panel

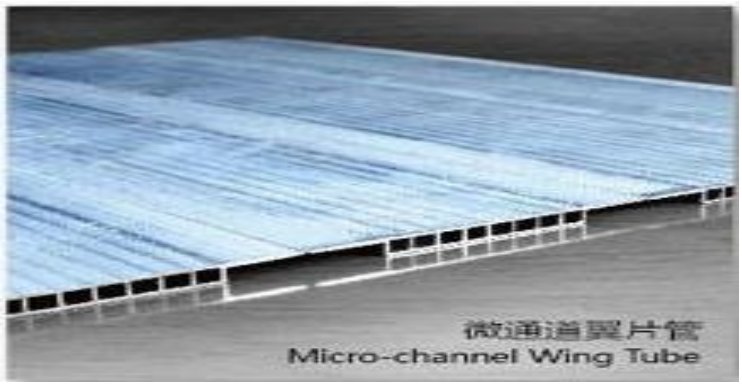

Fig. 2- 31: Finned micro-channel tube [2.138]

The current and commercial PV/T products normally use the welding as the connection method between the tube and thermal absorber, which has the weak of poor jointing effect, high thermal resistance and impacts the heat transfer coefficient between the cooling medium and thermal absorber. The thermal absorber and tube can be manufactured to be one component, as shown in **Fig. 2-31**. The fin of the micro-channel tube is designed as the thermal absorber, which has a low resistance and large heat transfer area.

2.4.2 Relieving the inequality thermal stress between the PV cell and thermal absorber

The EVA is usually used as the hot melt glue to connect the PV cell and glass or thermal absorber, while with the PV cell and absorber are being heated, the thermal stress between them is different which will cause the wires to break, leading to outage of PV cell. Two methods are presented to solve the inequality thermal stress, which are new melt thermal glue and another material of PV cell. The amorphous silicon (a-Si) cells may perform better at higher operating temperature, regarding the effect of thermal annealing. They are able to exhibit positive power temperature coefficients at degraded steady state (DSS). Unlike c-Si cells-based PV/T collectors suffering from poor thermal conductivity and large thermal stress due to the fluctuation in operating temperature, a-Si PV/T collectors are made of thin and flexible cells that can be easily deposited on metal (i.e., stainless steel), and are thus

promising in the medium/high temperature applications [2.139]. The method of replacing EVA with new thermal glue is another solution to relieve the impaction of different thermal stress [2.140], which allows the different thermal expansion between the PV cell and thermal absorber.

2.5 Chapter summary

An extensive review on the R&D and practical application of PV/T technology has been carried out. The review work provides a foundational information about the current level of development, the remaining barriers and develop direction to improve the PV/T technology, testing standards, the evaluating methods, costing and the difficulties to promote it in practical application.

There are several types of PV/T panels, unglazed with/without of insulation, glazed PV cells placed under the glass or on the thermal absorber, PV/T panel with concentrators. It is common for the PV/T panel which could be combined with other equipment to work together. The solar direct-expansion and indirect-expansion heat pump systems are mostly investigated, which can keep the working temperature of PV/T at low point, achieving a higher overall energy efficiency.

The professional testing standard for PV/T technology is not available in current, but the performance of it can be evaluated by the electrical, thermal and overall efficiencies, the cost, lifetime, payback time and environmental benefit.

The technical barriers are that the connection method between the heat exchanger tube, thermal absorber and PV cell need to be improved for achieving a much higher efficiency and longer lifetime. The application barriers are that the promotion of it needs the policy support from the government to shorten the payback time.

The review results helped to (1) identify the technical barriers existing in current PV/T technologies, (2) establish a scientific methodology for the PV/T research, (3) propose new research opportunities, and (4) build the research direction for subsequent chapters.

CHAPTER 3: CONCEPTUAL DESIGN AND DEVELOPMENT THEORETICAL SIMULATION MODELS OF THE SOLAR DIRECT-EXPANSION HEAT PUMP SYSTEM

3.1 Chapter introduction

This chapter proposes the designing scheme and theoretical simulation program of a novelty solar direct-expansion heat pump system for space heating, with the novelty micro-channel PV/T panel acting as the evaporator. It is intended to complete the following missions:

(1) Describe the working principle and strength of the system;
(2) Deliver designing drawings and parameters of all the components;
(3) Build the computer models of the PV/T panel (evaporator), compressor, water storage tank (condenser) and electronic expansion valve;
(4) Simulate and analyse the performance of this system with a typical weather data;

These work gives a detailed introduction on the solar direct-expansion heat pump system. The design on the components and theoretical simulation provide basic data for the experiment and result comparison in the future.

3.2 System description and working principle

The PV/micro-channel direct-expansion heat pump is designed for space heating in winter and generating electricity annually. The schematic diagram of it is shown in **Fig. 3-1**.

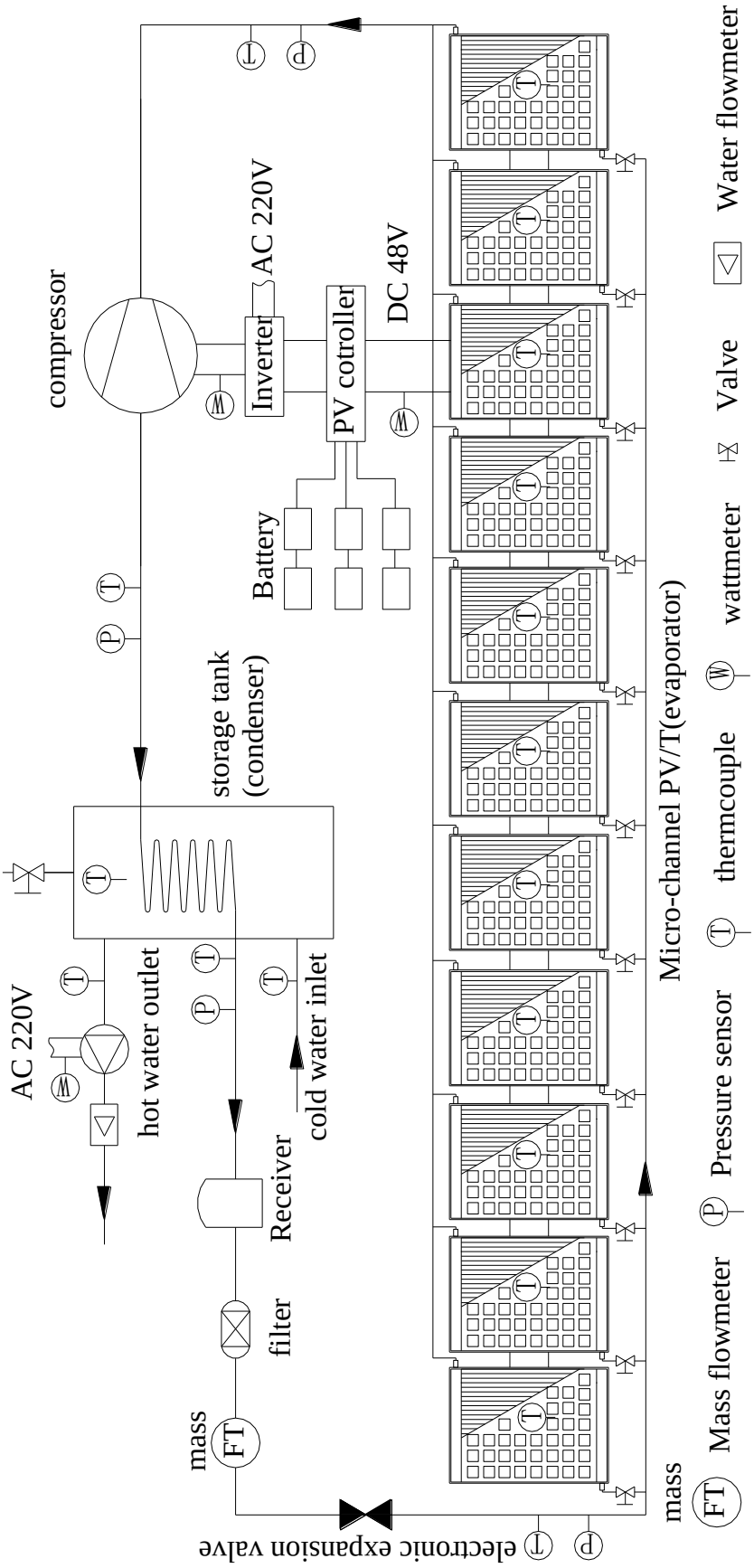

Fig. 3- 1: Schematic diagram of a novelty solar direct-expansion heat pump system for space heating

The entire PV/micro-channels-evaporator modules based heat pump system is shown schematically in **Fig. 3-1**. The system comprised four major components: (1) the PV/micro-channels-evaporator modules, each of which is the combination of the traditional PV panel and micro-channel evaporator; (2) a brushless motor driven compressor; (3) a condenser that also acts as the heat exchanger to transfer the heat from the refrigerant to the passing water; and (4) an electro-magnetic expansion valve that is to lower the pressure of the condensed refrigerant from the high to low level as required. Furthermore, the system also contained several supplementary components including a heat storage tank, PV controller, batteries and an inverter; all of which are functioned to support the smooth and stable operation of the system. On the hot water side, the piping layout is such configured to deliver the hot water directly to the embedded under-floor heating elements, which can emit the heat to the room space at the designed rate.

When the refrigerant (R410A) passed through the PV/micro-channel-evaporator modules, it changes phase from the liquid to vapour state by absorbing the heat from the rear of the PV panel. The vaporized refrigerant is then directed into a compressor where it is pressurized and heated, becoming high-pressure super-critical vapour. This part of vapour is then delivered to the condenser where heat exchange between the vapour refrigerant and heating loop water takes place. This action leads to temperature rise of the heating loop water which is used for providing heating for the targeted flat space in a building. It, meanwhile, leads to the condensation of the refrigerant vapour, generating the liquid refrigerant at the outlet of the condenser. The liquid refrigerant is then forced through the electro-magnetic expansion valve, leading to significant fall in both the pressure and temperature. After that, the low temperature liquid refrigerant is once again delivered into the PV/micro-channels-evaporator to absorb the heat from the PV panel. Operation of the heat pump will require an electrical input that, for this system, will be supplied by the PV/micro-channel-evaporator modules, thus creating a net-zero-external-powered operation. As the PV cells will generate electricity all year round while the heat pump will only be used during summer and winter seasons. The PV generated electricity could be fed into the local grid system at the first instance and then transferred to the heat pump. Use of the local

grid system as the electricity reserve/balance pool will reduce the sizes of the PVs, thus minimizing the cost of the heat pump system.

3.3 Unique features of the system and predicted system operational performance

The unique feature of this system lies in the employment of the micro-channel PV/T panels which act as the evaporator of the heat pump system. For this design, the refrigerant can absorb the solar energy directly with phase changing from liquid to vapour. Furthermore, the special structure of micro-channel tube can improve the heat exchange rate of the refrigerant inside, and the heat pump can keep the evaporating temperature at a low point. These superiorities make the PV/T panel operating at a low temperature, which increase both the electrical and thermal efficiencies of it.

The expected operational conditions of the PV-micro-channel direct expansion heat-pump system are shown in **Table 3-1**, while the refrigerant cyclic illustration in Log P-h chart is shown in **Fig. 3-2**. Owing to the performance limitation of the compressor, its maximum evaporation temperature is 12 ^{o}C. Similarly, the mass flow rate is determined by the operating frequency of the compressor and the evaporation temperature of refrigerant, then it can be calculated precisely. The superheat temperature is controlled by the EEV. The condensation and supercooled temperature is set by the required water temperature (40 ^{o}C). With these design parameters, the system is expected to provide hot water for building, which can meet the space heating demand and operate under a high COP at the same time.

Table 3- 1: Design parameters of the system

Evaporation temperature	Condensation temperature	Superheat temperature	Subcooled temperature	Refrigerant mass flow rate
12℃	45℃	5℃	5℃	50g/s

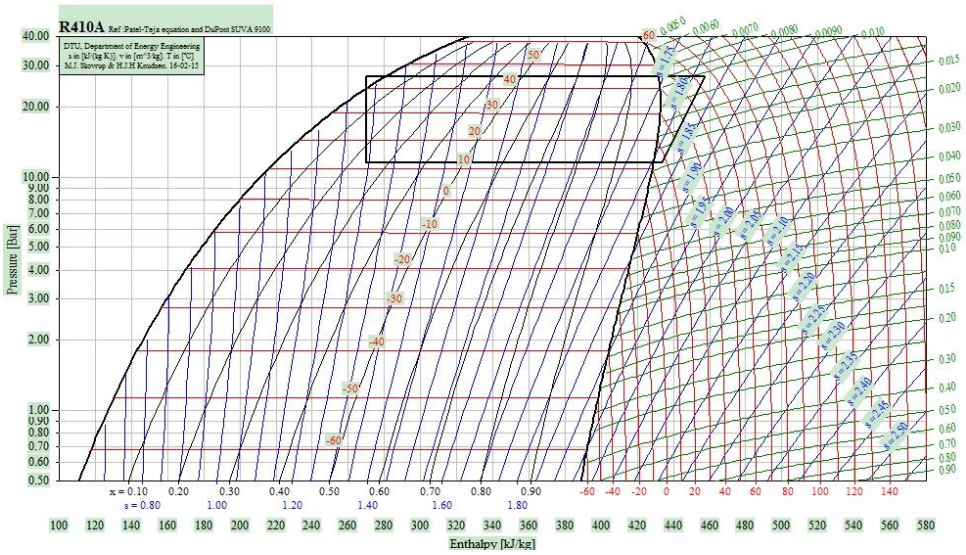

Fig. 3- 2: Log P - h chart illustration of the PV-micro-channel direct expansion heat-pump system

3.4 The system components and associated parameters

This section presents the all kinds of parameters of the components in the system. These details, i.e., the micro-channel, PV panel, compressor, condenser, expansion valve, could be applied as the input figure of the simulation program.

3.4.1 Micro-channel PV/T panels

Micro-channels are ideally suited for conducting heat transfer within small spaces, i.e., electronics, aerospace, and super-scale computing devices, where large sized heat transfer elements are difficult to incorporate. This kind of application has been in use for decades and in recent years, the 'micro-channel' concept has been brought into the heat exchanger design and manufacturing. This new development has been proved to be effective in increasing heat transfer within a heat exchanger, thus leading to the reduced size, weight, as well as manufacturing cost of the heat exchanger [1.17, 1.18]. The evaporator and condenser within a refrigeration (or heat pump) system could be such kinds of heat exchangers [1.17, 1.18]. In particular, the micro-channel tubes could be well applied to the PV integrated evaporator. Owing to the flat surfacing structure, the micro-channel tubes could be perfectly combined with PV modules, thus removing the difficulties remaining with the fin-tubing structure, and leading to the increase in heat transfer rate by 30% [2.100]. These elments, owing to the numerous partitions fitted inside, create

numerous interior micro-channels that can further enhance the heat transfer between the refrigerant and surrounduing heat source. Compared to existing flat-plate evaporators, the micro-channels have the reduced interior sizes, thus creating an increased vapour flow velocity within the channels; while the high vapor velocity will exert a higher shear stress onto the liquid film on the wall, which can greatly decrease the thickness of the liquid film, thus resulting in very high evaporation rate of the liquid [1.19]. Owing to such a notable feature of the micro-channels, the PV integrated evaporator made of micro-channels would be highly efficient in heat absorption, conversion and transportation.

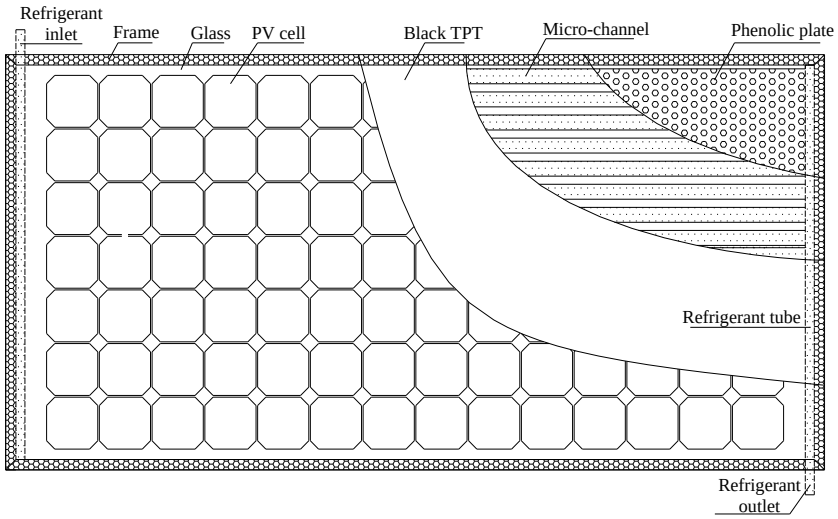

Fig. 3- 3: Structure of the PV/micro-channel-evaporator module

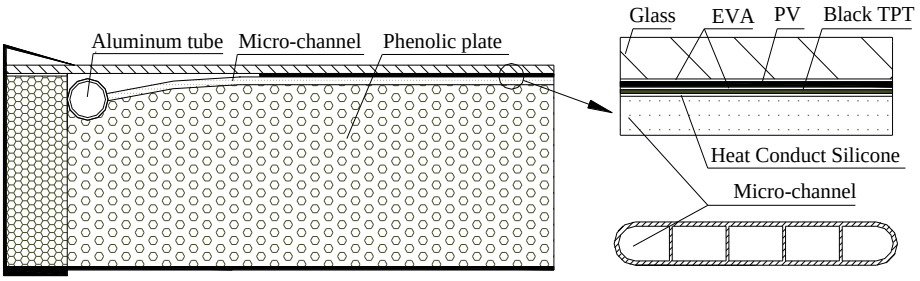

Fig. 3- 4: Sectional view of the PV/micro-channels-evaporator module

The PV/micro-channel-evaporator module was sized by 1 m x 2 m. The PV/T panel comprises a series of functional layers: (1) glazing cover; (2) PV cell; (3) EVA layer; (4) TPT layer; (5) thermal grease layer (6) micro-channels layer; (7) insulation layer to minimize the heat loss of the panel to the surrounding; and (8) holding-up framework. The structure of it is shown in **Fig. 3-3** and **Fig. 3-4**.

3.4.1.1 Glassing cover

Basically, the glassing cover is acted as the baseboard for the PV panel or unglazed PV/T panel. The function of it is to prevent the excessive convective heat loss to the surrounding and protecting the PV from being damaged, i.e., rain, dust and hail. The parameters of it would affect the performance of the PV or PV/T panel, because of that it can determine the percentage of sunlight going through it. The parameters of current production are shown in **Table 3-2**.

Table 3- 2: Parameters of the solar glass

Glassing	Emissivity	Transmittance	Size (mm)	Conductivity (W/m/K)
Super White Low Iron Tempered Glass	0.89	0.92	1980 × 980 ×3.2	1.2

3.4.1.2 PV cell

PV cell is used for converting part of the striking solar radiation into electricity. In this panel, 98 pieces of PV cell are placed on the glass, with the size of 125 × 125 × 0.3 mm and the total area of 1.53 m^2. The performance of the PV/T panel under the standard testing condition [3.1], 1,000 W/m^2 of solar radiation and 25 ^oC of ambient temperature, was estimated, and the detailed technical data are listed in **Table 3-3**.

Table 3- 3: Performance parameters of PV/T panel under standard testing conditions [3.1]

Item		Value
Electrical efficiency at maximum output power	η_{rc}	18%
Maximum output power, W	E_{max}	270
Output voltage at maximum output power, V	U_{max}	49.49
Output current at maximum output power, A	C_{max}	5.46
Open-circuit voltage, V	U_{oc}	60.35
Short-circuit current, A	C_{su}	5.87

3.4.1.3 EVA and black TPT

The EVA is the melt thermal glue which will connect the glass, PV cell and TPT together. The black TPT layer performs as the electrical isolation and the thermal absorber, to convert part of the striking solar radiation into heat

and take it away from the panel. These two components have the same size as the glass whose parameters are shown in Table 3-4.

3.4.1.4 Micro-channel layer

The micro-channel layer has 17 micro-channel rectangular pipes (**Fig. 3-5**, size 36 mm × 3 mm × 23) connected to the head tubes on both ends. And between theses tubes where the refrigerant will go through and has a phase change, 16 infill tubes (**Fig. 3-6**, size 20 mm × 3 mm × 5) are inserted into the gap and act as the fins. The structure and size of the micro-channel layer is shown in **Fig. 3-7**.

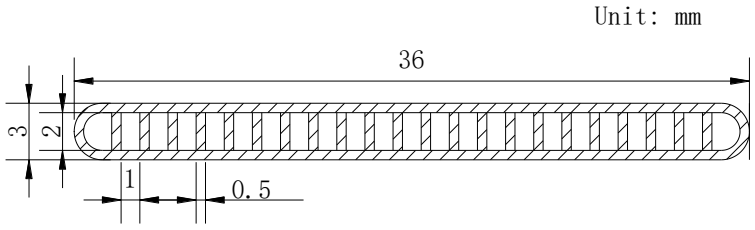

Fig. 3- 5: Structure of the micro-channel tube

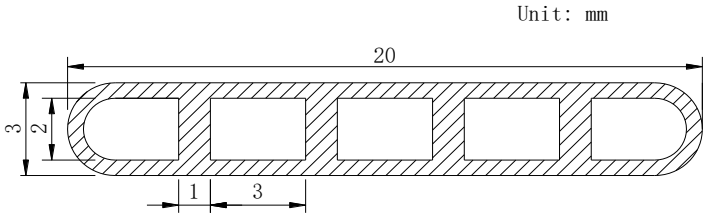

Fig. 3- 6: Structure of the infill tube

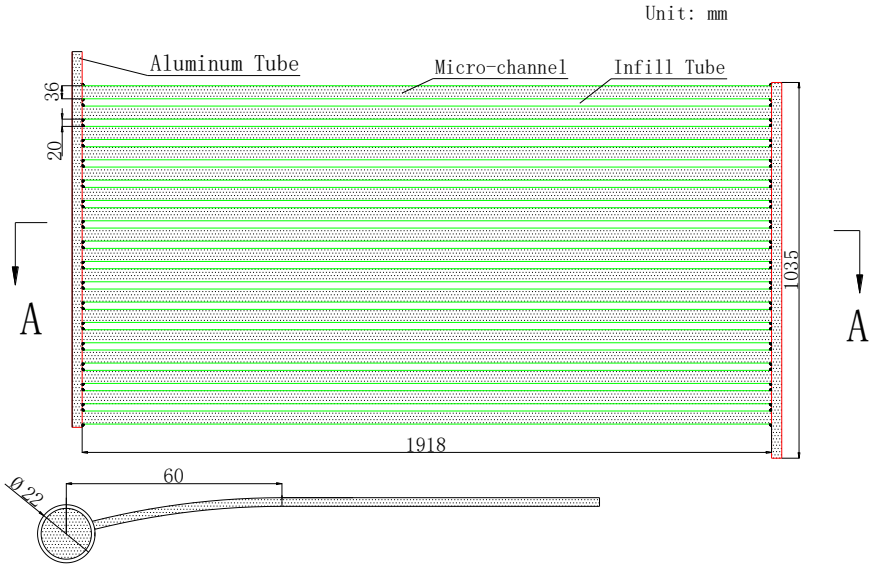

Fig. 3- 7: Structure and size of the micro-channel layer

3.4.1.5 Insulation layer and frame

The insulation layer is used to reduce the heat loss of the panel to the surrounding from the backside. The frame keeps all the components together and protect them. The structure of the frame is shown in **Fig. 3-8.**

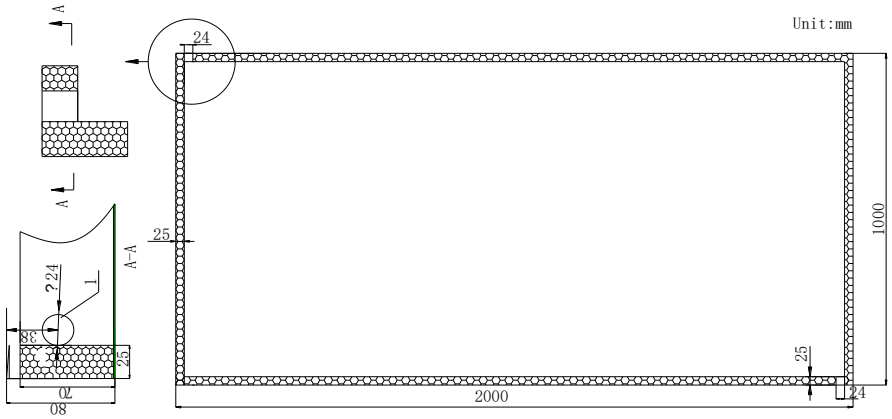

Fig. 3- 8: Structure of the frame

In summary, the size, material and function of each component of micro-channel PV/T panel are collected in **Table 3-4**. The super-heating temperature and evaporation temperature are designed at 5 ^{o}C and 12 ^{o}C, respectively. The evaporation pressure is set at 11.6 Bar.

Table 3- 4: Sizes and materials of the elements contained in the micro-channel PV/T panel

No	Element	Thickness	Function
1	Low-iron tempered glass plate	3.2mm	Based panel; prevent dust and rain water
2	Ethylene-vinyl acetate (EVA)	0.5mm	The hot melt glue
3	PV cell	200μm	Generate electricity
4	Ethylene-vinyl acetate (EVA)	0.5mm	The hot melt glue
5	Black tedlar-polyester-tedlar (TPT)	0.35mm	Electric insulator for the PV cells, enhanced the absorption of solar irradiation.
6	Heat conduct silicone	0.2mm	Reduce the contact thermal resistance
7	Micro-channel tube	4mm	The flow channel of Refrigerant
8	Phenolic plate	62mm	Thermal insulation layer
9	Frame	80mm	Packaging, fixing, protection

3.4.2 Compressor

The compressor is mechanical device that can increase the pressure with reduce its volume. It is the most important component in the heat pump system, which connect the evaporator and condenser together. The low-pressure and low-temperature vapour from evaporator enter into the compressor, then it be condensed by the piston driven by the motor to be high-pressure and high-temperature vapour and then enter into the condenser, preparing for heat transformation in the condenser.

Based on the required heat output and operational conditions, a brushless motor-powered compressor was selected. This compressor, as shown in **Fig. 3-9**, was delivered with a set of catalogue data which, as outlined in **Table 3-5** and **Fig. 3-10**, show the technical specifications and testing result under the standard testing condition [3.2].

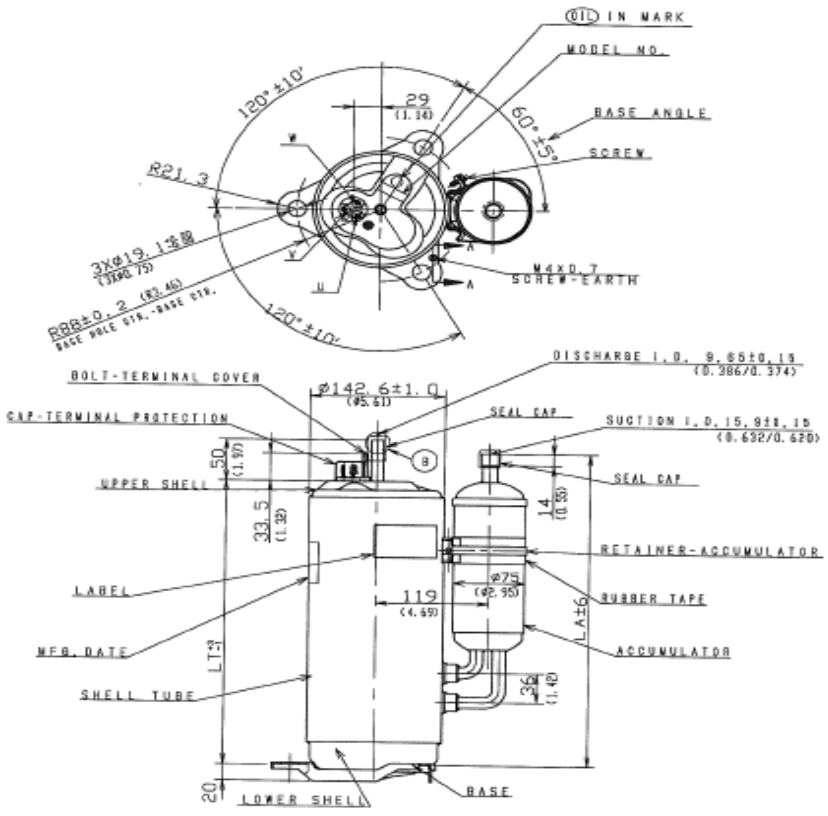

Fig. 3- 9: Structure of the compressor

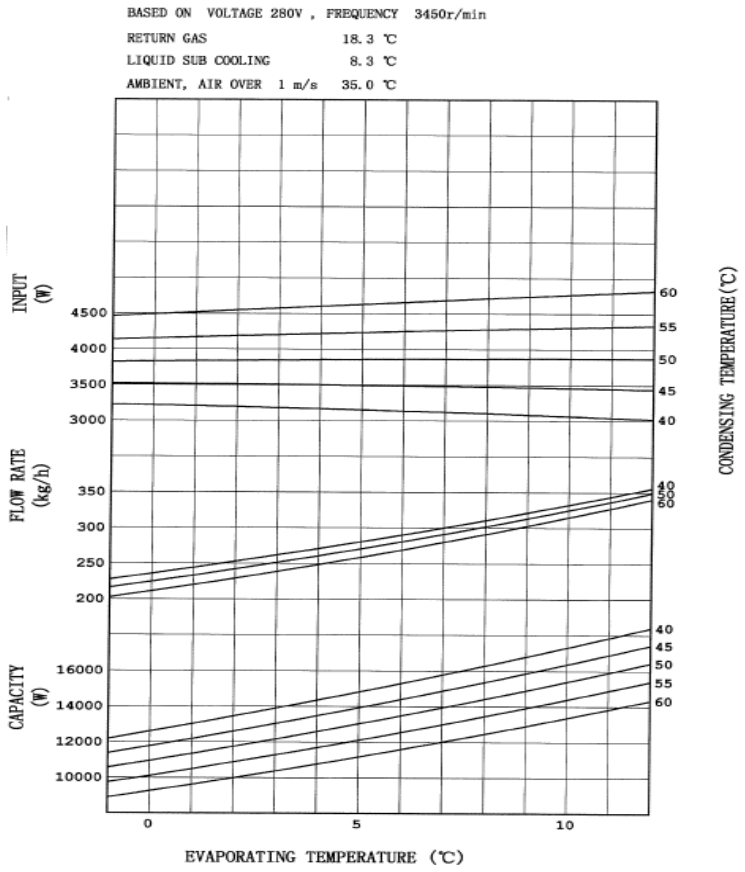

Fig. 3- 10: Testing result of the compressor under standard condition

Table 3- 5: Parameters of the compressor

Module	Refrigerant	Rated Frequency	Rated Power	Frequency Range	Suction pressure	Discharge pressure
5VD420			3.75		0.5-1.2	
ZAA21	R410A	50Hz	KW	25-80Hz	Mpa	3.2Mpa

3.4.3 Condenser

The condenser of the system is a copper coil heat exchanger, which is embedded into a heat storage water tank to transfer the condensation heat to the tank water. The heat storage tank was designed for multiple functions, including (1) receiving the condensation heat from the refrigerant; (2) delivering the hot water to the heating loop and collecting the cold water from the heating loop; and (3) reserving the surplus heat during the sunny daytime and discharging the reserved heat to loop water during the less or no sunny time. The image of the condenser/tank is shown in **Fig. 3-11**, while its technical specifications are given in **Table 3-6**.

Table 3- 6: Parameters of the condenser, heat storage tank and thermodynamic parameter

Storage tank	Value	Condenser	Value	Thermodynamic parameter	Value
Height	2 m	Diameter	12.7 mm	Condensation Enthalpy	185 kJ/kg
Diameter	900 mm	Thickness	1 mm	Condensation Pressure	27.3 Bar
Thickness of insulation	50 mm	Length	48 m	Condensation Temperature	45℃
Volume	1 m^3	Area	1.92 m^2	Sub-heating Temperature	5℃

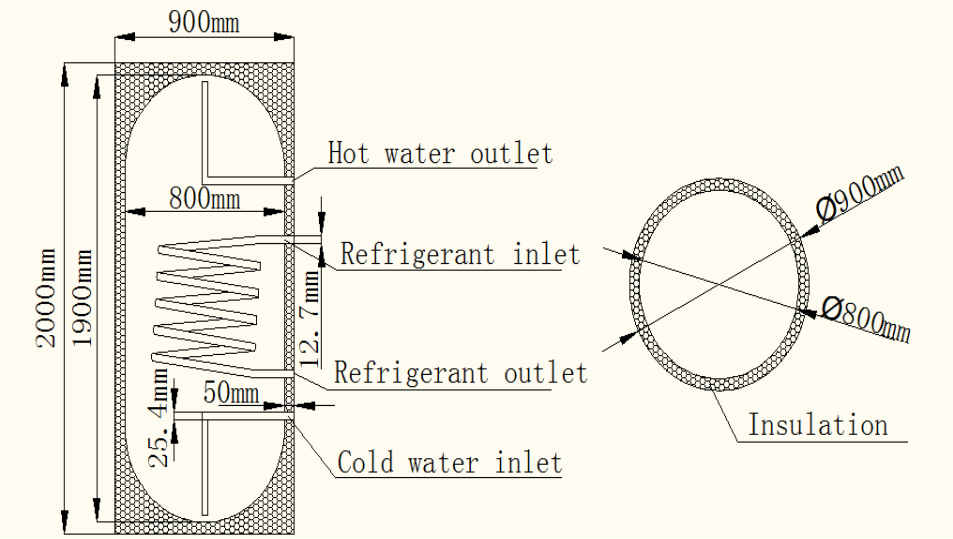

Fig. 3- 11: Condenser/tank selected in the system

3.4.4 Expansion valve

The expansion valve removes pressure from the liquid refrigerant to allow expansion or change of state from a liquid to a vapour in the evaporator.

The high-pressure liquid refrigerant entering the expansion valve is quite warm. This may be verified by feeling the liquid line at its connection to the expansion valve. The liquid refrigerant leaving the expansion valve is quite cold. The orifice within the valve does not remove heat, but only reduces pressure. Heat molecules contained in the liquid refrigerant are thus allowed to spread as the refrigerant moves out of the orifice. Under a greatly reduced pressure the liquid refrigerant is at its coldest as it leaves the expansion valve and enters the evaporator.

Pressures at the inlet and outlet of the expansion valve will closely approximate gauge pressures at the inlet and outlet of the compressor in most systems. The similarity of pressures is caused by the closeness of the components to each other. The slight variation in pressure readings of a very few pounds is due to resistance, causing a pressure drop in the lines and coils of the evaporator and condenser.

The electronic expansion valve normally comprises the stepper-motor valve and a controller. The Emerson EX4-121 electronic expansion valve was selected. It combines the superior control resolution of a stepper-motor valve with the automatic shut-off of a solenoid in a full take-apart body design. The IP67 rating ensures outstanding performance even under the most severe working conditions. No battery is required, and the take-apart design offers flexible inventory management and allows for each on-site installation and service making this valve is the ideal solution for today's commercial refrigeration applications. Its technical specifications are given in **Table 3-7**, while the image of the valve is shown in **Fig. 3-12**.

Table 3- 7: Technical specifications of the expansion valve

Brand	Module	Refrigerant	Capacity (10%~100%)
EMERSON	EX4-I21	R410A	2-19.3 KW

Fig. 3- 12: Stepper-motor valve and a controller

3.4.5 Heating loop and the circulating water pump

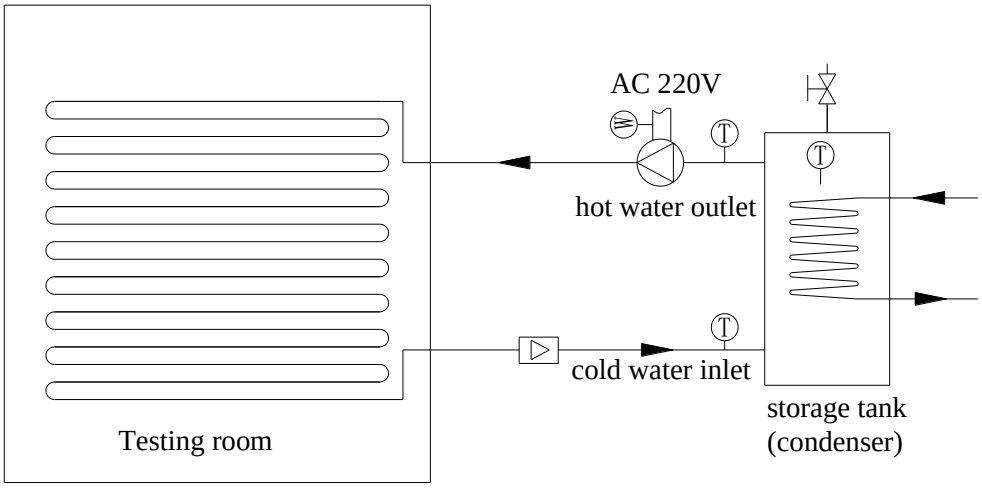

Fig. 3- 13: Schematic of the heating loop system

The heating loop was laid to connect the heat storage tank and underfloor heating coil that enable the effective heat delivery to the flat space. A circulating water pump was selected to enable this function. The image of the heating loop system is shown in **Fig. 3-13**.

3.4.6 Solar battery

The solar battery is specially designed for the Solar Off-grid System. It can be charged, store electricity and discharge the electricity generated by the PV panel. The image and parameters of battery are shown in **Fig. 3-14** and **Table 3-8**, respectively. The features of it are as blow:

- No free acid, the battery can be safely used by placing back to 90 °.
- Very low electrolyte weight, extending life.
- Strict selection of materials and advanced manufacturing technology, minimising the self-discharge.
- Very low float current to ensure life.
- Sealing reaction efficiency is high.
- The electrolyte composition: Compound silicate, dilute sulfuric acid, deionized water

Fig. 3- 14: Image of the battery

Table 3- 8: Parameters of the battery

Brand	Model	Voltage	Capacity	Size	Weight	Working temperature
Guanghe guineng	GHGN-12V200AH	DC 12V	200AH	522×219×239mm	58kg	-40℃-70℃

3.4.7 Solar control & inverter machine

Inverter is an electronic device or circuitry that changes direct current (DC) to alternating current (AC). The input voltage, output voltage and frequency, and overall power handling depend on the design of the specific device or circuitry. The inverter does not produce any power; the power is provided by the DC source.

A power inverter can be entirely electronic or may be a combination of mechanical effects (such as a rotary apparatus) and electronic circuitry. Static inverters do not use moving parts in the conversion process. It comprises the maximum power point tracker (MPPT), toroidal transformer and display. The image, schematic diagram and parameters of the inverter selected in this system are shown in **Fig. 3-15**, **Fig. 3-16** and **Table 3-9**.

Fig. 3- 15: Image of the inverter

Table 3- 9: Specifications of the inverter

Input voltage (AC)	**Input Voltage (DC PV)**	**Output voltage (AC)**	**Output power**	**Maximun current (A)**
220V	<100V	220V	3000W	30
Operating model	**Input frequency**	**Output frequency**	**Output waveform**	**Size (mm)**
AC priority & DC priority	48-52HZ	50HZ +/- 5%	Pure sine wave	475×342×195

Fig. 3- 16: Schematic diagram of the inverter

3.4.8 Insulation

Several different kinds of insulation material are applied in this system to minimum the heat loss, i.e., phenolic resin board, expanded polystyrene, rubber insulation cotton. The performance of insulation is evaluated by its thermal resistance. The parameters of them are listed in **Table 3-10**.

Table 3- 10: Thermal resistance of different insulation material

Material	Thermal resistance
Phenolic resin board	0.03 W/(m·K)
Expanded polystyrene	0.02-0.03 W/(m·K)
Rubber insulation cotton	0.034 W/(m·K)

3.5 Simulation models

Based on the design of above, the computer simulation models will be built to describe the energy relationship between all the components in this system, including solar energy, electricity generated, energy absorbed by the PV/T panel, electricity consumed by the compressor, the heat exchanged in water tank and testing room. With the input data, which is from the real testing condition, the theoretical simulation results will be analysed.

3.5.1 Thermal physical properties of refrigerating

In the solar direct-expansion heat pump system, all the energy is transferred by the refrigerant, hence the precision of the simulation result is depended on the precision of parameters and physical properties of the refrigerating. The calculation of the refrigerant in this chapter comprises two parts: (1) calculation of parameters under the condition of saturation; (2) calculation of parameters under the condition of superheated. These data can be used to calculate the energy transferred, the heat transfer eco-efficiency of refrigerant and confirm the status of it.

3.5.1.1 Calculation of parameters under the condition of saturation

In this section, several parameters of refrigerant under the condition of saturation should be calculated. They are saturation pressure, saturation temperature, enthalpy of saturated liquid, enthalpy of saturated vapour, density of saturated liquid and density of saturated vapour. Normally, these

parameters are a single function of the saturation temperature and have a one-to-one correspondence with it.

The equation of saturation pressure can be given as [3.3]:

$$P_{sat} = \exp(A + \frac{B}{T} + CT_{sat} + DlnT_{sat}) \quad [3\text{-}1]$$

Where, P_{sat} is the vapour pressure (bar); T_{sat} is the saturated temperature (K).

The equation of saturation temperature can be given as [3.3]:

$$T_{sat} = \frac{A}{\ln(P_{sat})+B} + C \quad [3\text{-}2]$$

The equation of saturated liquid enthalpy can be given as [3.3]:

$$h_l = \mathrm{A} + \mathrm{BX} + \mathrm{CX}^2 + D\mathrm{X}^3 + E\mathrm{X}^4 \quad [3\text{-}3]$$

$$h_g = \mathrm{A} + \mathrm{BX} + \mathrm{CX}^2 + D\mathrm{X}^3 + E\mathrm{X}^4 \quad [3\text{-}4]$$

$$\mathrm{X} = (1 - \frac{T}{T_c})^{(\frac{1}{3})} \quad [3\text{-}5]$$

Where, h_l and h_g are the saturated liquid and vapour enthalpy (kJ/kg), T is the temperature of liquid (K), T_c is the critical temperature of refrigerant (344.15 K).

The equation of liquid density can be given as [3.3]:

$$\rho_l = \mathrm{A} + \mathrm{BX} + \mathrm{CX}^2 + D\mathrm{X}^3 \quad [3\text{-}6]$$

Where, ρ_l is the liquid density of refrigerant (kg/m^3).

The equation of Saturated Vapour Density can be given as [3.3]:

$$\rho_g = (1 - \mathrm{y}^3) \times \rho_c \quad [3\text{-}7]$$

$$\mathrm{y} = \mathrm{A} + \mathrm{BX} + \mathrm{CX}^2 + D\mathrm{X}^3 + E\mathrm{X}^4 + F\mathrm{X}^5 \quad [3\text{-}8]$$

Where, ρ_g is the Saturated Vapour Density (kg/m^3); ρ_c is the Critical Density (493 kg/m^3). The coefficient of the calculation equation of refrigerant is shown in **Table 3-11**.

Table 3- 11: Coefficient of the equation [3.3]

	A	B	C	D	E	F
$Q_{3\text{-}1}$	78.003928	-4076.4422	0.2065787	11.878228	/	/
$Q_{3\text{-}2}$	-2348.18978	- 22.24929	-271.30340	/	/	/
$Q_{3\text{-}3}$	275.71426	-280.52509	577.11261	-1430.1314	685.7202	/
$Q_{3\text{-}4}$	275.71426	34.40354	490.727346	-818.05424	170.41778	/
$Q_{3\text{-}6}$	493	930.2971	416.4226	-86.8832	/	/
$Q_{3\text{-}8}$	0.36359063	2.6775079	-5.9330937	9.5070291	-9.1236153	3.5429932

3.5.1.2 Calculation of parameters under the condition of superheated

In the existing implicit curve-fitting method, the implicit equation for superheated region is constructed by an indirect way consisting of two steps, and the saturated vapour state is used as the reference state. In the first step, the implicit equation for saturated vapour state is constructed, and explicit formulae for saturated thermodynamic properties are obtained accordingly. In the second step, an equation describing the difference between superheated properties and saturated vapour properties under the same pressure is constructed. The implicit equation in the first step obviously only contains two variables, and it is not difficult to be established. For the implicit equation in the second step, it can be treated as two-variable implicit equation if the saturated property is considered as known, then it is still easy to establish such a high accuracy implicit equation by curve-fitting. In fact, the explicit formulae for saturated vapour state can describe the effect of the third variable, thus, the implicit equation for superheated region can still reflect the relationship among three variables.

The following implicit cubic equation is applied for superheated region and it can be given as [3.4, 3.5]:

$$\left(\frac{1}{u_{sat}}-\frac{1}{u}\right)+a_1\left(\frac{T_{sat}}{u_{sat}}-\frac{T}{u}\right)+a_2\left(\frac{{T_{sat}}^2}{u_{sat}}-\frac{T^2}{u}\right)+a_3\left(\frac{{T_{sat}}^3}{u_{sat}}-\frac{T^3}{u}\right)+$$

$$a_4\left(\frac{1}{{u_{sat}}^2}-\frac{1}{u^2}\right)+a_5\left(\frac{T_{sat}}{{u_{sat}}^2}-\frac{T}{u^2}\right)+a_6\left(\frac{{T_{sat}}^2}{{u_{sat}}^2}-\frac{T^2}{u^2}\right)+a_7\left(\frac{{T_{sat}}^3}{{u_{sat}}^2}-\frac{T^3}{u^2}\right)$$

$$+a_8\left(\frac{1}{{u_{sat}}^3}-\frac{1}{u^3}\right)+a_9\left(\frac{T_{sat}}{{u_{sat}}^3}-\frac{T}{u^3}\right)+a_{10}\left(\frac{{T_{sat}}^2}{{u_{sat}}^3}-\frac{T^2}{u^3}\right)+a_{11}\left(\frac{{T_{sat}}^3}{{u_{sat}}^3}-\frac{T^3}{u^3}\right)=$$

0 [3-9]

Where, a_1 , a_2 ,….. a_{11} are the coefficients to be regressed; u is a thermodynamic property or a transformation of that; subscript ref indicates the value of the reference state. In actual regression, the thermodynamic property except T and P is normally transformed before regression in order to improve regression precision.

In this equation, the P is the given parameter, the vapour enthalpy or density of refrigerant can be calculated based on the temperature of superheated refrigerant. The equation can be described as a standard cubic equation, which can be given as [3.4, 3.5]:

$$Ay^3 + By^2 + Cy + D = 0 \quad [3\text{-}10]$$

When the temperature T is known, let:

$$A = -\left(\begin{array}{c} \frac{1}{u_{sat}} + a_1 \frac{T_{sat}}{u_{sat}} + a_2 \frac{{T_{sat}}^2}{u_{sat}} + a_3 \frac{{T_{sat}}^3}{u_{sat}} + a_4 \frac{1}{{u_{sat}}^2} + a_5 \frac{T_{sat}}{{u_{sat}}^2} + \\ a_6 \frac{{T_{sat}}^2}{{u_{sat}}^2} + a_7 \frac{{T_{sat}}^3}{{u_{sat}}^2} + a_8 \frac{1}{{u_{sat}}^3} + a_9 \frac{T_{sat}}{{u_{sat}}^3} + a_{10} \frac{{T_{sat}}^2}{{u_{sat}}^3} + a_{11} \frac{{T_{sat}}^3}{{u_{sat}}^3} \end{array} \right) \quad [3\text{-}11]$$

$$B = 1 + a_1 T + a_2 T^2 + a_3 T^3 \quad [3\text{-}12]$$

$$C = a_4 + a_5 T + a_6 T^2 + a_7 T^3 \quad [3\text{-}13]$$

$$D = a_8 + a_9 T + a_{10} T^2 + a_{11} T^3 \quad [3\text{-}14]$$

When the vapour enthalpy or density are known, let:

$$A = a_{11} + a_7 u + a_3 u^2 \quad [3\text{-}15]$$

$$B = a_{10} + a_6 u + a_2 u^2 \quad [3\text{-}16]$$

$$C = a_9 + a_5 u + a_1 u^2 \quad [3\text{-}17]$$

$$D = a_8 + a_4 u + u^2 - \left(\begin{array}{c} \frac{1}{u_{sat}} + a_1 \frac{T_{sat}}{u_{sat}} + a_2 \frac{{T_{sat}}^2}{u_{sat}} + a_3 \frac{{T_{sat}}^3}{u_{sat}} + a_4 \frac{1}{{u_{sat}}^2} + a_5 \frac{T_{sat}}{{u_{sat}}^2} + \\ a_6 \frac{{T_{sat}}^2}{{u_{sat}}^2} + a_7 \frac{{T_{sat}}^3}{{u_{sat}}^2} + a_8 \frac{1}{{u_{sat}}^3} + a_9 \frac{T_{sat}}{{u_{sat}}^3} + a_{10} \frac{{T_{sat}}^2}{{u_{sat}}^3} + a_{11} \frac{{T_{sat}}^3}{{u_{sat}}^3} \end{array} \right) u^3 \quad [3\text{-}18]$$

When the parameters in the equation are temperature, pressure and vapour enthalpy, the equation [3-9] is $f(P, T, h) = 0$ and its coefficient (Q1) is

shown in Table 3-12 [3.5]. Then the $u = \mathrm{h}/1000$, and $u_{sat} = h_g/1000$. When the parameters in the equation are temperature, pressure and specific volume, and the equation [3-9] is $f(P,T,\rho) = 0$ and its coefficient (Q2) is shown in Table 3-12 [3.5]. Then the $u = (\rho 10^{-4})^{1/128}$, and $u_{sat} = (\rho_g 10^{-4})^{1/128}$.

Table 3- 12: Coefficients of the two equations [3.5]

	a_1	a_2	a_3	a_4	a_5
Q1	-192.461×10^{-5}	482.153×10^{-8}	-209.822×10^{-11}	-447.288×10^{-3}	115.444×10^{-5}
Q2	-123.292×10^{-6}	215.858×10^{-9}	-171.258×10^{-12}	-998.373×10^{-3}	237.873×10^{-6}
	a_6	a_7	a_8	a_9	a_{10}
Q1	-251.355×10^{-8}	239.851×10^{-12}	620.716×10^{-4}	-161.257×10^{-6}	261.355×10^{-9}
Q2	-420.103×10^{-9}	337.988×10^{-12}	331.902×10^{-9}	-114.927×10^{-6}	204.853×10^{-9}
	a_{11}				
Q1	217.634×10^{-12}				
Q2	-167.067×10^{-12}				

3.5.2 Refrigerant flow heat transfer model

During the operating process of the direct-expansion heat pump, the state of the refrigerant can be in subcooled region, two-phase region or superheated region. It is a very difficult to analyse the process of the mass and heat transfer in these regions. Therefore, in order to simplify the calculation, the mass and heat transfer model of refrigerant in this thesis is simplified by the following assumptions:

- The flow process of the refrigerant is a one-dimensional, which is along the axial direction of the pipe. In the two-phase region, it is considered that the working fluid in the vapour and liquid are uniformly mixed, ignoring the interphase slip in the flow process;
- The pressure of vapour and liquid in the same flow section is equal in the two-phase region;
- Ignoring the impact of gravity of refrigerant;
- Taking no account of the frosting problem;

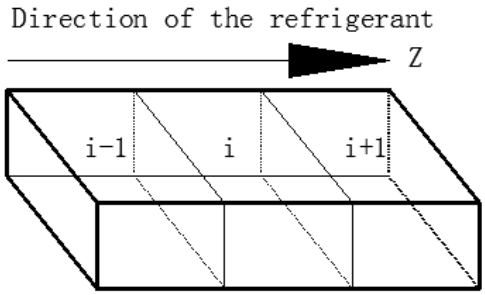

Fig. 3- 17: Image of flow process of refrigerant

As shown in **Fig. 3-17**, based on the selected section i and the above assumptions, the equation on it can be described with equation of mass conservation, equation of momentum conservation and equation of energy conservation.

The equation of mass conservation can be given as [3.6]:

$$\frac{\partial \rho}{\partial t} + \frac{\partial \dot{m}}{\partial z} = 0 \qquad [3\text{-}19]$$

$$\rho = \frac{\rho_g \rho_l}{\chi \rho_l + (1-\chi)\rho_g} \qquad [3\text{-}20]$$

Where, $\dot{m}$ is the mass flow rate (kg/(m^2·s)), the χ is the dryness of the refrigerant that describes the state of the refrigerant, and the details are shown in **Table 3-13**.

Table 3- 13: State of refrigerant at different dryness

χ	0	0<χ<1	1
	Subcooled	Two-phase	Superheated

The equation of momentum conservation can be given as [2.52]:

$$\frac{\partial(\dot{m})}{\partial t} + \frac{\partial(\frac{\dot{m}^2}{\rho})}{\partial z} = -\frac{\partial P}{\partial z} - (\frac{\partial P}{\partial z})_{ref} \qquad [3\text{-}21]$$

Where, P is the pressure (Pa), $(\frac{\partial P}{\partial z})_{fric}$ is the pressure drop of the refrigerant.

The equation of energy conservation can be given as [2.52]:

$$\frac{\partial(\rho h)}{\partial t} + \frac{\partial(\dot{mh})}{\partial z} = \frac{\pi D_{p.in}}{A_{ref}} \alpha_{ref}(T_p - T_{ref}) \qquad [3\text{-}22]$$

$$h = \chi h_l + (1 - \chi) h_g \quad [3\text{-}23]$$

Where, h is the average specific enthalpy of the refrigerant (J/kg); h_l and h_g are the liquid and vapour specific enthalpy of the refrigerant (J/kg); $D_{p.in}$ is the internal diameter of pipe which the refrigerant flows through (m); T_p and T_{ref} are the temperature of pipe and refrigerant (K), respectively. α_{ref} is the heat transfer coefficient between the pipe and refrigerant (W/(m^2·K)).

3.5.3 Simulation model for the micro-channel PV/T panels

The micro-channel PV/T panels are designed as the evaporator of the heat pump system (**Fig. 3-18**), by which the solar energy be converted into the electrical energy that can be stored or sold and thermal energy that is brought away through the evaporation of the refrigerant for space heating. In this section, the mathematical models of the sunlight incidence, glass cover, PV cell and micro-channel tube are established. These models describe the energy relationship between all of the components in the panel.

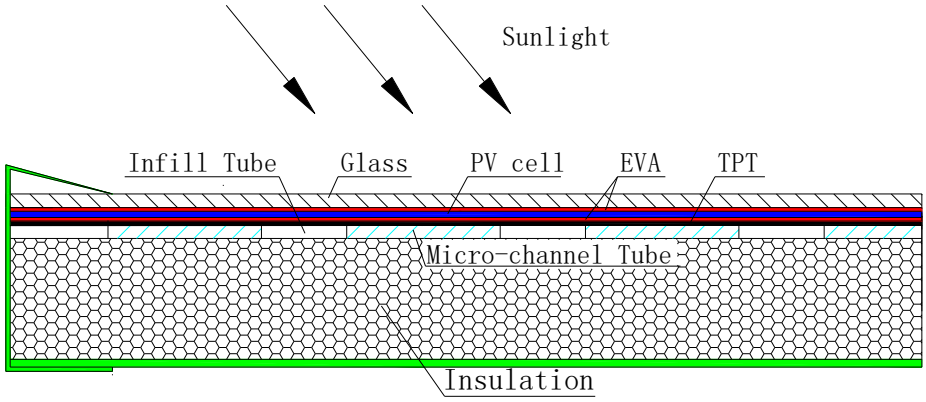

Fig. 3- 18: Image of the Micro-channel PV/T panel

3.5.3.1 Mathematical model of the sunlight incidence

The installation angle of the panel is fixed (35.6^o), but the incident angle of sunlight has been changing all the time from the morning to the afternoon. Therefore, the energy collected by the panel is not only impacted by the solar radiation but also the incident angle. The incident angle of sunlight to a plane is related to the dip and azimuth of this plane, the local latitude, the solar angle and the declination of the sun, the equation of the incident angle can be given as [3.6]:

$$\cos\theta = \cos\phi \cos\delta \cos\omega + \sin\phi \sin\delta \quad [3\text{-}24]$$

Where,θ is the incident angle of sunlight to the plane; δ is the declination of the sun; ϕ is the latitude of local place; ω is the solar hourly angle. The solar angle will be changed 15 degrees per hour, and it is 0 at 12:00, positive in the afternoon and negative in the morning.

The panel is installed face to south, and the equation can be given as [3.6]:

$$\cos\theta = \cos(\phi - \beta)\cos\delta\cos\omega + \sin(\phi - \beta)\sin\delta \quad [3\text{-}25]$$

$$\delta = 23.45\sin(360\frac{284+n}{365}) \quad [3\text{-}26]$$

Where, β is the angle of inclination of the plane with the horizontal; n is the n^{th} day of the year.

3.5.3.2 Mathematical model for the glass cover

The glass cover acts as the baseboard of the PV cell, and it is assumed that the temperature of glass cover is constant, and each part of the cover receives the same amount of the solar energy. The transient energy balance equation for the glass cover can be given by [2.52]:

$$G\lambda_{gc} + \mathrm{Q}_{pv\_gc} = \mathrm{d}_{gc}\rho_{gc}\mathrm{C}_{p.gc}\frac{\partial T_{gc}}{\partial t} + \mathrm{Q}_{am\_gc} + \mathrm{Q}_{s\_gc} \quad [3\text{-}27]$$

Where, d_{gc} is the thickness of glass cover (m); ρ_{gc} is the density (kg/m^3); $C_{p.gc}$ is the specific heat capacity (J/(kg·K)); G is the solar radiation intensity (W/m^2); $\lambda_{gc}$is absorption rate of the glass cover; Q_{pv_gc}, Q_{am_gc} and Q_{s_gc} are the heat transfer between the glass cover and the photovoltaic cell, the ambient air and the surrounding environment.

The absorption rate of the glass cover can be given as [3.6, 3.7]:

$$\lambda_{gc} = 1 - \gamma_{gc} \quad [3\text{-}28]$$

$$\gamma_{gc} = [1.005\times10^{-4}\times(90-\theta)\times\vartheta] - \left(5.204\times10^{-3}\times d_{gc}\times\vartheta\right) + (0.095\times\vartheta^2) + (0.029\times\vartheta) + \left[3.837\times10^{-4}\times(90-\theta)\times d_{gc}\right] - \left(3.299\times10^{-3}\times {d_{gc}}^2\right) - \left(0.028\times d_{gc}\right) + [9.117\times10^{-4}\times(90-\theta)] + [2.417\times10^{-7}\times(90-\theta)^2] + 0.859 \quad [3\text{-}29]$$

Where, γ_{gc} is the transmittance of glass cover; ϑ is the diffused radiation fraction with the range of 0 to 1; θ is the solar incidence angle in degree with the range of 0 to 90◦.

The equation of heat transfer between the glass cover and air can be given as [3.8]:

$$Q_{am\_gc} = \alpha_{am\_gc}(T_{gc} - T_{am}) \quad [3\text{-}30]$$

$$\alpha_{am\_gc} = 2.8 + 3.0S_{wd} \quad [3\text{-}31]$$

T_{gc} is the temperature of the glass cover (K); T_{am} is the ambient temperature (K); α_{am_gc} is the heat transfer coefficient between the glass cover and the ambient air (W/(m^2·K)); S_{wd} is the wind speed (m/s).

The heat transfer between the glass cover and PV cell comprises the direct contact heat transfer and radiative heat transfer, the equation of can be given as [2.52]:

$$Q_{pv\_gc} = \alpha_{pv\_gc}(T_{gc} - T_{pv}) \quad [3\text{-}32]$$

$$\alpha_{pv\_gc} = \sigma(T_{pv}^{\ 2} + T_{gc}^{\ 2})(T_{pv} + T_{gc})\left(\frac{\zeta}{\frac{1}{\varepsilon_{pv}}+\zeta\left(\frac{1}{\varepsilon_{gc}}-1\right)} + \frac{1-\zeta}{\frac{1}{\varepsilon_{TPT}}+(1-\zeta)\left(\frac{1}{\varepsilon_{gc}}-1\right)}\right) + \frac{K_{EVA}}{d_{EVA}} \quad [3\text{-}33]$$

Where, T_{pv} is the temperature of the photovoltaic cell (K); α_{pv_gc} is the heat transfer coefficient between the glass cover and photovoltaic cell (W/(m^2·K)); ζ is the coverage factor of the photovoltaic cell; ε_{pv} and ε_{TPT} are the emissivity of the photovoltaic cell and the black TPT, respectively; K_{EVA} and d_{EVA} are the heat conductivity coefficient (W/(m·K)) and thickness (m) of EVA layer, respectively; σ is the Stefan-Boltzmann constant, which is 5.6697 × 10^{-8} (W/(m^2·K^4)).

The equation of the heat transfer between the glass cover and the surrounding environment can be given as [3.7]:

$$Q_{s\_gc} = \alpha_{s\_gc}(T_{gc} - T_s) \quad [3\text{-}34]$$

$$\alpha_{s\_gc} = \varepsilon_{gc}\sigma(T_s^{\ 2} + T_{gc}^{\ 2})(T_s + T_{gc}) \quad [3\text{-}35]$$

$$T_s^{\ 4} = \kappa_{sky\_gc}T_{sky}^{\ 4} + \kappa_{gr\_gc}T_{gr}^{\ 4} + \kappa_{s\_gc}T_{sr}^{\ 4} \quad [3\text{-}36]$$

Where, $\alpha_{s_gc}$is the heat transfer coefficient between the glass cover and the surrounding environment (W/(m^2·K)); T_s is the background equivalent temperature (K); ε_{gc} is the emissivity of glass cover; κ_{sky_gc}, κ_{gr_gc} and κ_{s_gc} are the view factors of the glass surface to the sky, ground and surroundings, respectively.

3.5.3.2 Mathematical model for the PV cell layer

To simplify the simulation, the PV layer is defined as the composite module, which comprises two layers of EVA, one layer of PV cell and black TPT. It is assumed that the temperature of the PV layer is constant, and the specific heat capacity of EVA and TPT is ignored, because of their very thin thickness.

The equation of the PV cell can be given as [2.52]:

$$\zeta d_{pv}\rho_{pv}C_{p.pv}\frac{\partial T_{pv}}{\partial t} = \mathrm{Q}_{pv\_gc} + \mathrm{Q}_{pv\_p} + G(\tau\alpha)_{pv} - E_{pv} \quad [3\text{-}37]$$

Where, d_{pv} is the thickness of PV layer (m); ρ_{pv} is the density (kg/m^3); $C_{p.pv}$ is the specific heat capacity (J/(kg·K)); Q_{pv_p} is the heat transfer between the PV layer and the pipe, $(\tau\alpha)_{pv}$ is the effective absorption of PV layer; E_{pv} is the output power of PV layer.

The equation of heat transfer between the PV layer and the pipe can be given as [2.52]:

$$\mathrm{Q}_{pv\_p} = (T_{pv} - T_p)/R_{pv\_p} \quad [3\text{-}38]$$

Where, T_p is the temperature of the wall of micro-channel (K); R_{pv_p} is the thermal resistance between PV layer and micro-channel (K·m^2/W).

The equation of effective absorption of PV layer can be given as [3.7]:

$$(\tau\alpha)_{pv} = \frac{\gamma_a\gamma_r\lambda_{pv}}{1-(1-\lambda_{pv})r} \quad [3\text{-}39]$$

Where, γ_{al} and γ_{rl} are transmittance of glass cover which is only considering absorption losses and reflection losses, respectively; λ_{pv} is the absorption of the PV layer; r is the reflectance of glass for diffuse radiation.

The equation of output power of the PV layer can be given as [3.7]:

$$E_{pv} = \zeta G\eta_{rc}(1 - \beta_{t\_c}(T_{pv} - T_{rc}) \quad [3\text{-}40]$$

Where, η_{rc} is the electrical efficiency of PV under standard condition (18%); β_{t_c} is the temperature coefficient (0.0045 K^{-1}); T_{rc} is the reference operating temperature (298.15 K).

3.5.3.3 Mathematical model for the micro-channel tube and infill tube

Micro-channel tube acts as the heat exchanger between the refrigerant and the panel. The micro-channel layer can be divided into two parts: the two-phase region and superheated region. As shown in **Fig. 3-19**, the temperature of refrigerant is constant in the two-phase region, while it keeps increasing in the superheated region. Therefore, the temperature is changing in the X direction. The evaporation of refrigerant is taken place in the micro-channel, resulting in a much lower temperature. While the infill tube acts as the fin of micro-channel, storing and transferring energy to micro-channel tube, owning a higher temperature. Therefore, the temperature is also different in the y direction. Based on the inconstant temperature of the tubes, the two-dimensional heat transfer models of them are built.

The equation of infill tube can be given as [2.52]:

$$\rho_{if} C_{p.if} \frac{\partial T_{if}}{\partial t} = \mathrm{K}_{if} \frac{\partial^2 T_{if}}{\partial y^2} + \mathrm{K}_{if} \frac{\partial^2 T_{if}}{\partial x^2} + \frac{1}{A_{if}} \left[(T_{am} - T_{if}) / R_{am\_if} + (T_{pv} - T_{if}) / R_{pv\_if} \right] \quad [3\text{-}41]$$

Where, ρ_{if}, $C_{p.if}$ and K_{if} are the density (kg/m^3), specific heat capacity (J/(kg·K)) and thermal conductivity (W/(m·K)) of the micro-channel tube, respectively; $A_{if}$is the cross-sectional area of the tube wall (m^2); R_{am_if} and R_{pv_if} are the thermal resistance between the infill tube and ambient, PV layer (K/W). The equations of them can be given as [2.52]:

$$R_{am\_if} = \frac{d_{pr}}{K_{pr}} + 1/\alpha_{s\_gc} \quad [3\text{-}42]$$

$$R_{pv\_if} = \frac{d_{sg}}{K_{sg}} \quad [3\text{-}43]$$

Where, d_{pr}, K_{pr} are the thickness (m) and thermal conductivity coefficient (W/(m·K)) of the phenolic resin, respectively; d_{sg}, K_{sg} are the thickness (m) and thermal conductivity coefficient (W/(m·K)) of the silicone grease, respectively.

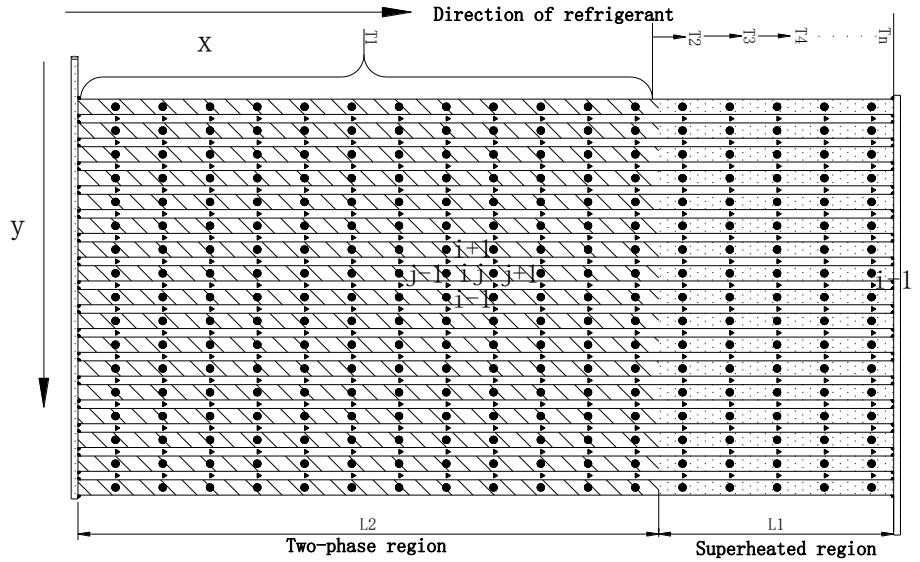

Fig. 3- 19: Structure of the micro-channel layout

The equation of micro-channel tube can be given as [2.52]:

$$\rho_p C_{p.p} \frac{\partial T_p}{\partial t} = \mathrm{K}_p \frac{\partial^2 T_p}{\partial y^2} + \mathrm{K}_p \frac{\partial^2 T_p}{\partial x^2} + \frac{1}{A_p}\left[(T_{am} - T_p)/R_{am\_p} + (T_{pv} - T_p)/ R_{pv\_p} + L_p \alpha_{r\_p}(T_{ref} - T_p)\right] \quad [3\text{-}44]$$

Where, ρ_p, $c_{p.p}$ and K_p are the density (kg/m^3), specific heat capacity (J/(kg·K)) and thermal conductivity (W/(m·K)) of the micro-channel tube, respectively; $A_p$is the cross-sectional area of the tube wall (m^2); L_p is the perimeter of the tube (m); α_{r_p} is the heat transfer coefficient between the tube and refrigerant (W/(m^2·K)).

The heat transfer coefficient of refrigerant in micro-channel in two-phase region can be given as [3.9]:

$$\alpha_{r\_p} = (\alpha_{nb}{}^2 + \alpha_{cb}{}^2)^{0.5} \quad [3\text{-}45]$$

$$\alpha_{nb} = [2345\left(B_o \frac{L_H}{L_F}\right)^{0.7} P_R{}^{0.38}(1-\chi)^{-0.51}](0.023\mathrm{Re}_l{}^{0.8} Pr_l{}^{0.4} \frac{K_l}{D_h}) \quad [3\text{-}46]$$

$$\alpha_{cb} = [5.2\left(B_o \frac{L_H}{L_F}\right)^{0.08} We_{lo}{}^{-0.54} + 3.5\left(\frac{1}{\chi_{tt}}\right)^{0.94} (\frac{\rho_g}{\rho_l})^{0.25}](0.023\mathrm{Re}_l{}^{0.8} Pr_l{}^{0.4} \frac{K_l}{D_h}) \quad [3\text{-}47]$$

$$B_o = \frac{q_H{}''}{\bar{m} h_{gl}} \quad [3\text{-}48]$$

$$P_R = \frac{P}{P_{crit}} \quad [3\text{-}49]$$

$$\mathrm{Re}_f = \frac{D_h(1-\chi)\bar{m}}{\mu_l} \quad [3\text{-}50]$$

$$We_{lo} = \frac{D_h \bar{m}^2}{\rho_l \sigma} \quad [3\text{-}51]$$

$$\chi_{tt} = \left(\frac{\mu_l}{\mu_g}\right)^{0.1} \left(\frac{1-\chi}{\chi}\right)^{0.9} \left(\frac{\rho_g}{\rho_l}\right)^{0.5} \quad [3\text{-}52]$$

Where, α_{nb} and α_{cb} are the nucleate boiling dominant and convective boiling dominant heat transfer coefficient (W/(m^2·K)), respectively; B_o is the boiling number; L_H and L_F are heated perimeter and wetted perimeter of channel (m), respectively; P_R is reduced pressure; Re_l and Pr_l are the superficial liquid reynolds number and prandtl number of the liquid refrigerant; K_l is the thermal conductivity (W/(m·K)); D_h is the hydraulic diameter (m); We_{lo} is the Weber number of liquid refrigerant; χ_{tt} is the Lockhart–Martinelli parameter based on turbulent liquid-turbulent vapour flows; q_H" is effective heat flux averaged over heated perimeter of channel (W); $\bar{m}$ is mass velocity (kg/(m^2·s)); h_{gl} is the latent heat of vaporization (kJ/(kg·K)); μ_l and μ_g are the liquid and vapour dynamic viscosity of the refrigerant (Pa·s).

The heat transfer coefficient of refrigerant in micro-channel in superheated region can be given as [3.10]:

$$\alpha_{r\_g} = 0.0023 \frac{Re_g^{0.8} Pr_g^{0.4} K_g}{D_p} \quad [3\text{-}53]$$

Where, Re_g, Pr_g and K_g are the superficial liquid reynolds number, prandtl number and thermal conductivity (W/(m·K)) of the superheated vapour refrigerant, respectively; D_p is the equivalent diameter of the micro-channel tube (m).

3.5.4 Simulation model for the compressor

The compressor is the power component in the heat pump system, which can raise the pressure and temperature of the vapour from the evaporator. The type of compressor selected in this system is scroll compressor. The models of it include the equation of refrigerant mass flow, equations of the theoretical input power and energy balance of the compressor. These mathematical

models can simplify describe the energy relationship between them, avoiding reducing operation reliability of the simulation program.

3.5.4.1 Mathematic model for the refrigerant mass flow

Normally, the mass flow of refrigerant is an important parameter which presents the refrigerating (heating) capacity of the heat pump system. The refrigerant is the energy carrier of the heat pump system, which absorbs and releases energy with the phase-changing in the evaporator and condenser.

The equation of mass flow of refrigerant can be given as [3.11]:

$$m_{r\_com} = \eta_{gt} n' V_{com} \rho_{r\_com} \quad [3\text{-}54]$$

Where, m_{r_com} is the mass flow of refrigerant (kg/s); $n'$is the rotational speed of compressor (r/s); V_{com} is the displacement per revolution (m^3); ρ_{r_com} is the density of the refrigerant (kg/m^3); η_{gt} is the gas transmission efficiency of compressor.

The equation of gas transmission efficiency can be given as [3.11]:

$$\eta_{gt} = \psi_v \psi_p \psi_T \psi_{lk} \quad [3\text{-}55]$$

$$\eta_{gt} = 0.94 - 0.085[(\frac{P_{out}}{P_{in}})^{\frac{1}{\varrho}} - 1] \quad [3\text{-}56]$$

Where, ψ_v is the volumetric coefficient, which is related to the clearance volume; ψ_p is the pressure coefficient, which is related to the pressure loss during the inspiratory process; ψ_T is the temperature coefficient, which is related to the temperature of cylinder; ψ_{lk} is the leakage coefficient, which is related to sealing level of the compressor; P_{out} and P_{in} are the pressure at inlet and outlet of the compressor (Pa); ϱ is the adiabatic compressibility factor of the refrigerant.

The equation of rotational speed of compressor can be given as [3.11]:

$$n = 2f''/\Pi \quad [3\text{-}57]$$

Where, f'' is the frequency of power input (Hz); Π is the number of poles in the motor.

3.5.4.2 Mathematic model for the input power of compressor

The models of the input power of compressor comprises the theory of input power and the actual input power.

The equation of theory input power of compressor can be given as [3.11]:

$$WI_{com\_to} = \mathrm{n}\eta_{gt} V_{com} \frac{\varpi}{\varpi - 1} \left(\left[\frac{P_{out}}{P_{in}} (1 + \varsigma) \right]^{\frac{\varpi - 1}{\varpi}} - 1 \right) \quad [3\text{-}58]$$

Where, WI_{com} is the theory input power of the compressor (W); ς is the relative pressure loss during the during the compression process; ϖ is the ratio of specific heats at constant pressure and at constant volume.

The equation of actual input power of compressor can be given as [3.11]:

$$W_{com\_ac} = \frac{W_{com\_to}}{\eta_{ie}\eta_{em}} \quad [3\text{-}59]$$

$$\eta_{ie} = 0.36997 \times \left(4.4818 + 1.4772 \times 10^{-2} \times T_{g\_e}\right) \times$$

$$\left(-2.6883 + 2.8745 \times {T_{st}}^{(-0.012584)}\right) \times$$

$$(1.4387 + 3.3657 \times {T_{g\_c}}^{-0.058049}) \quad [3\text{-}60]$$

Where, W_{com_ac} is the actual input power of compressor (W); η_{ie} is the indicated efficiency; T_{g_e}, T_{st} and T_{g_c} are the evaporating, superheated and condensing temperature (K), respectively; η_{em} is the efficiency of the electrical motor.

3.5.4.3 Mathematic model for the compressor

To simplify the model of energy balance of compressor, it is assumed that the temperature of the compressor is constant and equal to the temperature of refrigerant at outlet. The equation of it can be given as [3.12]:

$$M_{com} \mathrm{C}_{p.com} \frac{\partial T_{com}}{\partial t} = \mathrm{Q}_{in} - \mathrm{Q}_{out} \quad [3\text{-}61]$$

Where, M_{com} is the quality of the compressor (kg); $\mathrm{C}_{p.com}$ is the heat capacity of compressor (J/kg.K); T_{com} is the temperature of compressor (K); Q_{in} and Q_{out} are the input and output energy of the compressor (W), respectively.

The input and output energy of the compressor can be given as [3.12]:

$$\mathrm{Q}_{in} = WI_{com\_ac} + m_{r\_com} h_{com\_in} \quad [3\text{-}62]$$

$$Q_{out} = m_{r\_com} h_{com\_out} + \alpha_{com} A_{com} (T_{com} - T_a) \quad [3\text{-}63]$$

Where, h_{com_in} and h_{com_out} are the enthalpy of the refrigerant at the inlet and outlet (kJ/kg), respectively; α_{com} is the total heat transfer coefficient between the compressor and surrounding (W/(m^2·K)); A_{com} is the superficial area of the compressor (m^2).

3.5.5 Simulation model for the condenser

The low-quality energy in the evaporator with low pressure and temperature is improved into high quality by the compressor, and it will be delivered into the condenser in the storage tank. In this section, the mathematic model of refrigerant, the pipe of condenser and water will be analysed. It is assumed that the temperature of water in the tank is constant.

The equation of the refrigerant can be given as [2.52]:

$$Q_{con} = m_{r\_com} (h_{con\_in} - h_{con\_out}) = A_{pc\_in} \alpha_{r\_c} (T_{ref} - T_{p\_c}) \quad [3\text{-}64]$$

Where, Q_{con} is the release energy of the refrigerant (W); the h_{con_in} and h_{con_out} are the enthalpy of the refrigerant at the inlet and outlet of condenser (kJ/kg)); A_{pc_in} is the internal surface area (m^2); α_{r_c} is the heat transfer coefficient between the pipe and refrigerant (W/(m^2·K)); T_{ref} and T_{p_c} are the temperature of refrigerant and copper pipe (K), respectively.

The equation of the pipe of condenser can be given as [3.12]:

$$\rho_{p\_c} C_{p.p\_c} \frac{\partial T_{p\_c}}{\partial t} = \mathrm{K}_{p\_c} \frac{\partial^2 T_{p\_c}}{\partial x^2} + \frac{1}{A_{p\_c}} \left[\pi D_{pc\_in} \alpha_{r\_c} (T_{ref} - T_{p\_c}) + \pi D_{pc\_out} \alpha_{p\_w} (T_w - T_{p\_c}) \right] \quad [3\text{-}65]$$

Where, ρ_{p_c}, $C_{p.p\_c}$ and K_{p_c} are the density (kg/m^3), specific heat capacity (J/(kg·K)) and thermal conductivity (W/(m·K)) of the copper pipe, respectively; A_{p_c} is the cross-sectional area of the copper pipe wall (m^2); D_{pc_in} and D_{pc_out} are the inside and outside diameter (m), respectively; and α_{p_w} is the heat transfer coefficient between the pipe and water (W/(m^2·K)); T_w is the temperature of water in the tank (K).

The equation of the water in the tank can be given as [3.12]:

$$M_w C_{p.w} \frac{\partial T_w}{\partial t} = A_{pc\_out}\, \alpha_{p\_w}(T_{p\_c} - T_w) - \alpha_{tk} A_{tk}(T_w - T_a) - M_{w\_c} C_{p.w}(T_{w\_out} - T_{w\_in}) \quad [3\text{-}66]$$

Where, M_w and M_{w_c} are the quality of water in the tank (kg) and circulating water (kg/s); $C_{p.w}$ is the specific heat capacity of water (J/(kg·K)); A_{pc_out} is the exterior surface area of the copper pipe (m^2); α_{tk} is the total heat transfer coefficient between the tank and surrounding ($W/(m^2 \cdot K)$); A_{tk} is the superficial area of the tank (m^2). T_{w_in} and T_{w_out} are the temperature of water at the inlet and outlet of tank (K).

The equation of the heat transfer coefficient between the pipe and refrigerant (α_{ref_p}) can be given as [3.13]:

$$\alpha_{ref\_p} = \left[1 + 10.3\left(\frac{D_{pc\_in}}{RC}\right)^3\right] \alpha_{ref\_l} \left[(1-\chi)^{0.8} + \frac{3.8\chi^{0.76}(1-\chi)^{0.04}}{Pr^{0.38}}\right] \quad [3\text{-}67]$$

$$\alpha_{ref\_l} = 0.023 \frac{Re_l^{0.8} Pr_l^{0.3} K_l}{D_p} \quad [3\text{-}68]$$

Where, RC is the radius of curvature of coil (m); Re_l, Pr_l and K_l are the superficial liquid reynolds number, prandtl number and thermal conductivity (W/(m·K)) of the refrigerant in condenser, respectively.

The equation of the heat transfer coefficient between the pipe and water (α_w) can be given as [3.12]:

$$\alpha_w = \frac{0.685 Ra^{0.295} K_w}{D_{pc\_out}} \quad [3\text{-}69]$$

$$Ra = GrPr = \frac{g\beta' \Delta T_{p\_w} L^3}{\nu o} \quad [3\text{-}70]$$

Where, Ra is the Rayleigh number; Gr is Grashof number; g is the acceleration of gravity (m/s^2); β' is the thermal diffusivity (m^2/s); ν is the kinematic viscosity (m^2/s); o is the volumetric thermal expansion coefficient of air (K^{-1}); ΔT_{p_w} is the temperature difference between the pipe and water (K); L is the characteristic length (m).

3.5.6 Simulation model for the electronic expansion valve

Electronic expansion valve (EEV) is widely applied in inverter-type heat pump and refrigeration system, because that it can control the mass flow intelligently to match to a wide range of operating conditions.

The accurate simulation model of EEV is very important to ensure the entire system simulation working successfully in steady-state simulation or dynamic simulation. In the dynamic simulation, the opening value of EEV is driven to adjust the mass flow rate into evaporator and push the temperature at outlet of evaporator approaching the set superheat. This real-world mass flow regulation can implement the optimal economic and reliable operating strategies of the heat pump/refrigeration systems. Since the throttling process in the EEV is much faster than the refrigerant processes in the other system components, the transient effects in the EEV can be neglected without significant error in system simulations. Therefore, a steady-state modelling of mass flow characteristics in EEV is also suitable for dynamic modelling.

The equation of mass flow of refrigerant in the EEV can be expressed as [3.14]:

$$m_{ref} = \mathrm{C}_D A_{eev}\sqrt{2\rho_{ref}(p_{eev\_in} - p_{eev\_out})} \quad [3\text{-}71]$$

Where, $m_{ref}$is the mass flow rate (kg/s); A_{eev} is the geometric throat area (mm^2), $\rho_{ref}$is the inlet density of refrigerant (kg/m^3), $p_{eev_in}$and p_{eev_out} are the upstream and downstream pressures (MPa), respectively, C_D is the mass flow coefficient.

As shown in the equation, the mass flow rate in EEV is mainly influenced by inlet condition (pressure, temperature or supercooled), outlet pressure and flow area. Generally, the mass flow rate through the EEV will increase with the rise of supercooled at the EEV inlet. The refrigerant density at the EEV inlet will increase with the increase of supercooled, resulting in higher mass flow rate at the same volumetric flow rate. The mass flow rate increases as the condensing temperature rises for any opening pulse. As the outlet pressure decreases, the mass flow rate increases accordingly until the chocking flow occurs.

The mass flow coefficient can be expressed as [3.14]

$$C_D = 0.689 - 0.015 \times p_{eev\_in} + 0.01 \times p_{eev\_out} + 0.001 \times {p_{eev\_out}}^2 + 0.007 \times \Delta T_{sc} + 0.201 \times A_{eev} - 0.089 \times {A_{eev}}^2 \quad [3\text{-}72]$$

Where, ΔT_{sc} is the supercooled temparature (K).

When the refrigerant through the EEV, it can be regarded as the isenthalpic process. The equation of it can be expressed as [3.14]:

$$h_{eev\_in} = \mathrm{h}_{eev\_out} \quad [3\text{-}73]$$

Where, h_{eev_in} and h_{eev_out} are the enthalpy of refrigerant at the inlet and outlet of EEV (kJ/kg).

3.5.7 Simulation model for the testing room

The energy transferred from the water tank will balance the heat loss from the room to the surrounding, keeping the temperature of the room to meet the requirement of space heating. To simplify the simulation model, it is assumed that the temperature of all the room is constant and the wall of the building would not store energy. The models of circulating water, water pipe and testing room are developed to describe the energy balance between them.

The equation of the circulating water can be expressed as [3.12]:

$$Q_{ro} = M_{w\_c}\mathrm{C}_{p.w}(T_{w\_out} - T_{w\_in}) \quad [3\text{-}74]$$

The equation of the water pipe can be expressed as [2.52]:

$$\rho_{ppr} C_{p.ppr} \frac{\partial T_{ppr}}{\partial t} = \mathrm{K}_{ppr} \frac{\partial^2 T_{ppr}}{\partial x^2} +$$

$$\frac{1}{A_{ppr}}\left[\pi D_{ppr\_\mathrm{in}} \alpha_{w\_ro}(T_{w\_c} - T_{ppr}) + (T_{ppr} - T_{ro})/R_{ppr\_ro}\right] \quad [3\text{-}75]$$

$$\alpha_{w\_ro} = \frac{K_w}{D_{ppr\_in}} \times 0.023 \times Re^{0.8} \times Pr^{0.3} \quad [3\text{-}76]$$

Where, ρ_{ppr}, $C_{p.ppr}$ and K_{ppr} are the density (kg/m^3), specific heat capacity (J/(kg·K)) and thermal conductivity (W/(m·K)) of the PPR pipe, respectively; A_{ppr} is the cross-sectional area of the PPR pipe wall (m^2); D_{ppr_in} is the inside diameter (m); and α_{ro_w} is the heat transfer coefficient between the PPR pipe and water; K_w is the thermal conductivity of water (W/(m·K)); T_{w_c}, T_{ppr} and T_{ro} are the temperature of the circulating water, the PPR pipe and the room (K), respectively; R_{ppr_ro} is the thermal resistance between the PPR pipe and the room (K/W). The equation of it can be given as [3.15, 3.16]:

$$R_{ppr\_ro} = \frac{d_{ml}}{K_{ml}} + \frac{d_{gf}}{K_{gf}} + \frac{d_{pt}}{K_{pt}} + \frac{1}{\alpha_{gf\_ro}} \quad [3\text{-}77]$$

$$\alpha_{gf\_ro} = 2.17(T_f - T_{ro})^{1.31} + 4.98[\left(\frac{T_{gf}+273}{100}\right)^4 - \left(\frac{T_{ro}+271.82}{100}\right)^4] \quad [3\text{-}78]$$

Where, d_{ml}, d_{gf} and d_{pt} are the thickness of the mortar levelling layer, ground floor and pea stone layer (m), respectively; K_{gf}, K_{ml} and K_{pt} are the thermal conductivity of the ground floor, mortar levelling layer and pea stone layer (W/(m·K)), respectively; T_{gf} is the temperature of the ground floor (K).

The equation of the room can be expressed as [3.13]:

$$M_{air}\mathrm{C}_{p.air}\frac{\partial T_{ro}}{\partial t} = (T_p - T_{ro})/R_{ppr\_ro} - U_{ro}A_{ro}(T_{ro} - T_{am}) \quad [3\text{-}79]$$

Where, M_{air} is the quality of air in the building (kg); $\mathrm{c}_{p.air}$ is the specific heat capacity of the air (J/(kg·K)); A_{ro} is the exterior surface area of building (m^2); U_{ro} is the total heat transfer coefficient between the room and surrounding ($W/(m^2 \cdot K)$).

3.5.8 Simulation model for the refrigerant flow pressure loss

Pressure drop is defined as the difference in total pressure between two points of a fluid carrying network. It includes (1) friction pressure drop along a pipe, which is caused by the friction between the fluid and the wall; (2) pressure drop by gravity, which is caused by the different liquid level of the refrigerant; (3) acceleration pressure drop, which is caused by the change of density or velocity; and (4) pressure drop by partial shape, which is caused by the change of flow direction and pipeline shape. Many models of the pressure drop have been studied, and the model developed by Müller-Steinhagen-Heck has a wide range of application, i.e., supercooled region, two-phase region and superheated region. Therefore, in this section, it is adopted to calculate the pressure drop of refrigerant in the pipeline.

The equation of the pressure drop can be expressed as [3.17]:

$$\left(\frac{\partial p}{\partial x}\right)_{ref} = \left\{\left(\frac{dp}{dx}\right)_l + 2\chi\left[\left(\frac{dp}{dx}\right)_g - \left(\frac{dp}{dx}\right)_l\right]\right\}(1-\chi)^{1/3} + \left(\frac{dp}{dx}\right)_g \chi^3 \quad [3\text{-}80]$$

Where, $\left(\frac{dp}{dx}\right)_g$ and $\left(\frac{dp}{dx}\right)_l$ are the friction pressure drop of the refrigerant under the only vapour and only liquid condition (Pa). The equation of them can be expressed as [3.15]:

$$\left(\frac{dp}{dx}\right)_g = \mathrm{f}_g \frac{2(m_{r\_total})^2}{D_{p\_in}\rho_g} \quad [3\text{-}81]$$

$$\left(\frac{dp}{dx}\right)_l = \mathrm{f}_l \frac{2(m_{r\_total})^2}{D_{p\_in}\rho_l} \quad [3\text{-}82]$$

$$f = \frac{0.079}{\mathrm{Re}^{0.25}} \quad [3\text{-}83]$$

$$Re = \frac{m_{total} D_{p\_in}}{\mu} \quad [3\text{-}84]$$

Where, f_g and f_l are the friction factor of vapour and liquid refrigerant; m_{total} is the total mass velocity (kg/(m^2·s)); μ is the dynamic viscosity (N·s/m^2).

3.5.9 Simulation model for the combined micro-channel PV/T based heat pump system

In this section, the models of the electrical efficiency, thermal efficiency and overall efficiency of the micro-channel PV/T panel, the COP of the heat pump will be developed. They are the most important parameters to evaluate the performance of the system.

The equation of the electrical efficiency of micro-channel PV/T panel can be given as [2.52]:

$$\eta_{pv} = \frac{\mathrm{E}_{pv}}{\mathrm{GA}_{pv}} \times 100\% \quad [3\text{-}85]$$

Where, η_{pv} is the electrical efficiency of micro-channel PV/T panel; E_{pv} is the electrical power output of the micro-channel PV/T panel (W); A_{pv} is the area of the PV cell (m^2).

The equation of heat gain of the micro-channel PV/T panel can be given as [2.52]:

$$Q_{eva} = m_{ref\_eva}(h_{eva\_out} - h_{eva\_in}) \quad [3\text{-}86]$$

Where, Q_{eva} is the heat gain of the refrigerant (W); m_{ref_eva} is the mass flow rate of refrigerant (kg/s); h_{eva_in} and h_{eva_out} are the enthalpy of the refrigerant at the outlet and inlet of evaporator (kJ/kg));

The equation of the thermal efficiency of micro-channel PV/T panel can be given as [2.52]:

$$\eta_{th} = \frac{Q_{eva\_in}}{\mathrm{GA}_{pvt}} \times 100\% \quad [3\text{-}87]$$

Where, η_{th} is the thermal efficiency of micro-channel PV/T panel; A_{pvt} is the area of the PV /T panel (m^2).

The equation of the overall efficiency of micro-channel PV/T panel can be given as [2.52]:

$$\eta_{overall} = \eta_{th} + \xi\eta_{pv} \quad [3\text{-}88]$$

Where, $\eta_{overall}$ is the overall efficiency of micro-channel PV/T panel; ξ is the PV cell covering factor of the PV/T panel.

The equation of the COP of the heat pump can be given as [2.52]:

$$COP = \frac{Q_{con\_out}}{WI_{com}} \quad [3\text{-}89]$$

The relative error and mean relative error are applied to analyse the difference between the simulation result and experimental result. The equation of them can be given as [2.52]:

$$RE = \frac{X_{exp} - X_{sim}}{X_{exp}} \times 100\% \quad [3\text{-}90]$$

$$MRE = \frac{\sum_{i=1}^{i=N} |X_{exp} - X_{sim}|}{\sum_{i=1}^{i=N} X_{exp}} \times 100\% \quad [3\text{-}91]$$

Where, RE and MRE are relative error and mean relative error, respectively; X_{sim} and X_{exp} are the simulation and experimental result, respectively.

3.6 Model operation and results discussion

3.6.1 Model operational principle and procedure

The micro-channel PV/T panel is the most important and complicated component in this system. It is the energy source of the heat system, which can directly impact the performance of the entire system.

For the micro-channel PV/T panel, the equations of all the components are all implicitly and discretized. The second-order central differential mode is adopted for the battery substrate equation and the working-tube wall equation. The flow heat transfer equation of the working fluid is discretized by the upwind scheme. Two-order centre scheme model are developed to describe

the equation of PV layer and pipe. The equation of flow heat transfer of the refrigerant is solved by the discrete upwind schemes. The iterative calculation of the above equations is solved by the computer language C.

This project was funded by a Chinese company: Shanxi Jingxu renewable energy Co.,Ltd. To test the stability and reasonability and achieve the operating performance of the system in real-world condition quickly, the system was constructed and an experiment on the system was carried out firstly with the help of the funded company in Lvliang city, China. When the final design of the system was determined, the computer model based on the selected components was developed, and a typical day's weather data was selected as the input parameters to simulate the performance of the system. By comparing the experimental and simulation results, the computer model was verified and adjusted to be able to predict the annual performance of the system. According to the contract, all the achievements about the system belongs to the funded company (data, patent and computer model code), therefore, the computer model code, which included all the details about the system, was the funded company's commercial secret and thus cannot be provided in this thesis.

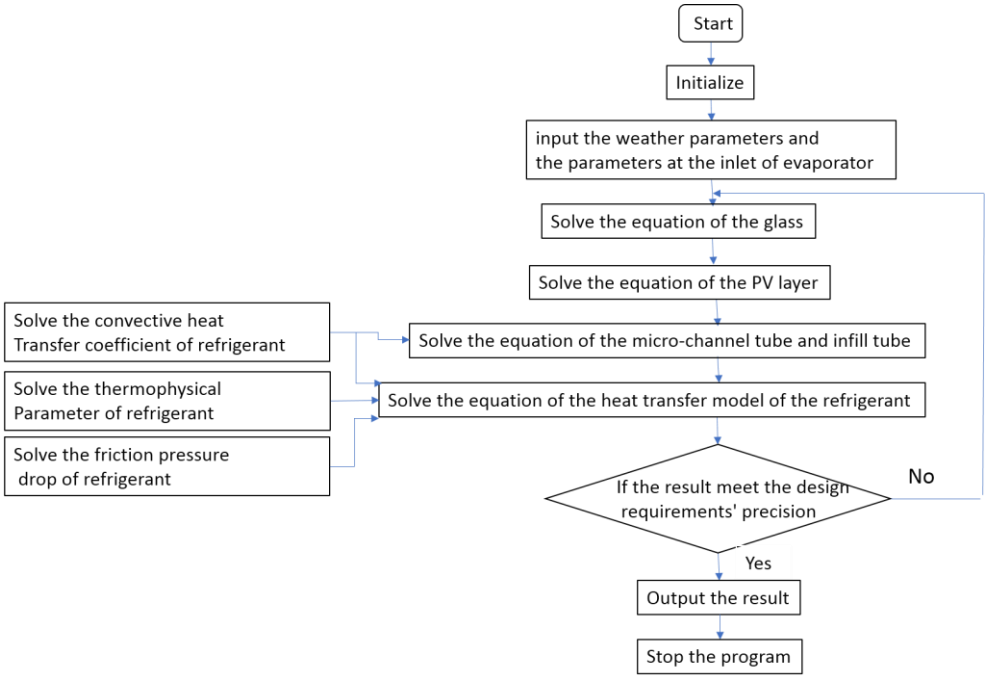

Fig. 3- 20: Calculation flow chart of the micro-channel PV/T

The calculation flow chart of the micro-channel PV/T is shown in the **Fig. 3-20**, and the calculation steps are as follows:

1) Start the program, and initialize the parameters of the micro-channel PV/T panel;
2) Input the weather parameters (solar radiation, ambient temperature, etc.), and input the parameters at the inlet of the evaporator, including the temperature, pressure, mass flow rate and specific enthalpy of the refrigerant;
3) Solve the equation of the glass cover, and calculate the temperature of glass cover T_{gc};
4) Solve the equation of PV layer based on the glass cover temperature T_{gc}, and calculate the temperature of the PV layer T_{pv} and output power of the PV/T panel E_{pv};
5) Solve the equation of the micro-channel tube and infill tube based on the temperature of PV layer T_{pv}, and calculate the temperature of micro-channel tube T_p and infill tube T_{if};
6) Solve the flow heat transfer model of the refrigerant, based on the equation of the mass conservation, equation of momentum conservation and equation of energy conservation. Solve the equations of the convective heat transfer coefficient, the thermophysical parameter and friction pressure drop of refrigerant, and calculate the parameters of the temperature, density, specific enthalpy, dryness, pressure and mass flow of the refrigerant.
7) Check if the calculated value of each parameter has reached the calculation accuracy ($|T_{sim} - T_{set}|/T_{set} < 10^{-3}$, $|P_{sim} - P_{set}|/P_{set} < 10^{-5}$) If no, return to step 3) and continue iterative solution; if yes, then output the results.
8) End the calculation program.

In the solar direct-expansion heat pump system, the input and output of the energy both are rely on the phase changing of the refrigerant; all of the components are related to and connected together by the refrigerant. Therefore, it is very important and necessary to select a reasonable pointcut to simplify the calculation process. The compressor which connected with the both the evaporator and condenser is an appropriate pointcut to calculate the density, mass flow rate, enthalpy of the refrigerant with its assumed temperature and pressure. The calculation flow chart of the heat pump is shown in **Fig. 3-21**, and the calculation steps are as follows:

1) Start the program, and initialize the parameters of all the components in the heat pump system;
2) Input the weather parameters (solar radiation, ambient temperature, etc.), and assume the parameters at the inlet of the compressor, i.e., the pressure, temperature, specific enthalpy, density, the parameter at the outlet, i.e., the pressure, and the inlet pressure of the evaporator;
3) According to compressor inlet parameters and compressor outlet pressure, the parameters such as working fluid mass flow rate, temperature, density, specific enthalpy and power consumption at compressor outlet are calculated;
4) According to the parameters at outlet of the compressor, the condenser model is solved to calculate the heat gain and the temperature of the water in the tank, the parameters of the refrigerant at the outlet of condenser, i.e., the mass flow, temperature, specific enthalpy and density;
5) According to the parameters at the outlet of condenser and the assumed pressure at the inlet of evaporator, the model of the EEV is solved to calculate the mass flow rate through the EEV and the parameters of the refrigerant at the outlet of the EEV;
6) Compare the mass flow rate of refrigerant through the EEV and condenser. If they have the same value ($|M_{ref\_sim} - M_{ref\_set}|/M_{ref\_set} < 10^{-3}$), then go to the next step 7); Otherwise, return to the step 3) and adjust the pressure at the outlet of the compressor to recalculate it again;
7) According to the parameters at the outlet of the EEV, the model of the PV/T panel is solved to calculate the output power of the PV and parameters of the refrigerant at the outlet of the evaporator;
8) Compare the parameters (pressure, specific enthalpy) at the outlet of the evaporator and inlet of the compressor ($|T_{sim} - T_{set}|/T_{set} < 10^{-3}$, $|P_{sim} - P_{set}|/P_{set} < 10^{-5}$). If they have the same values, then go to the next step 9); otherwise, return to step 3) and adjust the pressure at the inlet of the EEV to recalculate it again;
9) Check if the simulation time has reached the set time (450 minters). If no, return to the step 2) and make t = t + dt to calculation it again; if yes, then output the results and end the program.

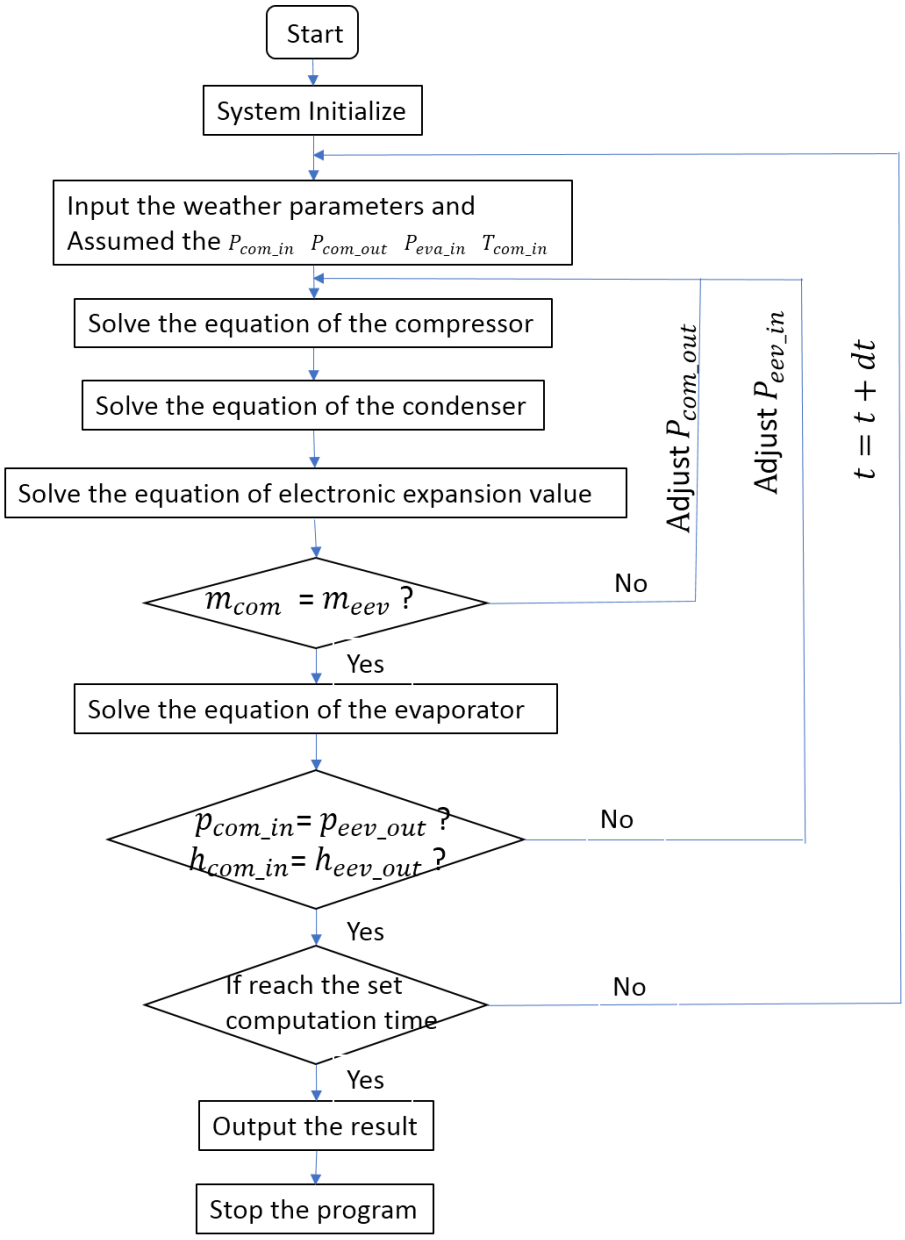

Fig. 3- 21: Calculation flow chart of the heat pump system

3.6.2 Modelling results and discussion

The investigation of this system is carried out in Lvliang City, China. And a typical local sunny day weather data is selected as the input data to simulate the performance of this system. The simulation results are shown in **Fig. 3-22** to **Fig**. **3-28**. **Fig. 3-22** show the variation of solar radiation and ambient temperature of this testing period. The solar radiation increased from 390 W/m^2 to 760 W/m^2 in the morning, and then decreased to 330 W/m^2 in the afternoon. The ambient temperature kept increasing from 6 ºC to 15.3 ºC during the testing time.

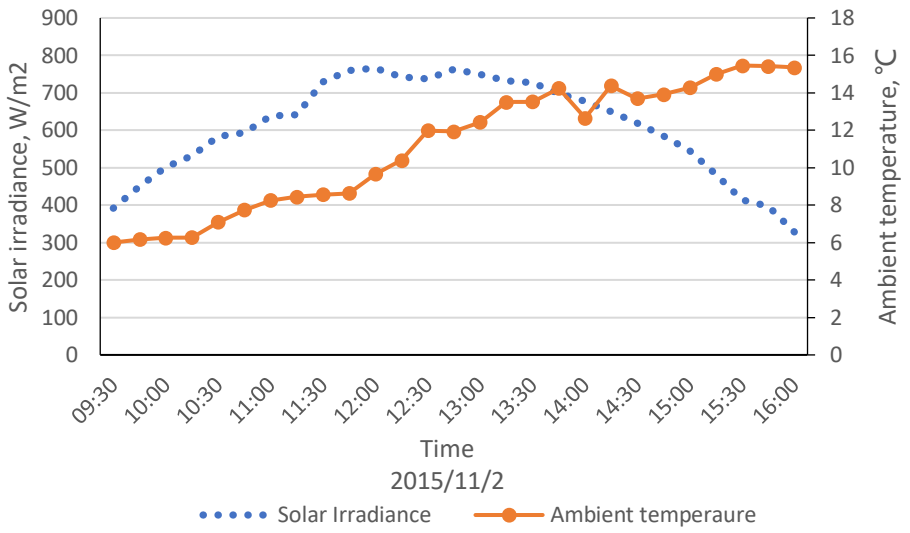

Fig. 3- 22: Variation of the solar radiation and ambient temperature

Fig. 3-23 shows the simulation temperature of the PV/T panels, and the refrigerant temperature at the inlet and outlet of the PV/T panels. The PV/T surface temperature increased from 9:30 to 13:30 and decreased from 13:30 to 16:00. The maximum value of the PV/T surface temperature was 36 ^{o}C, while its initial value at 9:30 was 15 ^{o}C and final value at 16:00 was 19 ^{o}C. This variation is similar to that of the solar radiation but gives 1-hour time lag between the maximum value appearance times of the temperature and the solar radiation. This indicates that the PV/T surface temperature is less affected by the ambient temperature and instead, it was largely impacted by the solar radiation.

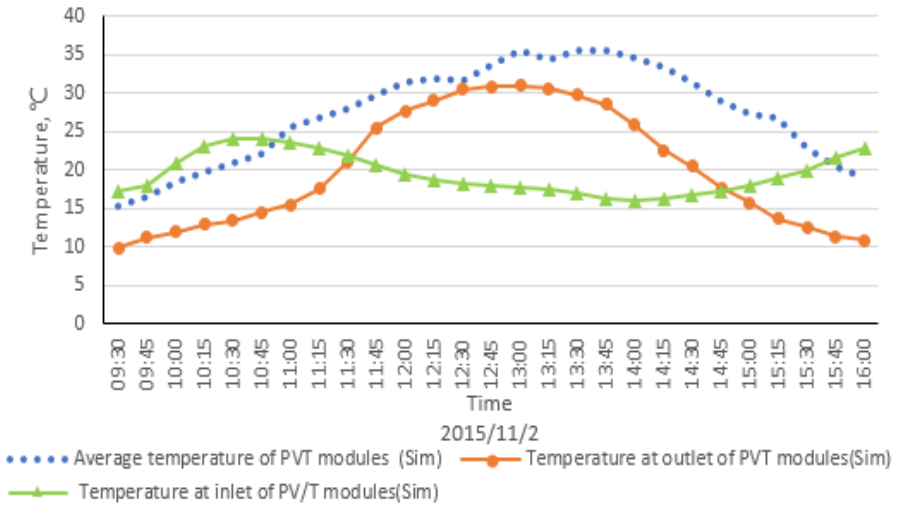

Fig. 3- 23: Simulation temperature of the PV/T panels, refrigerant temperature at the inlet and outlet of the PV/T panels

The temperature of the refrigerant at the outlet of the PV/T modules shows a similar trend of variation as the solar radiation. The reason for this is clear: a higher solar radiation led to a higher thermal energy collection, which resulted in a higher module outlet temperature. However, the temperature of the refrigerant at the inlet of the PV/T modules was found to be stable (at around 20 ^{o}C). This is owing to the use of the automatic expansion valve, which could automatically adjust the expansion rate and give a constant temperature/pressure at the inlet of the PV/T modules (i.e., evaporators).

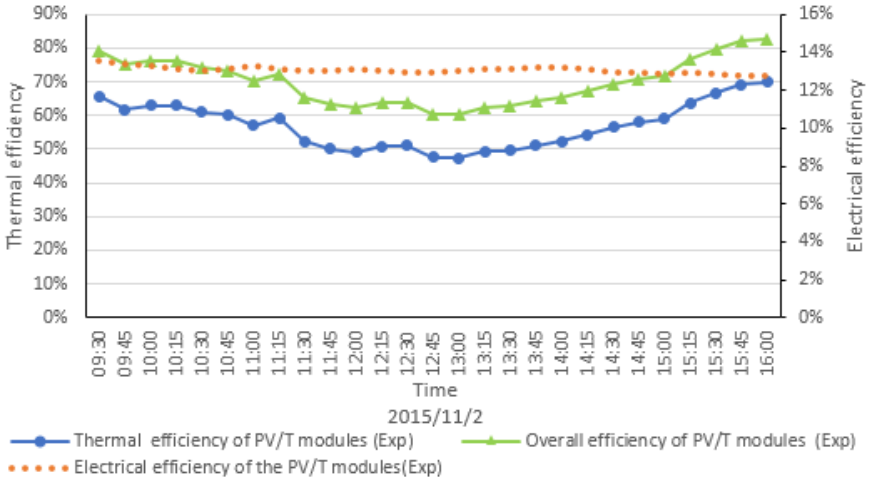

Fig. 3- 24: Simulation results of the electrical, thermal and overall efficiency of the PV/T panels

Fig. 3- 24 shows the simulation electrical, thermal and overall efficiencies of the PV/T panels. It is founded that all the three efficiencies show the opposite trend of variation with the solar radiation, which were higher in the early morning (14.7%, 67.0% and 82.0%, respectively) and in the late afternoon (13.9%, 67.0% and 81.0%, respectively) and were lower during the mid-day time (13.2%, 45.0% and 59.0%, respectively between 12:30 to 13:00). The reason for this is clear: a higher temperature of the modules resulted from higher solar radiation during the mid-day, while the electrical efficiency is depended on the operating temperature (high temperature with low efficiency). When the system operates stable, the evaporating pressure and mass flowrate of the refrigerant (**Fig. 3-26**) is also stable, leading to the stable heat absorption capacity of the system. With the solar radiation increasing, the thermal efficiency shows an opposite variation trend. After the calculation, the average electrical, thermal and overall efficiencies of the PV/T panels are 13.7%, 55.0%, and 68.7%, respectively.

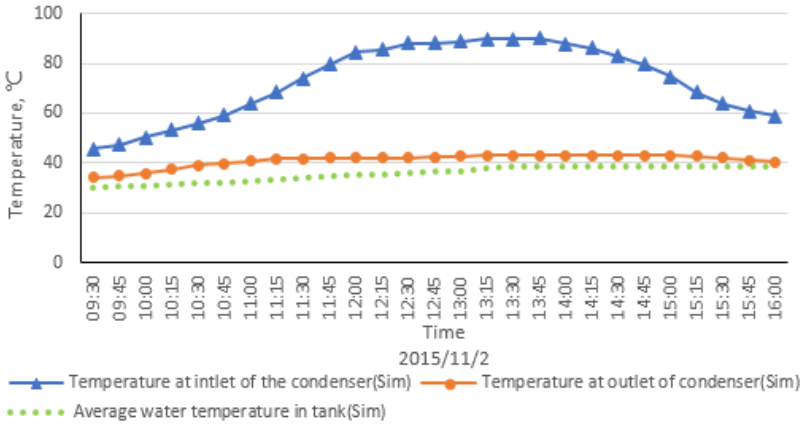

Fig. 3- 25: Simulation temperature of water in the tank, refrigerant temperature at the inlet and outlet of the condenser

As shown in **Fig. 3-25**, the refrigerant temperature at the inlet and outlet of the condenser has a similar variation trend as the PV/T panels, which is also impacted by the solar radiation. With the energy exchange between the water and refrigerant, the temperature of water increases slowly (from 9:30 to 14:00) and then keep stable (from 14:00 to 16:00), which indicates that the input energy from the heat pump system and the output energy to the testing room is nearly balanced in the afternoon.

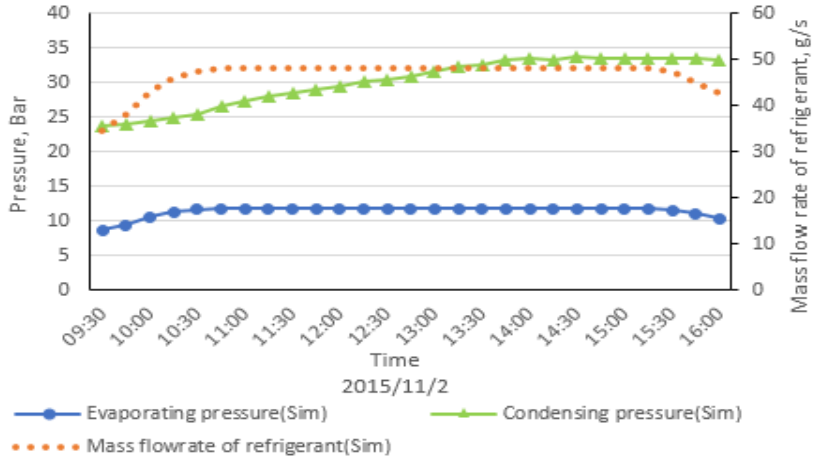

Fig. 3- 26: Simulation results of the refrigerant mass flow rate, the evaporating and condensing pressure

As shown in **Fig. 3-26**, at the earlier hours of the testing, the sharp rising solar radiation resulted in the fast growth of the refrigerant mass flow rate owing to the growing evaporation rate. This led to the sharp increase in the evaporation pressure from 8.6 bar to 11.7 bar within the first hour operation. Afterwards, the evaporation pressure remained relatively stable owing to the

stabilized operational condition of the system. However, the condensation pressure of the system continued to grow over the remaining testing duration, which was resulted from the increased water temperature in the water storage tank (**Fig. 3-25**).

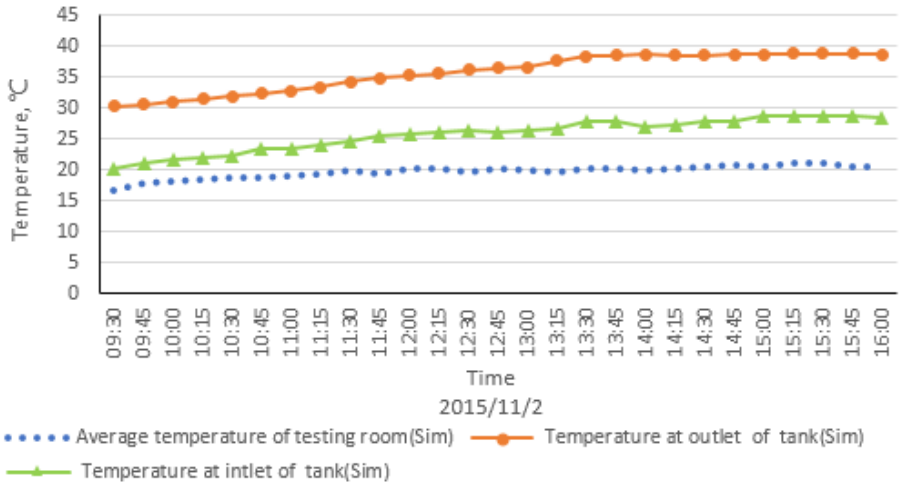

Fig. 3- 27: Simulation temperature of testing room, water temperature at the inlet and outlet of the tank

The water in the tank stores the energy from the heat pump system, and meantime, it goes through the testing room and releases energy for space heating. During this period, the flowrate of the water is set at 0.5 m^3/h. As shown in **Fig. 3-27**, the water temperature at the outlet of the tank is the same as the water temperature in the tank, and the temperature at the inlet shows a similar variation as it releases energy to the testing room. The temperature of the testing house increases slowly from 16 ºC to 20 ºC, and the average value remained at around 18.5 ºC, indicating that the system could provide the required heat capacity effectively.

Fig. 3-28 shows the variations of the simulation COP and compressor input power during this period. It was seen that the COP had a similar trend of variation as to solar radiation. When the solar radiation was rising from 390 W/m^2 to 760 W/m^2 in the morning, the COP of the system was rising from 5.1 to 5.9. When the solar radiation was decreasing from 760 W/m^2 to 320 W/m^2, the COP of the system was falling to 3.4. The average simulation COP of the heat pump system during the single-day period was 5.0. On the other hand, the power input to the compressor was increasing from 2,200 W to 3,070 W during the simulation period, owing to the increased condensation

pressure (**Fig. 3-26**); both the compressor power and condensation pressure had the similar trend of variation, which were all rising throughout the simulation period.

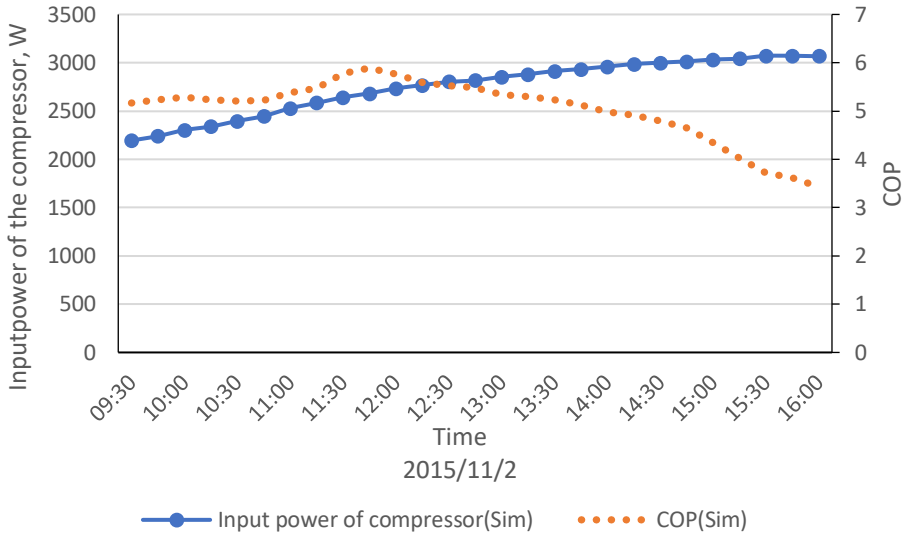

Fig. 3- 28: Simulation results of the input power of the compressor and COP of the system

3.7 Chapter summary

This chapter has described the design concept and working principle of the novelty solar direct-expansion heat pump system for space heating. The outstanding features lay in as the following: (1), the micro-channel PV/T panel acts as the evaporator of the heat pump, which can absorb the solar energy directly with the phase-changing of refrigerant; (2), the low evaporation temperature of the refrigerant can cool down the PV/T panel effectively, reducing the heat loss to surrounding; (3) the micro-channel tube acts as the heat exchanger between the refrigerant and panel, which can increase the vapour flow velocity and generate a higher shear stress exerted upon the film interface, resulting in very high evaporation rate of the liquid on the channel wall. This innovation structure applied in the PV/T panel can increase both the thermal and electrical efficiencies obviously; (4) the PV/T panels can generate electricity annually, which not only can balance the electricity consumption of the heat pump, but also can be sold to government for increasing the income.

The parameters and working principle of all the components in this heat pump are described, including the micro-channel PV/T panel, compressor,

condenser and electronic expansion value. These designed parameters provide fundamental data for the following simulation and experimental test.

Based on the design concept and parameters of all the components, the simulation models of the system are developed, including the thermodynamic parameter of the refrigerant, the sunlight incidence, the components of the system (micro-channel PV/T panel, the compressor, condenser, the EEV and testing room), the heat transfer rate and pressure drop of the refrigerant. In term of the refrigerant, the model of its thermodynamic parameter in saturation region and superheated region are developed, which are the basic data to calculate the heat transfer rate and heat transfer capacity. In term of the sunlight incidence, the model describes the time impaction on the solar radiation during the whole day. In term of the micro-channel PV/T panel, the models of glass cover, PV layer, micro-channel tube and infill tube are built to calculate the temperature of the panel, electrical and thermal efficiencies of it. In term of the compressor and EEV, the models are applied to figure out the mass flow rate of the refrigerant through them, which will be compared to determine the accuracy in simulation programme. In term of condenser, the heat gain of the water in the tank from the condenser and heat output to the building are calculated based on the equations of refrigerant, copper pipe and water tank. The models of the heat transfer rate of refrigerant in the micro-channel tube (evaporator) and copper tube (condenser) are built under the two-phase and superheated condition.

The calculation flow chart of the micro-channel PV/T panel and the entire heat pump system are developed to describe the process and steps of the simulation program. These works completed the preparation for the simulation and experiment testing in practice condition.

The performance of the system is simulated with a selected weather condition. The result indicates that the temperature of the panels, the temperature of refrigerant at the outlet of the panel (evaporator), inlet and outlet of the condenser show a similar variation trend as the solar radiation. The temperature at inlet of the panel (outlet of the electric expansion valve) keeps stable which is impacted by the expansion valve. The simulation average electrical, thermal and overall efficiencies are 13.7%, 55.0% and 68.7%, respectively. The average COP of the system is 5.0. With the solar heat pump

system providing energy for the room, the temperature of the room can remain at 18.5 ^{o}C which is high enough for the space heating.

CHAPTER 4: EXPERIEMNTAL TESTING OF THE SOLAR MICRO-CHANNEL PV/T HEAT PUMP SYSTEM AND MODEL VALIDATION AND REFINEMENT

4.1 Chapter introduction

This chapter introduces the manufacturing process of the components and experimental testing of the solar direct-expansion system in real weather condition. The works will be completed in this chapter are as follows:

(1) All of the components selected in this system are described, especially the innovation component micro-channel PV/T panel;
(2) Based on the selected components and test instruments, the solar direct-expansion heat pump is set up and tested in the real weather condition in a city of China;
(3) Based on the experimental and simulation results under the same real weather condition, the comparison and analysis between them are presented.

4.2 Components selected in the system

This solar direct-expansion heat pump system comprises four components, the micro-channel PV/T panels, a compressor, condenser and electronic expansion valve, which have been introduced in **Chapter 3**. Based on the heat demand of the building, 11 pieces of PV/T panels are selected, and the picture of it are shown in **Fig. 4-1**. 17 micro-channel tubes are welded to two header pipes in parallel mode. Silicone grease is placed between the micro-channel tube and PV layer to enhance the heat transfer. An inverter compressor and frequency converter (**Fig. 4-2**) with the input power of 3.5 kW is selected to push the refrigerant (R410A) to circulate in the heat pump system. The condenser is spiral copper pipe inserted in the water tank (**Fig. 4-3**). The electronic expansion value is composed of the stepper motor driven valves and superheat controller to control the refrigerant mass flow with the set superheated temperature (**Fig. 4-4**).

Fig. 4- 1: Image of the micro-channel layer and PV/T panel

Fig. 4- 2: Image of the inverter compressor and frequency converter

Fig. 4- 3: Image of the condenser

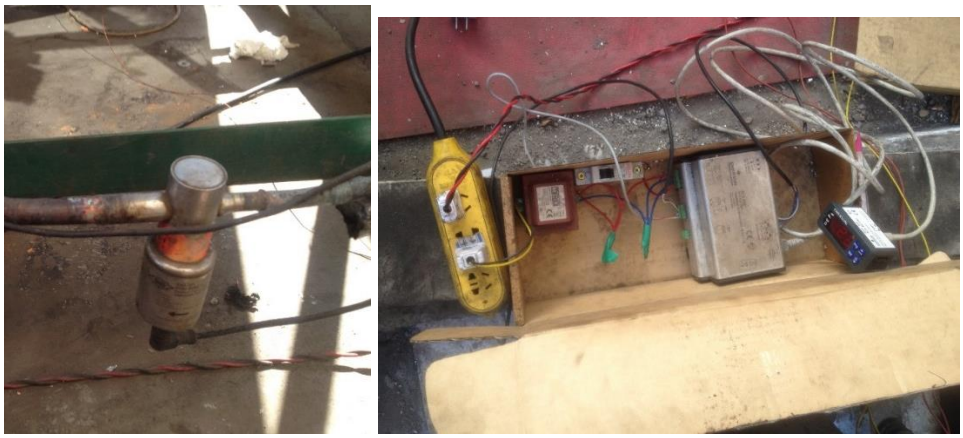

Fig. 4- 4: Image of the EEV and superheat controller

4.3 Measuring components

The parameters of this system need to be collected, including the temperature, pressure, solar radiation, wind speed, mass flow rate and so on. Some measuring instruments are selected and installed to make it. The details of them are as follows:

4.3.1 Thermoelectric couples

The thermoelectric couple is a T-type of thermocouple whose material are copper and constantan, and the accuracy of the measurement is ±0.2 ^{o}C. The ice-water mixture is set as the fixed point and the temperature of the measured point can be calculated by the difference of voltage between them. The picture of the thermoelectric couple is shown in **Fig. 4-5**. The number and place of the thermoelectric couple are listed in **Table 4-1**.

Fig. 4- 5: Image of the thermoelectric couple

Table 4- 1: List of the thermoelectric couples

No	Place	Number	Function
1	Back of PV/T panel	3	Average temperature of the panel
2	Outlet of panel / inlet of compressor	2	Superheated temperature of the refrigerant at outlet of evaporator
3	Outlet of compressor / inlet of condenser	2	Superheated temperature of the refrigerant at inlet of condenser
4	Water storage tank	4	Average temperature of the water in tank
5	Outlet of tank / inlet of building	2	Water temperature at outlet of tank
6	Outlet of building / inlet of tank	2	Water temperature at inlet of tank
7	Three Rooms	3	Average temperature of the testing room
8	Outlet of condenser / inlet of EEV	2	Supercooled temperature of the refrigerant at outlet of condenser
9	Outlet of EEV / inlet of panel	2	Water temperature at inlet of evaporator
10	Under the panel	2	Ambient temperature

4.3.2 Flowmeter and mass flowmeter

The water flowmeter is a liquid turbine flow meter, which is placed at the outlet of the tank (**Fig. 4-6**). It can display and collect the flow rate of the water, and the parameters of it is listed in **Table 4-2**.

Fig. 4- 6: Image of the water flowmeter

Table 4- 2: Parameters of the water flowmeter

Brand	Connector size	Connection type	Test Range	Power	Output
Meacon	DN 25	Thread	0.5-10 m^3/h	DC 24 V	4-20 mA

A mass flow meter is placed at the inlet of the EEV, which is used to collect the quality variation of the refrigerant. The DMF-1 Series mass flow meters are based on the Coriolis force principle, and it is composed of sensor and transmitter. It can measure the fluid mass flow directly without any conversion or fixed on the pressure, temperature, viscosity, density and other parameters. It has the following features: (1) high accuracy (0.1% to 0.2%); (2) wide range of applications (measurable for non-Newtonian fluids, slurries, suspensions, high-viscosity fluids, etc.); (3) low installation requirements (no special requirement on the straight pipe before or behind meter), (4) reliable operation, stability, low maintenance rates. The picture of it is shown in **Fig. 4-7** and the parameters are listed in **Table 4-3**.

Fig. 4- 7: Image of the mass flowmeter

Table 4- 3: Parameters of the water flowmeter

Brand	Connector size	Connection type	Test Range	Working pressure	Power	Output
Sincerity	DN 6	Thread	0.5-100 kg/h	0-25 Mpa	DC 24 V	4-20 mA

4.3.3 Pressure transmitter

The pressure transmitter is supplied by the Huba control company, and it is suitable for different applications in the field of industrial refrigeration due to its application specific pressure connections. Four pressure transmitters are selected to test the pressure of inlet and outlet at the evaporator and condenser. The pictures are shown in **Fig. 4-8** and the parameters are listed in **Table 4-4**.

Fig. 4- 8: Image of the pressure transmitter

Table 4- 4: Parameters of the pressure transmitter

Brand	Connector size	Connection type	Test Range	Working Temperature	Power	Output
Huba	G1/4	Thread	0-30 bar	-40-80°C	DC 24 V	4-20 mA

4.3.4 Solar radiation sensor

The solar radiation sensor is provided by JinZhou TINEL Environment Energy Instrument Co.,Ltd. The type is JTBQ-2, which can measure the radiation from the sun ranging from 0.28-3.2 μm. It is developed according to the principal of photoelectricity conversion. It was placed on the top of the water tank. The picture of it is shown in **Fig. 4-9**, and the parameters are listed in **Table 4-5**.

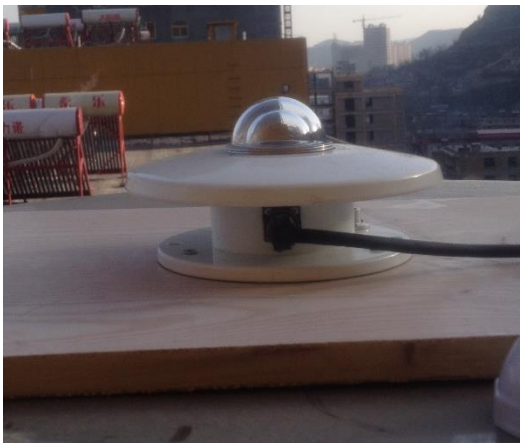

Fig. 4- 9: Image of the solar radiation sensor

Table 4- 5: Parameters of the solar radiation sensor

Model	Sensitivity	Response time	Yearly stability	Power	Output
JTBQ-2	11.675 mv/kw/m^2	<30s	< ±2%	DC 24 V	4-20 mA

4.3.5 Power sensor

The input power of the compressor is measured by the active power sensor, and the output current of the PV/T panel is measured by the DC power sensor. The picture is shown in **Fig. 4-10**, and the parameters of them are listed in **Table 4-6**.

Fig. 4- 10: Image of the power sensor and current sensor

Table 4- 6: Parameters of the AC and DC power sensor

	Model	Input voltage	Input current	Power	Output
AC Power sensor	WBP112S91	AC 220V	AC 20A	DC 24 V	DC 0-5V
DC power sensor	CE-P03-34BS	DC 0-500V	DC 0-5A	DC 24 V	DC 0-10V

4.3.6 Anemometer

An anemometer is fixed on the roof to measure the wind speed. The picture and parameters of it are shown in **Fig. 4-11** and **Table 4-7**, respectively.

Fig. 4- 11: Image of the anemometer

Table 4- 7: Parameters of the anemometer

Brand	Model	Measuring range	Starting speed	Power	Output
Huakong	HS-FS01	0-30 m/s	0.4-0.8 m/s	DC 24 V	0-5 V

4.3.7 Data logger and computer

Two of Agilent 34970A are selected and connected with desk computer as the instrument to collect all the needed data, i.e., the temperature, pressure, mass flow rate, wind speed and output power etc. The picture of it is shown in **Fig. 4-12**.

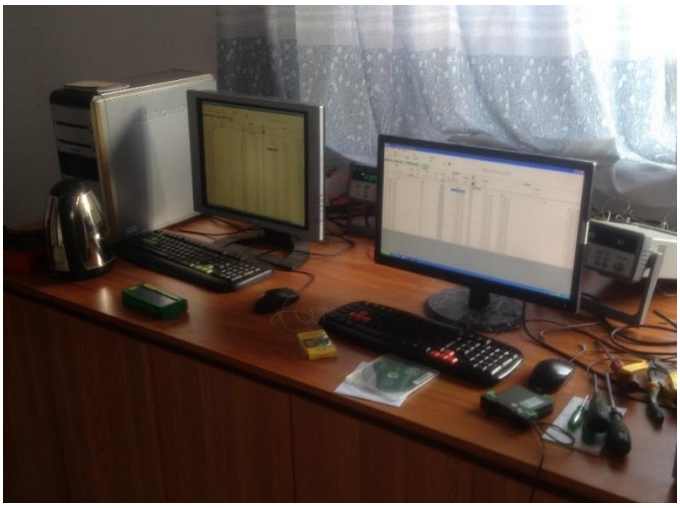

Fig. 4- 12: Image of the data logger

4.4 System installation, commission and testing procedure

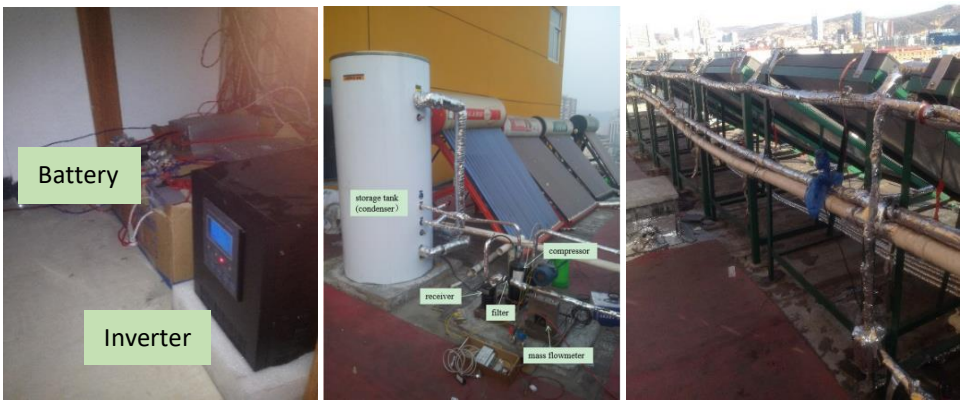

Fig. 4- 13: Image of the PV/micro-channel direct-expansion heat pump system

The experiment was based on a flat space in a high rising residential building, located at Lvliang City of China (**Fig. 4-13**). The flat has a floor area of 150 m^2 which needs heating service throughout the winter, i.e., from November to March. For this space, the maximum heat load is 6.75 kW that occurs in January, while the average heating load is 5.75 kW. The average heat output

of the PV-micro-channel direct expansion heat pump system was designed to be around 9 kW on the sunny day.

Based on the above design and components selection, an integrated experimental direct expansion heat pump system was constructed. This system, as shown in **Fig. 4-13**, was equipped with various measurement instruments and sensors. Within the system, the temperature, pressure and flow rate of the refrigerant and water flows were measured using the thermocouples/temperature probes, pressure transmitters and flow sensor respectively, by implementing them into the appropriate positions; the irradiance of the solar simulator was measured by using a pyrometer; while the power output of the PV/T modules and power input of the compressor were measured by means of two power meters. All the outputs of the sensors and instruments were transmitted into a Data Logger and then to the computer.

The tests were carried out at the real-world operational conditions for a duration between 9:30 and 16:00 in consecutive seven days, from 2nd to 11th November 2015. Lvliang city has a typical dry climatic condition and enjoys sun shining on most of the days in a year. All the testing results were obtained for clear day conditions in the consecutive seven days.

In addition to the sensor/meter arrangement illustrated in **Table 4-8**, further details of the measurement points are as follow: the temperature of each collectors were measured for three points, i.e., at the top, middle and bottom of collector panel. The temperature of the water storage was measured for 4 points to obtain the average water temperature inside the water tank; meanwhile the inlet/outlet temperatures of storage tank were measured as well and the water flow rate to the radiator was measured simultaneously, the data obtained was used to estimate the heat gain by the flat house. The local wind speed was monitored using an anemometer. Two data loggers were used to record the testing results at 15 seconds time interval. The measured data was used to evaluate the performance of the system.

Table 4- 8 List of experimental testing and monitoring devices

Devices	Specification	Quantity	Location
Pressure sensor	Huba 506.931A13101W (Huba Sweden)	4	Evaporator entrance and exit, condenser entrance and exit
Power sensor	WBP112S91(Wei bo China) and CE-P03-32BS(SSET China)	11	Compressor input (AC), PV module output (DC)
Pyranometer	TQB-2 (Sunlight, China)	1	Top of the storage tank
Mass flowmeter	DMF-1-3-A (SINCERITY China)	1	Between the tank and electronic expansion valve
Water flowmeter	LWGY-C(MEACON China)	1	Water tank exit
Thermocouple	0.2 mm copper-constantan (Zhongjia China)	60	PV/T modules/evaporator; collectors/evaporator entrance and exit; condenser entrance and exit; water storage tank; ambient, etc.
Data logger and computing unit	34970A (Agilent, USA)	2	Control room

4.4 Testing results and discussions

The daily average testing results on 2^{th} - 4^{th} and 8^{th} - 11^{th} November 2015 are shown in **Table 4-9**, while the testing results on 5^{th} - 7^{th} were ignored owing the cloud and sunless weather condition during that period. On each single day, the testing was carried out between 9:30 and 16:00.

The performance of the system on a typical day (2^{th} November 2015) are analysed and compared to simulation result. The results are shown in **Fig**. **4-14** to **Fig. 4-20**. The weather data is the same as it used in the simulation program, which is shown in **Fig. 3-22.**

Table 4- 9: Testing results under the selected testing days

Date	Radiation (W/m^2)	Mass flower of refrigerant, g/s	Temperature (°C)						System performance (%)			
2015	G	M_R	T_a	T_{wo}	$T^{'}_{wi}$	$T^{'}_{avg}$	T_o	T_i	η_e	η_{th}	η_{sh}	COP
02/Nov	608.7	47.2	10.9	29.8	30.2	39.1	40.1	30.4	15.4	56.6	69.7	4.7
03/Nov	621.5	48.7	11.3	30.6	31.1	39.3	40.7	30.1	15.4	56.8	69.8	4.65
04/Nov	570.2	44.1	12.1	28.3	30.5	38.9	40.6	30.8	15.4	57.1	70.1	4.72
08/Nov	556.9	43.3	6.8	27.4	30.2	38.4	39.4	30.3	15.5	54.2	67.2	4.68
09/Nov	511.7	39.1	9.3	29.1	30.3	38.6	40.3	30.5	15.4	55.4	68.5	4.65
10/Nov	560.4	43.9	9.5	29.3	30.4	38.8	40.2	30.3	15.4	55.9	68.9	4.66
11/Nov	523.6	41.8	9.4	29.7	30.6	38.2	40.3	30.4	15.4	56.2	69.2	4.66

Fig. 4-14 shows the variation of the experimental temperature of the PV/T panels, refrigerant temperature at the inlet and outlet of the PV/T panels. The PV/T surface temperature and refrigerant temperature at the outlet of panels show a similar trend as the solar radiation. Increasing from 15 ^oC and 13 ^oC at the 9:30, reaching at the maximum value was 36.5 ^oC and 32.5 ^oC at 13:00, dropping to 18 ^oC and 12 ^oC at 16:00. The refrigerant temperature at the inlet of the panels is controlled by the expansion valve, keeping around 20 ^oC.

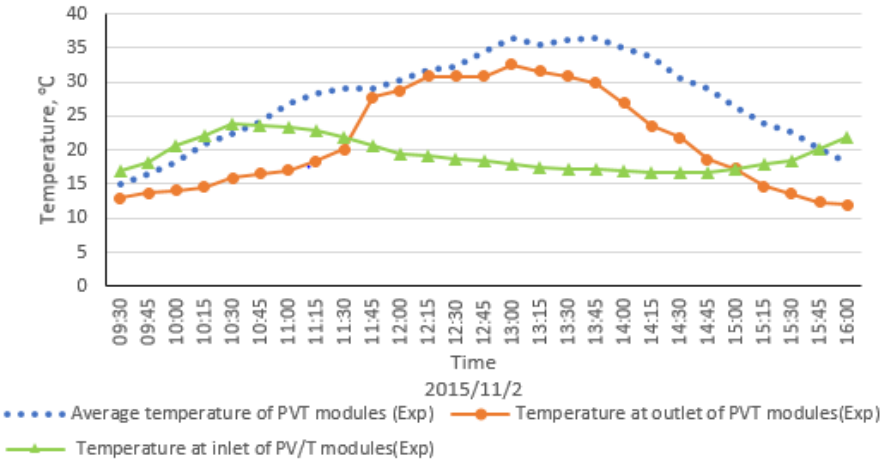

Fig. 4- 14: Experimental temperature of the PV/T panels, refrigerant temperature at the inlet and outlet of the PV/T modules

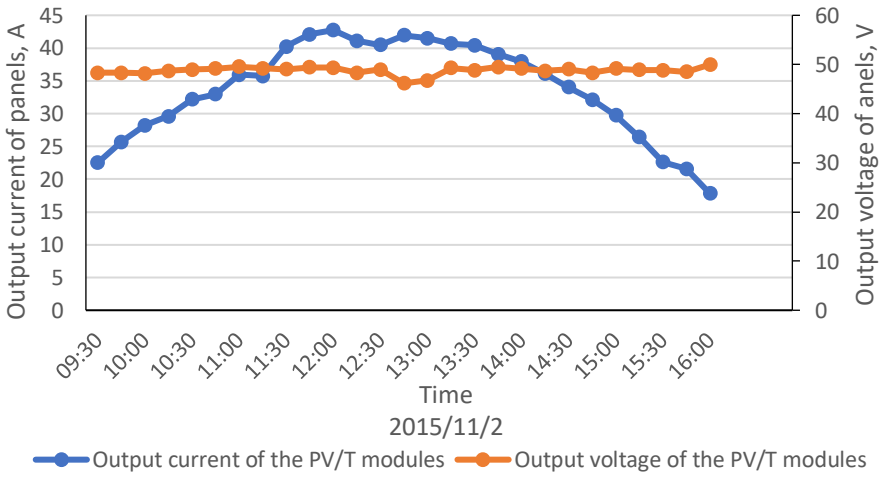

Fig. 4- 15: Output current and voltage of the PV/T modules

Fig. 4-15 shows the variation of the output power of the PV/T models during the testing period. The output voltage of PV/T modules kept at 49 V and the output current show a similar variation trend as the solar radiation, which increased from 22 A to 43 A in the morning and then dropped to 18 A in the afternoon.

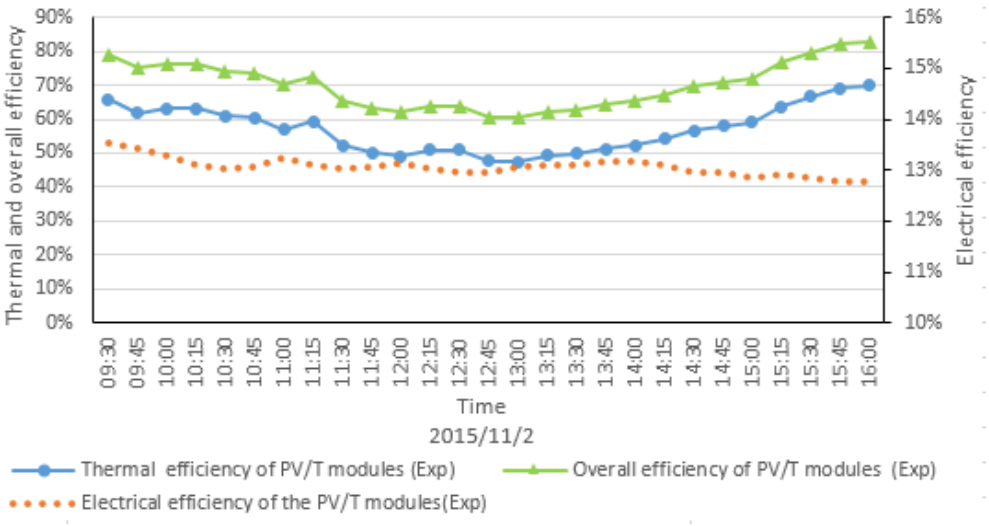

Fig. 4- 16: Experimental results of the electrical, thermal and overall efficiency of the PV/T modules

As shown in **Fig. 4-16**, the experimental electrical, thermal and overall efficiencies of PV/T modules show an opposite trend with the solar radiation, which is impacted by the operating temperature of modules and the working status of the heat pump system. The average value of them are 13.1%, 56.6% and 69.7%, respectively.

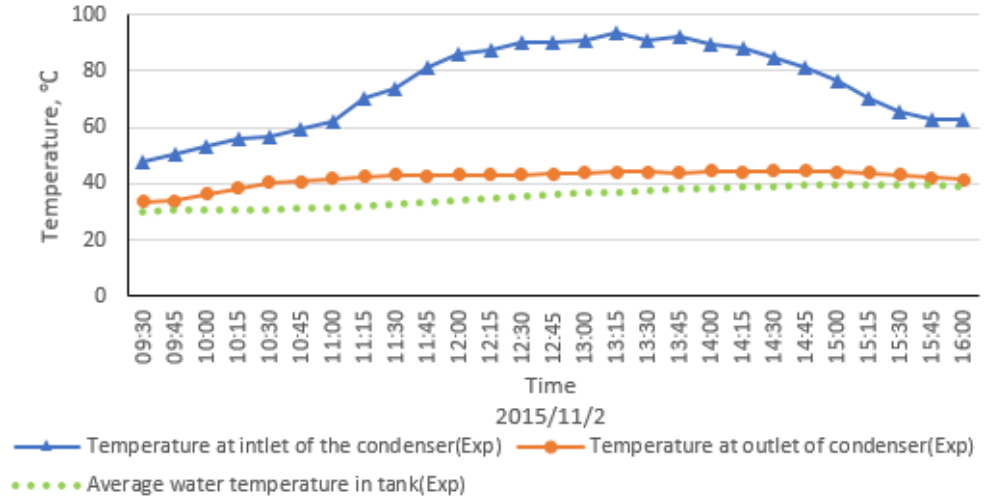

Fig. 4- 17: Experimental temperature of water in the tank, refrigerant temperature at the inlet and outlet of the condenser

As shown in **Fig. 4-17**, the refrigerant temperature at the inlet and outlet of the condenser shows a similar trend as the temperature at the outlet of PV/T modules, which is influenced by the solar radiation. With being heated by the system continually, the water temperature keeps increasing from 30 ^{o}C to 39 ^{o}C.

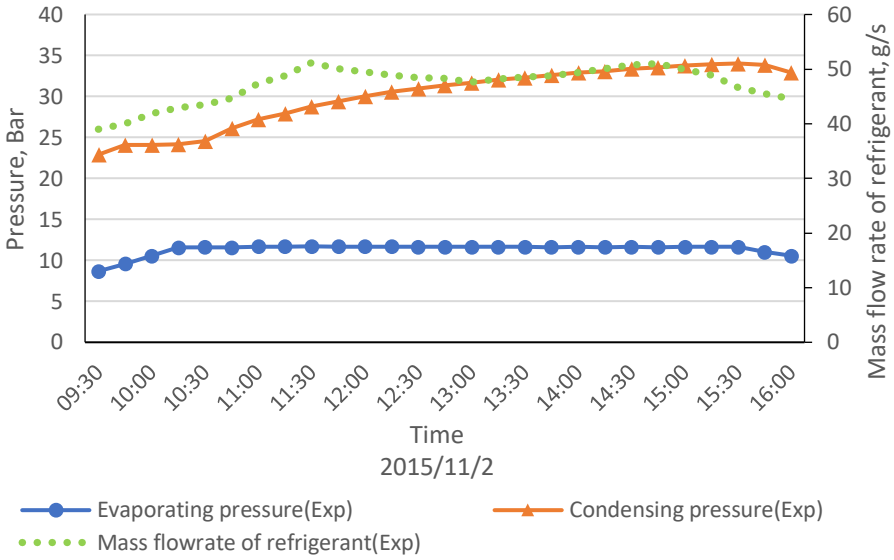

Fig. 4- 18: Experimental results of the refrigerant mass flow rate, the evaporating and condensing pressure

As shown in **Fig. 4-18,** the evaporating temperature and mass flowrate show a similar variation trend, which increase first, then keep stable, and drop finally. With the solar radiation increasing, the energy of the system collected is increasing, too. When the evaporating pressure reach at its limitation, then keep stable, and the mass flowrate is controlled by the evaporating pressure and frequency (50 Hz) of the compressor. Therefore, the mass flowrate shows a similar trend as the evaporating pressure. With the water temperature in the tank increasing, the condensation pressure and temperature increase too, showing a same variation trend.

As shown in the **Fig. 4-19**, the water temperature at the inlet and outlet of the tank show a similar trend, and the temperature difference between them keeps at around 10^{o}C. With the warm water going through the testing room, the room temperature is increasing from 16 ^{o}C to 19 ^{o}C slowly.

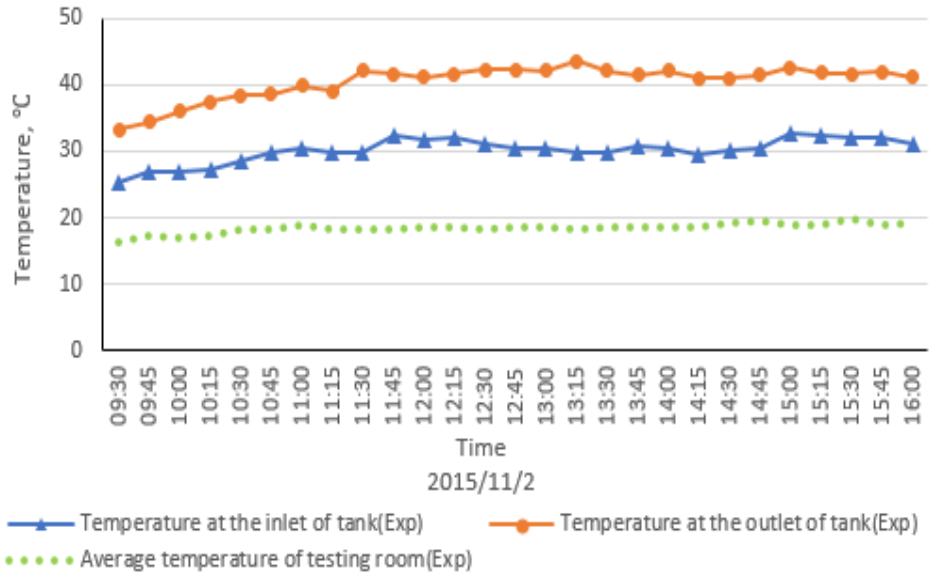

Fig. 4- 19: Experimental temperature of testing room, water temperature at the inlet and outlet of the tank

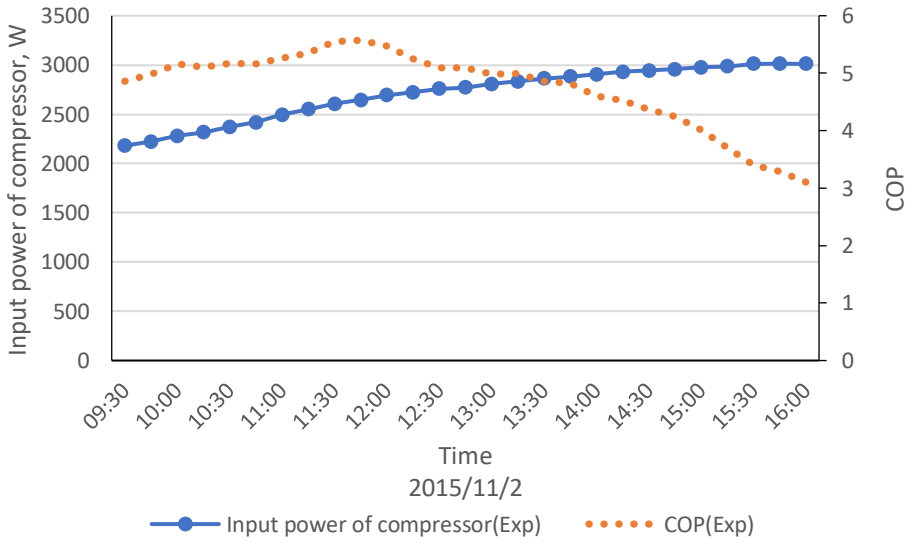

Fig. 4- 20: Experimental input power of the compressor and COP

Fig. 4-20 shows the variations of the experimental COP and compressor power input during the testing period. It was seen that the COP had a similar trend of variation as to solar radiation, and the average COP is 4.7 during the testing period. Owing to the increased condensation pressure (**Fig. 4-18**), the input power of compressor increases slowly from 2,180 W to 3,010 W.

4.5 Model validation/refinement via the comparison between the testing and simulation results

Comparing the simulation and experimental results of the system, it can be found that the variation trend of all the results is the same, i.e., temperature, pressure, flowrate and energy efficiency. The error is mainly from the measurement (temperature, pressure, power) and calculation (efficiency, COP). The comparison between the most important experimental and simulation results (PVT temperature, energy efficiency, COP and room temperature) in one figure are shown from **Fig. 4-21** to **Fig. 4-25**.

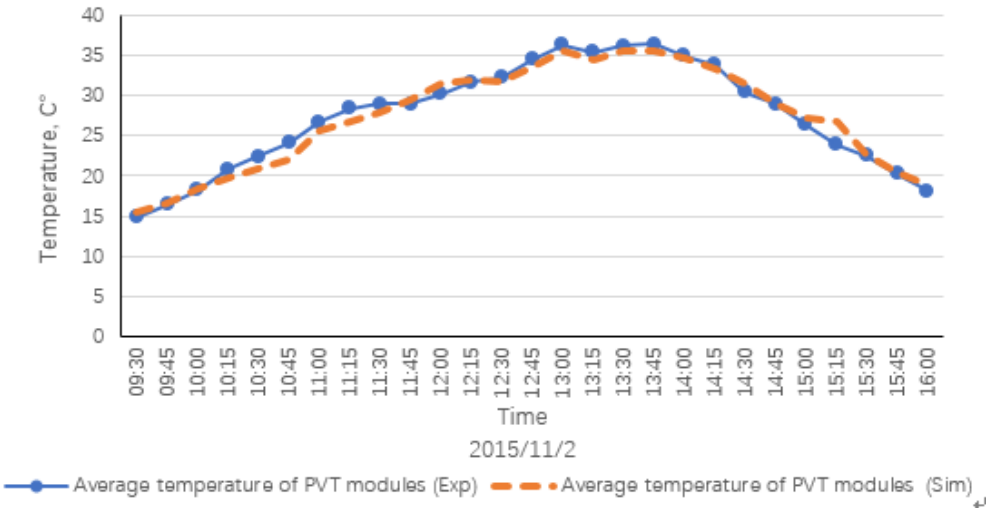

Fig. 4- 21 Variation of the experimental and simulation average surface temperature of the PV/T modules

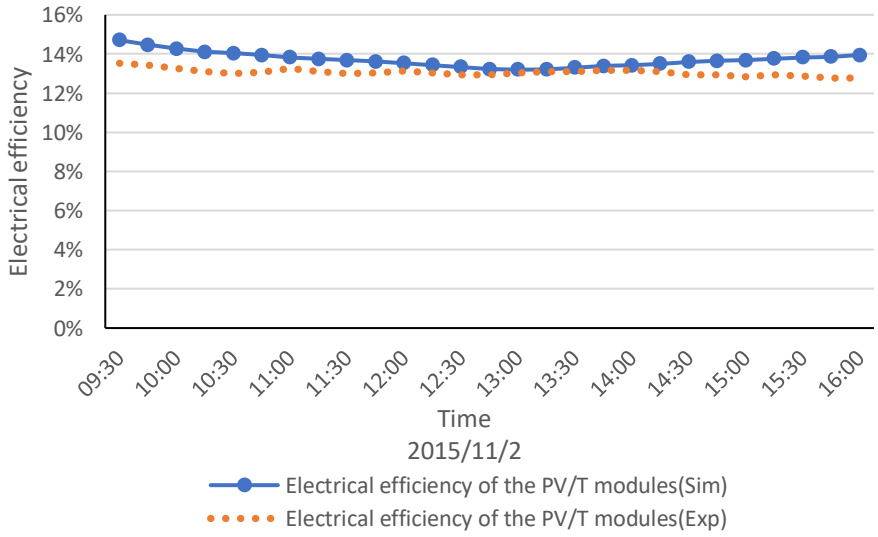

Fig. 4- 22 Variation of the experimental and simulation electrical efficiency of the PV/T modules

Fig. 4-21 and **Fig. 4-22** show the experimental and simulation surface temperature and electrical efficiency of the PV/T modules respectively. The results are good and agree with each other. The maximum temperature difference between them was 2.2 ^{o}C, and the average error is 3.2%. After the calculation, the experimental and simulation results were 13.1% and 13.7%, respectively with the error of 5.0%.

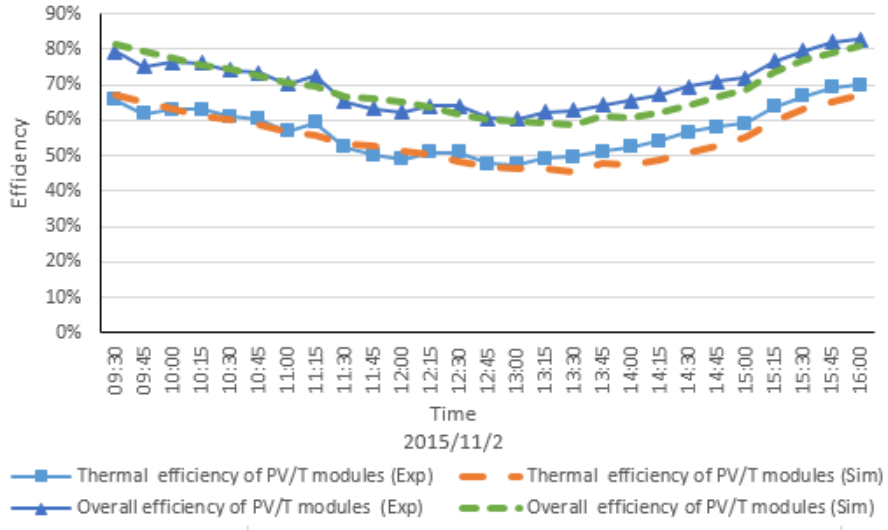

Fig. 4- 23 Variation of the experimental and simulation thermal and overall efficiency of the PV/T modules

Fig. 4-23 shows the variation of the experimental and simulation thermal and overall efficiencies of the PV/T modules during the testing period. The average experimental and simulation thermal efficiency and overall efficiency of the PV/T modules during the testing day were 56.6%, 55.0%, 69.7% and 69.1%, respectively, and the average error of them is 4.8% and 4.3%, respectively.

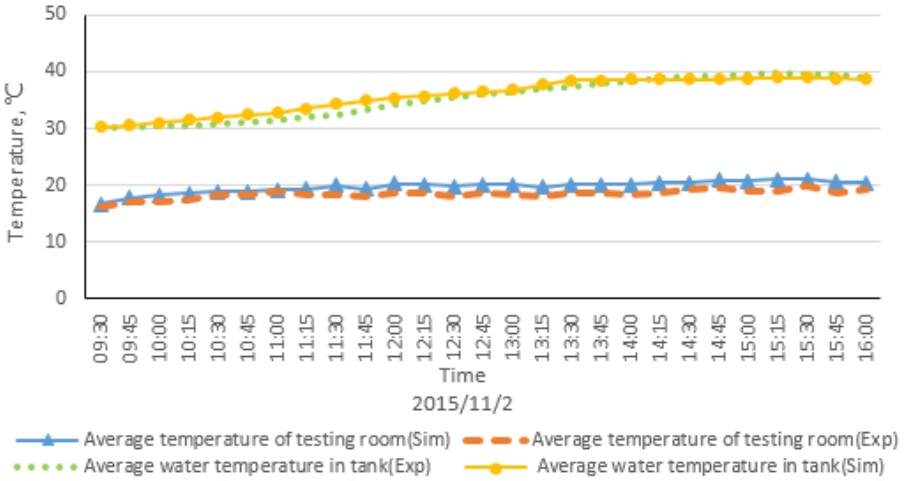

Fig. 4- 24 Variation of the experimental and simulation water temperature in the tank and room temperature

Fig. 4-24 shows the variation of the experimental and simulation tank water and room air temperatures during the testing period. Both them displayed a similar variation trend with small difference between them. The average error of them is 2.3% and 5.2%, respectively.

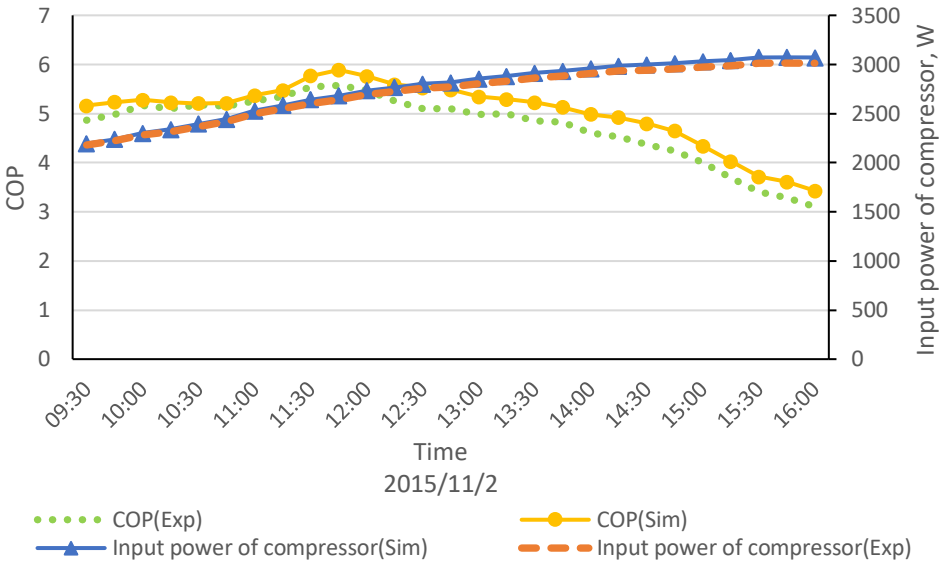

Fig. 4- 25 Variations of the experimental and simulation input power of compressor and COP of the system

Fig. 4-25 shows the variations of the experimental and simulation COP and compressor power input during the testing period. The average experimental and simulation COP of the heat pump system during the single-day period was 4.7 and 5.0, respectively. On the other hand, the power input to the compressor was increasing from 2,200W to 3,000W during the testing period, owing to the increased condensation pressure (**Fig. 4-18**); both the compressor/pump power and condensation pressure had the similar trend of variation, which were all rising throughout the testing period. The average error of them is 1.9% and 6.3%, respectively.

After the calculation, the COP of the compressor has the maximum error which is 6.3%, while the input power of compressor has the mini error which is 1.9%. The average error of the system is shown in **Table 4-10**.

Table 4- 10: Average error of the system and performance

		T	η_{t_pvt}	η_{e_pvt}	η_{o_pvt}	COP
Error	Winter	5.2%	4.8%	5.0%	4.3%	6.3%

The simulation and experimental results match each other very well, and the comparison result between them indicated that the simulation models is reasonable and credible, and it can be used to predict the performance of the system annually in the future.

4.6 Chapter summary

This chapter described the experimental and simulation results of a solar powered direct-expansion heat pump system employing the novel PV/micro-channels-evaporator modules. This system can provide electrical and thermal energy for the residential house annually. The dedicated system design, construction, and field-testing were conducted, and on this basis, the system was investigated in terms of the solar thermal, electrical and overall efficiencies, as well as coefficient of performance (COP), under the real-world operational condition in city of Lvliang, China.

Compared the experimental and simulation results, it was found that the electric power output and thermal energy production of the micro-channel based PV/T module show the similar trend of variation as to the solar radiation. The experimental and simulation electrical efficiencies of the module was stable with an average value of 13.1% and 13.7%, during the single day testing period. Higher temperatures of the PV/T modules resulted from the higher solar radiation led to the reduced thermal and overall energy efficiencies. The average experimental and simulation thermal and overall energy efficiencies of the new PV/T modules are 56.6%, 55.0%, 69.7%, 69.1%, respectively. The COP of the system had a similar trend of variation as to the solar radiation and the average experimental and simulation COP in the testing day was 4.7 and 5.0, respectively.

During the testing time, the room temperature can keep at around 18.5 ^{o}C, which can meet the space heating demand of the selected flat house. This indicated that the system was appropriately designed and configured, and thus can be rated as a highly efficient and practically feasible heat and power system applicable to the cold climatic condition, in particular, to the northern China condition. The results obtained from this experimental work would provide valuable data for the theoretical analysis and further development of the micro channel PV/T heat pump system in the future.

CHAPTER 5: CONCEPTUAL DESIGN AND DEVELOPMENT OF THEORETICAL SIMULATION PROGRAM OF A MINI-CHANNEL PV/T MODULES BASED SOLAR INDIRECT-EXPANSION HEAT PUMP SYSTEM

5.1 Chapter introduction

This chapter describes the design conception of a solar indirect-expansion heat pump system for space heating and hot water employing the mini-channel PV/T and thermal panels. Both the solar direct and indirect expansion heat pump systems have the similar function and used the similar novel heat exchange structure PV/T panel (micro-channel tube and mini-channel tube) which can improve the efficiency of panel as the energy source to provide energy for space heating. Additionally, the heat pump system was installed into them which can improve the energy efficiency. While the solar direct expansion heat pump has the advantage of high efficiency and COP, and the system presented in previous chapter (Chapter 3 and Chapter 4) owns 22 m^2 PV/T panel, but it is wasteful to supply hot water in other seasons, because of its high operating cost. Therefore, the solar indirect expansion heat pump system was introduced and can provide energy for space heating and hot water in different seasons with little operating cost. Compared to the micro-channel tube, which is suitable for two-phase medium, the mini channel tube owns a large size of section and equivalent diameter which make the working fluid inside own low-pressure loss and high flow rate, resulting in low electricity consumption and operating cost. The simulation models based on the all the components in it are developed. It is intended to complete the following task:

(1) Describe the different operational principles based on the different working time, i.e., day time, night.
(2) Present the sketch drawings, construction and features of all the components.

(3) Based on the parameters of the components, the simulation models of them are developed to describe the heat transfer process between them and the performance of the system, i.e., thermal efficiency, electrical efficiency, COP of the heat pump system.

(4) The performance of the system is simulated and analysed based on a real weather data.

These achievements build the foundational works for the theoretical simulation and experimental testing in real weather condition in the future.

5.2 Operational principle in different working condition

The system with the combined solar thermal and PV/T panels and a heat pump is shown schematically in **Fig. 5-1**. The system comprises seven major components: (1) the mini-channel-based solar thermal panels; (2) the mini-channel-based PV/T panels; each of which is the combination of the traditional PV module and mini-channel thermal panel; (3) a heat pump; (4) a heat storage tank; (5) a water pump; (6) a gas heater; and (7) batteries and an inverter. These components were appropriately linked together using the dedicated pipe lines, thus forming a hybrid experimental space heating system that can make use of the benefits of each component.

In view of the IEA SHC-Task 26 for solar combi-systems [5.1], the performance evaluation indicators for the solar heating system with auxiliary heaters are recognized as fractional solar consumption and fractional energy savings. These parameters could be extended to the proposed thermal and PV/T based solar heat pump system. By referring to the literatures relating to performance optimization and analysis of solar combi-system [5.2, 5.3] and local climatic conditions in winter, ratio of the PV/T panels to the total panel areas is estimated, giving a value in the range 0.3 to 0.5. In this application, 10 pieces of micro-channel thermal and 10 pieces of PV/T panels, each with the size of 1000 mm × 2000 mm, are selected.

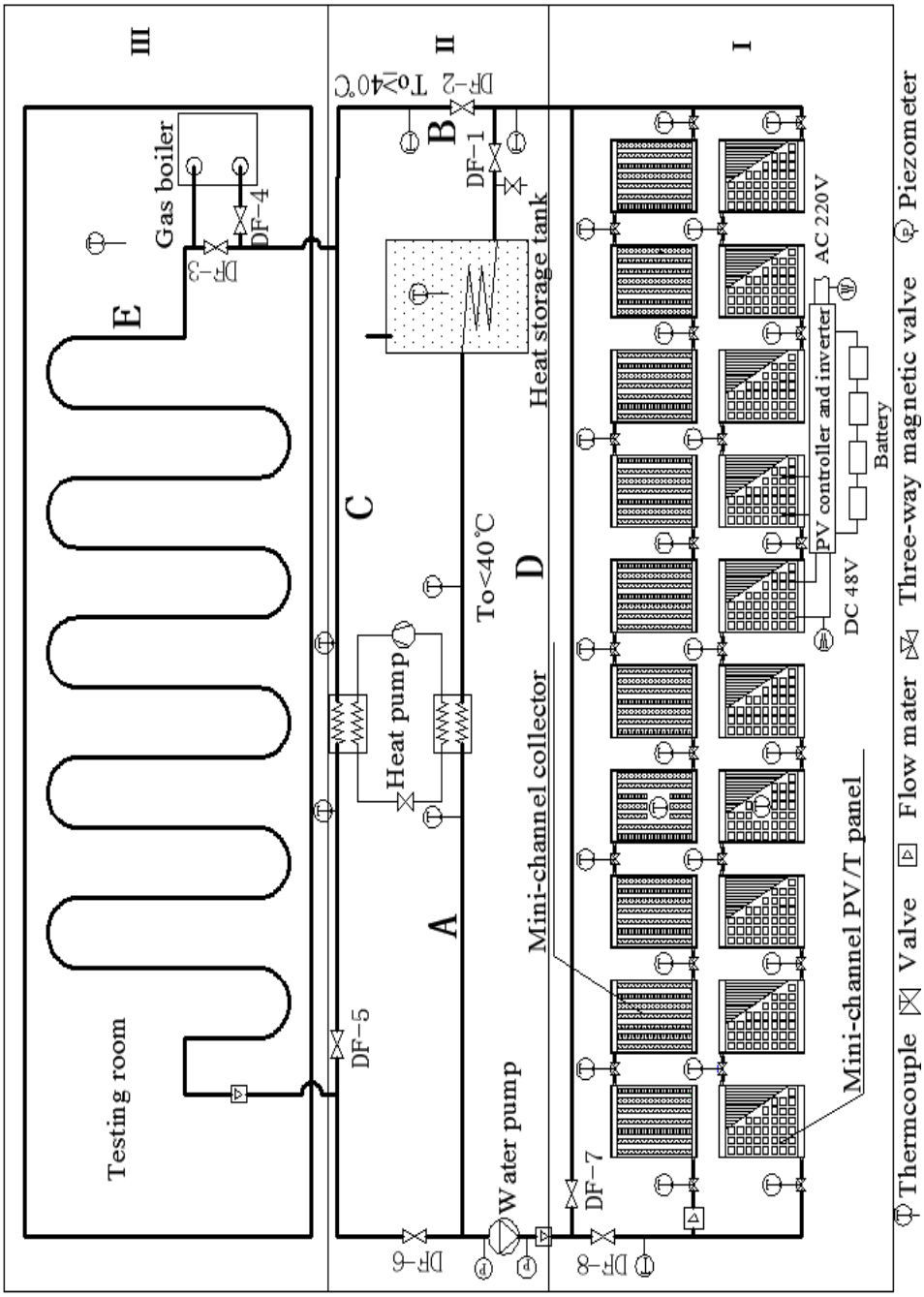

Fig. 5- 1: Schematic of the hybrid space heating system employing the mini-channel solar thermal and PV/T panels and a heat pump

In overall, the proposed system can be divided into three functional parts: (I) energy collection part, (II) energy upgrading and transportation part, and (III) energy releasing part. Within the part I, 10 pieces of solar thermal panels were linked together in series, thus forming the panels-group 1, and 10 pieces of PV/T panels were also linked together in series, thus forming the panels-group 2. The two groups of panels were arranged in parallel to provide hot water to part II and also electricity to the batteries. Meanwhile, a by-pass line

was also incorporated that allows the working fluid to pass through when solar radiation is weak or unavailable, during which the solar thermal and PV/T lines are closed. It should be addressed that the working fluid within the energy collection loop is a mixture of water and an anti-freezing liquid (i.e., glycol); these two fluids have the volume ratio of 60 to 40. Within the part II, which is for energy upgrading and transportation, there are multiple flow paths laid off that allow the working fluid to pass selectively. Within the part III, a heating loop comprising several heat emitters and a heat exchanger is integrated into the service house. This allows the heat carried by the loop fluid to be released to room space, Furthermore, the heating loop has a few channels that allow the fluid from the solar loop to be fed in (via the paths A and B) and the fluid within the loop to be released (via the path E). It should be noted that a gas heater is incorporated in the heating loop and used to deliver the additional heat when the heat from the solar loop is insufficient. It should also be stressed that the same fluid, i.e., mixture of water and glycol, is used in both the heating loop and solar loop, as both are inter-linked.

As shown in **Fig. 5-1**, during the daytime, the system is controlled by the temperature of the fluid at the joint outlet of the two panels groups. If To is less than 40^{o}C, the fluid will travel through the path A. If To is greater than 40 ^{o}C, the fluid will be divided into two parts: one will travel through the heat storage via the path A, continuing to release energy to the heat storage tank, and the second will travel through the path B and then go straight to the heating loop fixed in the part III, thus providing heat required for space heating. During the night time operation, the system was controlled by the time which imposes the function to the heat pump and gas heater. When the temperature of water in the water storage tank is above 15 ^{o}C, the fluid will flow through the paths C and D, where the heat exchange will take place between the working fluid and the refrigerant within the heat pump. When tank water temperature is below 15 ^{o}C, the gas heater will be turned on to replace the heat pump to provide energy for space heating.

5.3 Unique features of the system

The unique features of the system lie in the multiple functions of providing energy for space heating in winter, domestic hot water in other seasons and generating electricity annually to balance the electricity demand of the system.

Compared to traditional flat-plate solar collectors, the mini-channel solar thermal and PV/T panels have the smaller cross-sectional area, higher fluid flow velocity and thus higher heat transfer rate between the heat-carrying fluid and panel walls, thus leading to enhanced solar thermal and electrical efficiencies.

5.4 System components and their performance data

5.4.1 Mini-channel PV/T panels

The mini-channel PV/T panel, as shown in **Fig. 5-2** and **Fig. 5-3**, comprises two major parts: (1) a standard PV panel, which is laminated with one glazed cover (preventing the heat loss and protecting the PV cells), 72 pieces of PV cells (converting solar energy into electricity), two pieces of EVA layers (as the adhesive to connect the cover) and one piece of black TPT layer (as the electrical isolation); (2) a mini-channel thermal panel, which is comprised of an aluminium plate (designed as the fin of micro-channel tubes, to transfer heat between the PV and mini-channel thermal panel), mini-channels (sized 28 mm x 5 mm), the air vent (for cooling down the aluminium plate when no working fluid passes across the channels), the insulation layer, and holding-up framework. The photo is shown in **Fig. 5-4**.

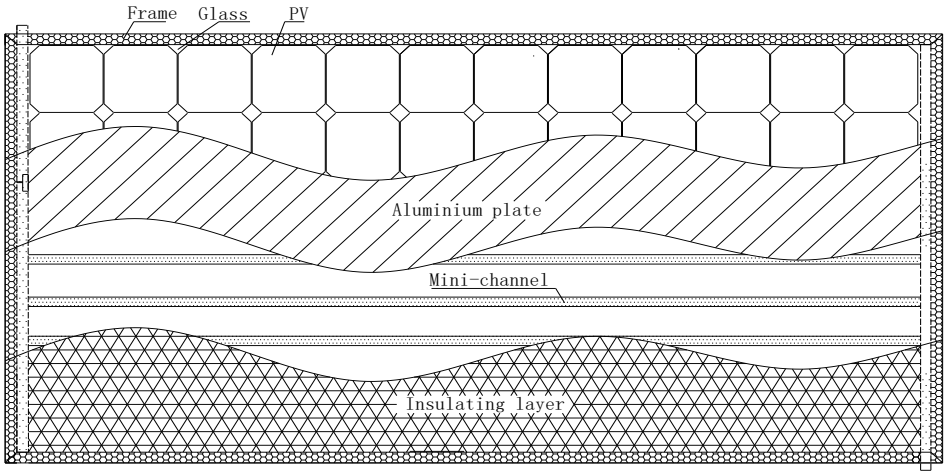

Fig. 5- 2: Structure of the mini-channel PV/T panel

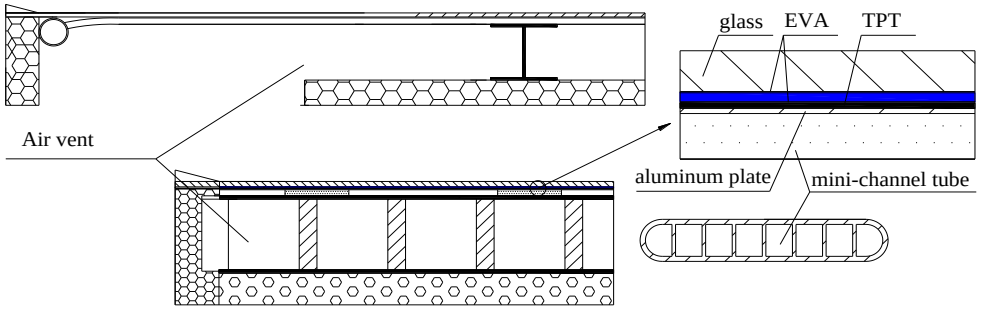

Fig. 5- 3: Sectional view of the mini-channel PV/T panel

Fig. 5- 4: Mini-channel PV/T panel

The mini-channel PV/T panels have a similar structure as the micro-channel PV/T panels, the difference between them are as follows:

5.4.1.1 PV panel

The material of the PV cell selected in this panel is polycrystalline silicon (**Fig. 5-5**), with the size of 156 × 156 × 0.3 mm, number of 72 (12 × 6) and area of 1.752 m^2 per panel. The performance of the PV modules in the panel was measured under the standard testing condition. Thus, giving their technical data listed in **Table 5-1**.

Table 5- 1: Performance parametrical data of the PV modules under the standard testing condition

Item		Value
Electrical efficiency at maximum output power	η_{rc}	17%
Maximum output power, W	E_{max}	310
Output voltage at maximum output power, V	U_{max}	35.2
Output current at maximum output power, A	C_{max}	8.83
Open-circuit voltage, V	U_{oc}	40.2
Short-circuit current, A	C_{su}	8.84

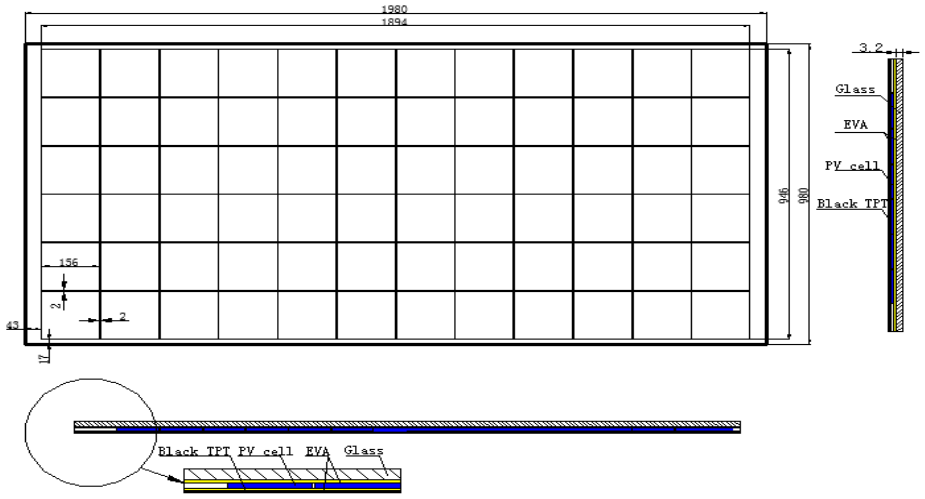

Fig. 5- 5: Drawing of the PV panel

5.4.1.2 Mini-channel layer

The mini-channel layer is composed of a piece of aluminium plate (size 1950 × 950 × 0.4 mm) and mini-channel heat exchanger, which are connected by thermally conductive glue. As shown in **Fig. 5-6**, nine mini-channel tube (**Fig. 5-7**) are welded into the two header pipes in parallel, and each of the header pipes is composed of two blind pipes, which work together to separate the nine mini-channel tubes to be three parts. This structure can increase the flow velocity of the working fluid and form turbulence as well as increase the heat transfer rate.

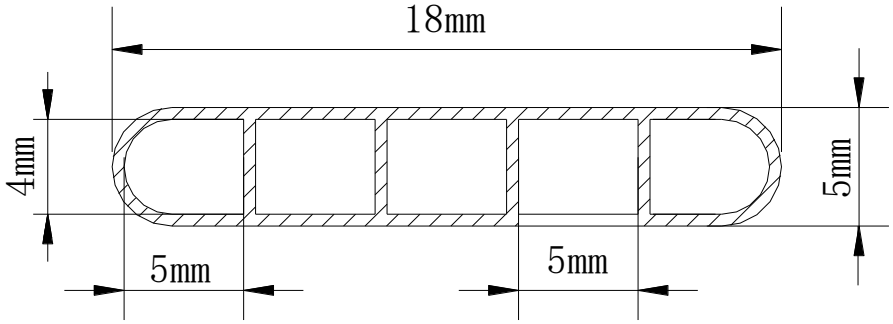

Fig. 5- 6: Drawing of the mini-channel tube

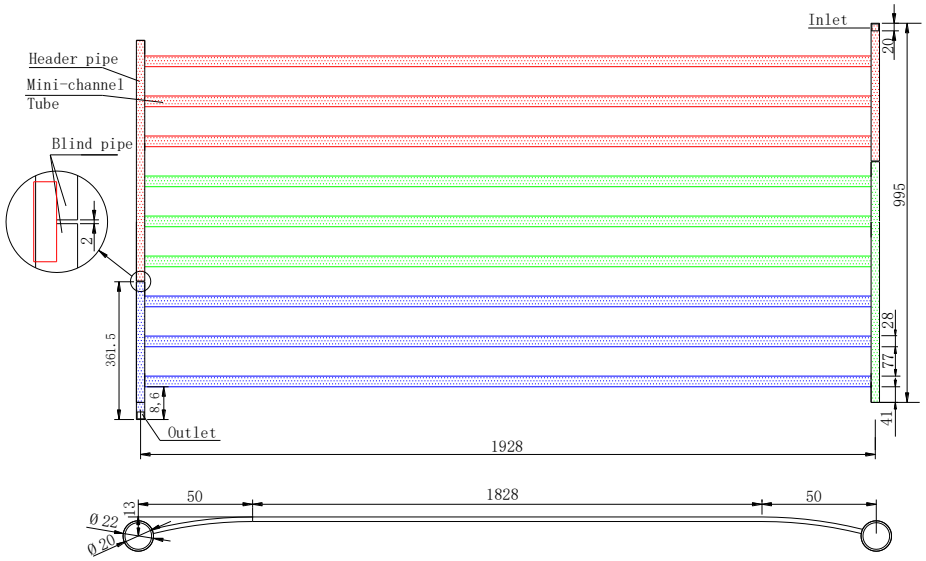

Fig. 5- 7: Drawing of the mini-channel layer

5.4.1.3 Air vent

It is known that the electrical efficiency of the PV/T panel is impacted by its working temperature. When the working temperature increases, the electrical efficiency of PV/T panel will decrease. In winter, the electricity and thermal energy are both needed, hence the air vent is closed and acts as the insulation layer to prompt the PV/T panel operating at high overall efficiency; while in other seasons, the PV/T panels only need to generate electricity, but the high ambient temperature and strong solar radiation will push the PV/T panel working at a very high temperature, impacting the performance of it. Therefore, as shown in **Fig. 5-3**, an air vent is designed under the micro-channel tube to cool down the PV/T panel.

5.4.2 Thermal panel

The mini-channel thermal panels, as shown in **Fig. 5-8** and **Fig**. **5-9**, comprises of (1) the glazed cover, which is to prevent excess heat loss and

protect the thermal panel; (2) the core part, which is a black chrome absorber plate to increase the absorptivity of the panel to solar radiation; (3) the mini-channels layer (28 mm ×5 mm), which has numerous mini-channel rectangular pipes and is connected to the head tubes on both ends; and (4) holding-up framework. The photo is shown in **Fig. 5-10**.

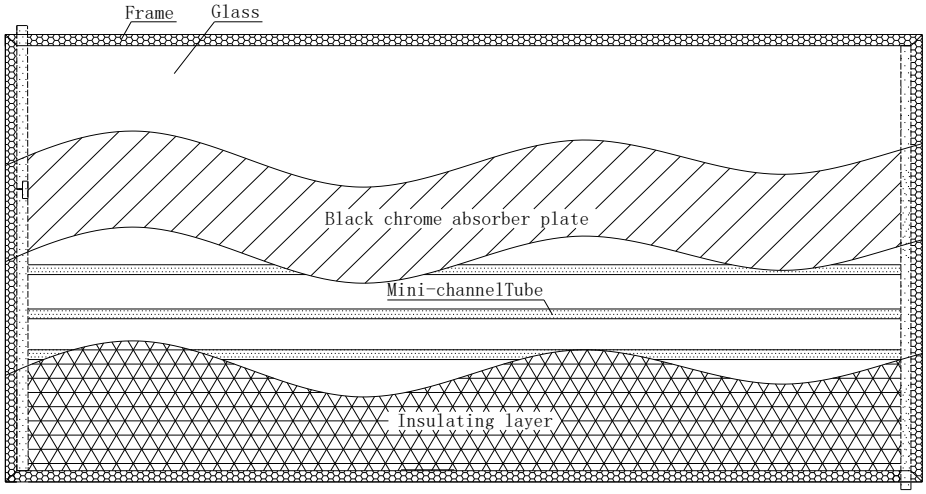

Fig. 5- 8: Front view of the mini-channel solar thermal panel

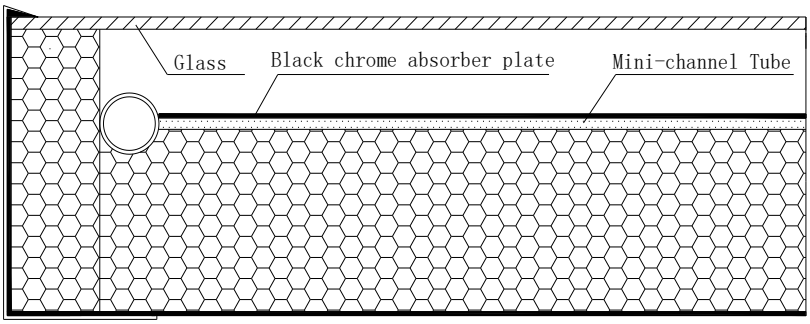

Fig. 5- 9: Sectional view of the mini-channel solar thermal panel

Fig. 5- 10: Image of the mini-channel solar thermal panel

The mini-channel PV/T and thermal panels have the similar structure, while the differences are that (1) an air gap is designed between the glass and absorber, which can prevent the heat loss from the glass cover; (2) the air vent is removed, because of not involving the PV cell.

5.4.3 Heat storage tank

There are two sets of coil-type-heat-exchangers embedded into the heat storage tank, which are dedicated to store heat to the tank water when the solar radiation is high and collect heat from the tank water when solar radiation is low.

The heat storage tank was constructed with multiple functions: (1) reserving the surplus heat from the passing water when the panel temperature is higher than water temperature; (2) delivering the reserved heat to the passing water when the heat pump is turned on. The structural design and photograph of the heat storage tank are shown in **Fig. 5-11** and **Fig. 5-12**, respectively, while its technical data are listed in **Table 5-2**.

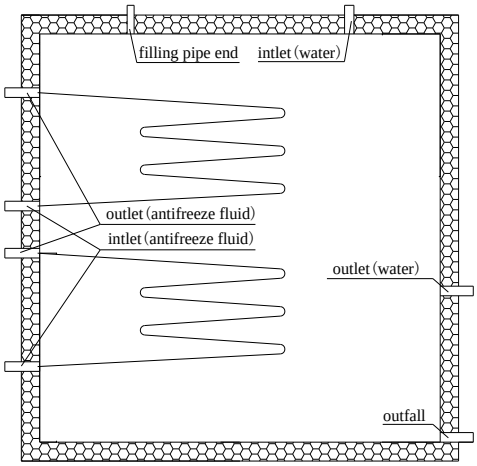

Fig. 5- 11: Structural design of the heat tank

Fig. 5- 12 : Image of the heat tank

Table 5- 2: Parameters of the storage tank

Heat storage tank	**Volume**	**Height**	**Diameter**	**Thickness of insulation**	
	$1m^3$	1,180 mm	1,190 mm	50 mm	
Coil-type-heat-exchanger	**Surface area**	**Quantity**	**Diameter**	**Thickness**	**Length**
	$1.32\ m^2$	2	15 mm	1 mm	14 m

5.4.4 Heat pump

The heat pump is used to upgrade the low temperature energy stored in the solar loop water and feed the upgraded energy into the heating loop. In this system, the heat pump is in operation only at the period when solar radiation is weak and unavailable. The photograph of the selected heat pump is presented in **Fig. 5-13**, while its technical data are listed in **Table 5-3**.

Table 5- 3: Parameters of the heat pump

Brand	**Volume**	**Refrigerant**	**Input power**	**Cooling capacity**	**Heating capacity**
GREE	880×660×1470mm	R-22	2.1 kW	9.9 kW	12 kW

Fig. 5- 13: Image of the heat pump

5.4.5 Gas boiler

The gas boiler is the supplementary heat source which will provide energy for building in the night and rain days. The photograph of the selected gas boiler is presented in **Fig. 5-14**, while its technical data are listed in **Table 5-4**.

Table 5- 4: Technical data of the gas boiler

Brand	Size	Output power	Flow rated	Space-heating area
Renon	750×440×240mm	24 kW	9.4 L/min	170 m^2

Fig. 5- 14: Image of the selected gas boiler

Other system components, i.e., inverter, battery and the testing room, are also selected which has the same parameters as the selected in the solar direct-expansion heat pump system.

5.5 Simulation model

Based on the design concept and parameters of the selected components, the simulation models about the mini-channel thermal and PV/T panel, storage tank, heat pump are developed. These models integrate the data of the solar radiation, flow rate, temperature and heat transfer rate to analyse the performance of the system, including the thermal efficiency, electrical efficiency and COP of the heat pump, while the simulation model of solar radiation is the same as the one which is described in Chapter 3, therefore, only the different models will be developed in this chapter, compared to the solar direct expansion heat pump system. These models set up the foundation for the theoretical analysis and comparison between the simulation and experimental results in the following chapter.

5.5.1 Simulation model for the mini-channel PV/T panel

The mini-channel PV/T panel has a similar structure with the mini-channel PV/T panel, and the simulation models of some parts are the same, i.e., the glass cover. The difference is that an aluminium plate is applied to replace the infill tube as the fin of the mini-channel tube.

5.5.1.1 PV layer

The equation of the PV layer can be given as [2.52]:

$$\zeta d_{pv}\rho_{pv}C_{p.pv}\frac{\partial T_{pv}}{\partial t} = \frac{T_{pv}-T_b}{R_{b\_pv}} + \alpha_{pv\_gc}\left(T_c - T_{pv}\right) + G(\tau\alpha)_{pv} - E_{pv} \qquad [5\text{-}1]$$

Where, T_b is the temperature of the aluminium plate (K); R_{b_pv} is the thermal resistance between PV layer and aluminium plate (K·m^2/W).

5.5.1.2 Aluminium plate

As shown in the **Fig. 5-15**, all the energy has been absorbed by the working fluid in the mini-channel tube, and it is assumed that the temperature is constant in the X direction because of the temperature difference is small enough to be ignored. The plate can be divided into two regions: (1) the first

part which connects the mini-channel directly; (2) the second part which acts as the fin. The models of them are given as follows:

The equation of the first part can be expressed as [2.52]:

$$\rho_b \mathrm{C}_{p.b} \frac{\partial T_b}{\partial t} = \mathrm{K}_b \frac{\partial^2 T_b}{\partial y^2} + d_b[\frac{T_{am}-T_b}{R_{b\_am}} + \frac{T_{pv}-T_b}{R_{b\_pv}} + \frac{T_p-T_b}{R_{p\_b}A_{bi}}] \quad [5\text{-}2]$$

The equation of the second part can be expressed as [2.52]:

$$\rho_b \mathrm{c}_{p.b} \frac{\partial T_b}{\partial t} = \mathrm{K}_b \frac{\partial^2 T_b}{\partial y^2} + d_b[\frac{T_{am}-T_b}{R_{b\_am}} + \frac{T_{pv}-T_b}{R_{b\_pv}}] \quad [5\text{-}3]$$

Where, ρ_b, $C_{p.b}$, d_b and K_b are the density (kg/m^3), specific heat capacity (J/(kg·K)), thickness (m) and thermal conductivity (W/(m·K)) of the aluminium plate, respectively; R_{b_am}, R_{b_pv}, R_{p_b} is the thermal resistance between the aluminium plate and ambient, PV layer and mini-channel tube (K/W). A_{bi} is the heat exchange area of the selected microelement (m^2), and the equation of it can be given as [2.52]:

$$A_{bi} = W_b \times dy \quad [5\text{-}4]$$

Where, W_b is the length of the panel (m); dy is the width of the selected microelement (m).

$$R_{p\_b} = d_{hcg}/(K_{hcg}A_{p\_b}) \quad [5\text{-}5]$$

Where, d_{hcg} and K_{hcg} are the thickness (m) and thermal conductivity (W/(m·K)) of the heat-conducting glue, respectively; A_{p_b} is the contact area between the mini-channel tube and aluminium plate (m^2).

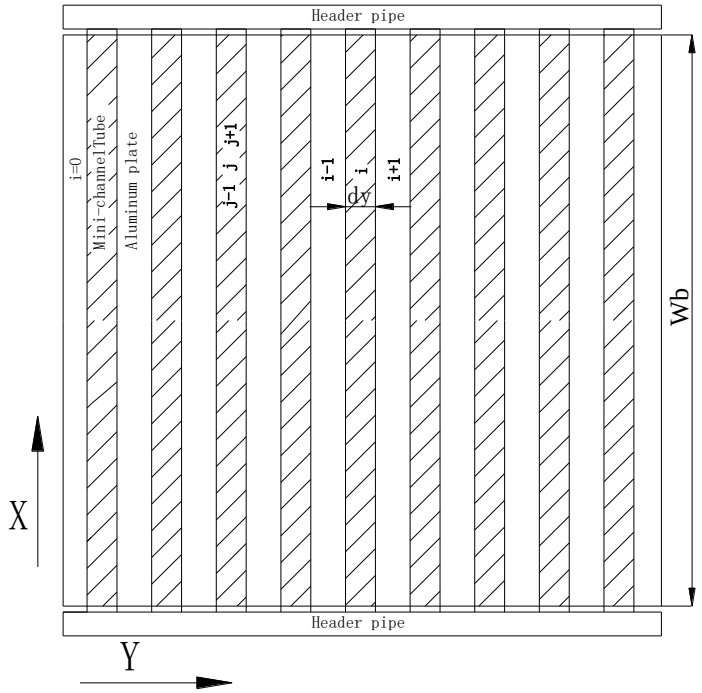

Fig. 5- 15: Drawing of the aluminium plate

5.5.1.3 Mini-channel tube

The mini-channel tube is the heat exchanger where the solar energy is taken away by the working fluid, the equation of it can be given as [2.52]:

$$\rho_p C_{p.p} \frac{\partial T_p}{\partial t} = \mathrm{K}_p \frac{\partial^2 T_p}{\partial y^2} + \frac{1}{A_p}\left[(T_b - T_p)/R_{b\_p} + L_p \alpha_{wf}(T_{wf} - T_p)\right] \qquad [5\text{-}6]$$

Where, T_{wf} is the temperature of the working fluid (K); α_{wf} is the heat transfer coefficient between the tube and working fluid (W/(m^2·K)), and the equation of it can be given as [2.52]:

$$\alpha_{wf} = \frac{K_{wf}}{D_{mc}} \times 0.023 \times Re^{0.8} \times Pr^{0.3} \qquad [5\text{-}7]$$

Where, K_{wf} is the thermal conductivity of the working fluid (W/(m·K)); D_{mc} is the equivalent diameter of mini-channel tube (m).

5.5.1.4 Working liquid in mini-channel tube

The working liquid is used to transfer the heat from the panel to the storage tank. The node division is shown in **Fig. 5-13**, and the equation of it can be given as [2.52]:

$$m_{wf} C_{p.wf} \frac{\partial T_{wf.j}}{\partial t} + \dot{m_{wf}} C_{p.wf}\left(T_{wf.j} - T_{wf.j-1}\right) = (T_a - T_{wf.j})/R_{wf\_am} + (T_p - T_{wf.j})/R_{wf\_p} \qquad [5\text{-}8]$$

Where, m_{wf} is the quality of the working fluid in a single control volume (kg); $\dot{m_{wf}}$ is the mass flow rate through a single-piece tube (kg/s); C_{wf} is the specific heat capacity of the working fluid (J/(kg·K)); R_{wf_am} is the total thermal resistance between the working fluid and the external environment (K/W); R_{wf_p} is the thermal resistance between the working fluid and mini-channel tube (K/W).

5.5.2 Simulation model for the mini-channel thermal panel

The mini-channel thermal panel has a similar structure as the conventional thermal collector. The model of the glass cover, absorber and mini-channel tube are developed. The difference between them are as blow.

5.5.2.1 Glass cover

To simplify the simulation model, it is assumed that the temperature of the glass cover is constant. The equation of it can be given as [5.1]:

$$d_{gc}\rho_{gc}C_{p.gc}\frac{\partial T_{gc}}{\partial t} = \alpha_{am\_gc}(T_{gc} - T_{am}) + \alpha_{s\_gc}(T_{gc} - T_s) + \alpha_{b\_gc}(T_{gc} - T_b) + G\alpha_{gc} \quad [5\text{-}9]$$

$$\alpha_{b\_gc} = \sigma(T_b{}^2 + T_{gc}{}^2)(T_b + T_{gc})\frac{1}{\frac{1}{\varepsilon_b}+\frac{1}{\varepsilon_{gc}}-1} + \frac{Nu\cdot K_{air}}{l} \quad [5\text{-}10]$$

Where, α_{b_gc} is the heat transfer coefficient between the glass cover and absorber (W/(m^2·K));T_b and ε_b are the temperature (K) and emissivity of the absorber, respectively; K_{air} is the thermal conductivity of the air (W/(m·K)); l is the thickness of the air gap (m); Nu is the Prandtl number of the air between the glass cover and absorber, which can be expressed as [5.2]:

$$Nu = 1 + 1.14\left(1 - \frac{1708\times(\sin 1.8\beta)^{1.6}}{Ra\times\cos\beta}\right)[1 - \frac{1708}{Ra\cos\beta}]^{+} + [(\frac{Ra\times\cos\beta}{5830})^{1/3} - 1]^{+} \quad [5\text{-}11]$$

Where, β is the angle of inclination of the plane with the horizontal; Ra is the Rayleigh number. + presents that if the figure in the$[\quad] > 0$, then keep on, if not, the figure will be set at 0.

5.5.2.2 Absorber plate

The simulation models of the absorber plate are similar with the aluminium plate, they are divided into two parts: (1) the first part which connects the mini-channel directly; (2) the second part which acts as the fin. The models of them are given as follows:

The equation of the first part can be expressed as [2.52]:

$$\rho_b \mathrm{C}_{p.b} \frac{\partial T_b}{\partial t} = \mathrm{K}_b \frac{\partial^2 T_b}{\partial y^2} + d_b[\frac{T_{am}-T_b}{R_{b\_am}} + \frac{T_{gc}-T_b}{R_{b\_gc}} + \frac{T_p-T_b}{R_{p\_b}A_{bi}} + G(\tau\alpha)_b] \quad [5\text{-}12]$$

The equation of the first part can be expressed as [2.52]:

$$\rho_b \mathrm{c}_{p.b} \frac{\partial T_b}{\partial t} = \lambda_b \frac{\partial^2 T_b}{\partial y^2} + d_b[\frac{T_a-T_b}{R_{b\_a}} + \frac{T_c-T_b}{R_{b\_c}} + G(\tau\alpha)_b] \quad [5\text{-}13]$$

Where, $(\tau\alpha)_b$ is the effective absorptance of the absorber plate.

5.5.3 Simulation model for the water storage tank

The water in the tank will be heated by the working fluid which is from the panels, storing the surplus energy and acting as the energy source of the heat pump. The models of working fluid, heat exchanger pipe and water in the tank are developed. It is assumed that the temperature of the water in it is constant.

The equation of the working fluid can be given as [3.12]:

$$\mathrm{Q}_{wf} = \rho_{wf} V_{wf} C_{p.wf}(T_{wf\_in} - T_{wf\_out}) \quad [5\text{-}14]$$

Where, Q_{wf} is the release energy of the working fluid (W); ρ_{wf}, v_{wf} and $c_{p.wf}$ are the density (kg/m^3), volume flow rate (m^3/s) and specific heat capacity (J/(kg·K)) of the working fluid, respectively; T_{wf_in} and T_{wf_out} are the temperature of working fluid at the inlet and outlet tank (K), respectively.

The equation of the pipe of heat exchanger can be given as [3.12]:

$$\rho_{pst} C_{p.pst} \frac{\partial T_{p\_st}}{\partial t} = \mathrm{K}_{pst} \frac{\partial^2 T_{p\_st}}{\partial x^2} +$$

$$\frac{1}{A_{pst}}\left[\pi D_{pst\_in}\alpha_{wf\_pst}(T_{wf} - T_{pst}) + \pi D_{pst\_out}\alpha_w(T_w - T_{pst})\right] \quad [5\text{-}15]$$

Where, ρ_{pst}, $C_{p.pst}$ and K_{pst} are the density (kg/m^3), specific heat capacity (J/(kg·K)) and thermal conductivity (W/(m·K)) of the stainless steel pipe,

respectively; A_{pst} is the cross-sectional area of the stainless steel pipe wall (m^2); D_{pst_in} and D_{pst_out} are the inside and outside diameter (m), respectively; and α_w is the heat transfer coefficient between the pipe and water (W/(m^2·K)); T_w is the temperature of water in the tank (K).

The equation of the water in the tank can be given as [3.12]:

$$M_w C_{p.w} \frac{\partial T_w}{\partial t} = A_{pst\_out}\, \alpha_w (T_{pst} - T_w) - U_{tk} A_{tk} (T_w - T_{am}) \quad [5\text{-}16]$$

Where, M_w and M_{w_c} are the quality of water in the tank (kg) and circulating water (kg/s); $c_{p.w}$ is the specific heat capacity of water (J/(kg·K)); A_{pst_out} is the exterior surface area of the copper pipe (m^2); U_{tk} is the total heat transfer coefficient between the tank and surrounding (W/(m^2·K)); A_{tk} is the superficial area of the tank (m^2).

The equation of the heat transfer coefficient between the pipe and working fluid (α_{r_c}) can be given as [3.13]:

$$\alpha_{wf\_pst} = \left[1 + 10.3 \left(\frac{D_{pst\_in}}{R}\right)^3\right] 0.023 \frac{Re_{wf}^{0.8} Pr_{wf}^{0.3} K_{wf}}{D_{pst}} \quad [5\text{-}17]$$

Where, R is the radius of curvature of coil (m); Re_{wf}, Pr_{wf} and K_{wf} are the superficial liquid reynolds number, prandtl number and thermal conductivity (W/(m·K)) of the working fluid.

5.5.4 Simulation model for the heat pump

The components of the water-source heat pump are similar with the solar direct-expansion heat pump, which is presented in **Chapter 3**. The simulation model of the compressor, electronic expansion valve and flow pressure drop in the two systems is the same, and the differences between them are as follows:

(1) The selected refrigerant of the indirect-expansion heat pump is R22, while the solar direct-expansion heat pump is R410a;
(2) The evaporator of the indirect-expansion heat pump is a double-pipe heat exchanger, while the solar direct-expansion heat pump is mini-channel PV/T panel;

(3) The condenser of the indirect-expansion heat pump is a double-pipe heat exchanger, while the solar direct-expansion heat pump is water storage tank with a copper coil heat exchanger in it;

The evaporator and condenser of the water-source heat pump are both double-pipe heat exchanger, and they have the same simulation models, which including the refrigerant model, pipe model and heat transfer liquid model. The model of refrigerant and pipe are the same as the condenser presented in **Chapter 3** (Equ. [3-67]), and the heat exchange liquid model can be given as [2.52]:

$$\alpha_{w\_l} = 0.023 \frac{Re_{wf}{}^{0.8} Pr_{wf}{}^{0.4} K_{wf}}{D_p} \quad [5\text{-}18]$$

5.5.5 Performance of the system

The average electrical efficiency of the PV/T panels is given by [2.41]:

$$\eta_e = \frac{\sum_{j=1}^{10} P_{pvj}}{\sum_{j-1}^{10} (GA_{cl})_j} \quad [5\text{-}19]$$

The thermal efficiency of the PV/T panels is given by [2.41]:

$$\eta_{t\_pvt} = \frac{C_{p.wf} M_{wf} (T_{pvt\_out} - T_{pvt\_in})}{\sum_{j-1}^{10} (GA_{cl})_j} \quad [5\text{-}20]$$

Where, C_{p_wf} is the specific heat of the working fluid (J/(kg·K)); M_{wa} is the mass flowrate of the working fluid (kg/s); T_{PVT_in} and T_{PVT_out} is the temperature at the inlet of the first PV/T panel and the outlet of the last PV/T panel (K), respectively.

The average thermal efficiency of the panels is the ratio of the thermal output of the panels to the solar radiation striking on them, given by [2.40]:

$$\eta_{t\_th} = \frac{C_{p.wf} M_{wf} (T_{pvt\_out} - T_{pvt\_in})}{\sum_{j-1}^{10} (GA_{cl})_j} \quad [5\text{-}21]$$

Where, T_{Th_in} and T_{Th_out} is the temperature at the inlet of the first thermal panel and the outlet of the last thermal panel (K), respectively.

The energy performance of the heat pump was assessed by the coefficient of performance (COP), which is expressed as [2.52]:

$$COP = \frac{C_{p.wf} M_{wf} (T_{CHE\_out} - T_{CHE\_in})}{WI_{com}} \quad [5\text{-}22]$$

Where, T_{CHE_in} and T_{CHE_out} is the temperature at the inlet and the outlet of the condenser heat exchanger (K), respectively.

5.5.6 Mathematic model of the gas boiler

The solar energy and water-source heat pump system only can cover part of the energy demand of the building. When the solar energy is unavailable (in the night or rain day), the gas boiler will turn on to provide energy for the building. The simple equation of the gas boiler can be given as:

$$m_{gas} h_{gas} \eta_{gas\_b} = C_{p\_wf} M_{wf} (T_{gas\_out} - T_{gas\_in}) \quad [5\text{-}23]$$

Where, m_{gas} is the consumption quality of the gas (kg/s); h_{gas} is the combustion calorific value of the gas (kJ/kg); T_{gas_out} and T_{gas_in} was the temperature of working fluid at inlet and outlet of the gas boiler.

5.6 Model set-up and operational procedure

The mini-channel PV/T panel and mini-channel thermal panel are the energy source of the system, and the equations of the glass, PV cell, aluminium plate and the mini-channel tube are all implicitly and discretized. The storage tank and testing room are the storage and consumable components respectively. The water-source heat pump is the auxiliary source. All the equations of them combine and describe the energy flow process. The second-order central differential mode is adopted for the battery substrate equation and the working-tube wall equation. The flow heat transfer equation of the working fluid is discretized by the upwind scheme. Two-order centre scheme model are developed to describe the equation of PV layer and pipe. The equation of flow heat transfer of the working fluid is solved by the discrete upwind schemes. The iterative calculation of the above equations is solved by the computer language C. The calculation flow chart is shown in **Fig. 5-16** and **Fig. 5-17**, and the calculation steps are as follows:

1) Start the program, and initialize the parameters of the mini-channel PV/T and thermal panel;
2) Input the weather parameters (solar radiation, ambient temperature, etc.), and input the parameters at the inlet of the panels, including the temperature, mass flow rate and specific enthalpy of the working fluid;

3) Solve the equation of the glass cover, and calculate the temperature of glass cover T_{gc};
4) Solve the equation of PV layer based on the glass cover temperature T_{gc}, and calculate the temperature of the PV layer T_{pv} and output power of the PV/T panel E_{pv};
5) Solve the equation of the aluminium plate and min-channel tube based on the temperature of PV layer T_{pv}, and calculate the temperature of mini-channel tube T_p and absorber T_b;
6) Solve the equation of the working fluid; calculate the temperature at outlet of PV/T T_{wf_out}.
7) Solve the equation of the glass cover, and calculate the temperature of glass cover T_{gc};
8) Solve the equation of the absorber and mini-channel tube, and calculate the temperature of it T_b and T_p;
9) Solve the equation of the working fluid; calculate the temperature at outlet of thermal panel T_{wf_out}.
10) Solve the equation of the storage tank and testing room, calculate the temperature of the water T_w and room T_{room};
11) Solve the equation of the working fluid; calculate the temperature at outlet of tank T_{tk_out} and T_{room}.
12) Check if the calculated value of each parameter has reached the calculation accuracy ($|T_{sim} - T_{set}|/T_{set} < 10^{-3}$, computation time 480 minters)) If no, return to step 3) and continue iterative solution; if yes, then output the results.
13) End the calculation program

For the water-source heat pump, the process is similar as the direct-expansion heat pump, i.e., the evaporator, compressor, condenser and expansion value. The difference is that the evaporator is the double-tube heat changer, replacing the PV/T panel, and the storage tank acts as the energy source, replacing the solar energy.

For the gas boiler, the energy from the burning gas is absorbed by the working fluid, then the hot working fluid go through the floor of the room and provide energy for space heating.

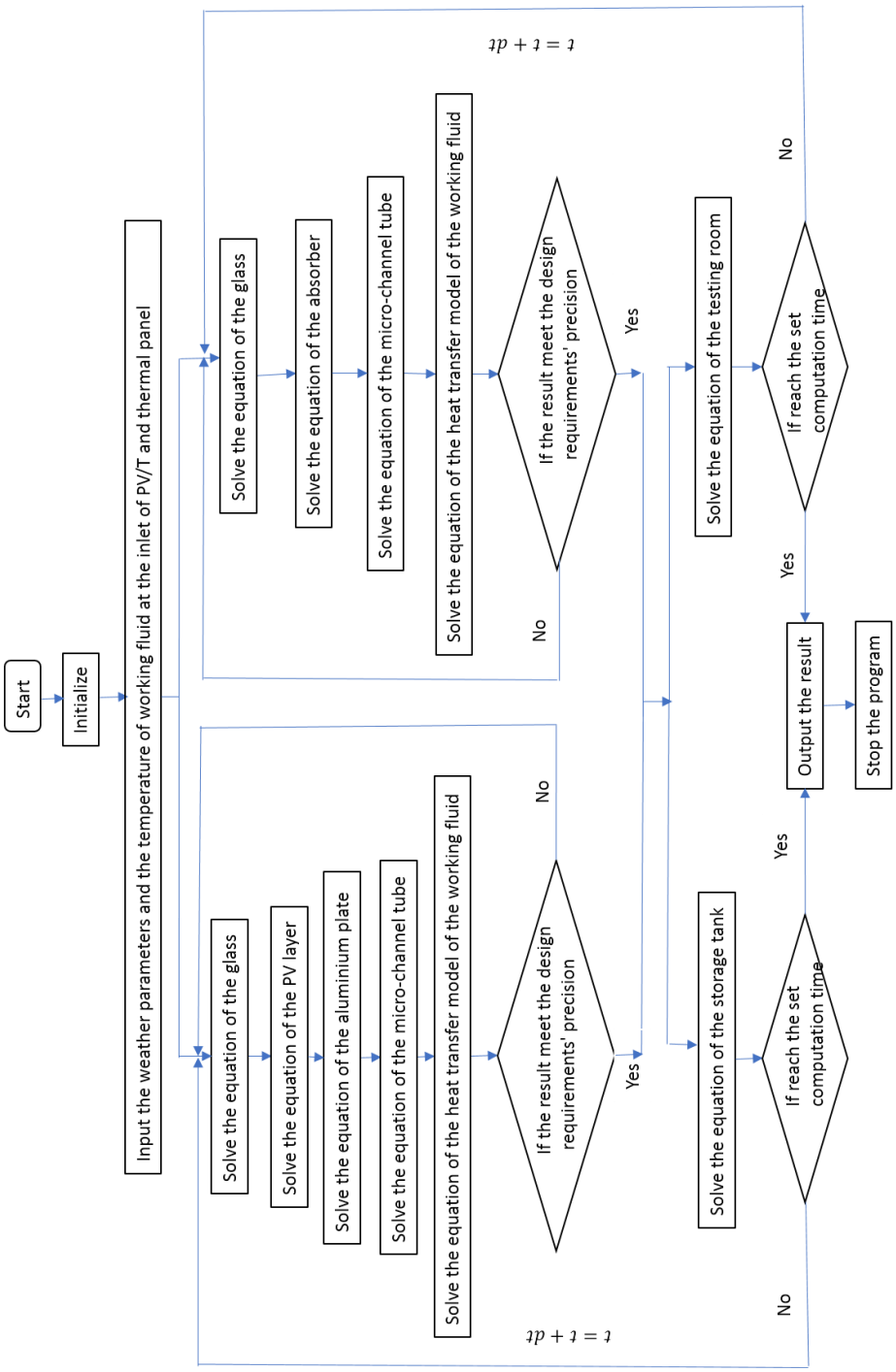

Fig. 5- 16: Calculation flow chart of the solar indirect-expansion heat pump system

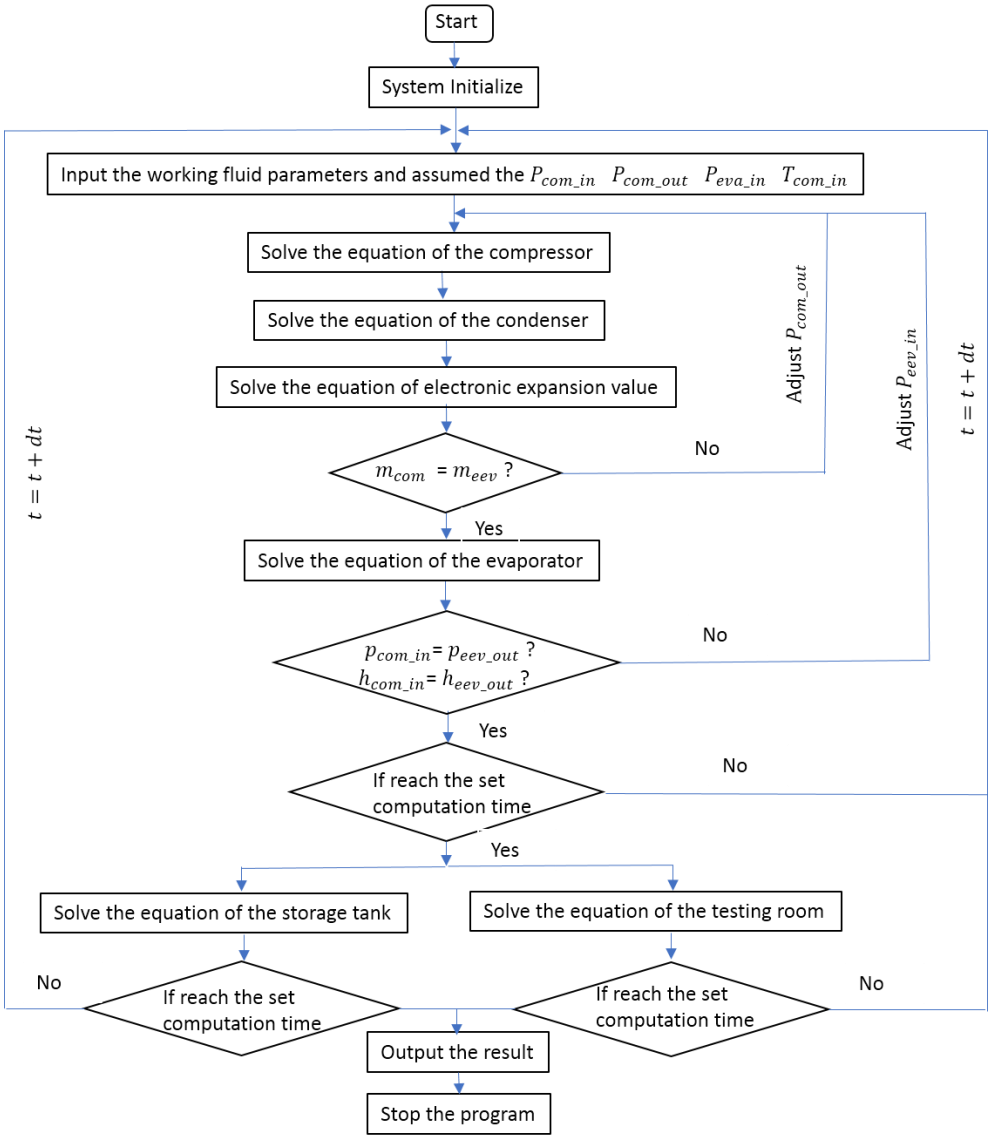

Fig. 5- 17: Calculation flow chart of the solar indirect-expansion heat pump system

5.7 Modelling results and discussion

5.7.1 Simulation performance of the system in winter

A clear weather data is selected as the input data of the system models, and the simulation result, i.e., temperature, efficiency, and COP, are shown as follow.

5.7.1.1 Simulation performance of the system during the solar available period (9:00 to 16:00)

The average flowrate of working fluid in the thermal and PV/T panel is set at 0.505 and 0.442 m^3/h, respectively. **Fig. 5-18** shows the variation of the solar radiation and ambient temperature during a solar available period. The solar

radiation increases from 215 W/m^2 to 610 W/m^2 (between 9:00 and 13:30), and then fell to 290 W/m^2 (between 13:30 and 16:00). The ambient temperature increases from 4.3 ºC to 17.2 ºC (between 9:00 and 14:30) and dropped slowly to 16.0 ºC (between 14:30 and 16:00).

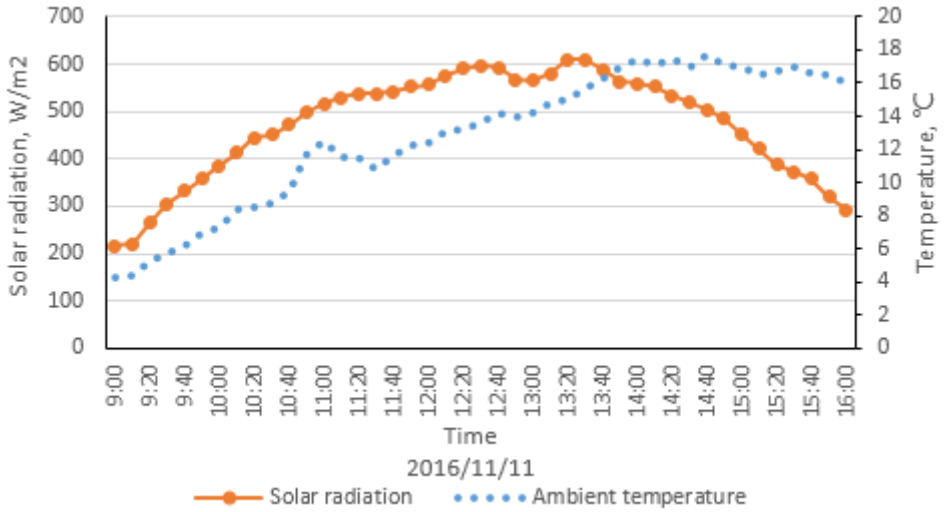

Fig. 5- 18: Variation of solar radiation and ambient temperature on the test day

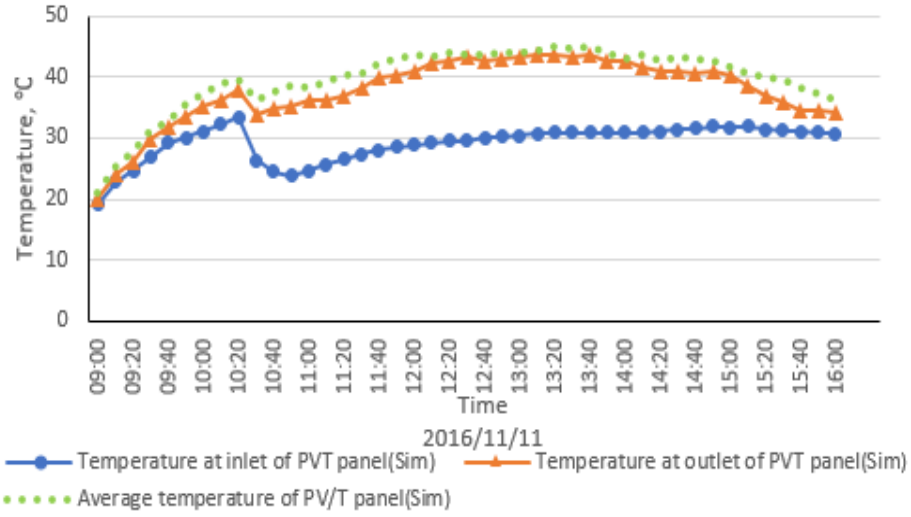

Fig. 5- 19: Simulation results of the surface temperature of panels, working fluid temperature at inlet and outlet of the PV/T panels

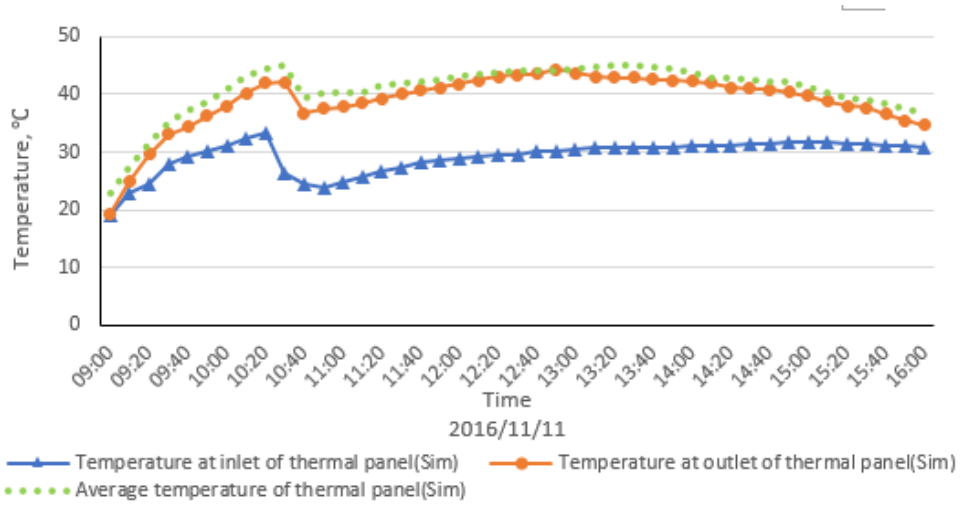

Fig. 5- 20: Simulation results of the surface temperature of panels, working fluid temperature at inlet and outlet of the thermal panels

Fig. 5-19 and **Fig. 5-20** show the surface temperature, working fluid temperature at the inlet and outlet of the PV/T /thermal panels. It is clear that during earlier morning between 9:00 and 10:30, both the inlet and outlet temperatures of the fluid were steadily growing when the solar radiation increased, during which the fluid travelled through the heat storage tank path, undertaking heat exchange with the water in the tank. As soon as the outlet fluid temperature of the panels increased to above 40 ^{o}C which was occurring at around 10:30, one part of the fluid continued to release energy to the water in the tank, and the other part was directed toward the heating loop fixed in the room space. This led to a sharp fall in the fluid temperature at the exit of the heating loop owing to the heat release of the fluid to the room space. With the solar radiation increasing, the outlet temperature began to increase again.

As shown in **Fig. 5-21**, the electrical efficiency is impacted by the temperature of the PV/T panel, they have an opposite variation trend, meaning that the temperature is higher, and the electrical efficiency is lower. During the daytime testing result, the average simulation electrical efficiency of the PV/T panel is 14.9%. The thermal efficiency shows a similar variation trend as the solar radiation, which increases from 6% to 65% between 9:00 and 13:00 and then fell to 31% in the afternoon. During the daytime working period, the average simulation thermal and overall efficiencies of the PV/T panel are 33.9% and 48.8%, respectively.

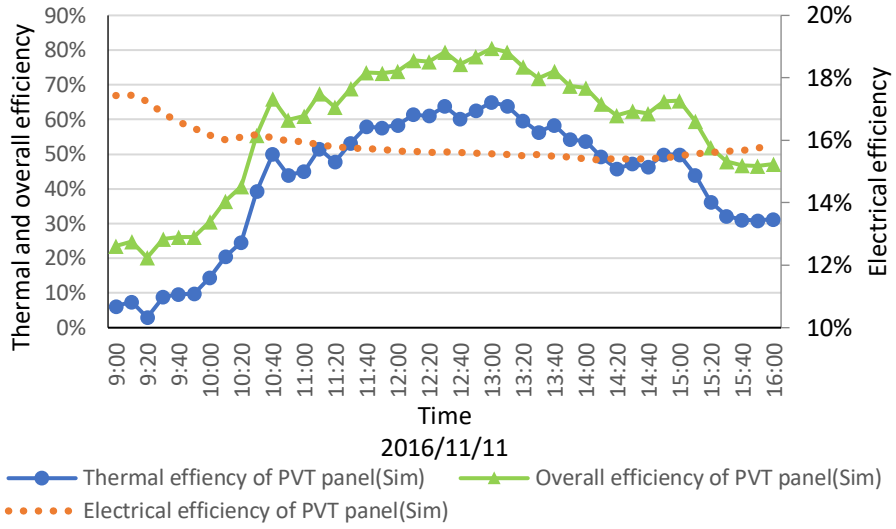

Fig. 5- 21: Simulation results of the electrical, thermal and overall efficiency of the PV/T panels

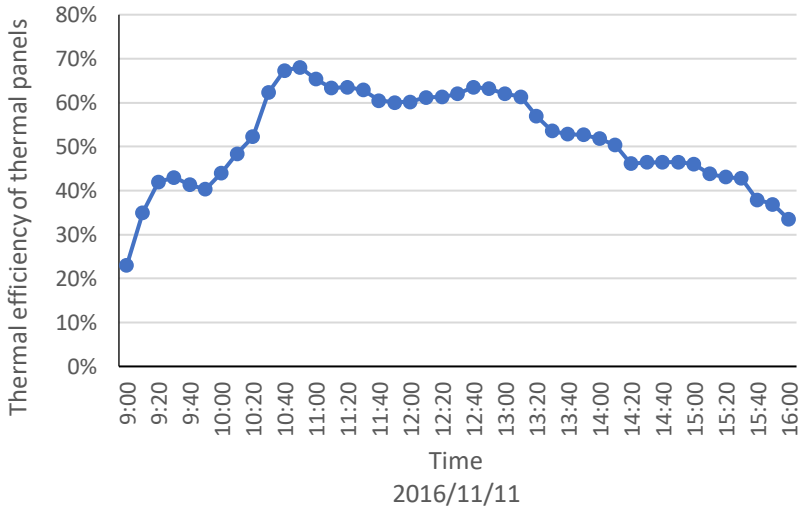

Fig. 5- 22: Simulation thermal efficiency of the thermal panels

The simulation thermal efficiency of the thermal panels (**Fig. 5-22**) increased from 23.0% to 67.9% between 9:00 and 12:00 and then fell to 33.4% after 12:00. During the daytime working period, the average simulation thermal efficiency of the thermal panel is 51.3%.

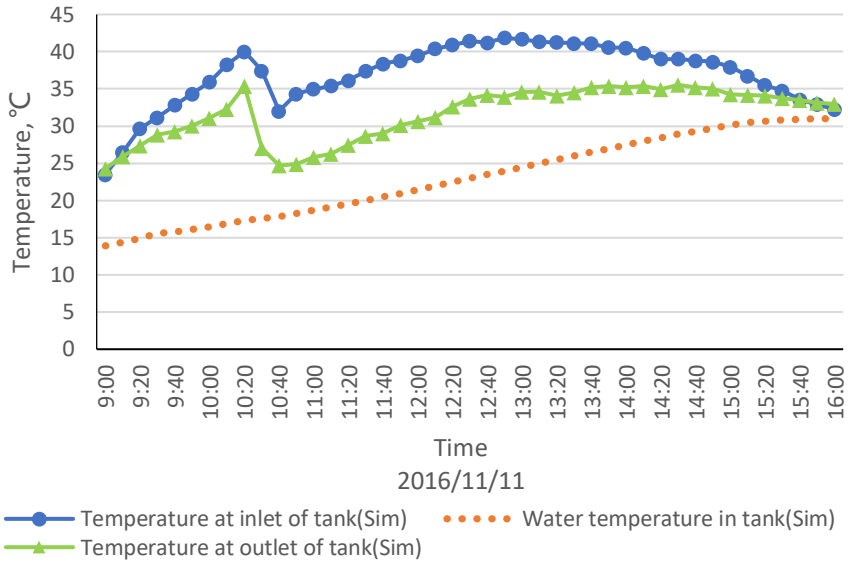

Fig. 5- 23: Simulation results of the water temperature in the tank, working fluid temperature at inlet and outlet of the tank

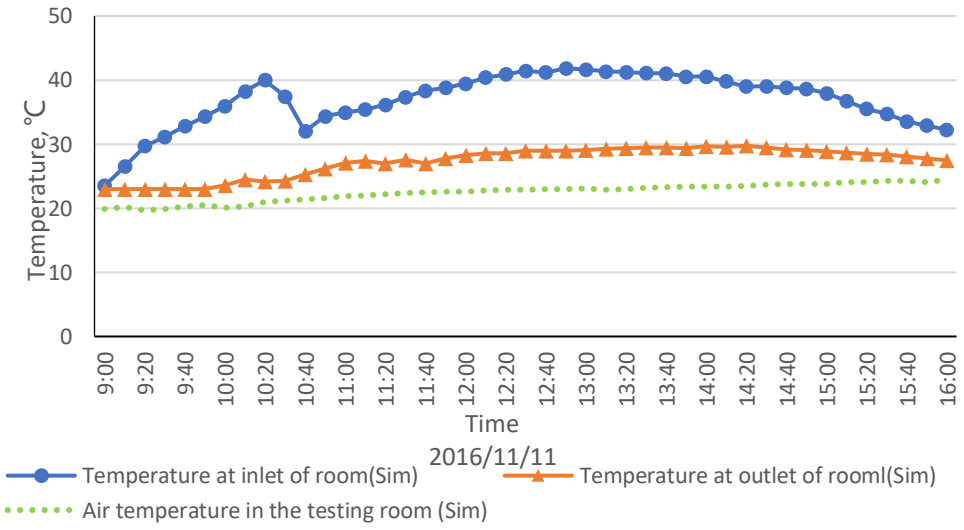

Fig. 5- 24: Simulation results of the air temperature of the room, working fluid temperature at inlet and outlet of the room

Fig. 5-23 and **Fig. 5-24** show the simulation water temperature, room temperature, working fluid temperature at inlet and outlet of the tank and room. The average flowrate of working fluid in the tank and testing room is set at 0.4 m^3/h and 0.55 m^3/h, respectively. Temperature of the water within the storage tank increased steadily from 13.9 ^oC to 31.0 ^oC during the solar system operating period, i.e., 9:00 - 16:00, indicating that the storage water stored the surplus heat from the passing fluid. The water in the storage tank was heated under two working modes. When the mixed outlet temperature was blow 40 ^oC, all the thermal energy produced by the collectors and PV/T

panels were collected to heat up the storage tank water, which occurred between 9:00 and 10:30. When the mixed outlet temperature was high than 40 °C which occurred after 10:30, the circulating fluid was divided into two parts: one part of the fluid went straight to the testing room to provide space heating, while the remaining was directed into the heat storage tank where it released heat to the storage water, and then went into solar panels.

The temperature of working fluid at the inlet of the water tank and testing room is the mixed temperature from the thermal and PV/T panels, it shows a similar variation rend with the temperature at the inlet of them. With transferring thermal energy to the water tank and testing room steadily, the temperature of working fluid at the outlet of tank and testing room follows the similar trend with the temperature at inlet. With the ambient temperature increasing and heat load decreasing, the temperature of air in the testing room is increasing slowly from 19.8 °C to 24.5 °C.

5.7.1.2 Simulation performance of the system during the heat pump operational period (18:00 to 20:00)

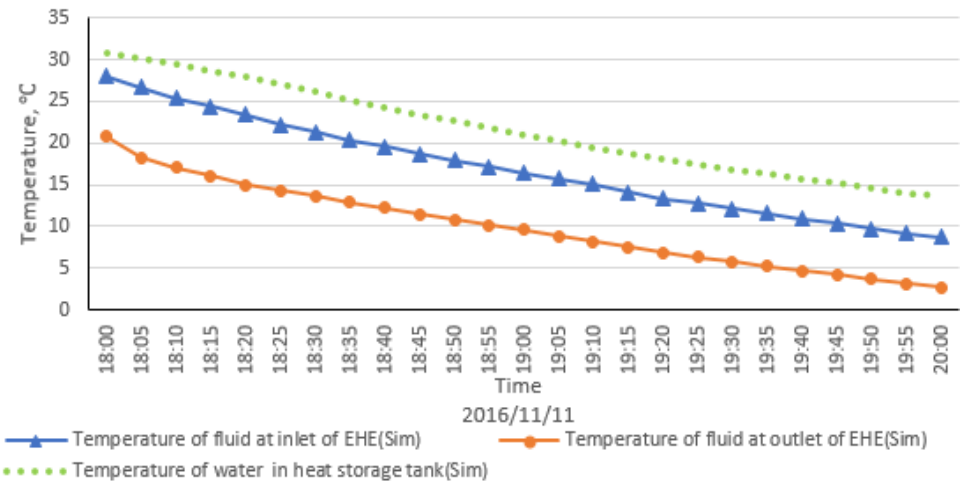

Fig. 5- 25: Simulation results of the water temperature in the tank, fluid temperature at inlet and outlet of the EHE

During the evening time between 18:00 and 20:00, the heat pump was turned on and the water within the storage tank became the heat source of the heat pump. **Fig. 5-25** shows the simulation variation of the fluid temperature at the inlet and outlet of the evaporative heat exchanger (EHE) and the temperature of the water within the storage tank. The flowrate of working fluid in the EHE is set at 1.53 m^3/h. Both the temperature of the water within the tank and the

working fluid at the inlet and outlet of the EHE fell gradually during the testing period between 18:00 and 20:00.

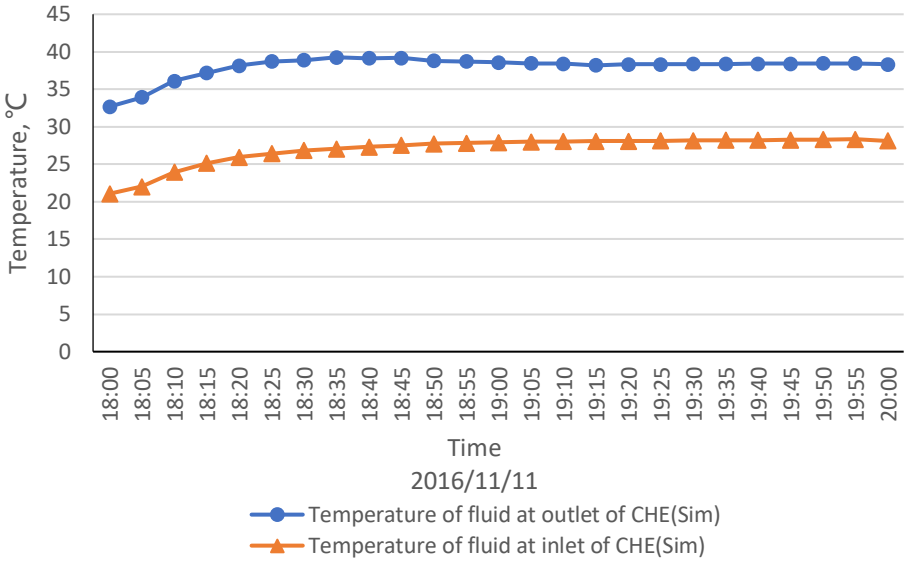

Fig. 5- 26: Simulation results of the working fluid temperature at inlet and outlet of the CHE

Similarly, the simulation temperature of the heating loop fluid at the inlet and outlet of the heat pump condensing heat exchanger (CHE) are shown in **Fig. 5-26**. And the flowrate of working fluid in the CHE is set at 1.3 m^3/h. The temperatures of the heating loop fluid at the inlet and outlet of the CHE remained a very similar variation trend. The temperature of them increases first and then keep steady. It because the temperature difference between the room air and working fluid is small at the beginning, and part energy is transferred to the room and other is absorbed by the working fluid. With the temperature difference increasing, the energy gain from the heat pump and heat release to the room is similar, then the temperature keeps steady.

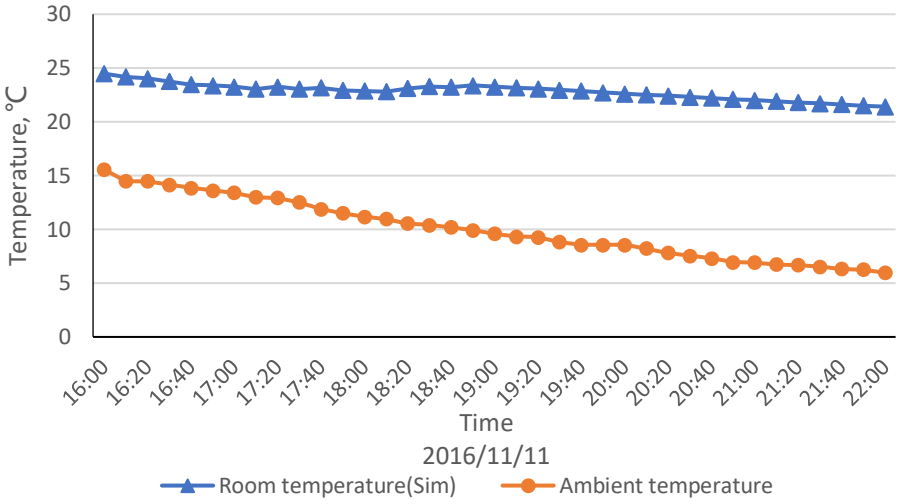

Fig. 5- 27: Simulation temperature of testing room and ambient temperature

The simulation room temperature and ambient temperature from 16:00 to 22:00 is shown in **Fig. 5-27**. The room temperature falls down slowly (16:00-18:00) when the system is stopped, and the thermal energy is from the building which is stored in the daytime. When the heat pump starts (18:00-22:00), the room temperature keeps steady, meaning that part of energy is released to the room and the other is stored by the building. When the heat pump is stopped, the energy stored in the building continue to release energy to keep the room warm.

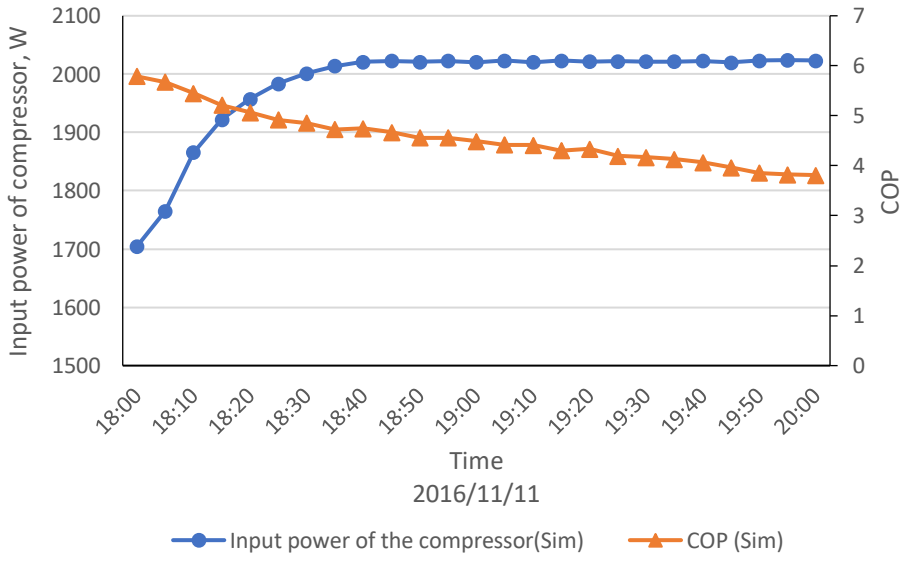

Fig. 5- 28: Simulation results of the input power of compressor and COP of the heat pump

Fig. 5-28 shows the variation of the simulation input power to the compressor and COP of the heat pump. During the two-hours' testing period, the input power to the compressor increased gradually while the COP of the heat pump presented the opposite variation trend. This indicated that the reduced tank water temperature, referring to the reduced source heat, led to the increased power input to the compressor and decreased energy efficiency of the heat pump. The average simulation COP of the heat pump 4.9.

5.7.1.3 Simulation performance of the system during the night time (22:00 to 9:00)

During the night timing between 22:00 at evening and 9:00 in the second morning, the gas heater was activated periodically, with the scheme of one hour on and one hour off. Variation of the working fluid experimental and simulation temperature at the inlet and outlet of the gas heater during the operational periods is shown in **Fig. 5-29**. The flowrate of the working fluid is 0.506 m^3/h, and it is seen that the both the inlet and outlet temperatures of the fluid increased steadily during the operating hour.

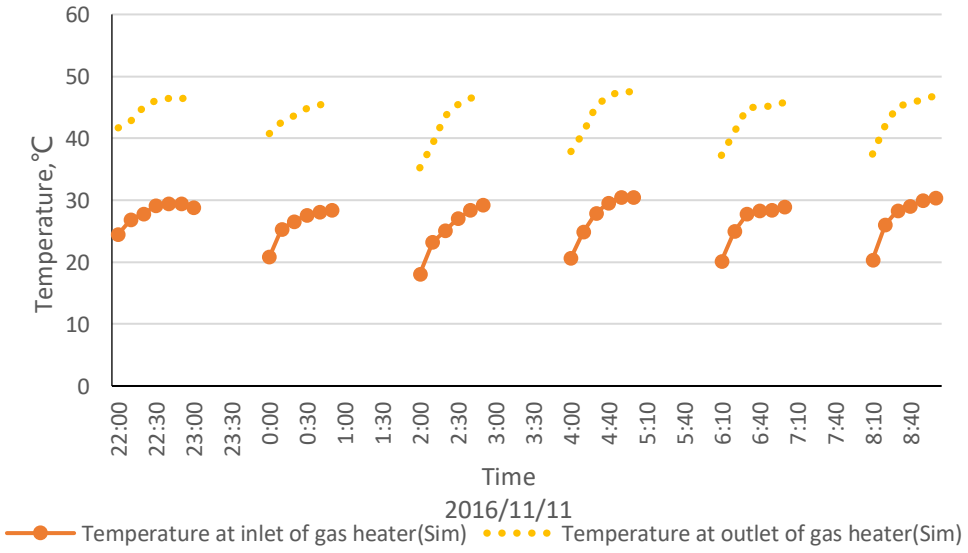

Fig. 5- 29: Fluid temperature at the inlet and outlet of the gas heater

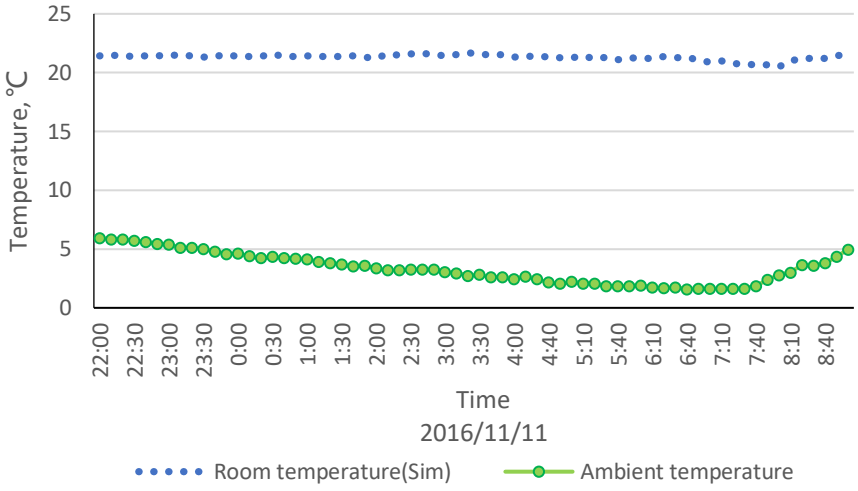

Fig. 5- 30: Variation of the ambient temperature, room temperature of testing room

Variation of the ambient temperature, room air temperature of the testing room during the night time was shown in **Fig. 5-30**. During the first working hour when the gas heater was on, the room air temperature increased while the surplus heat was stored into the building fabrics. During the follow-on one hour when the gas heater was off, the room air temperature fell by a few degrees and the stored heat by the fabric was released to the room space in order to keep the room warmth at an adequate level.

5.7.2 Simulation performance of the system in summer

In the summer, the system can provide hot water and generate electricity for the user. For the thermal panels, the main function was providing hot water, with the working fluid going through them. For the PV/T panel, its function was generating electricity. The air vent, which is designed at the back of the PV/T panel, was opened and the air would cool down the PV cell without requiring fluid to pass through them. One day's simulation result was selected to show the performance of the system in summer.

The variation of the solar radiation and ambient temperature were shown in **Fig. 5-31.** The ambient temperature increased from 23.5 ^{o}C to 33.8 ^{o}C during 8:00 to 16:00. The solar radiation increased from 330 W/m^2 to 950 W/m^2 (8:00 - 12:40), and then dropped to 610 W/m^2 (12:40 - 16:00).

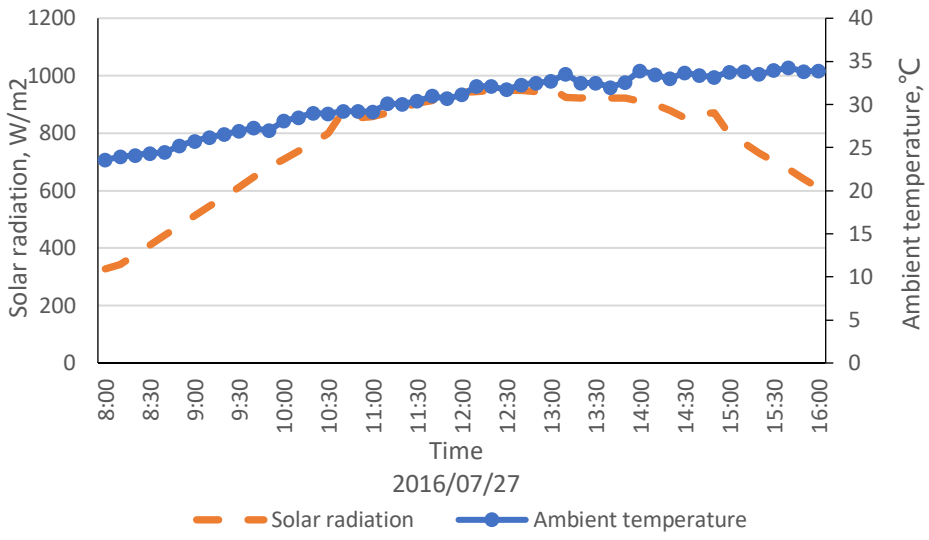

Fig. 5- 31: Variation of the solar radiation and ambient temperature in a sunny day

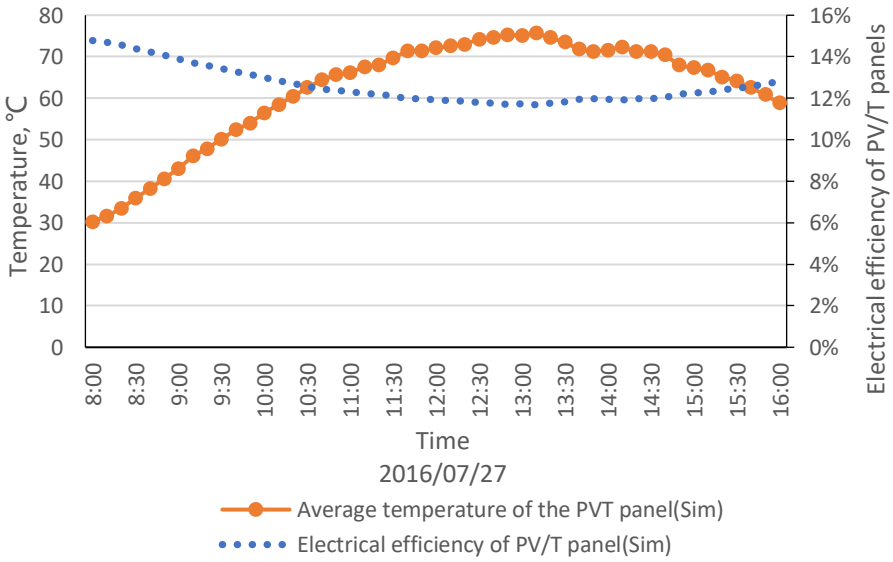

Fig. 5- 32: Simulation result of the surface temperature and electrical efficiency of the PV/T panels

As shown in the **Fig. 5-32**, the average simulation temperature of the PV/T panel has a similar variation as the solar radiation, which increased from 30.2 ºC to 75.6 ºC, and then dropped to 58.8 ºC. The simulation electrical efficiency of the PV/T panels is impacted by the temperature of the panel, showing a converse variation trend and the average simulation result is 12.6%.

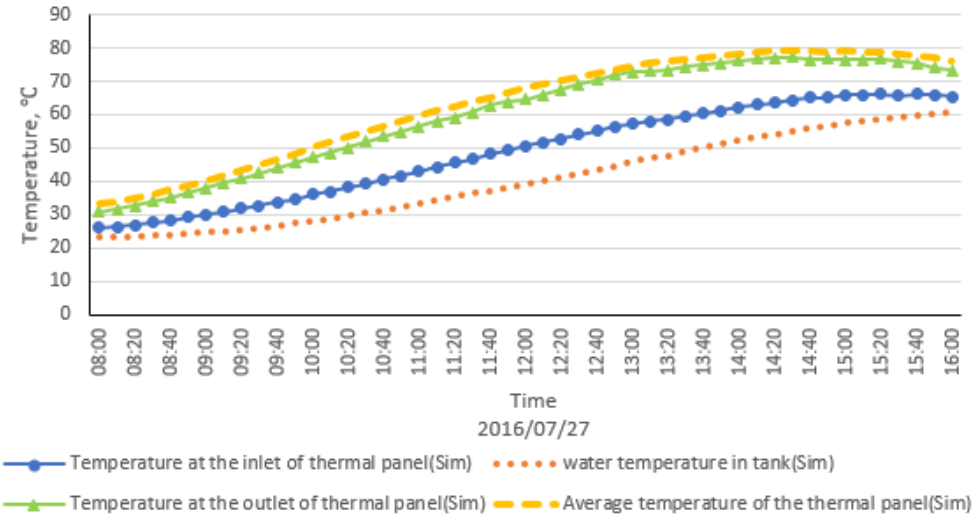

Fig. 5- 33: Simulation results of the surface temperature, water temperature in tank, fluid temperature at inlet and outlet of thermal panels

As shown in the **Fig. 5-33**, the average simulation temperature of the thermal panel has a similar variation as the solar radiation, which increased from 33.1 °C to 79.1 °C, and then dropped to 76.3 °C. With the solar radiation increasing, the temperature at the inlet and outlet show a similar variation trend. The flowrate of the working fluid was set at 0.56 m^3/h. With being heated by the panels, the temperature of the water in the tank increase from 23.2 °C to 60.9 °C slowly.

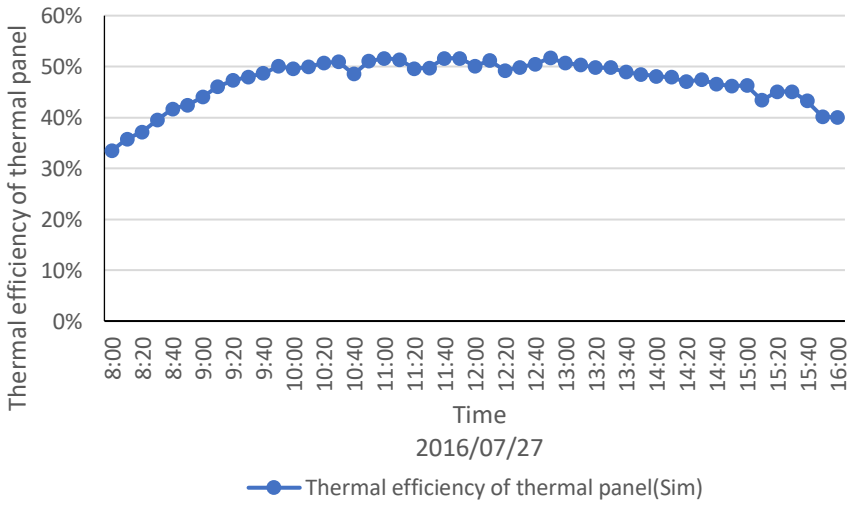

Fig. 5- 34: Simulation thermal efficiency of the thermal panel in sunny day

The simulation thermal efficiency of the thermal panel was shown in the **Fig. 5-34.** The thermal efficiency was impacted by the solar radiation, and shows a similar variation trend as it, increasing first and then dropping. After the calculation, the average simulation thermal efficiency was 47.0%.

5.8 Chapter summary

This chapter has described the design concept and working principle of the solar indirect-expansion heat pump system for space heating. The outstanding features lay in as the following: (1), this system can provide energy for space heating in the winter and hot water in other seasons, and generate electricity annually; (2), in the winter, multiple energy source work together to provide energy for space heating, meeting the building demand at any condition; (3) the mini-channel tube acts as the heat exchanger which have a high heat exchange rate and larger contact area.

The parameters and working principle of all the components in this heat pump are described, including the mini-channel PV/T panel, the mini-channel thermal panel, storage tank, water-source heat pump and gas boiler. These designed parameters provide fundamental data for the simulation and experimental test.

Based on the design concept and parameters of all the components, the simulation models of the system are developed, including the sunlight incidence, the components of the system (mini-channel PV/T panel, the mini-channel thermal panel, storage tank, water-source heat pump and gas boiler). In term of the mini-channel PV/T panel and thermal panel, the models of glass cover, PV layer, absorber and the mini-channel tube are built to calculate the temperature of the panel, electrical and thermal efficiencies of it. In term of the storage tank, the models of the heat exchanger inside and water are built to calculate the temperature of water and working fluid. In term of water-source heat pump, the models of evaporator, condenser, EEV and compressor are built to calculate the working pressure and temperature of the refrigerant. In the item of gas boiler, the parameters of the working fluid and room can be calculated.

The calculation flow chart of the entire heat pump system is developed to describe the process and steps of the simulation program. Based on these

works, simulation on the system is carried out with a real weather data. In winter, it was found that the mini-channel PV/T panels had the average electrical, thermal and overall efficiencies of 14.9%, 33.9% and 48.8% respectively, while the mini-channel thermal panels had the average solar thermal efficiency of 51.3%, and the heat pump had an average COP of 4.9. The temperature of the testing room remained at above 18 ^{o}C throughout the whole testing period, indicating that the system has the capacity to meet the comfort standard of the building. In summer, the average electrical efficiency of the PV/T panel was 12.6%, and the average thermal efficiency of thermal panel was 47.0%. The temperature of water in the tank increased from 23.2 ^{o}C to 60.9 ^{o}C which is high enough for different kinds of application.

These simulation models and results predict the performance of the system and make the preparation for the comparison between the simulation and experimental results.

CHAPTER 6: EXPERIEMNTAL TESTING OFTHE MINI-CHANNEL PV/T MODULES BASED SOALR INDIREC-EXPANSION HEAT PUMP SYSTEM IN REAL LIFE OPERATIONAL CONDITION

6.1 Chapter introduction

This chapter describes the experimental platform of the solar indirect-expansion heat pump system and the testing results in winter and summer condition. The experimental and simulation result is compared to each other and analysed.

6.2 System installation, commission and testing procedure

The components of the system contain the working and measurement components (**Fig. 6-1**). The working ones are mini-channel PV/T and thermal panel, storage tank, PPR pipe, heat pump battery, inverter and gas boiler whose parameters are described in **Chapter 5**; while the measurement components are the thermocouples, flowmeters, solar radiation sensor, power sensor, anemometer, data logger and computer which have the same parameters as the solar direct-expansion heat pump used. The specifications, quantity and installation position of the sensors/meters used in the measurement process are outlined in **Table 6-1**.

Fig. 6- 1: Set up of the system

The Control strategy of the system is shown in **Fig. 6-2**. In the day time, the water pump will push the working fluid to go through the mini-channel PV/T and thermal panel, then the hot water heats the room. In the night, the water heat pump will absorb energy from water tank, and continually provide

energy for the building. When the water temperature is too low, the gas boiler turns on and replaces heat pump to keep heating room in the night.

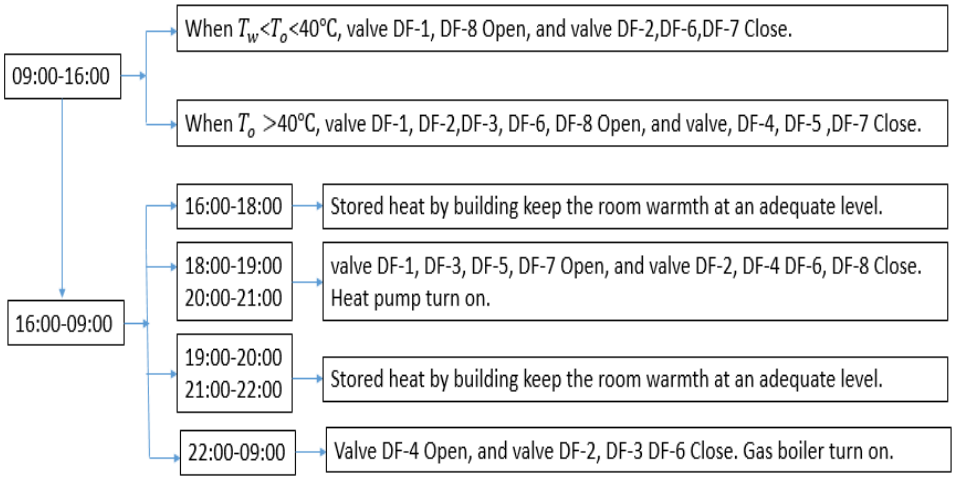

Fig. 6- 2: Control strategy of the system on clear days

Table 6- 1: List of measurement instruments and their positions in the system

Devices	Specifications	Quantity	Location
Power sensor	HK-D4I (Huakong xingye, China) and CE-P03-32BS(SSET China)	6	Heat pump input (AC), PV module output (DC)
Pyranometer	TQB-2 (Sunlight, China)	1	Top of the collector
Fluid flowmeter	LWGY-C(MEACON China)	3	PV/T and collector exit; PV/T entrance; condenser heat exchanger exit;
Anemometer	HS-FS01(Huakong xingye, China)	1	Top of the collector
Thermocouple	0.2 mm copper-constantan (Zhongjia China)	70	PV/T; collectors; PV/T and collector entrance and exit; heat exchanger entrance and exit; water storage tank; ambient, etc.
Data logger and computing unit	34970A (Agilent, USA)	2	Control room
Pressure gauge	YN60 0-0.6Mpa (Jiangyun, China)	2	Inlet and outlet of water pump

In addition to the information listed in **Table 6-1**, further description of the measurement points arrangement is as follows: (1), 3 measurement points

were selected to each panel to test the temperature of the panels; (2) to obtain the average temperature within the storage, four measurement points were selected (i.e., 1 on the top, 1 at the bottom and 2 in the middle); (3) to calculate the heat output of the gas heater, temperatures of the fluid at the inlet and outlet of the heater were measured; and (4) local wind speed was monitored using an anemometer.

6.3 Testing result and discussions

6.3.1 Experimental performance of the system in winter

The experiment was carried out in Lvliang city, China where is the same place as the solar direct-expansion heat pump system. The testing results during 10th to 13th, and 15th to 17th November 2016 are listed in **Table 6-2**. All the tests were carried out throughout the day, i.e., from 0:00 to 24:00.

Table 6- 2: Testing results at the selected dates

Date	Radiation (W/m^2)	Temperature °C			System performance (%)				
2016	G	T_a	T_{wt}^i	T_{wt}^f	$\eta_{t.Th}$	$\eta_{e.PVT}$	$\eta_{t.PVT}$	$\eta_{o.PVT}$	COP
10/11	454.2	13.2	14.2	30.6	49.1	14.2	32.2	46.4	4.53
11/11	472.6	12.8	13.6	29.4	50.2	14.5	31.6	46.2	4.93
12/11	466.4	11.1	14.5	29.9	50.8	14.0	30.7	44.7	4.81
13/11	439.3	9.1	15.6	30.8	50.1	14.1	31.9	46.0	4.9
15/11	451.9	8.4	13.1	28.6	50.5	14.2	32.4	46.6	5.05
16/11	460.6	8.7	14.4	27.8	48.3	14.0	31.5	46.5	5.09
17/11	423.6	6.4	14.6	29.2	47.4	14.1	30.7	44.8	4.93

The performance data of the system at a typical clear day is selected to show the testing and simulation result. The operational schedule of the experimental heating system is shown in **Table 6-3**.

Table 6- 3: Operational schedule of the hybrid heating system

Hour	1:00	2:00	3:00	4:00	5:00	6:00	7:00	8:00	9:00	10:00	11:00	12:00
Solar radiation, W/m^2	0	0	0	0	0	24	98	128	283	444	535	580
Heat demand, W	4302	4436	4588	4717	4834	4901	4731	4190	3758	2704	1891	1382
Solar panels									on	on	on	on
Heat pump												
Gas heater	on	on	on	on	on	on	on	on				
Hour	13:00	14:00	15:00	16:00	17:00	18:00	19:00	20:00	21:00	22:00	23:00	24:00
Solar radiation, W/m2	585	525	384	208	149	35	0	0	0	0	0	0
Heat demand, W	765	210	392	1170	1740	2310	2744	3160	3471	3697	3936	4120
Solar panels	on	on	on	on								
Heat pump						on	on	on				
Gas heater										on	on	on

During the day time period between 9:00 and 16:00, the solar radiation was sufficient to provide heating and thus no heat pump or gas heater was in need. There was certain amount of surplus heat that was stored in the water storage tank during this period and this amount of heat was used in later period as the heat source of the heat pump. During the period between 16:00 and 18:00 when the solar radiation was weak and thus insufficient to provide heating to building, the whole system was switched off and the room warmth was maintained by the thermal mass of the building fabrics. After 18:00, the heat pump was turned on to upgrade the stored solar heat in the water storage tank to meet the temperature and heat requirements of the room space. It was found that the stored heat in the water storage tank was depleted after 20:00 and thus the heat pump was switched off and the room warmth was again maintained by the thermal mass of the building fabrics. During the night time period between 22:00 at evening and 9:00 in the second morning, the gas heater was periodically switched on to deliver the energy required for the space heating.

6.3.1.1 Experimental performance of the system during the solar available period (9:00 to 16:00)

Fig. 6-3 and **Fig. 6-4** shows the variation of the surface temperature of PV/T and thermal panels, working fluid temperature at inlet and outlet of the PV/T and thermal panels. With the solar radiation and water temperature increasing (9:00-10:30), all the temperature increase quickly; when the mixed fluid temperature at the outlet of panels is over 40 ^{o}C, the part of the fluid will go

through the room, resulting in the dropping of all the temperature at 10:30. In this working model, all the temperature show a similar variation trend as the solar radiation.

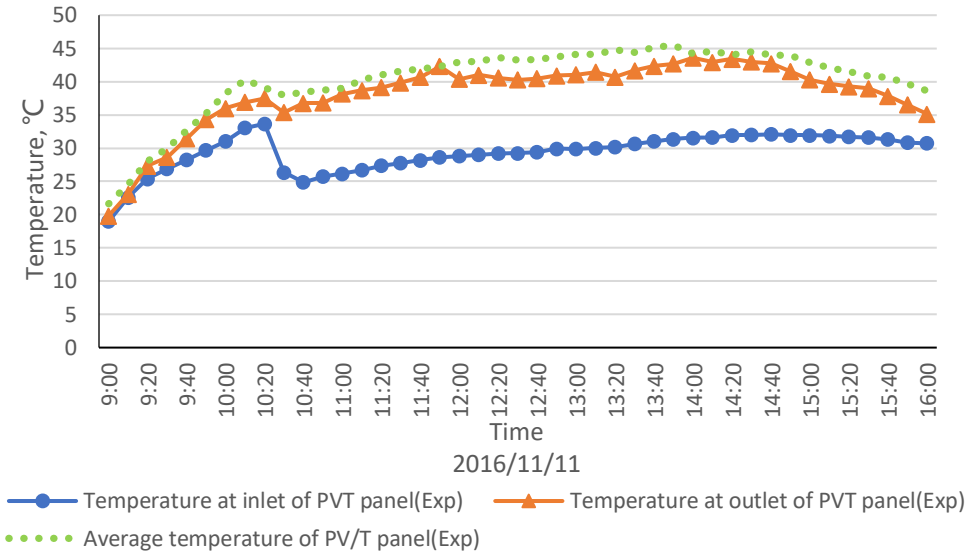

Fig. 6- 3: Experimental results of the surface temperature, working fluid temperature at inlet and outlet of the PV/T panels

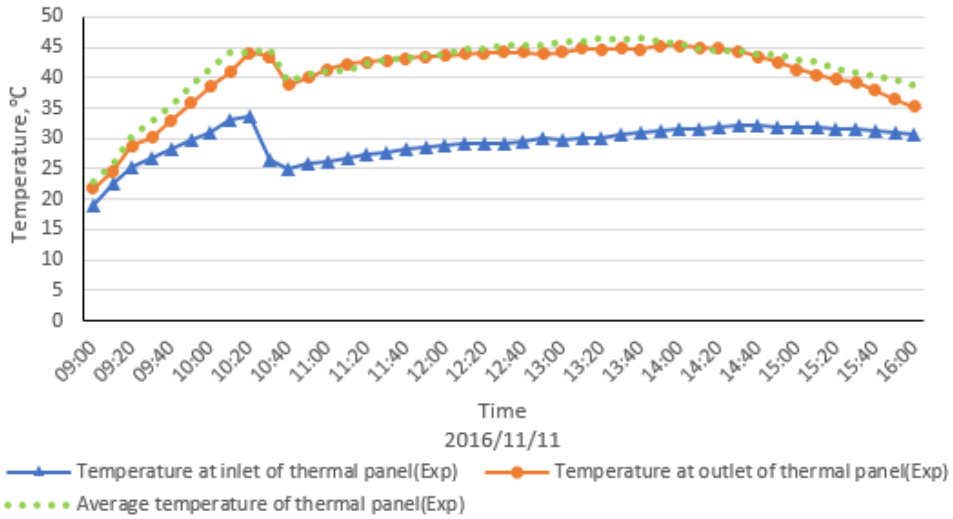

Fig. 6- 4: Experimental results of the surface temperature, working fluid temperature at inlet and outlet of the thermal panels

Fig. 6-5 shows the output voltage and current of the PV/T panels. The output voltage of the panels is around 72 V, and the current is impacted by the solar radiation, showing a similar trend as it. **Fig. 6-6** shows the electrical, thermal and overall efficiencies of the PV/T panels. **Fig. 6-7** shows the thermal efficiency of the thermal panels. The electrical efficiency is influenced by the temperature of the panels, high temperature with low efficiency. The thermal and overall efficiency show the similar trend as the solar radiation. During

the testing period, the average electrical, thermal and overall efficiencies of the PV/T panels are 14.5%, 31.7%, 46.2%, respectively. The thermal efficiency of thermal panels is 49.9%.

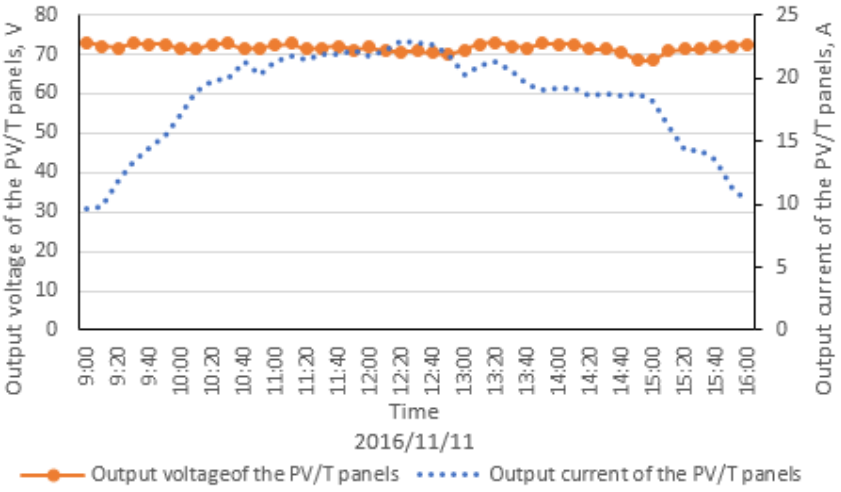

Fig. 6- 5: Output voltage and current of the PV/T panels

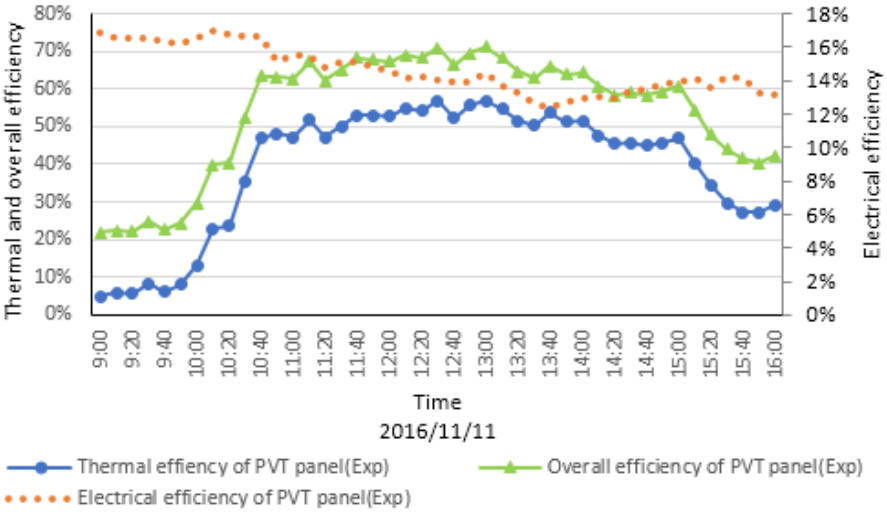

Fig. 6- 6: Electrical, thermal and overall efficiency of the PV/T panels

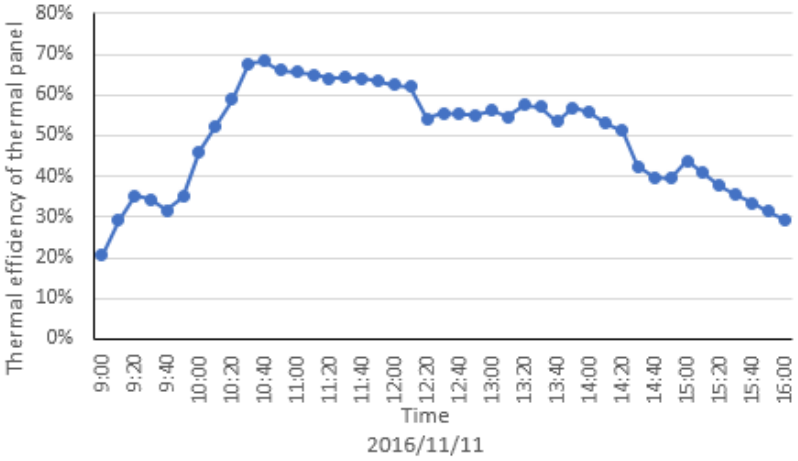

Fig. 6- 7: Thermal efficiency of the thermal panel

Variations of the tank water temperature, inlet and outlet temperatures of the working fluid at the storage tank and testing room during the test day are shown in **Fig. 6-8 and Fig. 6-9**. With being heated by the solar panels, the temperature of the water within the storage tank increased steadily from 13.6 ^{o}C to 29.4 ^{o}C during the solar system operating period, i.e., 9:00 - 16:00.

The temperature of working fluid at the inlet of the water tank and testing room is the mixed temperature from the thermal and PV/T panels, it shows a similar variation trend with the temperature at the inlet of them, which is impacted by the solar radiation and working model. During the testing period, the room temperature increased from 19.8 ^{o}C to 22.8 ^{o}C.

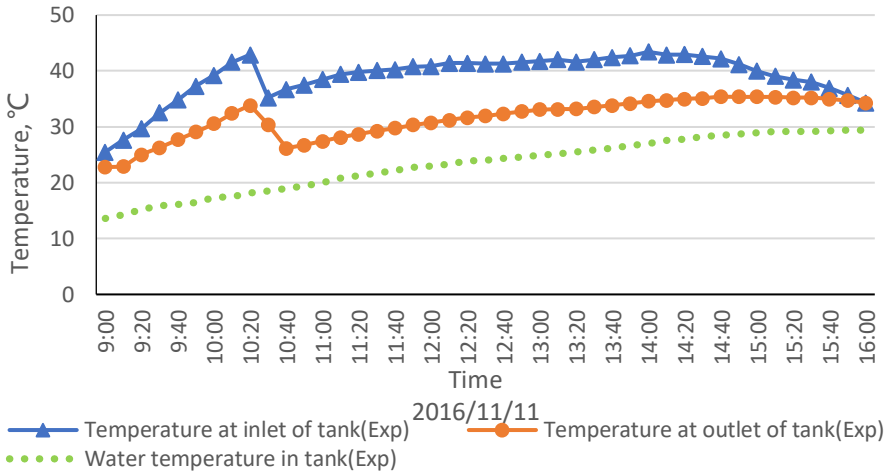

Fig. 6- 8: Experimental results of the water temperature, working fluid temperature at inlet and outlet of the tank

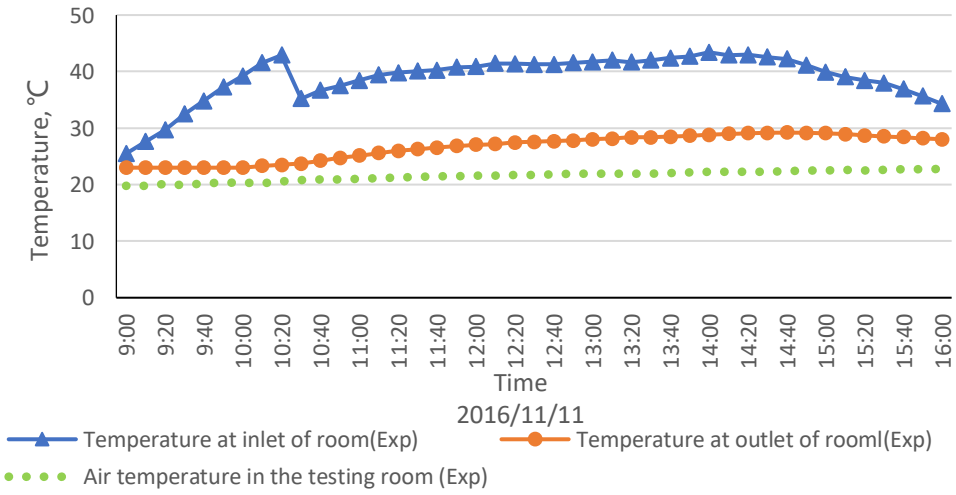

Fig. 6- 9: Experimental results of the room temperature, working fluid temperature at inlet and outlet of the testing room

6.3.1.2 Experimental performance of the system during the heat pump operational period (18:00 to 20:00)

During the time from 18:00 and 20:00, the heat pump and water tank worked together to provide energy for the room. **Fig. 6-10** shows the experimental variation of the water temperature in the tank, fluid temperature at the inlet and outlet of the evaporative heat exchanger (EHE). With the energy being absorbed by the heat pump, both the temperature of the water within the tank and the working fluid at the inlet and outlet of the EHE fell gradually during the testing period between 18:00 and 20:00.

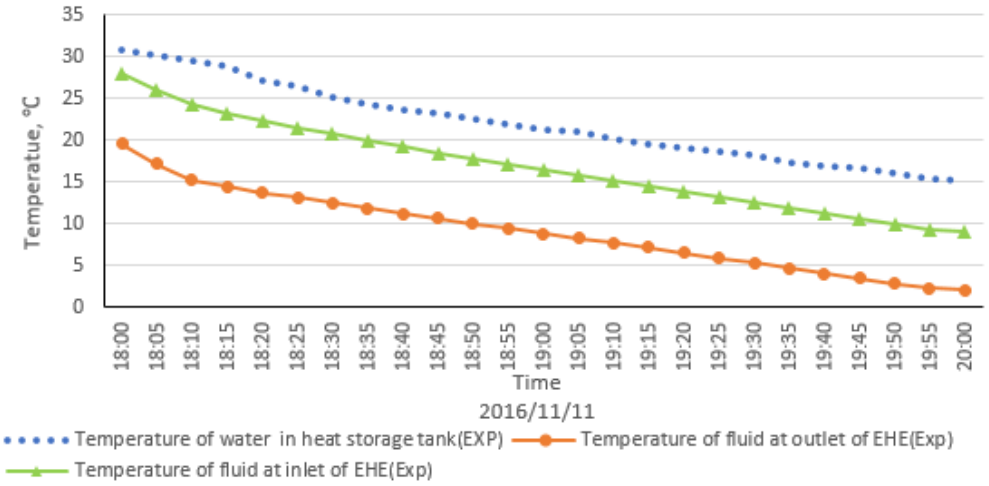

Fig. 6- 10: Experimental results of the water temperature, working fluid temperature at the inlet and outlet of EHE

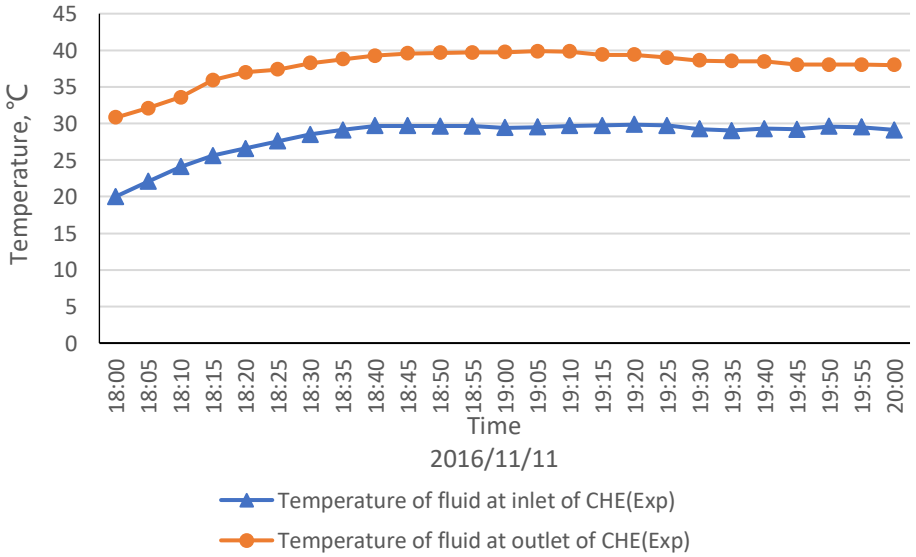

Fig. 6- 11: Experimental results of the working fluid temperature at the inlet and outlet of CHE

Fig. 6-11 shows the variation of the fluid temperature at the inlet and outlet of CHE. The temperature at inlet and outlet shows a same trend, increasing first and then keep steady.

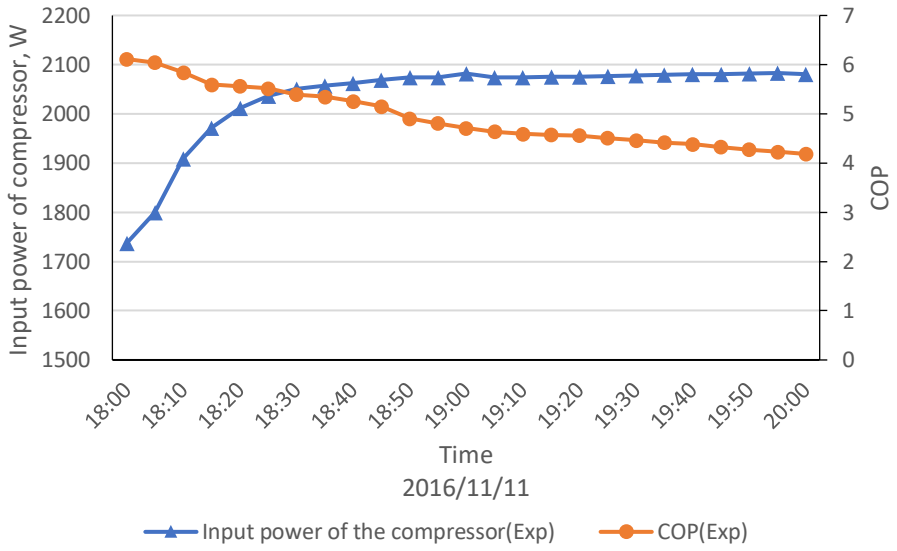

Fig. 6- 12: Input power of compressor and COP of the heat pump

Fig. 6-12 shows the variation of the experimental input power to the compressor and COP of the heat pump. The input power of the compressor is impacted by the output fluid temperature, showing a similar variation trend. With the absorbing energy from the tank decreasing and input power of compressor increasing, the COP decreased from 6.1 to 4.2. The average experimental COP of the heat pump was 4.6 during this working model.

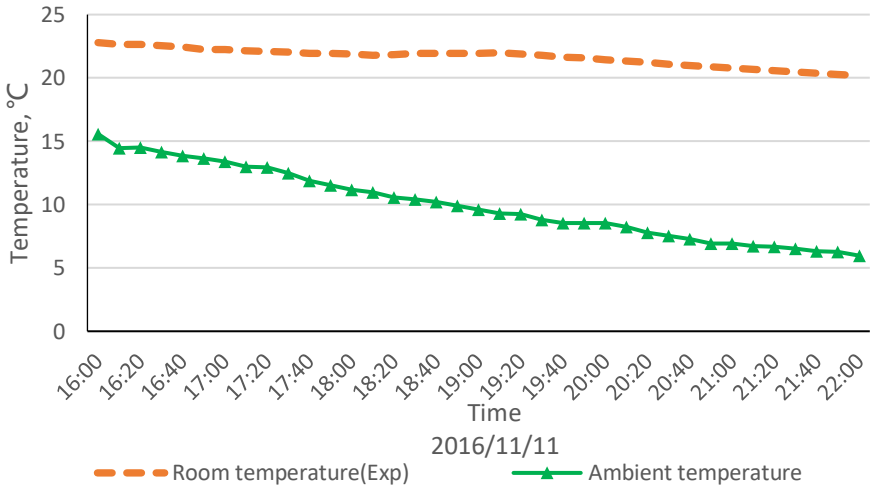

Fig. 6- 13: Temperature of testing room and ambient temperature

The room temperature and ambient temperature from 16:00 to 22:00 is shown in **Fig. 6-13**. The heating energy is from the building from 16:00 to 18:00 which is stored in the daytime. With the heat pump working from 18:00 to 20:00, one-part energy kept the temperature of the room, while the other is stored in the building which will release energy to the room when the heat pump is stopped.

6.3.1.3 Experimental performance of the system during the night time (22:00 to 9:00)

The gas boiler began to operate at 22:00 and stopped at 9:00. It was set to work one hour then off one hour. As shown in **Fig. 6-14**, the temperature at the inlet and outlet of the gas boiler shows a similar variation, and the temperature difference kept at around 17 ºC.

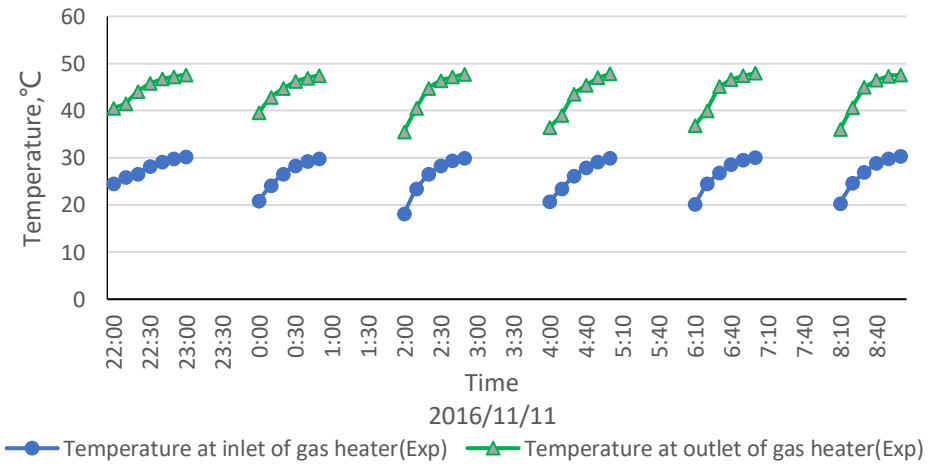

Fig. 6- 14: Fluid temperature at the inlet and outlet of the gas heater

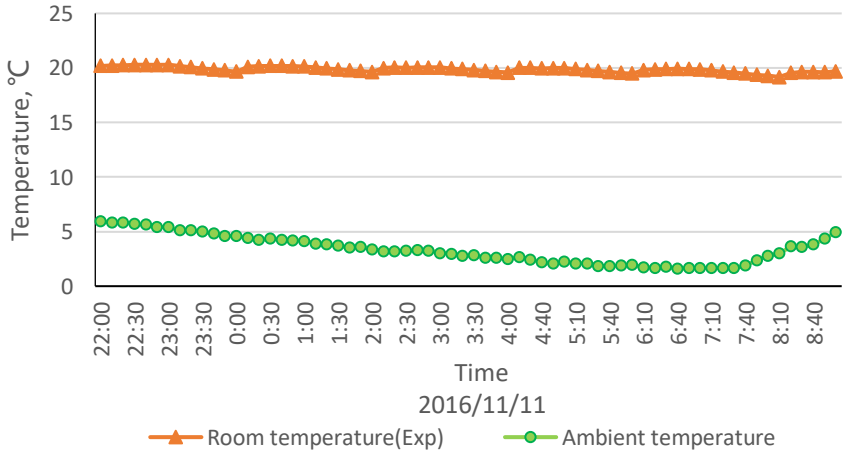

Fig. 6- 15: Variation of the ambient temperature, room temperature of testing room

Variation of the ambient temperature, room air temperature of the testing room during the night time was shown in **Fig. 6-15**. When the gas boiler is working, the room air is increasing slowly, while when it was stopped, the room temperature began to drop. During the testing period, the room temperature kept at around 20 ^{o}C.

6.3.2 Experimental performance of the system in summer

In the summer, the system can provide hot water and generate electricity for the user. The experiment was carried out from 21th to 27th July 2016. The testing result was shown in **Table 6-4**. The testing time were all from 8:00 to 16:00.

Table 6- 4: Testing result of the system in summer

Date	Radiation(W/m2)	Temperature ℃			System performance (%)	
2016	G	T_a	T_{wt}^i	T_{wt}^f	$\eta_{t.Th}$	$\eta_{e.PVT}$
21/07	685.6	13.2	22.2	56.1	45.6	11.9
22/07	703.4	12.8	22.7	57.4	46.2	11.5
23/07	697.5	11.1	23.1	56.9	45.8	11.8
24/07	736.4	9.1	22.9	57.8	44.9	12.0
25/07	743.8	8.4	22.5	58.6	47.0	11.0
26/07	723.6	8.7	21.6	56.9	46.3	11.2
27/07	765.5	6.4	23.2	59.3	46.8	11.4

The same day's testing result as the simulation was selected to show the performance of the system in summer.

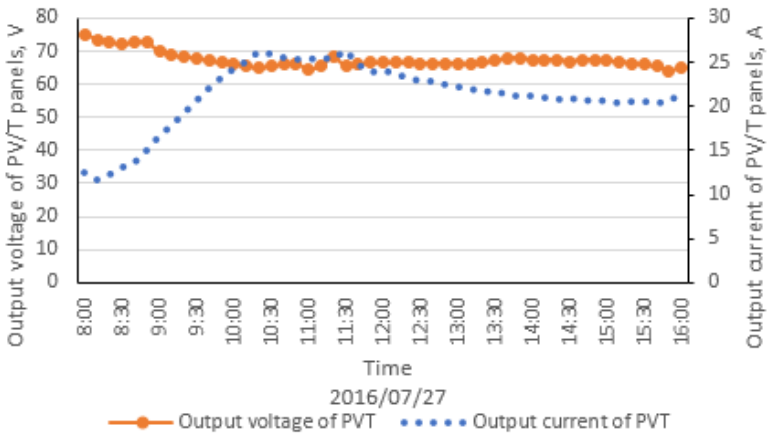

Fig. 6- 16: Output voltage and current of the PV/T panels in sunny day

The **Fig. 6-16** shows the output voltage and current of the PV/T panels. The output voltage of the PV/T panel kept at 68 V, and the output current

increased from 11.5 A to 26 A, and then dropped to 20 A. The output current was not only impacted by the solar radiation, but also the inverter. The inverter can show a good performance when the voltage of battery was between 46 V to 52 V. But the electrical load was stable, while the power input was changing all the time. Therefore, the output current didn't match the solar radiation very well.

As shown in the **Fig. 6-17**, the average experimental temperature of the PV/T panel has a similar variation as the solar radiation, which increased from 30 ºC to 75 ºC, and then dropped to 59 ºC. The electrical efficiency was impacted by the temperature of the panel, showing a converse variation trend. The average experimental result was 11.5% during the testing period.

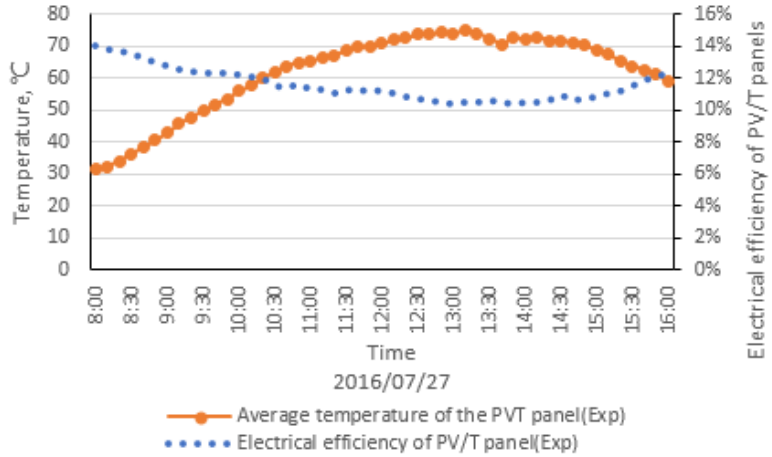

Fig. 6- 17: Experimental results of the surface temperature, electrical efficiency of the PV/T panels in sunny day

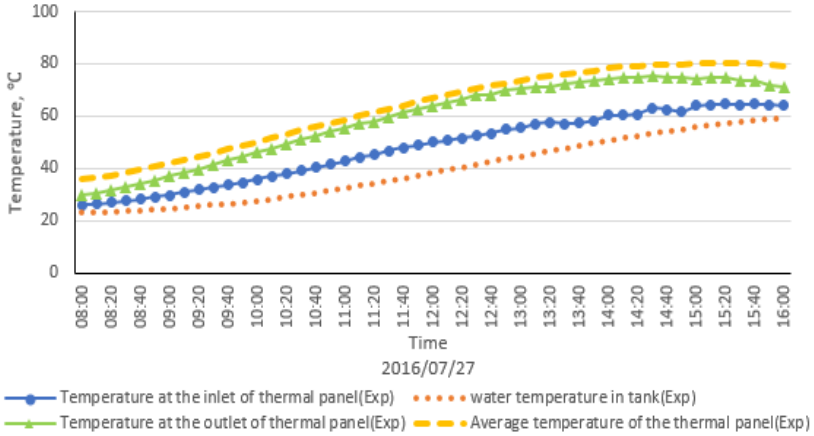

Fig. 6- 18: Experimental results of the surface temperature, water temperature in tank, fluid temperature at inlet and outlet of thermal panels

As shown in the **Fig. 6-18**, with the water being heated by the panels continually, the temperature of it increased from 23.2 ºC to 59.3 ºC from 8:00 to 16:00. The surface temperature, fluid temperature at inlet and outlet of thermal panels is influenced by the water temperature and solar radiation, showing a similar variation trend as them.

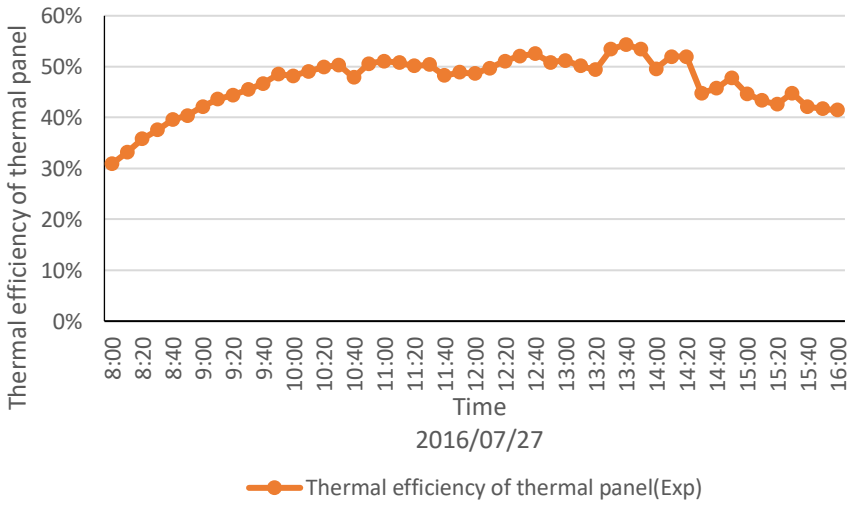

Fig. 6- 19: Thermal efficiency of the thermal panel in sunny day

The experimental thermal efficiency of the thermal panel was shown in the **Fig. 6-19.** The thermal efficiency was impacted by the solar radiation, and shows a similar variation trend as it, increasing first and then dropping. After the calculation, the average experimental thermal efficiency was 46.8% during the testing period.

6.4 Model validation/refinement via the comparison between the modelling and experimental results

Comparing the simulation (**Chapter 5**) and experimental result on the performance of the solar indirect-expansion heat pump system in winter and summer working models, several significant experimental and simulation results are shown in one figure to verify the computer model. Based on the simulation and experimental results, the error was calculated.

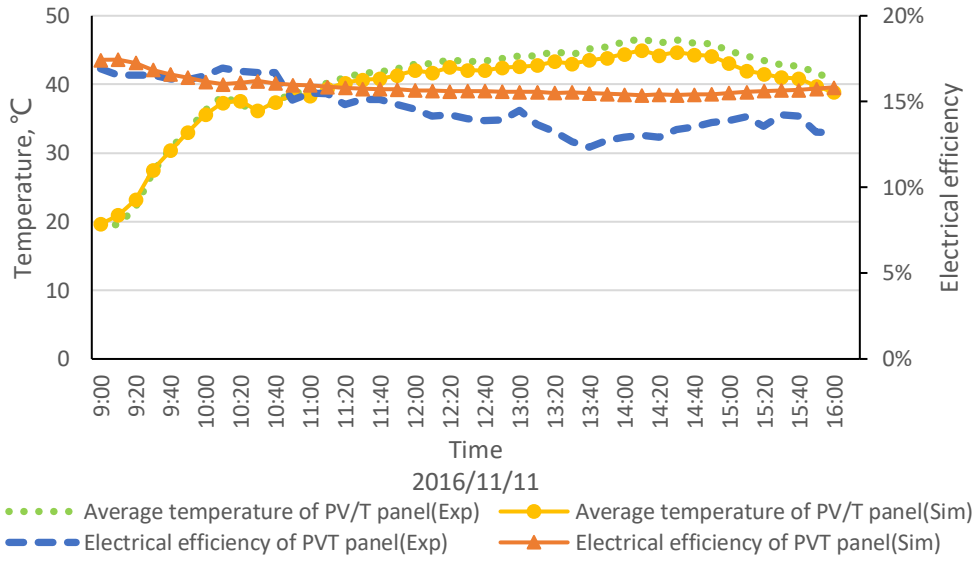

Fig. 6- 20 Average experimental and simulation panel surface temperature and electrical efficiency of the PV/T panels in winter

Fig. 6-20 shows the experimental and simulation variation trend of panel surface temperature and electrical efficiency, and a good agreement was found between them. The daily average experimental and simulation electrical efficiency is 14.5% and 14.9%, while the average temperature and electrical efficiency error is 3.3% and 9.1%, respectively.

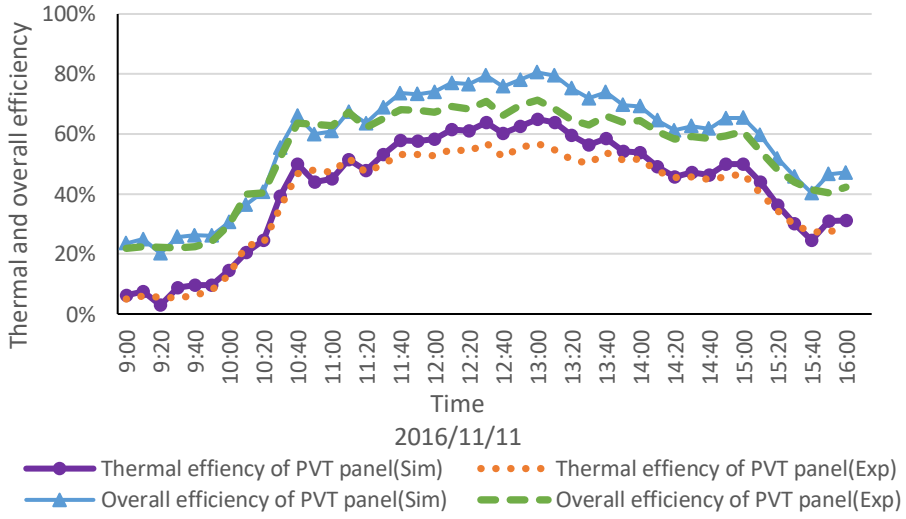

Fig. 6- 21 Comparison between the experimental and simulation thermal and overall efficiency of PV/T panels in winter

Fig. 6-21 shows the variation trend of thermal and overall efficiency which was mainly impacted by solar radiation. The average experimental and simulation value of them was 31.7% and 33.9%, 46.2% and 48.8%, while the error of thermal and overall efficiency is 8.8% and 7.3%, respectively.

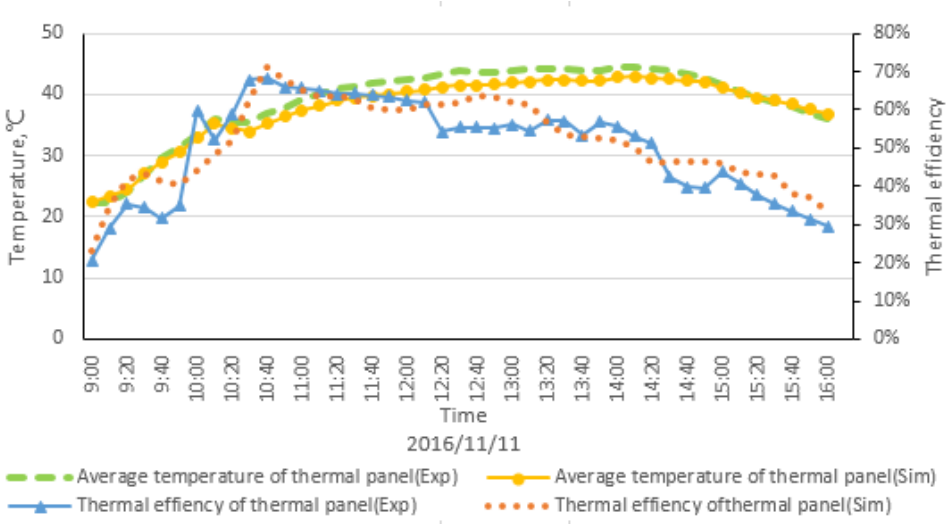

Fig. 6- 22 Average experimental and simulation panel surface temperature and thermal efficiency of thermal panels in winter

Fig. 6-22 shows the variation of panel surface temperature and thermal efficiency of thermal panel, both which was impacted by solar radiation. The average value of thermal efficiency was 49.9% and 51.3%, respectively. The error of the temperature and thermal efficiency is 3.7% and 8.5%.

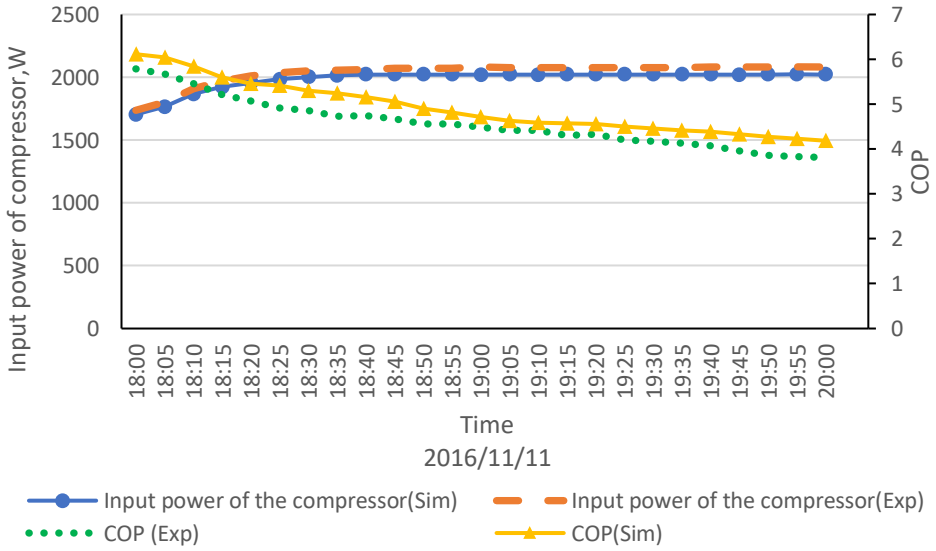

Fig. 6- 23 comparison between the experimental and simulation COP and input power of heat pump in winter

Fig. 6-23 shows the variation of the experimental and simulation input power of the compressor and COP of the heat pump, and the value of them agreed with each other very well. The average experimental and simulation COP of the heat pump was 4.6 and 4.9, respectively. The error of input power and COP is 2.5% and 7.4%, respectively.

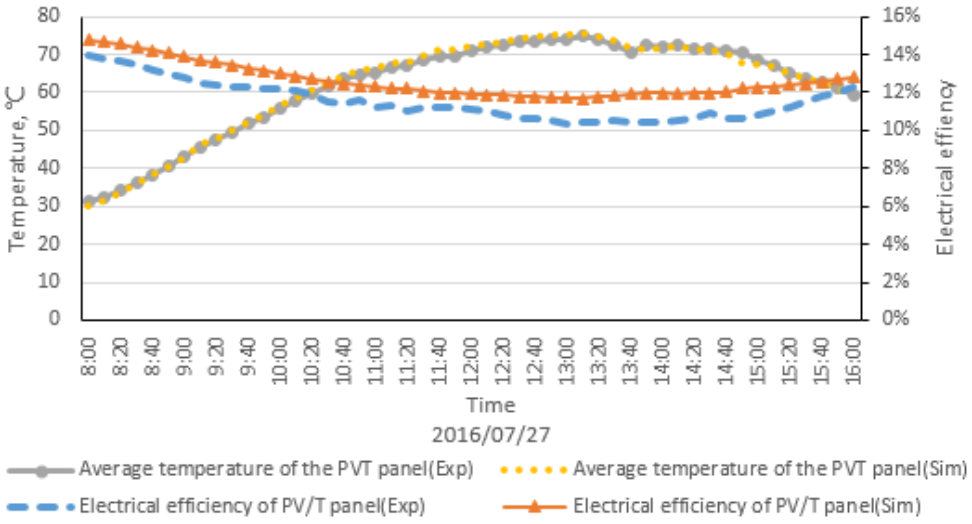

Fig. 6- 24 Average experimental and simulation panel surface temperature and electrical efficiency of the PV/T panels in summer

Fig. 6-24 shows the variation of panel surface temperature and electrical efficiency of the PV/T panels in summer. The experimental and simulation result was 11.5% and 12.6%. The error of the temperature and electrical efficiency was 1.2% and 9.5%, respectively.

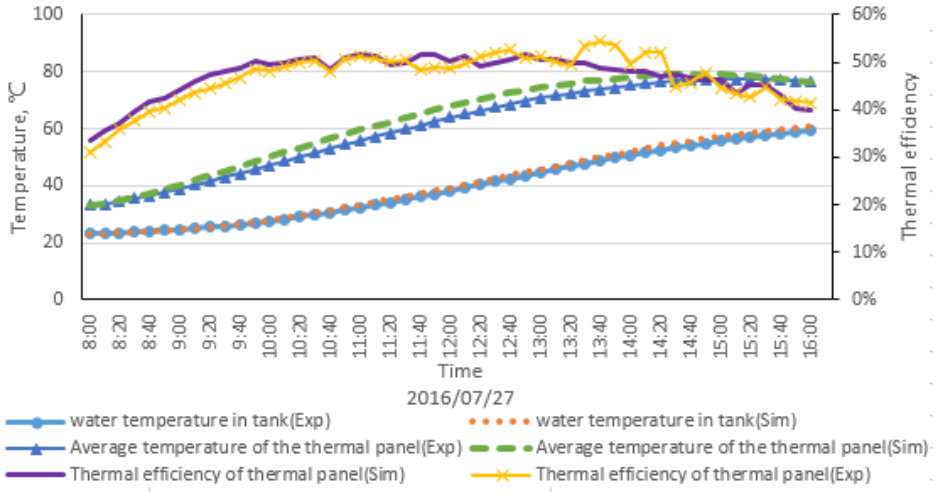

Fig. 6- 25 Average experimental and simulation panel surface temperature and thermal efficiency of the PV/T panels and water temperature in tank in summer

The surface temperature, thermal efficiency of thermal panel and water temperature in the tank was shown in **Fig. 6-25.** All of them were impacted by the solar radiation. The average experimental and simulation thermal efficiency was 46.8% and 47.0%, and the water temperature increased from

23 ºC to 60 ºC slowly. The error of them was 1.6%, 3.9% and 1.4%, respectively.

It can be found that most of the most significant results agreed with each other very well, and the error of them are shown in the **Table 6-5**. The high error of the performance efficiency is caused by several reasons, i.e., testing error, unstable practical operating condition. The electrical efficiency is impacted by the inverter and load, and the other efficiency is calculation value and affected by the mix measurement errors.

Table 6- 5: Average error of the system and performance

		T_{sur}	η_{t_pvt}	η_{e_pvt}	η_{o_pvt}	η_{t_th}
Average	Winter	3.7%	8.1%	9.1%	7.3%	8.5%
Error	Summer	1.4%	-	9.5%	-	3.9%

6.5 Chapter summary

This chapter described the experimental performance of the solar indirect-expansion heat pump for space heating in winter and hot water in summer. A hybrid space heating system comprising the mini-channel solar thermal and PV/T panels and a heat pump was designed, constructed and tested at the selected clear days of Lvliang city, China.

In overall, the system had three functional parts, namely, solar heat collection through the solar thermal and PV/T panels, heat transportation and upgrading through the solar loop, heat storage and heat pump, and heat release through the heating loop. These three parts were appropriately integrated via the appropriate piping network and control measures. In winter, it was found that the mini-channel PV/T panels had the average electrical, thermal and overall efficiencies of 14.5%, 31.7% and 46.2% respectively, while the mini-channel thermal panels had the average solar thermal efficiency of 49.9%, and the heat pump had an average COP of 4.6. The temperature of the testing room remained at above 18 ºC throughout the whole testing period, indicating that the system has the capacity to meet the comfort standard of the building. In summer, the average electrical efficiency of the PV/T panel was 11.5%, and the average thermal efficiency of thermal panel was 46.8%. The temperature of water in the tank increased from 23 ºC to 60 ºC which is high enough for different kinds of use. Compared the simulation and experimental results, the

experimental and simulation results revealed good agreement with each other, and the error of all the parameters ranged from 1.4% to 9.5%.

The experimental and simulation result of the system in winter and summer provided fundamental data and method for the performance analysis of whole year and improvement of the similar system in the future.

CHAPTER 7： ENERGY SAVING, ECONOMIC AND ENVIRONMENTAL ANALYSIS

7.1 Chapter introduction

This chapter predicted the annual performance of the two solar heat pump systems, based on the weather condition of Taiyuan, China and London, UK. The electrical, thermal efficiency and energy output of the panels, the performance of the economic and environment of the two systems are investigated. The works of these are as follows:

(1) The energy performance of the two systems are predicted with the computer model used in previous chapter.
(2) The economic performance of the two systems are analysed, compared to local space heating method.
(3) The environmental performance of the two systems are calculated based on the predicted result.

Based on the local weather data and computer model, the study on the energy, economic and environmental performance of the two systems are presented. The results give reasonable data to describe the total performance of the two systems.

7.2 Annual operational performance

The annual performance of the two system are based on the local weather and good computer model. Therefore, in this section, the weather data, i.e., solar radiation, ambient temperature, wind speed, electrical and thermal efficiencies of the panels, the monthly energy output of the two systems will be analysed successively.

7.2.1 Weather condition of Taiyuan and London

Both the weather data of the two cities is from the “energy plus” [7.1]. The variation of the hourly solar radiation, ambient temperature wind speed is shown in **Fig. 7-1, Fig. 7-2** and **Fig. 7-3**. The solar radiation and the ambient temperature of local city shows a similar trend, both of which are low in winter and high in summer. While the high wind speed occurs between April and May, and the low wind speed occurs in September. The hour-by-hour in

winter (January to March, November and December) is from 9:00 to 16:00, while it is from 8:00 to 16:00 in other seasons.

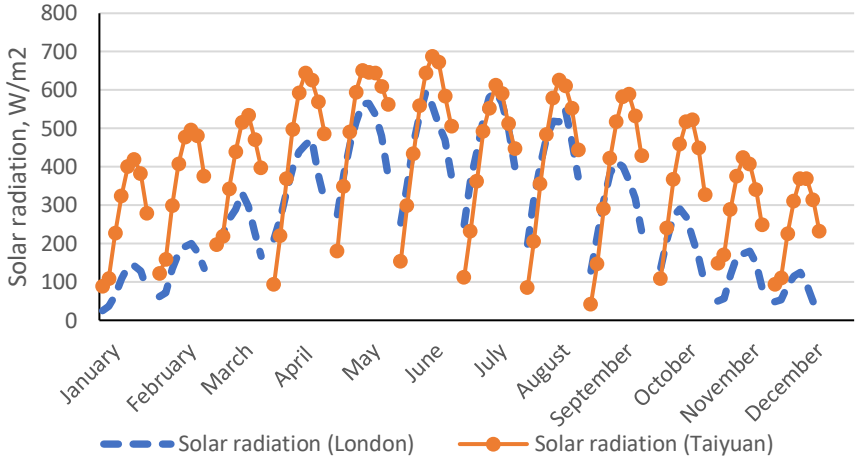

Fig. 7- 1: Hourly solar radiation of Taiyuan and London

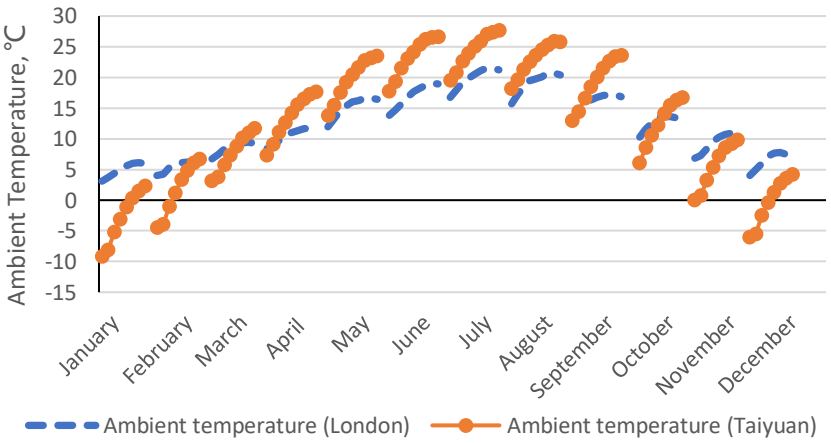

Fig. 7- 2: Hourly ambient temperature of Taiyuan and London

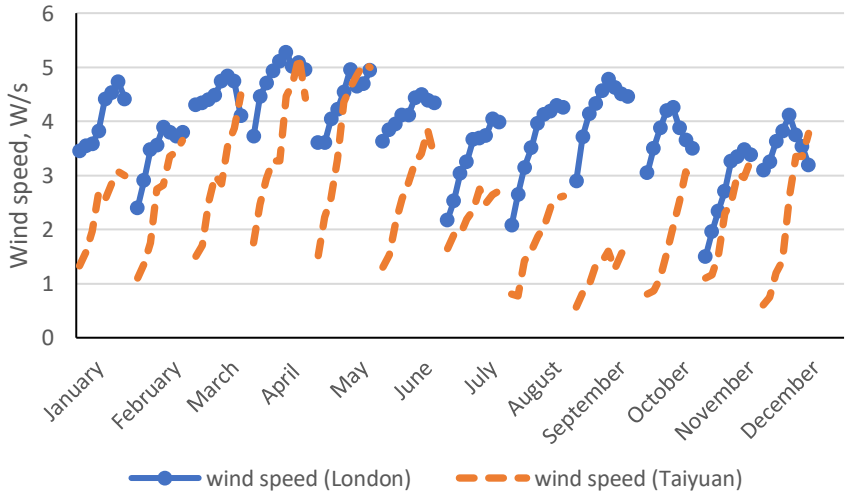

Fig. 7- 3: Hourly wind speed of Taiyuan and London

7.2.2 Energy performance of the solar direct-expansion heat pump system

The system is assumed to operate between 90:00 to 16:00 in the simulation model. In winter, the system provides thermal and electricity energy for building, and it is assumed that the initial water temperature in the tank is 30 ^{o}C. In summer, the PV/T panels will generate electricity for user.

The hourly simulation temperature of panel is shown in **Fig. 7-4**. In winter, it ranges from 7 ^{o}C to 40 ^{o}C; while in summer, it ranges from 13 ^{o}C to 68 ^{o}C, which is impacted by the weather data and operating model. The electrical and thermal efficiencies of the panel is shown in **Fig. 7-5** and **Fig. 7-6**, and the result is influenced by the operating temperature of the panels. The electrical efficiency ranges from 13.0 % to 16.2% in winter and 10.6% to 13.4% in summer. The thermal efficiency ranges from 54.2% to 57.0% in winter. The COP of the heat pump is shown in **Fig. 7-7**, it is based on the energy output of the system and input power of the compressor, which ranges from 3.6 to 5.0.

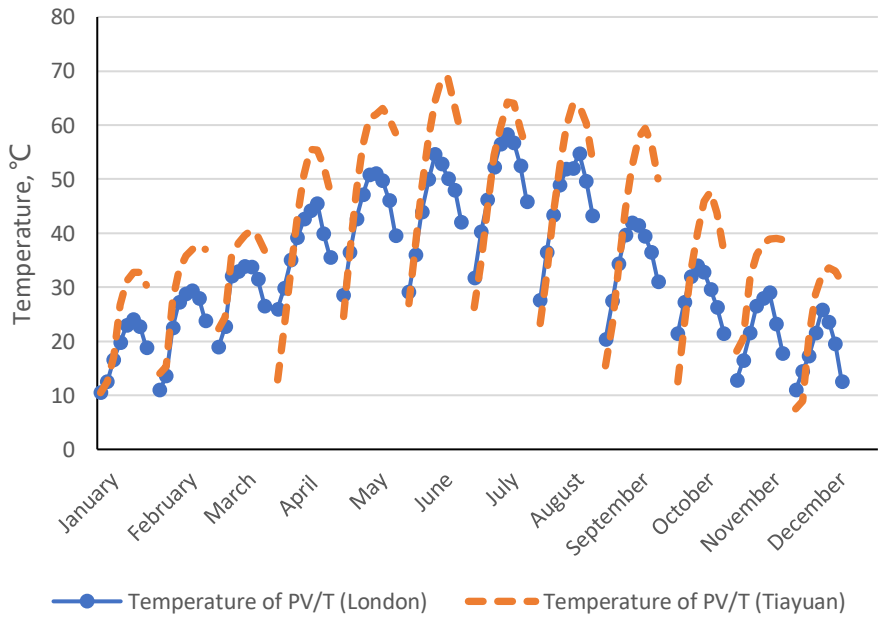

Fig. 7- 4: Simulation temperature of the PV/T panel in Taiyuan and London (DEHP)

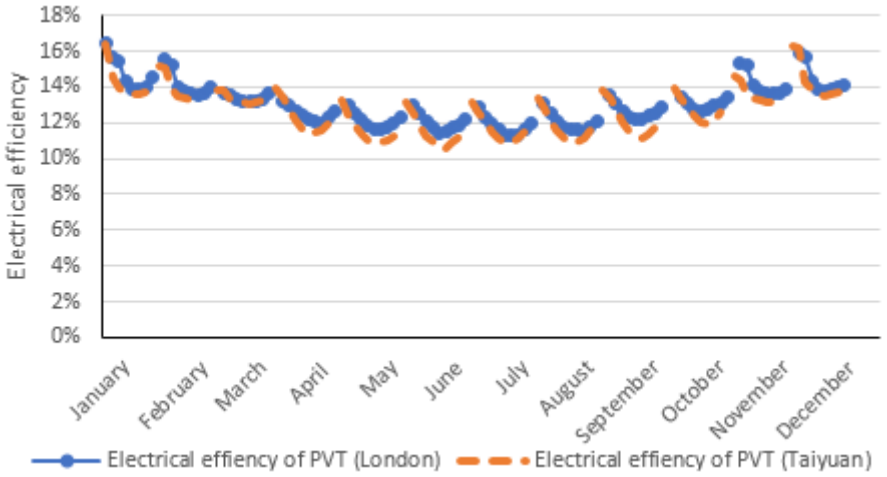

Fig. 7- 5: Simulation electrical efficiency of the PV/T panel in Taiyuan and London (DEHP)

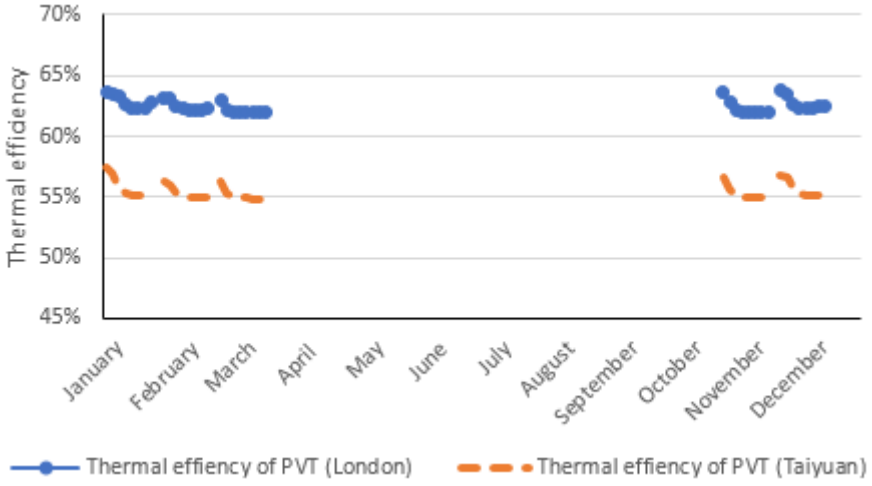

Fig. 7- 6: Simulation thermal efficiency of the PV/T panel in Taiyuan and London (DEHP)

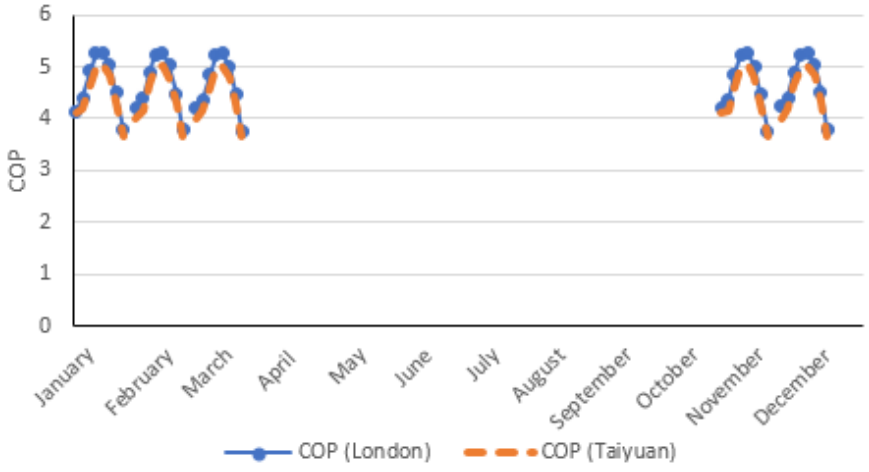

Fig. 7- 7: Simulation COP of the heat pump system in Taiyuan and London (DEHP)

The finial water temperature of Taiyuan and London in the tank is shown in **Table 7-1**. For the Taiyuan city, the lowest is 35 ºC in January while the highest is 45.4 ºC in March. For the London city, the lowest is 30.1 ºC in December, while the highest is 32.0 in March. It can be concluded that the result is decided by the solar radiation and ambient temperature, while the solar radiation will impact the energy which the water received from the solar heat pump system and the ambient temperature will influence the energy which the water released to the building.

Table 7- 1: Final water temperature in the tank (DEHP)

Month		Jan	Feb	Mar	Nov	Dec
Finial water temperature (℃)	Taiyuan	35.0	42.5	45.4	36.4	38.1
	London	30.8	31.2	32.0	30.5	30.1

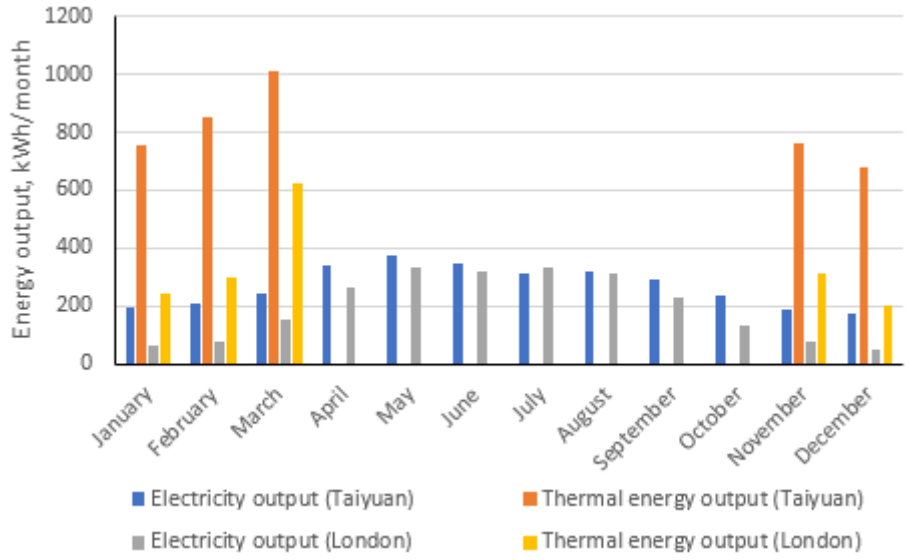

Fig. 7- 8: Monthly electricity output and thermal energy output of the system in Taiyuan and London (DEHP)

The monthly electricity output and thermal energy output of the system in Taiyuan and London is shown in **Fig. 7-8**. The energy output of the system mainly relies on the solar radiation. For Taiyuan city, the value of electricity output ranges from 172 kWh in December to 368 kWh in May. The value of thermal energy output ranges from 677 kWh in December to 1,014 kWh in March. For London city, the value of electricity output ranges from 52 kWh

in December to 334 kWh in May. The value of thermal energy output ranges from 199 kWh in December to 625 kWh in March

7.2.3 Energy performance of the solar indirect-expansion heat pump system

The output energy of the indirect-expansion heat pump system has two functions, which is for space heating in winter and hot water in other seasons. In winter, it is assumed that the solar panel provide energy during 9:00 to 18:00; the heat pump provide energy during 18:00 to 20:00; and the gas heater provides energy during 22:00 to 9:00. The initial water temperature in the tank is set at 15 ^{o}C, which will be heated by solar panel and then act as the energy source of heat pump to provide energy in the night. For the heat pump, the initial temperature at the inlet of evaporator and condenser is the water temperature in the tank and 20 ^{o}C respectively. The initial temperature at the inlet of gas heater is 20 ^{o}C. In other seasons, it is assumed that the operating time is from 8:00 to 16:00, and the initial water temperature is 23 ^{o}C that is the same as the experimental value.

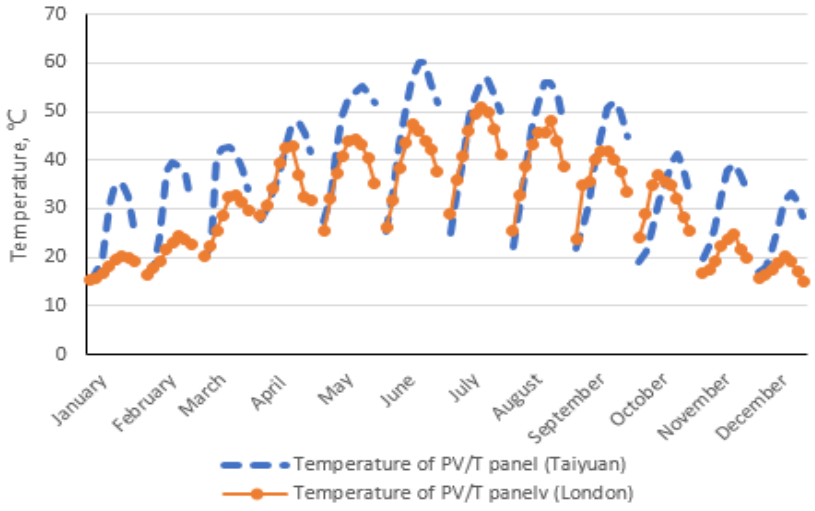

Fig. 7- 9: Simulation temperature of the PV/T panel in Taiyuan and London (IDEHP)

The hourly simulation result of the temperature of PV/T panel in Taiyuan and London is shown in **Fig. 7-9,** and it can be seen that the result is impacted by the weather condition. In winter, the solar radiation and ambient temperature is low, making the PV/T panel operating at a low temperature, ranging from 15.6 ^{o}C to 41.5 ^{o}C. While they are much higher in other seasons, then the

PV/T panels work at a high temperature, which ranges from 21.8 ºC to 60.1 ºC.

The hourly electrical efficiency of PV/T panels is shown in **Fig.7-10**. It is influenced by the working temperature of the PV/T panel, and shows a converse variation trend, ranging from 13.5% to 16.3% in summer and 15.6% to 18.0% in winter.

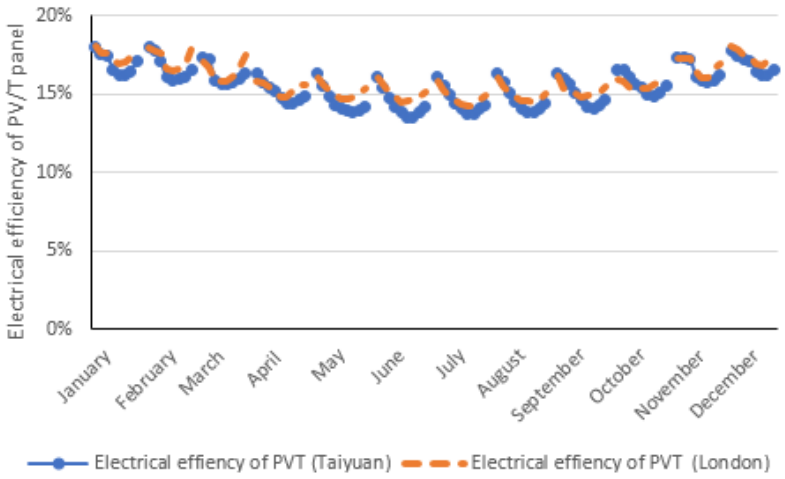

Fig. 7- 10: Simulation electrical efficiency of the PV/T panel in Taiyuan and London (IDEHP)

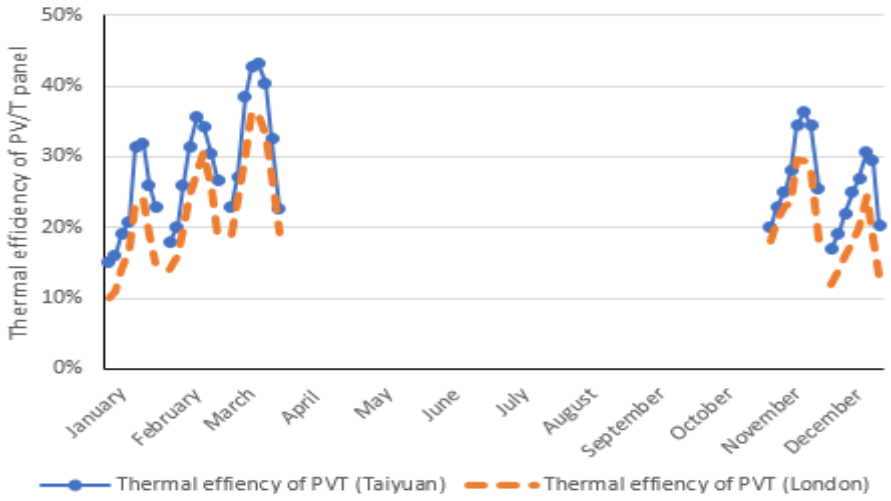

Fig. 7- 11: Simulation thermal efficiency of the PV/T panel in Taiyuan and London (IDEHP)

The thermal efficiency of PV/T panel is shown in **Fig. 7-11**, which shows a similar variation trend as the operating temperature, ranging from 10.7% to 43.2%.

The monthly electricity and thermal energy output of the PV/T panels is shown in **Fig. 7-12**. They have a similar trend as the solar radiation, and both minimum electricity and thermal energy output occurs in December. The maximum electricity output is in May (Taiyuan:428 kWh, London: 380kWh), while the thermal energy output is in March (Taiyuan: 511 kWh, London: 322 kWh).

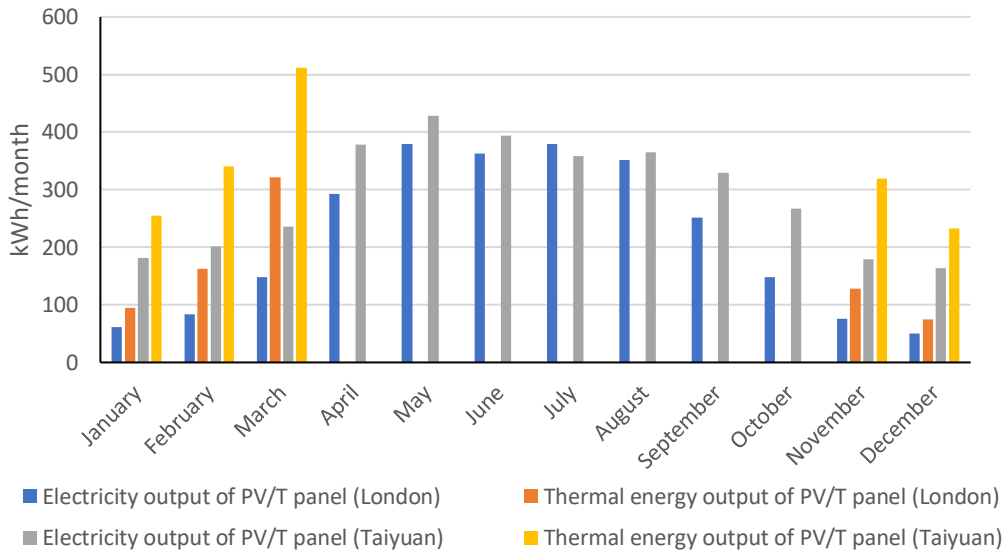

Fig. 7- 12: Monthly electricity and thermal energy output of the PV/T panels in Taiyuan and London (IDEHP)

The hourly operating temperature of thermal panel is shown in **Fig. 7-13**, it has a similar variation trend as the temperature of PV/T panel and also is impacted by the weather condition.

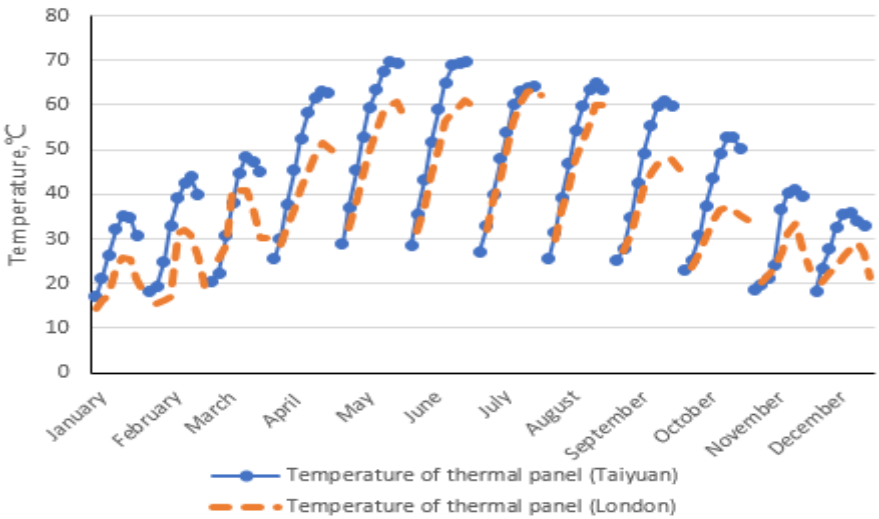

Fig. 7- 13: Simulation temperature of the thermal panel in Taiyuan and London (IDEHP)

The hourly thermal efficiency and water temperature is shown in **Fig. 7-14** and **Fig. 7-15,** respectively. In winter, the thermal efficiency of the thermal panel relies on the solar radiation and ambient temperature, ranging from 23.0% to 57.0%. In summer, it is affected by the water temperature of storage tank (**Fig. 7-15**) and the weather condition together.

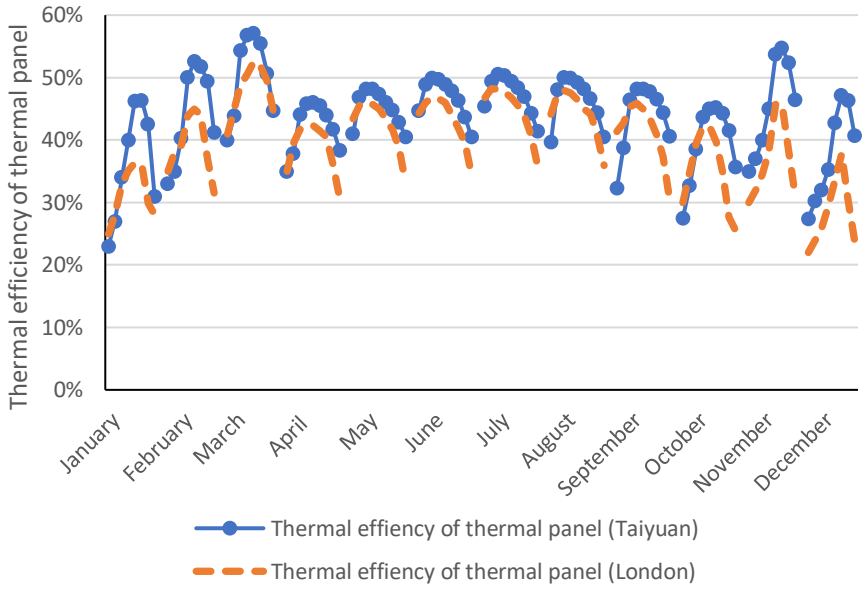

Fig. 7- 14: Simulation thermal efficiency of the thermal panel in Taiyuan and London (IDEHP)

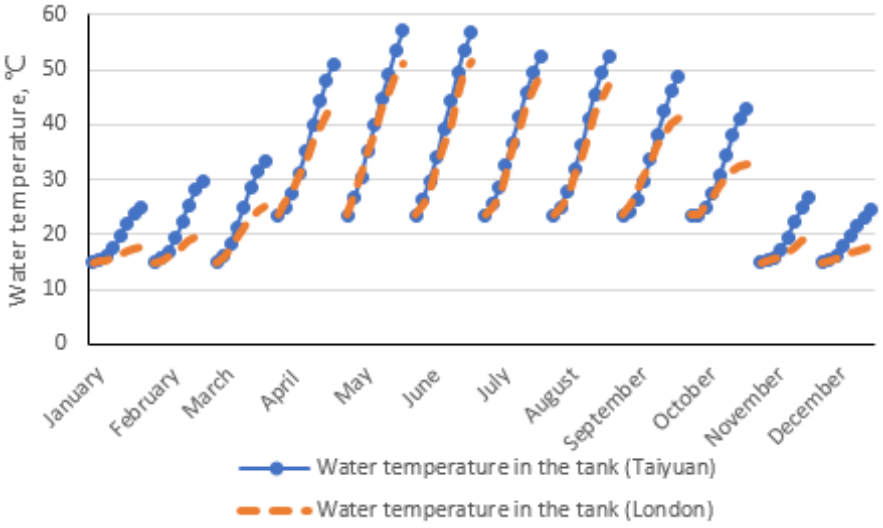

Fig. 7- 15: Simulation water temperature in the tank in Taiyuan and London (IDEHP)

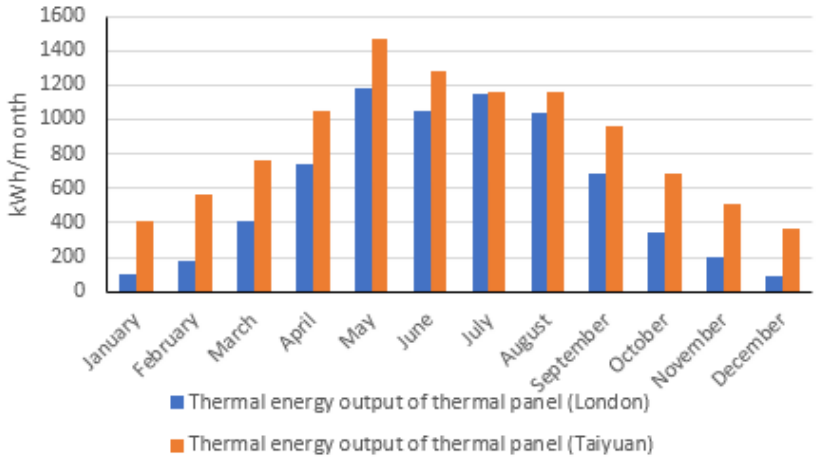

Fig. 7- 16: Monthly thermal energy output of the thermal panels in Taiyuan and London

Fig. 7-16 shows the monthly thermal energy output of the thermal panels, which has a similar trend as the solar radiation. For Taiyuan, it ranges from 396 kWh in December to 1,473 kWh in May. While for London, it ranges from 89 kWh in December to 1,183 kWh in May.

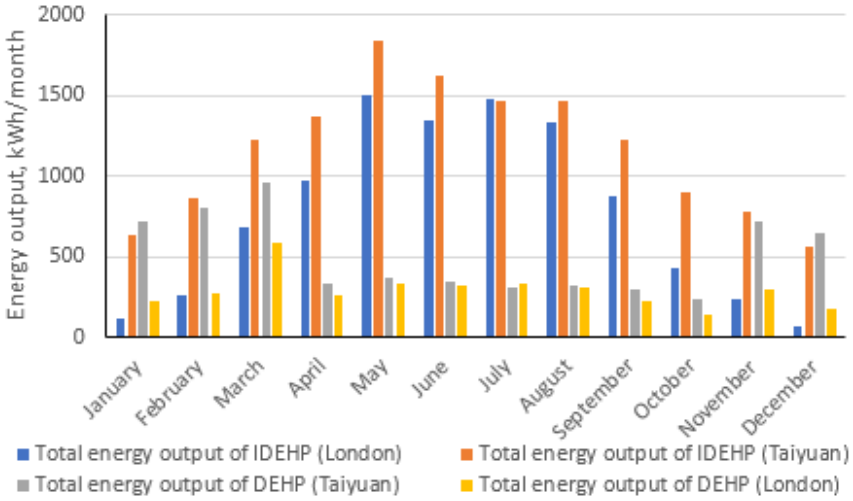

Fig. 7- 17: Comparison of total energy output by substituting the consumption of the two systems in Taiyuan and London

Fig. 7-17 shows the comparison of the two systems with substituting the system consumption on the total energy output in London and Taiyuan. It can be found that the solar indirect-expansion heat pump system has the maximum energy output in Taiyuan within the most of operating time, owning to the local strong solar radiation. While the solar direct-expansion heat pump system has the lowest energy output in London, owning to the local weak solar radiation.

7.2.4 Energy saving performance of the two systems compared to traditional boiler-based heating system with the equivalent capacity

The calculation of the operating cost and saving is based on a house with the area 150 m^2 and five people. The energy of this family need includes the space heating energy in winter and hot water annually. The initial water temperature of local city can be assumed to be 23 ^oC and the finial water temperature is 45 ^oC. The energy for hot water and space heating can be calculated as follow:

$$Q_{h.w} = C_{p.w} * M_{h.w.d} * \Delta T_{h.w} * n_{d.a} \quad [7\text{-}1]$$

$$Q_{s.h} = \sum_{i-0}^{i=24} K_{wall} * A_{wall} * \Delta T_{s.h} * n_{d.h} \quad [7\text{-}2]$$

Where, $Q_{h.w}$ is the thermal energy for hot water (kWh); $M_{h.w.d}$ is the quality of hot water needed per day (kg); $\Delta T_{h.w}$ is the temperature difference between the initial and finial water temperature (K); $n_{d.a}$ is the number of the days for hot water; $Q_{s.h}$ is the thermal energy for space heating (kWh); K_{wall} is the heat transfer rate between the inside and outside of the building ($W/m^2/K$); A_{wall} is the area of the wall (m^2); $\Delta T_{s.h}$ is the temperature difference between the indoor air and outdoor air; $n_{d.h}$ is the number of the days for space heating.

The solar heat pump system and gas boiler work together to provide the energy of the building demanded. The calculation result is shown in **Table 7-2**. It is assumed that the room air is set at 18 ^oC in winter. The efficiency of the coal boiler, gas boiler and electric heater is 35%, 80% and 90%, respectively. During the whole years' time, for Taiyuan city, the energy needed for space heating is much more than the hot water, which is 12,371 kWh and 3,194 kWh, respectively, while for London, the energy for space heating and hot water is around 3,750 kWh [7.2] and 15,000 kWh [7.3], respectively. Due to the limited function, the solar direct-expansion heat pump system only can provide thermal energy in winter; therefore, it has a lower proportion than the solar indirect-expansion heat pump system, accounting respectively for 26.1% and 47.9% of the whole years' energy demanded. For Taiyuan, the solar direct-expansion and indirect-expansion heat pump system can save energy about 4,054 kWh/year and 7,460 kWh/year, while for London, these two systems can save energy around 1,683 kWh/year and 5,518 kWh/year, respectively.

7.3 Life-cycle and economic performance analysis

7.3.1 Capital cost of the solar direct-expansion and indirect-expansion heat pump system

The capital cost of the two solar heat pump system consists of the price of all the components of the system and installation fee. **Table 7-2** gives a list of cost of the two systems. For the solar direct-expansion heat pump and gas boiler (efficiency 80%) [7.4] system, the initial cost of it is around GBP 5,975. The micro-channel PV/T panel accounts for the largest proportion, which is around 47.4%. For the solar indirect-expansion heat pump and gas boiler system, the capital cost is GBP 6,303, and the mini-channel PV/T and thermal panels are the largest component of the total cost, accounting for 50.4% of all the cost. For the traditional coal boiler (efficiency 30%-40%) [7.5] and electric heater (efficiency 90%) [7.4] system, the initial cost is GBP 907, and the coal boiler and electric heater are the most expensive, accounting for 60.0%.

Table 7- 2: Cost of the solar direct-expansion and indirect-expansion heat pump system

Solar direct-expansion heat pump system				
No.	**Item**	**Quantity/size**	**Unit Price (GBP)**	**Cost (GBP)**
1	**Micro-channel PV/T**	11/2m^2	234	2,575
2	**Compressor**	1/5P	245	245
3	**Water tank (condenser)**	1/1m^3	1,093	1,092
4	**Electric expansion valve & Controller**	1	248	248
5	**Copper tube**	40 meters/DN20	4	160
6	**Water pump**	1/90W	14	14
7	**Gas boiler**	1/24kW	541	540
8	**Refrigerant**	10 kg/R410a	89	89
9	**Solar battery**	4/ 12V 200Ah	100	401
10	**Inverter**	1/ 48V	256	256
11	**Electric wire**	30 meters/10A	1	18
12	**Panel support**	11/ 2m^2	13	147
13	**Insulation**	40meters	1	17
14	**Installation fee**	1	167	168
15	**Total cost (GBP)**			5,975

Solar indirect-expansion heat pump system				
1	**Mini-channel PV/T panel**	10/2m^2	234	2,340
2	**Mini-channel thermal panel**	10/2m^2	84	836
3	**Water tank and heat exchanger**	1/ 1t	446	446
4	**Water pump**	1/200W	78	78
5	**Heat pump**	1/3P	622	622
6	**valve**	6	14	87
7	**Solar battery**	4/ 12V 200Ah	100	400
8	**Inverter**	1/ 48V	256	256
9	**Gas heater**	1/24kw	541	541
10	**Electric wire**	30 meters/10A	1	18
11	**Antifreeze**	10/ 10L	13	130
12	**Electric wire**	30 meters/10A	1	19
13	**Panel support**	20/ 2m^2	13	260
14	**Insulation**	30meters	1	30
15	**Plastic tube**	30meters/DN25	1	30
16	**Installation fee**	1	223	223
17	**Total cost (GBP)**			6,303
Coal boiler and electric heater				
1	**Coal boiler**	1/150m^2	264	264
2	**Electric heater**	1/60L	279	279
3	**Heat sink**	4/720 x 670mm	36	145
4	**Tube**	30meters/ DN25	3	100
5	**Installation fee**	1	111	111
6	**Total cost (GBP)**			907

In China, many policies are made to encourage the local people to develop the renewable energy and clean energy system for space heating in winter. With the support of the local government, the installation subsidy is GBP 0.33 per W (PV installed capacity) [7.6], and the clean energy system can get GBP 250 per house to replacing the traditional coal boiler [7.7]. These policies can low down the capital cost of the new system. In London, the government encourage the uptake of renewable heating technologies within households, communities and businesses through the provision of financial incentives, which is GBP 0.192/kWh-year-heat [7.8].

7.3.2 Annual operational cost and bill saving

For the two solar heat pump systems, the operating cost is mainly caused by the consumption of the electricity and gas. With the policy support of the local

government, the generated electricity can be sale to the electricity company and the income form this can cover part annual operating cost of the two systems. Owning to the similar number of PV/T panels, the electricity generated by the two systems is also similar, which is 3,232 kWh and 3,481 kWh in Taiyuan, while 2,350 kWh and 2,583 kWh in London, respectively. Therefore, the finial operating cost of the two solar heat pump systems is GBP 175 and GBP 64 in Taiyuan, while 622 kWh and 431 kWh in London, respectively. The details of the operating cost and bill saving is shown in **Table 7-3**.

Table 7- 3: Operating cost of the solar direct-expansion and indirect-expansion heat pump systems

location	Taiyuan		London	
Energy price and demand				
Gas price (GBP/kWh)	0.03 [7.9]		0.05 [7.10]	
Electricity price (GBP/kWh)	0.06 [7.11]		0.14 [7.12]	
Coal price (GBP/kWh)	0.02 [7.13]		/	
Feed-In Tariff (GBP/kWh)	0.1[7.14]		0.15 [7.8]	
Total heat demand for hot water (kWh/yr)	3,194		3,750	
Total heat demand for space heating (kWh/yr)	12,371		15,000	
Cost for hot water (GBP)	Electric heater	198	Gas boiler	188
Cost for space heating (GBP)	Coal boiler	380	Gas boiler	750
Total operating cost (GBP)	578		938	
Solar direct-expansion heat pump system				
Heat produced from system for space heating (kWh/yr)	4,054		1,683	
Energy required from auxiliary heater for space heating (kWh/yr)	Gas boiler	8,317	Gas boiler	13,317
Heat produced from system for hot water (kWh/yr)	0		0	
Energy required from auxiliary heater for hot water (kWh/yr)	Gas heater	3,194	Gas boiler	3,750
Total electricity output from module (kWh/yr)	3,232		2,350	
Electricity consumed by heat pump (kWh/yr)	946		546	
Cost (GBP)	175		622	
Saving cost (GBP)	403		315	

Solar indirect-expansion heat pump system				
Heat produced from system for space heating (kWh/yr)	4,266		1,768	
Energy required from auxiliary heater for space heating (kWh/yr)	Gas boiler	8,150	Gas boiler	13,232
Heat produced from system for hot water (kWh/yr)	3,194		3,750	
Energy required from auxiliary heater for hot water (kWh/yr)	0		0	
Total electricity output from module (kWh/yr)	3,481		2,583	
Electricity consumed by system (kWh/yr)	1,448		1,123	
Cost (GBP)	64		431	
Saving cost (GBP)	514		507	

7.3.3 Annual maintenance costs

The main components of the two system are micro/mini-channel PV/T panels and heat pump; and they are all the standard products, which have a high quality and long lifetime. Normally the maintenance cost accounts for 2%-3% [7.15] of the initial cost. Therefore, the maintenance cost of the solar direct-expansion and indirect-expansion heat pump system is GBP 120 and GBP 127, respectively.

7.3.4 Cost payback time and life-cycle net cost savings

With replacing the traditional space heating system (coal boiler and electric heater) by the solar heat pump system and gas boiler, the payback period can be calculated as follow [7.15]:

$$CPT_{shp} = \frac{F_{cc} - F_{es} - F_{hps} - F_{tc}}{(F_{to} + F_{tm}) - (F_{so} + F_{sm})} \quad [7\text{-}3]$$

Where, CPT_{shp} is the payback time of the solar heat pump system (years); F_{cc} and F_{tc} is the initial cost the solar heat pump system and traditional space heating system (GBP); F_{es} and F_{hps} is the PV installation subsidy and clean energy system(GBP) respectively; F_{to} and F_{so} is the annual operating cost of the solar heat pump system and traditional space heating system (GBP); F_{tm} and F_{sm} is the annual maintenance cost of the new and traditional system (GBP).

For Taiyuan city, compared to traditional space heating system, the payback time of the solar direct-expansion and indirect-expansion heat pump system is 8.7 years and 5.8 years. For London city, the payback time of the solar direct-expansion and indirect-expansion heat pump system is 6.6 years and 3.5 years. The reason of this is that the thermal panels in solar indirect-expansion heat pump system can replace the gas boiler to provide hot water in most time of the year, which can save money directly. Compared to existing PV/T systems [2.10] whose payback time is between 15 to 21 years; these two systems have a much shorter payback time. The reason is that 1), the cost of PV/T is much higher in EU than it in China; 2), its function is too simple and just for hot water; 3) the bad weather data make it work in a poor performance which cannot provide enough thermal energy to cover the requirement of user and generate little electricity, resulting in rare income for sale; and 4) the support from the government is different. The new systems, although have a much higher initial cost, can overcome these drawbacks and meet multiple demand of user, saving others' consumption, then shorten the payback time.

Most of the components of the solar heat pump system has a long lifetime, i.e., the heat pump is over 20 years [7.16], the PV/T panels and thermal panels is around 25 years [7.17]. Therefore, the life-cycle net cost of the two systems can be given as [7.15]:

$$LCNC_{shp} = (20 - PT_{shp})[(F_{to} + F_{tm}) - (F_{so} + F_{sm})] \quad [7\text{-}4]$$

Where, $LCNC_{shp}$ is the life-cycle net cost of the system (GBP). Similarly, owning to the thermal panels which saves money, the life-cycle net cost of the solar indirect-expansion heat pump system is much higher which is GBP 8,391 in Taiyuan and GBP 8,366 in London, while the solar direct-expansion heat pump system is GBP 4,316 in Taiyuan and GBP 4,221 in London, respectively.

The analytical result indicates that it is reasonable to replace the traditional heater with the new solar heat pump system, which has a low operating cost. Compared the two solar heat pump systems, the solar indirect-expansion heat pump system has a much better economic perform than the direct-expansion one, although it has a higher initial cost.

7.4 Life-cycle environmental performance analysis - based on carbon emission performance of the systems relative to the traditional ones

Using solar energy to replace the traditional energy can reduce the CO_2 emission. For the traditional system, the CO_2 emission is main caused by the burning coal and electric heater. For the solar heat pump system, the CO_2 emission is from the gas boiler, operating of the compressor and water pump. The quality of the CO_2 emission saving in the lifetime can be given as [7.15]:

$$CS_{shp} = f'_{coal}Q_{coal} + f'_{ele}Q_{e.h} - f'_{ele}Q_{e.hp} - f'_{gas}Q_{gas} \quad [7\text{-}5]$$

Where, CS_{shp} is the quality of saving CO_2 emission (kg); f'_{coal} , f'_{ele} and f'_{gas} is the CO_2 emission factor of burning coal, electricity consumption and burning gas respectively (kg CO_2/kWh).; Q_{coal}, $Q_{e.h}$, $Q_{e.hp}$ and Q_{gas} is the energy provided by the coal boiler, electric heater, solar heat pump system and gas boiler (kWh).

Table 7- 4: Annual CO_2 emission saving of the solar heat pump system

CO_2 emission factor (kg/kWh)		
electric heater	0.997 [7.18]	
Coal boiler	0.43 [7.19]	
Gas boiler	0.26 [7.20]	
location	Taiyuan	London
CO_2 emission reduction		
Solar direct-expansion heat pump system (kg)	4,568	2,242
Life cycle CO2 emission reduction of DEHP (t)	91.4	44.8
Solar indirect-expansion heat pump system (kg)	5,451	3,812
Life cycle CO2 emission reduction IDEHP (t)	109.1	76.2

As shown in **Table 7-4**, compared to traditional coal boiler and electric heater, the annual CO_2 emission saving of the solar direct-expansion and indirect-expansion heat pump system combined gas boiler is 4.6 t and 5.5 t in Taiyuan, while 2.2 t and 3.8 t in London, respectively. The life-cycle CO_2 emission saving of the two new systems is 91.4 t and 109.1 t in Taiyuan, while 44.8 t and 76.2 t in London, respectively. It indicates that the two new systems can reduce the CO_2 emission obviously, and it is worth to promote solar heat pump system in the cold area.

7.5 Chapter summary

This chapter analysed the annual performance of the solar direct-expansion and indirect-expansion heat pump system based on the weather data of Taiyuan and London. The content includes the annual energy performance, the operating cost, the payback time and CO_2 emission saving of the two systems.

For the solar direct-expansion heat pump system, the performance is impacted by the capacity of the heat pump. When the solar radiation is low, it can absorb the energy more effectively, meaning that it owns a much better performance in electrical, thermal efficiency and COP. According to the result, the system has a better performance in London with the electrical efficiency ranges from 11.2 % in summer to 16.5% in winter. The thermal efficiency ranges from 61.2% to 64.5.0% in winter. The COP of the heat pump ranges from 4.2 to 5.3. For the solar indirect-expansion heat pump system, the thermal efficiency has a similar variation trend as the solar radiation, while the electrical efficiency has an opposite trend. Therefore, the system in Taiyuan has better thermal efficiency which ranged from 23.2% to 57.1%. while the electrical efficiency is from 14.4% to 18.1% in London.

The annual energy output was determined by the solar radiation, therefore, the energy output in Taiyuan is much higher than it in London. For the solar direct-expansion heat pump system, based on the weather data of Taiyuan city, the maximum electricity output is 368 kWh in May. The maximum thermal energy output is 1,014 kWh in March. Based on the weather data of London, the maximum electricity output is 334 kWh in May. The maximum thermal energy output is 625 kWh in March. For the solar indirect-expansion heat pump system, based on the weather data of Taiyuan, the maximum thermal output is 1,984 kWh in May, while for London, it is 1,505 kWh in May. The maximum electricity output of the system in Taiyuan and London is in May (Taiyuan:428 kWh, London: 380kWh).

The initial cost of solar direct-expansion and indirect-expansion system is GBP 5,973 and GBP 6,303. Compared to traditional coal boiler and electric heater system, the payback time of these two systems is 8.7 years and 5.8 years in Taiyuan, while 6.6 years and 3.5 years in London with the local

policy support. In Taiyuan, and the life-cycle net cost of these two systems is is GBP 4,316 and GBP 8,391, respectively, while it is GBP 4,221 and GBP 8,366 in London. The annual and life-cycle CO_2 emission saving of these two systems is 91.4 t and 109.1 t in Taiyuan, respectively, while it is 44.8 t and 76.2 t in London.

The excellent performance of the new clean systems indicates that there is a potential for developing them in cold area, especially with the support from the local government who is trying their best to encourage local people to replace the unreasonable old system.

CHAPTER 8: CONCLUSION AND FUTURE WORK

8.1 Conclusion

This research gave an investigation on the performance of the solar direct-expansion and indirect-expansion heat pump system. The works included a critical literature review, a concept design, development of simulation model, an experiment in real weather conditions, an analysis about the results, and an analysis of the economic and environmental performance.

The overall achievements include 1), two simulation models, which are developed based on the two solar heat pump systems; 2), two corresponding designed and constructed experimental platforms; 3) an economic analysis model which is presented to predict the energy, economic and environmental performance of the two systems in a local city.

The major conclusions summarized from the PhD work can be given as below.

(1) Micro-channel PV/T panel

For the existing PV/T panels, most of their heat exchange structure are copper tube, which has a limited contact area with the absorber and a complicated welding process. The method of combination between the PV cell and the absorber is lamination with EVA, which usually cause power outages, because of the different thermal stresses between the PV cells and the base panel. The novel PV/T panel developed in this research uses a micro-channel as the heat exchanger, whose special structure can improve the heat transfer rate of liquid inside, improving the electrical and thermal efficiencies of the panel. Furthermore, the micro-channel has a much larger contact area, which is beneficial for the heat transfer. The combination method between the PV cell and absorber is thermally conductive silicone grease, which avoids the unequal thermal stress and destruction of the PV cell. The low price of the micro-channel tube also provides economic support for the expansion of this new PV/T panel.

(2) Computer simulation models

Based on the design concept, and selected components of the solar heat pump systems, two computer simulation models are developed to predict the performance of the two systems. For the solar indirect-expansion heat pump system, the simulation model focuses on the four main components, micro-channel PV/T panels (evaporator), compressor, water tank (condenser), and electric expansion valve. It describes the heat transfer rate of refrigerant, the temperature of components, and the consumption of the system. For the solar indirect-expansion heat pump system, the simulation model focus on the solar panels, water tank, testing room and heat pump. It shows the energy flow process in this system, i.e., the input energy, collected energy and output energy. These works completed the preparation for the simulation and experimental testing in controlled conditions.

(3) Experiment and simulation based on the real-world conditions

The solar heat pump systems are constructed in city Lvliang, China. The performance of the two systems are tested in the real-world condition, and the simulation investigation is also carried out based on the same weather condition.

For the solar direct-expansion heat pump system, it is found that both of the electrical and thermal efficiencies are affected by the solar radiation and operating temperature. When the solar radiation and working temperature is high, the efficiency is lower. When this occurs the solar direct-expansion heat pump system works stably, and thus the energy it can collect also is stable. However, the energy loss will increase with the increasing solar radiation, causing it to perform at a lower energy efficiency. The result of testing the system on a sunny day shows that the experimental and simulation electrical efficiency of the micro-channel PV/T panels were stable with an average value of 13.1% and 13.7%. The average experimental and simulation thermal efficiency of the novel PV/T panels were 56.6%, 55.0%, and the overall energy efficiency were 69.7% and 69.1%, respectively, which were higher than the similar system, by 11.0%, 11.8% and 11.4% respectively. The COP of the system had a similar trend of variation with the solar radiation, and the average experimental and simulation COP in the testing day were 4.7 and 5.0,

respectively. Comparing the experimental and simulation results, the average error is less than 4.1%, the maximum error is the COP, which is 6.3%, and the minimum error is input power of compressor, which is 1.9%.

For the solar indirect-expansion heat pump system, the performance of this system was impacted not only by the solar radiation and operating temperature but also the working model and temperature of working fluid. It can be seen that the electrical efficiency of the PV/T panel has an opposite variation trend with the operating temperature, while the thermal efficiency has a similar trend with the operating temperature. In winter, it was found that the experimental average electrical, thermal and overall efficiencies of the mini-channel PV/T panels is 14.5%, 31.7% and 46.2%, respectively, while simulation results are 14.8%, 33.9% and 48.8%, respectively, which has 9.0%, 5.8% and 6.2% higher efficiency than the existing similar systems. The experimental and simulation thermal efficiency of the mini-channel thermal panels is 49.9% and 51.3%, respectively which increases by 5.0% compared to a similar collector. The experimental and simulation COP of the heat pump was 4.6 and 4.9 respectively. In summer, the average electrical efficiency of the PV/T panel was 11.5%, and the average thermal efficiency of thermal panel was 46.8%. While the simulation results yielded 12.6% and 47%, respectively. The temperature of water in the tank increased from 23 ^{o}C to 60 ^{o}C which is high enough for most domestic application. Comparing the experimental and simulation results, the average error is less than 7%, and the maximum error is the electrical efficiency, which is 9.5%, and the minimum error is the water temperature, which is 1.4%.

The experimental and simulation results of the two systems provided fundamental data, a method for the performance analysis of the whole year and indicated possible improvements for similar systems in the future.

(4) Socio-economic assessment

Hourly predicted performance of the two systems is presented based on the weather data of Taiyuan and London city. The energy efficiency, the initial cost, the operating cost, payback time, the life-cycle net cost and CO_2 emission saving have all been investigated.

Comparing the annual performance of the two solar heat pump systems, the indirect-expansion heat pump system has a better performance, in terms of the electrical efficiency and electrical output, than the direct-expansion heat pump system. This is caused by varying characteristics between of the different types, and sizes, of PV cell, leading to a different performance and PV cell covering factor. With a low temperature refrigerant continually passing through the micro-channel tube, the PV/T panel in solar direct-expansion heat pump system can achieve a high thermal efficiency and thermal energy output than the indirect-expansion type.

The initial cost of the direct-expansion and indirect-expansion systems is GBP 5,973 and GBP 6,303. With the income from the electricity generated by the PV/T panels and support of local government, the payback time of these two systems are 8.7 years and 5.8 years in Taiyuan, while 6.6 years and 3.5 years in London. In Taiyuan, and the life-cycle net cost of these two systems is is GBP 4,316 and GBP 8,391, respectively, while it is GBP 4,221 and GBP 8,366 in London. The annual and life-cycle CO_2 emission saving of these two systems is 91.4 t and 109.1 t in Taiyuan, respectively, while it is 44.8 t and 76.2 t in London.

The economic analysis results indicate that the two new clean energy systems can not only meet the demand of hot water and space heating, but also can increase the financial income of the owner and reduce the consumption of traditional fossil energy and CO_2 emission. Therefore, it is reasonable to replace the conventional coal boiler and electric heater with these systems.

8.2 Problems and future works

Two different solar heat pump systems are developed to provide energy for hot water, space heating and generating electricity. Although they show an excellent performance on energy efficiency and economic, there are still some problems which require addressing.

8.2.1 Structure and material of the PV/T panel

The micro-channel PV/T panel designed in this research introduced a new heat exchange structure to improve the heat transfer rate between the working fluid and absorber. This solved the problem of power outages caused by the different thermal stresses between the PV cell and base panel. However, this

process requires removing the air gap between the PV cell and glass, which will increase the heat loss at the front of the panel. Therefore, new technologies need to be developed to overcome the above drawbacks. Two methods are presented to solve the inequality in thermal stresses, which are a new melt thermal glue and a more suitable material for PV cells. The a-Si cells may perform better at higher operating temperatures, regarding the effect of thermal annealing. They are able to exhibit positive power temperature coefficients at degraded steady-state (DSS). Unlike c-Si cells-based PV/T collectors suffering from poor thermal conductivity and large thermal stress due to the fluctuation in operating temperature. Whereas a-Si PV/T collectors are made of thin and flexible cells that can be easily deposited on metal (e.g. stainless steel) and are thus promising in medium/high temperature applications. The method of replacing EVA with new thermal glue is another solution to relieve the impact of different thermal stress.

8.2.2 Manufacturing cost

Owing to the technical problems and application barriers, few companies can produce the PV/T panels, which need both the equipment for manufacturing PV panels and thermal panels. Therefore, the price of the PV/T panel is very high. A suitable manufacturing standard and testing standard also need to be established to make sure that the product possesses a high quality and good performance. The cost of the PV/T panel plays a very important role in its promotion, therefore, solving the technical problems and extending its application field can accelerate market development and reduce the price of the PV/T panel.

8.2.3 Optimization of the system

To obtain maximum energy from the solar panels, 11 and 20 panels are designed in the two solar heat pump systems. As this needs a large amount of space to construct, this system is limited to the rural houses, and furthermore, the scale also increases the initial cost of the system. Therefore, the size of the solar heat pump systems should be redesigned to reduce the scale of solar panels. The solar energy can provide a portion of energy for the building as needed, especially in winter. The energy source of the heat pump in the two system is limited to the solar energy. Hence, designing a double-source heat

pump (water and air source) to replace the single source heat pump not only can extend the energy source in winter but also can achieve the aim of providing cooling energy in summer.

8.2.4 Long-term measurement under real-world condition

Both of the two solar heat pump systems have been tested in practical conditions for more than one-month of time. However, long-term testing is also needed to evaluate their performance in different weather conditions. These testing results will give a much more reasonable and objective analysis on the performance of the systems.

8.2.5 Seeking policy support from the government

The PV/T system has a very long payback time with its high initial investment, i.e., PV/T panel, storage tank and grid-connected system. It is not easy to promote depending on its own performance of electrical and thermal energy, hence the government's support is very important. It is normal to receive allowance from the government for a huge solar photovoltaic plant, but the small scale of off-grid and on-grid systems is not easy, because of frequent maintenance, complex statistics and management.

REFERENCES

References for Chapter 1

[1.1] Report on the green energy and energy-saving technologies and resources and environmental technology progress in Jilin Province, Jilin Province Institute of Science and Technology Information. [7/06/2016]

[1.2] European Commission - 'EU energy and Transport in Figures - Statistical Pocket Book 2010' - 2010.

[1.3] Sustainable Buildings, https://ec.europa.eu/energy/en/topics/energy-efficiency/buildings.

[1.4] Yi Jiang. China Energy Consumption Research Report (2016), China Architecture & Building Press, ISBN：9787112192540.

[1.5] Bolin Sun, National defense construction enters a new era of low carbon economy, Defense in a New Era, [5/04/2010] http://news.163.com/10/0626/05/6A34NDFO00014AEE_mobile.html#

[1.6] Zheng Xinye, Ping Qin. 2014. "Characteristics of residential energy consumption in China: Findings from a household survey." Energy Policy 75: 126-135.

[1.7] 2010 Energy Efficiency Directive & 2012 Energy Efficiency Directive. https://ec.europa.eu/energy/en/topics/energy-efficiency/energy-efficiency-directive

[1.8] Anabela DuarteCarvalho, DimitrisMendrinos. Ground source heat pump carbon emissions and primary energy reduction potential for heating in buildings in Europe - results of a case study in Portugal. Renewable and Sustainable Energy Reviews 45 (2015) 755-768.

[1.9] Snapshot of Global Photovoltaic Markets 2017" report. International Energy Agency. 19 April 2017.

[1.10] Zhao Yuwen, Wang Sicheng,Wang Wenjing. Report on the development of the photovoltaic industry in China. China renewable energy development project (2006-2007). June 2008.

[1.11] Full steam ahead for low carbon energy by 2040, Bloomberg Brief June 20, 2016.

[1.12] SOLAR THERMAL MARKETS IN EUROPE, Trends and Market Statistics 2015, Published November 2016, Summary.

[1.13] Xiaoli Zhang, Solar Thermal Utilization Industry Development Report (2016).
http://www.escn.com.cn/news/show-375724.html

[1.14] Solar Energy Utilization 13th Five-Year Development Plan for Exposure Draft, National Energy Administration.
http://www.cspplaza.com/article-6377-1.html

[1.16] Lovedeep Sahotaa, G.N. Tiwar Review on series connected photovoltaic thermal (PVT) systems: Analytical and experimental studies. Solar Energy 150 (2017) 96-127.

[1.17] Henry T. Lancashire, Dai Jiang, Andreas Demosthenous, Nick Donaldson. An ASIC for Recording and Stimulation in Stacked Microchannel Neural Interfaces. Transactions on Biomedical Circuits and Systems.

[1.18] Ribatski, G. (2013) A Critical Overview on the Recent Literature Concerning Flow Boiling and Two-Phase Flows Inside Micro-Scale Channels, Experimental Heat Transfer: A Journal of Thermal Energy Generation, Transport, Storage, and Conversion, 26:2-3, 198-246, DOI:10.1080/ 08916152. 2012. 737189.

[1.19] Saisorn, S., Kuaseng, P., Wongwises, S., Heat transfer characteristics of gas-liquid flow in horizontal rectangular micro-channels. Experimental Thermal and Fluid Science 55 (2014) 54-61.

[1.20] Kim, S., Madawar, I., Universal approach to predicting saturated flow boiling heat transfer in mini/micro-channels - part II: two-phase heat transfer coefficient. International Journal of Heat and Mass Transfer 64 (2013-III) 1239-1256.

[1.21] Seyed Ebrahim Ghasemi, A.A. Ranjbar, M.J. Hosseini. Experimental and numerical investigation of circular minichannel heat sinks with

various hydraulic diameter for electronic cooling application. Microelectronics Reliability 73 (2017) 97–105

References for Chapter 2

[2.1] Test Method for Photovoltaic Module Power Rating, FSEC Standard 202-10, January 2010.

[2.2] Varkie C. Thomas, Basic Photovoltaic Principles and Methods, February 1982, SERI/SP-290-1448.

[2.3] Sandeep S. Joshi, Ashwinkumar S. Dhoble. Photovoltaic -Thermal systems (PVT): Technology review and future trends. Renewable and Sustainable Energy Reviews 92 (2018) 848-882.

[2.4] X. Zhao, X. Zhang, S. B. Riffat, X Su, Theoretical investigation of a novel PV/e roof module for heat pump operation, Energy Conversion and Management 2011; 52: 603-614.

[2.5] Wei He, Yang Zhang, Jie Ji. Comparative experiment study on photovoltaic and thermal solar system under natural circulation of water. Applied Thermal Engineering 31 (2011) 3369-3376.

[2.6] Xinshi Ge. Solar Engineering: Principles and Applications. Academic journals Press, 1988.

[2.7] Hottel H G, Woertz B B. The performance of flat plate solar collectors. Trans. of ASME (1942) 64:91-94.

[2.8] Hottel H G, Whillier A. Evaluation of flat plate collector performance. Trans. of the Conf. On the use of Solar Energy, 2, Part 1A, Univ. of Arizona Press (1955) 74-104.

[2.9] Coefficient of Performance, industrial heat pump. http://industrialheatpumps.nl/en/how_it_works/cop_heat_pump/

[2.10] Evidence Gathering – Low Carbon Heating Technologies - Hybrid Solar Photovoltaic Thermal Panels, BRE National Solar Centre and Delta-ee. September 2017.

[2.11] Madhu Sudan and G. N. Tiwari. Energy matrices of the building by incorporating daylight concept for composite climate - An

experimental study..Journal of Renewable and Sustainable Energy 6, 053122 (2014).

[2.12] Elzen, M.G.J.D., Hof, A.D., Beltran, A.M., Grassi, G., Roelfsema, M., Ruijven, B.V., Vliet, J.V., Vuuren, D.P.V. The Copenhagen accord: abatement costs and carbon prices resulting from the submissions. Environ. Sci. Policy 14 (2011), 28-39.

[2.13] Lovedeep Sahota, G.N. Tiwari, Review on series connected photovoltaic thermal (PVT) systems: Analytical and experimental studies. Solar Energy 150 (2017) 96-127.

[2.14] Caliskan, H., Dincer, I., Hepbasli, A. Exergoeconomic, enviroeconomic and sustainability analyses of a novel air cooler. Energy Build. 55 (2012) 747-756.

[2.15] Shyam, G.N. Tiwari, Olivier Fischer, R.K. Mishra, I.M. Al-Helal, Performance evaluation of N-photovoltaic thermal (PVT) water collectors partially covered by photovoltaic module connected in series: An experimental study. Solar Energy 134 (2016) 302-313.

[2.16] Sopiana, K., Othmana, M.Y., Yatima, B, Ruslan, M.H. Experimental studies on a solar assisted drying system for herbal tea, In Proceeding of World Renewable Energy Congress VI, 2000 1139-1142.

[2.17] Othman, M.Y.H., Sopian, K., Yatim, B. and Daud, W.R.W. Development of advanced solar assisted drying systems. Renewable Energy, 31 (2006) 703-709.

[2.18] Turhan, K. Performance of various design of solar air heaters for crop drying applications. Renewable Energy, 31 (2006) 1073-1088.

[2.19] Sarsavadia, P.N. Development of a solar-assisted dryer and evaluation of energy requirement for the drying of onion. Renewable Energy, 32 (2007) 2529-2547.

[2.20] Chantana Punlek, Rattanachai Pairintra, Sirinuch Chindaraksa, Somchai Maneewan. Simulation design and evaluation of hybrid PV/T assisted desiccant integrated HA-IR drying system (HPIRD). Food and bioproducts processing 87 (2009) 77-86.

[2.21] P. Barnwal, G.N. Tiwari. Grape drying by using hybrid photovoltaic-thermal (PV/T) greenhouse dryer: An experimental study. Solar Energy 82 (2008) 1131-1144.

[2.22] Ya Brigitte Assoa, François Sauzedde, Benjamin Boillot. Numerical parametric study of the thermal and electrical performance of a BIPV/T hybrid collector for drying applications. Renewable Energy 129 (2018) 121-131.

[2.23] A. Shahsavar, M. Ameri. Experimental investigation and modeling of a direct-coupled PV/T air collector. Solar Energy 84 (2010) 1938-1958.

[2.24] F. Sarhaddi, S. Farahat, H. Ajam, A. Behzadmehr, M. Mahdavi Adeli. An improved thermal and electrical model for a solar photovoltaic thermal (PV/T) air collector. Applied Energy 87 (2010) 2328-2339.

[2.25] J.K. Tonui, Y. Tripanagnostopoulos. Air-cooled PV/T solar collectors with low cost performance improvements. Solar Energy 81 (2007) 498-511.

[2.26] Jong-Gwon Ahn, Jin-Hee Kim, Jun-Tae Kim. A Study on Experimental Performance of Air-Type PV/T Collector with HRV. Energy Procedia 78 (2015) 3007-3012.

[2.27] Soudabeh Golzari, Alibakhsh Kasaeian, Majid Amidpour, Shahin Nasirivatan, Soroush Mousavi. Experimental investigation of the effects of corona wind on the performance of an air-cooled PV/T. Renewable Energy 127 (2018) 284-297.

[2.28] M.Y. Othman, S.A. Hamid, M.A.S. Tabook, K. Sopian, M.H. Roslan, Z. Ibarahim. Performance analysis of PV/T Combi with water and air heating system: An experimental study. Renewable Energy 86 (2016) 716-722.

[2.29] Krauter, S. Increased electrical yield via water flow over the front of photovoltaic panels. Sol. Energy Mater. Sol. Cells 82 (2004) 131-137.

[2.30] Ji, J., Han, J., Chow, T.T., Yi, H., Lu, J., He, W., Sun, W. Effect of fluid flow and packing factor on energy performance of a wall-

mounted hybrid photovoltaic/water heating collector system. Energy Build. 38 (2006) 1380-1387.

[2.31] Odeh, D.S., Mulaweh-Abu, I.H. Design and development of experimental setup of hybrid PV/thermal collector. Glob. J. Eng. Educ. 14 (2012) 170-176.

[2.32] Teo, H.G., Lee, P.S., Hawlader, M.N.A. An active cooling system for photovoltaic modules. Appl. Energy 90 (2012) 309-315.

[2.33] Bahaidarah, H., Subhan, A., Gandhidasan, P., Rehman, S. Performance evaluation of a PV (photovoltaic) module by back surface water cooling for hot climatic conditions. Energy 59 (2013) 445-453.

[2.34] Hussein, Hashim A., Numan, Ali H., Abdulmunem, Abdulmunem R. Improving of the photovoltaic/thermal system performance using water cooling technique. Mater. Sci. Eng. 78 (2015) 1-9.

[2.35] Y. Deng, Z. Quan, Y. Zhao, L. Wang, Z. Liu. Research on the performance of household-type photovoltaic-thermal system based on micro-heat pipe array in Beijing. Energy Convers. Manage., 106 (2015) 1039-1047.

[2.36] Nizetic, S., Coko, D., Yadav, A., Cabo, F.G. Water spray cooling technique applied on a photovoltaic panel: the performance response. Energy Convers. Manage. 108 (2016) 287-296.

[2.37] Jim Shiminski. Energy Recovery Heat Pipes-5 Advantages of using Heat Pipes for Air-To-Air Energy Recovery. Dynamic Air corporation, 2012, poster.

[2.38] Mawufemo Modjinou, Jie Ji, Weiqi Yuan, Fan Zhou, Sarah Holliday, Adeel Waqas, Xudong Zhao. Performance comparison of encapsulated PCM PV/T, microchannel heat pipe PV/T and conventional PV/T systems. Energy 166 (2019) 1249-1266.

[2.39] Longshu Hou, Zhenhua Quan, Yaohua Zhao, Lincheng Wang, Gang Wang. An experimental and simulative study on a novelphotovoltaic-thermal collector with micro heat pipe array (MHPA-PV/T). Energy and Buildings 124 (2016) 60-69.

[2.40] Wei He, JinZhi Zhou, Chi Chen, Jie Ji. Experimental study and performance analysis of a thermoelectric cooling and heating system driven by a photovoltaic/thermal system in summer and winter operation modes. Energy Conversion and Management 84 (2014) 41-49.

[2.41] Pei Gang, Fu Huide, Zhang Tao, Ji Jie. A numerical and experimental study on a heat pipe PV/T system. Solar Energy 85 (2011) 911-921.

[2.42] S. Launay, V. Sartre, J. Bonjour. Parametric analysis of loop heat pipe operation: a literature review. Int J Therm Sci, 45 (2007) 621-636.

[2.43] Wei He, Xiaoqiang Hong, Xudong Zhao, Xingxing Zhang, Jinchun Shen, Jie Ji. Operational performance of a novel heat pump assisted solar façade loop-heat-pipe water heating system. Energy 167 (2019) 866-888.

[2.44] Xingxing Zhang, Xudong Zhao, Jingchun Shen, Jihuan Xu, Xiaotong Yu. Dynamic performance of a novel solar photovoltaic/loop-heat-pipe heat pump system. Applied Energy 114 (2014) 335-352.

[2.45] Hong Li, Yue Sun. Operational performance study on a photovoltaic loop heat pipe/solarassisted heat pump water heating system. Energy and Buildings 158 (2018) 861-872.

[2.46] Thierno M.O. Diallo, Min Yu, Jinzhi Zhou, Xudong Zhao, Samson Shittu, Guiqiang Li, Jie Ji, David Hardy. Energy performance analysis of a novel solar PVT loop heat pipe employing a microchannel heat pipe evaporator and a PCM triple heat. Exchanger. Energy 167 (2019) 866-888.

[2.47] Luisa F. Cabeza, Aran Sol, Camila Barreneche. Review on sorption materials and technologies for heat pumps and thermal energy storage. Renewable Energy 110 (2017) 3-39.

[2.48] Guodong Qiua, Xinghua Wei, Zhenfei Xu, Weihua Cai. A novel integrated heating system of solar energy and air source heat pumps and its optimal working condition range in cold regions. Energy Conversion and Management 174 (2018) 922-931.

[2.49] Yin Liu, Jing Ma, Guanghui Zhou, Chao Zhang, Wenlei Wan. Performance of a solar air composite heat source heat pump system. Renewable Energy xxx (2015) 1-6.

[2.50] Xu Dong, Qi Tian, Zhen Li. Experimental investigation on heating performance of solar integrated air source heat pump. Applied Thermal Engineering 123 (2017) 1013-1020.

[2.51] Y. Bai, T. T. Chow, C.M´en´ezo, P. Dupeyrat. Analysis of a Hybrid PV/Thermal Solar-Assisted Heat Pump System for Sports Center Water Heating Application. Hindawi Publishing Corporation International Journal of Photoenergy Volume 2012, Article ID 265838, 13 pages, doi:10.1155/2012/265838.

[2.52] Wei He, Xiaoqiang Hong, Xudong Zhao, Xingxing Zhang, Jinchun Shen, Jie Ji. Theoretical investigation of the thermal performance of a novel solar loop-heat-pipe facade-based heat pump water heating system. Energy and Buildings 77 (2014) 180-191.

[2.53] Taehoon Kim, Byung-Il Choi,Yong-Shik Han, Kyu Hyung Do. A comparative investigation of solar-assisted heat pumps with solar thermal collectors for a hot water supply system. Energy Conversion and Management 172 (2018) 472-484.

[2.54] A.M. Omer, Ground-source heat pumps systems and applications, Renew. Sustain. Energy Rev. 12 (2008) 344-371.

[2.55] E.J. Lee, E.C. Kang, S.Y. Cho, E. Entchev, L. Yang, M. Ghorab, Performance Assessment and Integral Effect Test of Fuel Cell e Ground Source Heat Pump and Photovoltaic Thermal - Ground Source Heat Pump, Annex54-KIER e Subtask B Report, Available from: http://www.annex-54.sharepoint-live.de.

[2.56] S. Andrew Putrayudha, Eun Chul Kang, E. Evgueniy, Y. Libing, Euy Joon Lee. A study of photovoltaic/thermal (PVT)-ground source heat pump hybrid system by using fuzzy logic control Applied Thermal Engineering 89 (2015) 578-586.

[2.57] M. Bakker, H.A. Zondag, M.J. Elswijk, K.J. Strootman, M.J.M. Jong. Performance and costs of a roof-sized PV/thermal array combined with a ground coupled heat pump. Solar Energy 78 (2005) 331-339.

[2.58] Xu guoying, Zhang xiaosong, Zhao shanguo. Performance of flat-plate PV/T integrated heat pump water heating system. CIESC Journal, Vol. 63, No. S2, December 2012.

[2.59] Hongbing Chen, Saffa B Riffat. Investigation of a Hybrid Solar Heat Pump System. 2011 International Conference on Green Buildings and Sustainable Cities. Procedia Engineering 21 (2011) 311-318.

[2.60] Hongbing Chen, Saffa B. Riffat, Yu Fu. Experimental study on a hybrid photovoltaic/heat pump system. Applied Thermal Engineering 31 (2011) 4132-4138.

[2.61] Huan-Liang Tsai. Modeling and validation of refrigerant-based PVT-assisted heat pump water heating (PVTA–HPWH) system. Solar Energy 122 (2015) 36-47.

[2.62] Fu Huide, ZhangTao. Performance Analysis of an Integrated Solar-assisted Heat Pump System with Heat Pipe PV/T Collectors Operating Under Different Weather Conditions. Energy Procedia 105 (2017) 1143-1148.

[2.63] Jingyong Cai, Jie Ji, Yunyun Wang, Fan Zhou, Bendong Yu. A novel PV/T-air dual source heat pump water heater system: Dynamic simulation and performance characterization. Energy Conversion and Management 148 (2017) 635-645.

[2.64] Jingyong Cai, Jie Ji, Yunyun Wang, Wenzhu Huang. Operation characteristics of a novel dual source multi-functional heat pump system under various working modes. Applied Energy 194 (2017) 236-246

[2.65] Jingyong Cai, Jie Ji, Yunyun Wang, Wenzhu Huang. Numerical simulation and experimental validation of indirect expansion solar-assisted multi-functional heat pump. Renewable Energy 93 (2016) 280-290.

[2.66] Jie Ji, Gang Pei, Tin-tai Chow, Keliang Liu, Hanfeng He, Jianping Lu, Chongwei Han. Experimental study of photovoltaic solar assisted heat pump system. Solar Energy 82 (2008) 43-52.

[2.67] https://dualsun.fr/en/product/2-in-1-solar/

[2.68] http://www.anafsolar.eu/eng/H-NRG/H_ilsistema.html

[2.69] http://www.gseintegration.com/en/airsystem.html

[2.70] http://www.solator.cc/

[2.71] http://www.systovi.com/en/produit/r-volt-2/

[2.72] http://www.fototherm.com/en/

[2.73] http://www.solarangel.com/

[2.74] http://www.solimpeks.com/

[2.75] http://www.nakedenergy.co.uk/product/how-it-works/advantages/

[2.76] http://www.energyntegration.com/

[2.77] http://solarus.com/our-solution/powercollector-4/

[2.78] G.Fabbri, M.Greppi, M.Lorenzini. Optimization with genetic algorythms of PVT system global efficiency. Journal of Energy and Power Engineering 6 (2012) 1035-1041.

[2.79] Liao L, Athienitis AK, Candanedo L, Park KW, Poissant Y, Collins M. Numerical and Experimental Study of Heat Transfer in a BIPV Thermal System. J Solar Eng 2007; 129:423-30.

[2.80] Arvind Tiwari, M.S. Sodha. Performance evaluation of hybrid PV/thermal water/air heating system: A parametric study. Renewable Energy 31 (2006) 2460-2474.

[2.81] Zhongzhu Qiu, Xiaoli Ma, Peng Li, Xudong Zhao, Andrew Wrightd. Micro-encapsulated phase change material (MPCM) slurries: Characterization and building applications. Renewable and Sustainable Energy Reviews, 77 (2017) 246-262.

[2.82] R. Nasrin, N.A. Rahim, H. Fayaz, M. Hasanuzzaman. Water/MWCNT nanofluid based cooling system of PVT: Experimental and numerical research. Renewable Energy 121 (2018) 286-300.

[2.83] Ali H.A. Al-Waeli, Miqdam T. Chaichan, K. Sopian, Hussein A. Kazem,Hameed B. Mahood, Anees A. Khadom. Modeling and experimental validation of a PVT system using nanofluid coolant and nano-PCM. Solar Energy 177 (2019) 178-191.

[2.84] R. Nasrin, N.A. Rahim, H. Fayaz, M. Hasanuzzaman. Water/MWCNT nanofluid based cooling system of PVT: Experimental and numerical research. Renewable Energy 121 (2018) 286-300.

[2.85] Sakhr M Sultan, C P Tso, Ervina Efzan. The Effect of Mass Flow Rate and Solar Radiation on The Photovoltaic Efficiency of a Glazed Water Based PVT. AIP Conference Proceedings 2030,020309 (2018).

[2.86] J.K. Tonui, Y. Tripanagnostopoulos. Improved PV/T solar collectors with heat extraction by forced or natural air circulation. Renewable Energy 32 (2007) 623-637.

[2.87] Anand S. Joshi, Arvind Tiwari. Energy and exergy efficiencies of a hybrid photovoltaic–thermal (PV/T) air collector. Renewable Energy 32 (2007) 2223-2241.

[2.88] M. Rahou, M. Y. Othman, S. Mat and A. Ibrahim. Performance Study of a Photovoltaic Thermal System With an Oscillatory Flow Design. Solar Energy Engineering, 136 (2013) 21-26.

[2.89] Yanqiu Wang, Jie Ji, Wei Sun, Weiqi Yuan, Jingyong Cai, Chao Guo, Wei He. Experiment and simulation study on the optimization of the PV direct-coupled solar water heating system. Energy 100 (2016) 154-166.

[2.90] R. K. Koech, H. O Ondieki, J. K. Tonui, S. K Rotich. A Steady State Thermal Model For Photovoltaic/Thermal (PV/T) System Under Various Conditions. INTERNATIONAL JOURNAL OF SCIENTIFIC & TECHNOLOGY RESEARCH. 1 (2012) 2277-8616.

[2.91] Jingyong Cai, Jie Ji, Yunyun Wang, Fan Zhou, Bendong Yu. A novel PV/T-air dual source heat pump water heater system: Dynamic

simulation and performance characterization. Energy Conversion and Management 148 (2017) 635-645.

[2.92] Jingyong Cai, Jie Ji, Yunyun Wang, Wenzhu Huang. Numerical simulation and experimental validation of indirect expansion solar-assisted multi-functional heat pump. Renewable Energy 93 (2016) 280-290.

[2.93] Arash Kazemian, Mohammad Hosseinzadeh, Mohammad Sardarabadi, Mohammad Passandideh-Fard. Effect of glass cover and working fluid on the performance of photovoltaic thermal (PVT) system: An experimental study. Solar Energy 173 (2018) 1002-1010.

[2.94] Y. Tripanagnostopoulos, M. Souliotis, R. Battisti, A. Corrado. Performance, Cost and Life-cycle Assessment Study of Hybrid PVT/AIR Solar Systems. RESEARCH AND APPLICATIONS, 2006; 14:65-76.

[2.95] Jin-Hee Kim, Jun-Tae Kim. Comparison of Electrical and Thermal Performances of Glazed and Unglazed PVT Collectors.International Journal of Photoenergy Volume 2012, Article ID 9578.

[2.96] N.Aste, C. Del Pero, F. Leonforte. Water PVT collectors performance comparison. Energy Procedia 105 (2017) 961-966.

[2.97] Sanjay Agrawal, G.N. Tiwari. Energy and exergy analysis of hybrid micro-channel photovoltaic thermal module. Solar Energy 85 (2011) 356-370.

[2.98] Wenke Fan, Georgios Kokogiannakis, Zhenjun Ma. Optimisation of life cycle performance of a double-pass photovoltaic thermal-solar air heater with heat pipes. Renewable Energy 138 (2019) 90-105.

[2.99] María Herrando, Alba Ramos, James Freeman, Ignacio Zabalza, Christos N. Markides. Technoeconomic modelling and optimisation of solar combined heat and power systems based on flat-box PVT collectors for domestic applications. Energy Conversion and Management 175 (2018) 67-85.

[2.100] Jinwei Ma, Wei Sun, Jie Ji, Yang Zhang, Aifeng Zhang, Wen Fan. Experimental and theoretical study of the efficiency of a dual-function solar collector. Applied Thermal Engineering 31 (2011) 1751-1756.

[2.101] D.B. Tuckerman, R.F.W. Pease. High-performance heat sinking for VLSI. IEEE Electron Device Letters. 2 (1981) 126-129.

[2.102] MASOUD MOHAMMADI SARDOUEI, HAMID MORTEZAPOUR, KAZEM JAFARI NAEIMI. Temperature distribution and efficiency assessment of different PVT water collector designs. Sādhanā, (2018) 43:84.

[2.103] Swapnil Dubey, Andrew A.O. Tay. Testing of two different types of photovoltaic–thermal (PVT) modules with heat flow pattern under tropical climatic conditions. Energy for Sustainable Development 17 (2013) 1-12.

[2.104] Amin M. Elsafi, P. Gandhidasan. Comparative study of double-pass flat and compound parabolic concentrated photovoltaic–thermal systems with and without fins. Energy Conversion and Management 98 (2015) 59-68.

[2.105] A. Kroiß, M. Spinnler, T. Sattelmayer. Analysis of hybrid photovoltaic/thermal (PV/T) solar systems for small scale reverse osmosis desalination plants. 25th European Photovoltaic Solar Energy Conference and Exhibition (PVSEC 2010), At Valencia, Spain.

[2.106] M.Y. Othman, S.A. Hamid, M.A.S. Tabook, K. Sopian, M.H. Roslan, Z. Ibarahim. Performance analysis of PV/T Combi with water and air heating system: An experimental study. Renewable Energy 86 (2016) 716-722.

[2.107] Karima E. Amori, Hussein M. Taqi Al-Najjar. Analysis of thermal and electrical performance of a hybrid (PV/T) air based solar collector for Iraq. Applied Energy 98 (2012) 384-395.

[2.108] Ya Brigitte Assoa, François Sauzedde, Benjamin Boillot, Simon Boddaert. Development of a building integrated solar photovoltaic/thermal hybrid drying system. Energy 128 (2017) 755-767.

[2.109] F. Sarhaddi, S. Farahat, H. Ajam, A. Behzadmehr. Exergetic performance assessment of a solar photovoltaic thermal (PV/T) air collector. Energy and Buildings 42 (2010) 2184-2199.

[2.110] Corry de Keizer, Minne de Jong, Tiago Mendes, Munish Katiyar, Wiep Folkerts, Camilo Rindt, Herbert Zondag. Evaluating the thermal and electrical performance of several uncovered PVT collectors with a field test. Energy Procedia 91 (2016) 20-26.

[2.111] Jin-Hee Kim, Se-Hyeon Park, Jun-Gu Kang, Jun-Tae Kim. Experimental performance of heating system with building integrated PVT (BIPVT) collector. Energy Procedia 48 (2014) 1374-1384.

[2.112] Ahmad Fudholi, Kamaruzzaman Sopian, Mohammad H. Yazdi, Mohd Hafidz Ruslan, Adnan Ibrahim, Hussein A. Kazem. Performance analysis of photovoltaic thermal (PVT) water collectors. Energy Conversion and Management 78 (2014) 641-651.

[2.113] Haiping Chen, Heng Zhang, Mingjie Li, Haowen Liu, jiguang Huang. Experimental Investigation of a Novel LCPV/T System with Micro - channel Heat Pipe Array. Renewable Energy (2017), doi: 10.1016.

[2.114] Guoying Xu, Xiaosong Zhang, Shiming Deng. Experimental study on the operating characteristics of a novel low-concentrating solar photovoltaic/thermal integrated heat pump water heating system. Applied Thermal Engineering 31 (2011) 3689-3695.

[2.115] H.D. Fu, G. Pei, J. Ji, H. Long b, T. Zhang, T.T. Chow, Experimental study of a photovoltaic solar-assisted heat-pump/heat-pipe system. Applied Thermal Engineering 40 (2012) 343-350.

[2.116] China's crystalline silicon solar cell technology and cost status, China Renewable Energy Society. [14/04/2015]

[2.117] BoyleG. Renewable energy: power for a sustainable future. Second ed. UK: Oxford University Press; 2004.

[2.118] S.C. Solanki, Swapnil Dubey, Arvind Tiwari. Indoor simulation and testing of photovoltaic thermal (PV/T) air collectors. Applied Energy 86 (2009) 2421-2428.

[2.119] Zhang Heng, Li Mingjie, Chen Haiping, Ye Chentao. Experimental study of constant temperature operation and constant flow operation in concentrating PV/T system. The 8th International Conference on Applied Energy – ICAE2016. Energy Procedia 105 (2017) 869-874.

[2.120] Swapnil Dubey, S.C. Solanki, Arvind Tiwari. Energy and exergy analysis of PV/T air collectors connected in series. Energy and Buildings 41 (2009) 863-870.

[2.121] S. Nemati Jahromia, A. Vadiee, M. Yaghoubi. Exergy and economic evaluation of a commercially available PV/T collector for different climates in Iran. The 7th International Conference on Applied Energy – ICAE2015, Energy Procedia 75 (2015) 444-456.

[2.122] Majdi Hazami, Ali Riahi, Farah Mehdaoui, Omeima Nouicer, Abdelhamid Farhat. Energetic and exergetic performances analysis of a PV/T (photovoltaic thermal) solar system tested and simulated under to Tunisian (North Africa) climatic conditions. Energy 107 (2016) 78-94.

[2.123] Yongqiang Luo, Ling Zhang, Zhongbing Liu, Jing Wu, Yelin Zhang, Zhenghong Wu. Numerical evaluation on energy saving potential of a solar photovoltaic thermoelectric radiant wall system in cooling dominant climates. Energy 142 (2018) 384-399.

[2.124] Jan Cremers, Irina Mitina, Nansi Palla, Fritz Klotz, Xavier Jobard, Ursula Eicker. Experimental Analyses of Different PVT Collector Designs for Heating and Cooling. Applications in Buildings.Energy Procedia 78 (2015) 1889-1894.

[2.125] Matin Ghadiri, Mohammad Sardarabadi, Mohammad Pasandideh-fard, Ali Jabari Moghadam. Experimental investigation of a PVT system performance using nano ferrofluids. Energy Conversion and Management 103 (2015) 468-476.

[2.126] M. Proell, P. Osgyan, H. Karrer, C.J. Brabec. Experimental efficiency of a low concentrating CPC PVT flat plate collector. Solar Energy 147 (2017) 463-469.

[2.127] D.B. Singh, J.K. Yadav, V.K. Dwivedi, S. Kumar, G.N. Tiwari, I.M. Al-Helal. Experimental studies of active solar still integrated with two hybrid PVT collectors. Solar Energy 130 (2016) 207-223.

[2.128] Jiang Fan, Toh Peng Seng, Leung Kin On and Goh Leag Hua. Experimental Study on Glazed mc-Si Solar Photovoltaic/Thermal (PVT) System. Energy Procedia 61 (2014) 2787-2790.

[2.129] Diego Vittorini, Nicola Castellucci, Roberto Cipollone.Heat recovery potential and electrical performances in-field investigation on a hybrid PVT module. Applied Energy 205 (2017) 44-56.

[2.130] Ankita Gaur, Christophe Menezo, Stephanie Giroux-Julien. Numerical studies on thermal and electrical performance of a fully wetted absorber PVT collector with PCM as a storage medium. Renewable Energy 109 (2017) 168-187.

[2.131] D.B. Singh, G.N. Tiwari. Performance analysis of basin type solar stills integrated with N identical photovoltaic thermal (PVT) compound parabolic concentrator (CPC) collectors: A comparative study. Solar Energy 142 (2017) 144-158.

[2.132] Jee Joe Michael, Iniyan Selvarasan. Economic analysis and environmental impact of flat plate roof mounted solar energy systems. Solar Energy 142 (2017) 159-170.

[2.133] Samir Hassani, R. Saidur, Saad Mekhilef, Robert A. Taylor. Environmental and exergy benefit of nanofluid-based hybrid PV/T systems. Energy Conversion and Management 123 (2016) 431-444.

[2.134] Ka-Kui Tse, Tin-Tai Chow, Yan Su. Performance evaluation and economic analysis of a full-scale water-based photovoltaic/thermal (PV/T) system in an office building. Energy and Buildings 122 (2016) 42-52.

[2.135] Brian C. Riggs, Richard Biedenharn, Christopher Dougher, Yaping Vera Ji, Qi Xu, Vince Romanin, Daniel S. Codd, James M. Zahler, Matthew D. Escarra. Techno-economic analysis of hybrid PV/T systems for process heat using electricity to subsidize the cost of heat. Applied Energy 208 (2017) 1370–1378

[2.136] https://v.qq.com/x/page/s0529cae3it.html

[2.137] Keith A. Emery,J. Burdick,Y. Caiyem,D. Dunlavy. Temperature dependence of photovoltaic cells, modules and systems. Photovoltaic Specialists Conference, 1996., Conference Record of the Twenty Fifth IEEE.

[2.138] http://www.zpweirui.com/

[2.139] Jing LI, Xiao REN, Weiqi YUAN, Zhaomeng LI, Cagri KUTLU, Gang PEI2 Yuehong SU, Jie JI, Saffa RIFFAT. Design and test of novel photovoltaic/thermal collectors using amorphous silicon cells. 16th International Conference on Sustainable Energy Technologies (Set 2017), Italy, 17th -20nd July.

[2.140] A High Efficiency, Low Cost and Building Integrate-able Solar Photovoltaic/Thermal (PV/T) System for Space Heating, Hot Water and Power Supply, university of Hull and University of science and technology of China, Newton fund-China-UK research and innovation bridge. April 2017 – March 2019.

References for Chapter 3

[3.1] IEC 61215 standard “Crystalline silicium terrestrial photovoltaic (PV) Modules - Design qualification and type approval”.

[3.2] ISO/TC 86/SC 6, “Testing and rating of air-conditioners and heat pumps”.

[3.3] 2016 Klea 410A Phys Props Data, Mexichem refrigerant. Mexichem UK Limited

[3.4] Wu zhigang, Ding liangguo, The fast calculation of refrigerant thermodynamic properties:IPrinciple. Journal of Shanghai Jiaotong University, Volume 40 (2006) 297-300.

[3.5] Wu zhigang, Ding liangguo, The fast calculation of refrigerant thermodynamic properties: II Formulate for typical refrigerants. Journal of Shanghai Jiaotong University, Volume 40 (2006) 301-305.

[3.6] K. KALIDASA MURUGAVEL, K. SRITHAR, Effect of Cover Plate Transmittance on Solar Still Performance. International Journal of Green Energy (2015) 12, 431-439.

[3.7] T.T. Chow. Performance analysis of photovoltaic-thermal collector by explicit dynamic model. Solar Energy 75 (2003) 143-152.

[3.8] Watmuff J. H., Charters W. W. S, Proctor D. Solar and wind induced external coefficients for solar collectors. Comples 2, (1977).

[3.9] Sung-Min Kim, Issam Mudawar. Universal approach to predicting saturated flow boiling heat transfer in mini/micro-channels - Part II. Two-phase heat transfer coefficient International Journal of Heat and Mass Transfer 64 (2013) 1239-1256.

[3.10] Duffie JA, Beckman WA. 1991. Solar Engineering of Thermal Processes. Second ed., John Wiley & Sons, New York.

[3.11] Xi dongmin. Performance equation optimization and analysis for sopoll compressor based on experiment test. Master's Degree thesis, Shanghai jiaotong university. 2006-2-15.

[3.12] Pei Gang, Fu Huide, Zhang Tao, Ji Jie. A numerical and experimental study on a heat pipe photovoltaic/thermal system, Solar Energy 85 (2011) 911-921.

[3.13] Cuiping Lv. Analysis of Helical Coil Heat Exchanger in Thermal Storage Water Tank of Pressure - Separate Solar Hot Water System. Solar energy 11 (2013) 19-22.

[3.14] Wenhua Li. Simplified modeling analysis of mass flow characteristics in electronic expansion valve. Applied Thermal Engineering 53 (2013) 8-12.

[3.15] ZHAO Ming, YANG Mo，ZHANG Lixin. New Method of the Floor Surface Total Heat Flux Calculation, ENERGY CONSERVATION TECHNOLOGY, Vol. 29, Nov. 2011.

[3.16] ZHANG Juerong, LI Ke, LING Jihong, ZHANG Yufen. Heat Transfer Calculation of Floor Radiation Heating. Vol. 23 No. 11, Nov. 2003.

[3.17] Müller-Steinhagen H, Heck K. A simple friction pressure drop correlation for two-phase flow in pipes. Chemical Engineering Progress, 20 (1986) 297-308.

References for Chapter 5

[5.1] Chow TT. Performance analysis of photovoltaic-thermal collector by explicit dynamic model. Solar Energy, 75 (2003) 143-152.

[5.2] Hollands KGT, Unny TE, Raithby GD, et al. Free convection heat transfer across inclined air layers. Transactions of the American Society of Mechanical Engineers, Journal of Heat Transfer, 98 (1976) 189-193.

[5.3] Adachi, Y.; Lu, B. C. Y.; Sugie, H.: A four parameter equation of state. Fluid Phase Equilibria 11 (1983) 29-48.

[5.4] Lee, B. I.; Kesler, M. G.: A generalized thermodynamic correlation based on three-parameter corresponding states. A1ChE J.21 (1975) 510-527.

[5.5] Platzer, B.; Polt, A.; Maurer, G.: Thermophysical properties of refrigerants. Berlin Heidelberg New York: Springer 1990.

[5.6] Kim, W., Oh, J., Park, C., Cho, H., 2011. Study on Solar Hybrid Heat Pump System using Carbon Dioxide. In: 23rd International Conference of Refrigeration, Aug. 21-26, Prague, Czech Republic.

References for Chapter 7

[7.1] Weather profile, https://energyplus.net/

[7.2] R. Burzynski, M. Crane, R. Yao, V.M. Becerra, Heat demand analysis of residential development in London connected to district heating scheme. TSBE EngD Conference, TSBE Centre, University of Reading, Whiteknights, RG6 6AF, 5th July 2011

[7.3] Daniel Fosas, David A. Coley, Sukumar Natarajan, Manuel Herrera, Miguel Fosas de Pando, Alfonso Ramallo-Gonzalez. Mitigation versus adaptation: Does insulating dwellings increase overheating risk? Building and Environment 143 (2018) 740-759.

[7.4] Jin Xinghua, Greatly improve the efficiency of heat source to solve the problem of heating in rural areas in northern China. Application technology discussion, 2013, 80-85.

[7.5] Energy, www.greenspec.co.uk. [24/07/2013]

[7.6] Implementation advice on financial subsidies about distributed photovoltaic power generation projects in rural areas. Shanxi Province People's Government Office. [13/01/2018]

[7.7] Implementation plan for piloting the “coal to electricity” pilot project for urban and rural heating, Shanxi Province People's Government Office. [26/04/2016]

[7.8]. Renewable Heat Incentive (RHI), < www.energysavingtrust.org.uk>, [24/07/2013]

[7.9] Notice of Shanxi Provincial Price Bureau on Raising the Sales Price of Pipeline Natural Gas Residents in Taiyuan City, National energy Administration. [24/08/2012]

[7.10]. UK gas price, < www.britishgas.co.uk>, [26/06/2013]

[7.11] Electricity price in Shanxi province 2017. https://www.shfft.com/help/help_708963.htm

[7.12]. UK electricity price, < www.britishgas.co.uk>, [26/06/2012]

[7.13] Thermal Coal Price Index Weekly Review 2018. https://baijiahao.baidu.com/s?id=1601244254223101417&wfr=spider&for=pc

[7.14] Thoughts and plans for PV price adjustment in 2018. https://www.solarbe.com/toutiao/?id=122252

[7.15] S. Kalogirou, Economic analysis of solar energy systems using spread sheets, Proceedings of World Renewable Energy Congress IV, Denver, Colorado, US, 1996, 1303-1307.

[7.16] Rev. ed, Heating and Cooling With a Heat Pump, Natural Resources Canada’s Office of Energy Efficiency. December 2004.

[7.17] R. Kannan et al., Life cycle assessment study of solar PV systems: An example of a 2.7 kWp distributed solar PV system in Singapore, Solar Energy 80 (2006) 555-563.

[7.18] Global Energy & CO_2 Status Report 2017, International Energy Agency, March 2018.

[7.19] Electricity-to-CO_2 conversion ratio in China, www.china5e.com, [26/11/2012]

[7.20] Energy, www.greenspec.co.uk, [24/07/2013]